N° d'ordre 110 Année 2013-2014

جامعة عبد المالك السعدي
Université Abdelmalek Essaadi

UNIVERSITE ABDELMALEK ESSAADI
FACULTE DES SCIENCES et TECHNIQUES
TANGER

Centre d'Etudes Doctorales : « Sciences et Techniques de l'Ingénieur »
Formation Doctorale : « Sciences et Techniques de l'Ingénieur »

THESE DE DOCTORAT

Présentée

Pour l'obtention du

DOCTORAT EN SCIENCES ET TECHNIQUES DE L'INGENIEUR

Par :

AZRAR ABDELLHADI

Discipline : Sciences et Techniques de l'Ingénieur

Spécialité : Mécanique Numérique

Modélisation et simulation numérique des instabilités dynamiques des nanotubes de carbones multifeuillets

Modelling and numerical simulation of the dynamic instabilities of single and multiwalled Carbon NonoTubes

Soutenue le 27 / 12 / 2014 devant le Jury

Pr. Mustapha DIANI	*Faculté des Sciences et Techniques –Tanger*	*Président*
Pr. Abdulmalik Ali ALJINADI	*Université du Roi Abdulaziz, Jeddah, Arabie Saoudite*	*Rapporteur*
Pr. EL Mostafa DAYA	*Université de Lorraine, France*	*Rapporteur*
Pr. Miloud RAHMOUN	*École Supérieure de Technologie, Meknès*	*Rapporteur*
Pr. Adil CHAHBOUN	*Faculté des Sciences et Techniques –Tanger*	*Examinateur*
Pr. Khalid SBAI	*École Supérieure de Technologie, Meknès*	*Examinateur*
Pr. Zoubir EL FELSOUFI	*Faculté des Sciences et Techniques -Tanger*	*Examinateur*
Pr. Lahcen AZRAR	*Faculté des Sciences et Techniques -Tanger*	*Directeur de thèse*

Structure de recherche accréditée d'accueil :
Références : UAE/E05/FST : Equipe de Modélisation Mathématique et Contrôle de la FST de Tanger

بسم الله الرحمان الرحيم

الحمد لله رب العالمين، والصلاة و السلام على سيدنا ومولانا محمد وعلى آله و صحبه و سلم تسليما

عن أبي الدرداء، رضي الله عنه، قال سمعت رسول الله صلى الله عليه وعلى آله وصحبه يقول :

" من سلك طريقا يبتغي فيه علما سهل الله له طريقا إلى الجنة، وإن الملائكة لتضع أجنحتها لطالب العلم رضا بما يصنع، وإن العالم ليستغفر له من في السماوات و من في الأرض حتى الحيتان في الماء، وفضل العالم على العابد كفضل القمر على سائر الكواكب، وإن العلماء ورثة الأنبياء، وإن الأنبياء لم يورثوا دينارا ولا درهما وإنما ورثوا العلم، فمن أخذه أخذ بحظ وافر"

رواه أبو داود و الترمدي

Dédicace

A la mémoire de mon père

A toute ma famille :

A ma très chère mère

A mes très chers frères

A mes très chères sœurs

A tous ceux qui ont contribué de près ou de loin au bon déroulement

de ce travail

ACKNOWLEDGMENTS

I would like to sincerely and whole heartedly thank Prof. Lahcen AZRAR for his guidance and kindness throughout this work. His patience as an advisor, boundless energy while teaching, promptness while reviewing all my writing, and passion for research are to be commended and worth emulating. I am indebted to him for cajoling me into doing scientific research and thus opening a whole new exciting world for me.

I would like to thank all members of the research team of "Mathematical Modeling and Control" supervised by Prof. Lahcen AZRAR for various forms of help and assistance. I learned a lot from scientific and technical discussions with them.

The financial support provided by:

- "Bourse d'excellence" from the CNRST and the Ministry of Higher Education and Scientific Research "MESRSFC"
- The convention CNRST-CNRS, Morocco –French 'SPM06/12'
- The DSR the HiCi research project N^0 (7-4 - 1432/HiCi) at King Abdulaziz University in Jeddah, Saudi Arabia.

I thank Prof. Mahmoud HAMMADICH for his helpful suggestions. His financial assistance during recurrent invitations is acknowledged. A part of this work has been accomplished in "Laboratoire de Mécanique des Fluides et d'Acoustique (LMFA)" at Ecole Central of Lyon in France. I was delighted to take advantage to these kind invitations and the opportunity to use the facilities of this laboratory.

I would like to thank Professors Abdelmalik Ali-ALGHAMDI ALJINAIDI, Miloud RAHMOUN and El-Mostafa DAYA for accepting to be referees of this thesis and taking the charges of my thesis report.

I would like also to thank, Professors Mustapha DIANI, Adil CHAHBOUN, Khalid SBAI, Zoubir EL FELSOUFI and Mahmoud HAMMADICH-AL MOHAMED for accepting to be comity members of the jury and judging my thesis work.

I wish express my gratitude to the Dean Prof. Mohamed ADDOU and the vice Deans Prof. Mustapha DIANI and Prof Taoufik MOURABIT of the Faculty of Sciences and Techniques of Tangier.

My thinks also to all professors at the department of Mathematics, Physics and Mechanical Engineering of the FST of Tangier, for their kindness.

Most importantly, I would like to thank my Mother, Sisters, Brothers and all my family members for their unconditional support, love, and affection. Their encouragement and never-ending kindness made everything easier to achieve.

Gratitude

Le candidat a bénéficié d'une bourse d'excellence octroyée par le Centre National pour la Recherche Scientifique et Technique et ça dans le cadre du programme des bourses de recherche initié par le Ministère de l'Éducation National, de l'Enseignement Supérieur, de la Formation de Cadres et de la Recherche Scientifique.

CURRICULUM VITAE

ACTIVITÉS SCIENTIFIQUES

❖ Articles

[1] Azrar, A.; Azrar, L.; Aljinaidi, A. "**Length scale effect analysis on vibration behavior of single walled Carbon NanoTubes with arbitrary boundary conditions**" Revue de Mécanique Appliquée et Théorique, Vol. 2 pages 475-484, **2011**

[2] Azrar, A.; Azrar, L.; Aljinaidi, A. **"Dynamic instability analysis of single walled Carbone NanoTubes conveying fluid under generalized boundary conditions",** MATEC Web of Conferences 1, 09002, **2012**

Indexed by Scopus http://dx.doi.org/10.1051/matecconf/20120109002

[3] Azrar, A.; Azrar, L.; Aljinaidi, A.; Hammadich, M. "**Dynamics Instability Analysis of Multi-Walled Carbon Nanotubes Conveying Fluid**", **Journal of Advanced Materials Research**, ISSN 1022-6680, Vol. 682 , p 153-160, Trans Tech Publications Ltd, **2013**

[4] Azrar, A.; Azrar, L.; Aljinaidi, A **"Nonlinear free vibration of single walled Carbone NanoTubes conveying fluid",** MATEC Web of Conferences 11, 02015, **2014,**

Indexed by Scopus http://dx.doi.org/10.1051/matecconf/20141102015

[5] Azrar, A.; Azrar, L.; Aljinaidi, A. "**Analytical and numerical modeling of higher order free vibration characteristics of single walled Carbon NanoTubes**" Paper submitted to the journal '**Physica E 2014'.**

[6] Azrar, A.; Azrar, L.; Aljinaidi, A. "**Numerical modeling of dynamic and parametric instabilities of single-walled carbon nanotubes conveying pulsating and viscous fluid**" Paper submitted to the journal '**Composite Structures, 2014'.**

[7] Azrar, A.; Bensaid M. Azrar, L.; Aljinaidi, A. "**Parameters uncertainty effects on the dynamic behavior of fluid conveying carbon nanotubes under a random excitation"** Paper under finalization to be submitted to an international Journal

[8] Azrar, A.; Azrar, L.; Aljinaidi, A. "**Numerical modeling of dynamic and parametric instabilities of multi-walled carbon nanotubes conveying pulsating and viscous fluid**" Paper under finalization to be submitted to an international Journal.

[9] Azrar, A.; Azrar, L.; Aljinaidi, A. "**Nonlinear vibration analysis of multi-walled carbon nanotubes conveying fluid based on thermoelastic shell model**", Paper under finalization to be submitted to an international Journal

❖ ***Communications***

[1] Azrar, L. Azrar, A. Aljinaidi. "**Modélisation des vibrations aux ordres supérieurs des nano tubes en carbone**" in Proceedings of 10th Conference of Mechanics, Vol. 1, pages 44-46, Oujda, April 19-22, 2011.

[2] Azrar, A.; Azrar, L.; Aljinaidi, A. "**Dynamic instability analysis of single walled Carbone NanoTubes conveying fluid under generalized boundary conditions**" in **CD**, Proceedings of International Conference on Structural Nonlinear Dynamics and Diagnosis, Marrakech, Morocco, April 29-May 02, **2012,**

[3] Azrar, A.; Azrar, L.; Hammadiche, M. "**Dynamic instability analysis of multi-walled Carbon NanoTubes conveying fluid**'' in **CD**, Proceedings of International Symposium on Aircraft Materials, Fes, Morocco, May 9-12, **2012.**

[4] Azrar, A.; Azrar, L.; Aljinaidi, A. & Hamadiche, M. "**Vibration analysis of multi-walled carbon NanoTubes conveying fluid based on thermoelastic shell model**" in Proceedings of 11th Conference of Mechanics, Vol. 1, pages 35-37, Agadir, April 23-26, **2013**.

[5] Azrar, A.; Azrar, L.; Aljunaidi, A. "**Nonlinear free vibration of single walled Carbone NanoTubes conveying fluid**'' in **CD,** Proceedings of Congress on Materials & Structural Stability Rabat, Morocco, 27-30 November **2013.**

[6] A. Azrar, L. Azrar & A. Aljinaidi "**Dynamic stability analysis of single-walled carbon nanotubes conveying pulsating and viscous fluid with nonlocal effect**" in **CD,** Proceedings of 5th International Symposium on Aircraft Materials Marrakech**,** Morocco, April 23-26, **2014**

[7] A. Azrar, L. Azrar, A. Aljinaidi. **"Complex modes based numerical analysis of single-walled carbon nanotubes conveying pulsating and viscous fluid embedded in an elastic medium"** Journées sur la Modélisation et Analyse en Mécanique et Energétique Tanger, Maroc, 29-30 Avril **2014**

<u>Participation à la réalisation des Projets de recherche suivants:</u>

Mes travaux de recherche rentrent dans le cadre des projets suivants:

1) Projet de collaboration entre Prof. L. Azrar (FST, Tanger) et Prof. A. A. Aljinaidi (Université du Roi Abdulaziz à Jeddah en Arabie Saoudite).
   Intitulé : **Smart materials and active vibration Control**.

2) Projet de collaboration entre Prof. L. Azrar (FST, Tanger) et Prof. A. A. Aljinaidi (Université du Roi Abdulaziz à Djeddah en Arabie Saoudite), N^0 (7-4 - 1432/HiCi).

3) Projet de convention CNRS-CNRST Maroc-France 'SPM06/12', en collaboration entre Prof. L. Azrar (FST, Tanger) et Prof. Mahmoud Hamadiche (Université Claude Bernard Lyon/Ecole Centrale de Lyon, France).
   Intitulé : **Modélisation mathématique et biomécanique de l'interaction fluide-tubes biologiques**.

4) Projet de mémoire de fin d'études pour l'obtention du Diplôme Master.

Intitulé : **Contrôle Actif des Vibrations des Plaques Circulaires et Annulaires** ; modélisation et simulation numérique. Sous l'encadrement du Professeur Lahcen AZRAR. Département de Mathématiques, Faculté des Sciences et Techniques de Tanger, Maroc.

RESUME DE LA THESE

Au cours de ces dernières années les nanotubes de carbone (CNT) ont suscité un intérêt et un engouement grandissants dans le monde de la recherche et développement (R&D). Les propriétés physiques exceptionnelles des CNTs tant sur les plans mécaniques que thermiques ou électriques placent actuellement ces nano objets à la pointe de l'innovation. En nanotechnologie et particulièrement en NEMS (Nano-Electro-Mechanical-Systems). Cela donne actuellement lieu à une intense activité de recherche ayant pour but de poursuivre la miniaturisation et tirer profit des nouveaux phénomènes physique apparaissant au niveau nanométrique. Les propriétés mécaniques exceptionnelles des CNT en font des candidats potentiels pour la constitution des matériaux composites multifonctionnels et ultra-résistants. Leurs qualités de transport électronique en font des candidats pour la réalisation de nouvelles générations de transistors, de diodes, capteurs, actionneurs, nano oscillateurs, etc. L'étude vibratoire de ce type de structure est primordiale pour leur utilisation en technologie miniaturisée et de pointe.

L'objectif de cette thèse est de développer des modèles mathématiques et des simulations numériques pour les problèmes de vibrations et d'instabilités dynamiques et paramétriques des nanotubes de carbone simples et à écoulement fluide. Ces derniers sont classifiés comme mono feuillets (SWCNT) ou multi feuillets (MWNT) selon le nombre de tubes de carbone considéré. La modélisation et la simulation numérique des vibrations transversales et des instabilités dynamiques et paramétriques ont été élaborées dans ce travail. Ces études ont été basées sur la théorie d'élasticité non locale et les modèles de poutres et coques ainsi que sur l'interaction fluide-structure et de van der Waals. La méthode différentielle quadrature a été adaptée pour la résolution numérique en espace vu ses avantages numériques. Pour le problème temporel, différentes méthodes ont été utilisées. Le comportement vibratoire des nanotubes de carbone a été profondément analysé pour les faibles, moyennes et très hautes fréquences. Pour les nanotubes à écoulement fluide, les effets de la vitesse d'écoulement, stationnaire et instationnaire, sur les instabilités dynamiques et paramétriques ont été profondément étudiés. Les vibrations propres, vitesses critiques de divergence et de flutter ainsi que l'évolution de la fréquence en fonction de la vitesse d'écoulement ont été déterminées en se basant sur les modèles de poutre et coques et la théorie d'élasticité non locale. Les modes et fréquences complexes ainsi leurs évolutions en fonction de la vitesse d'écoulement ont été déterminés pour différents types de nanotubes de

carbone. Vu la sensibilité des paramètres physiques et géométriques des nanotubes de carbone, des paramètres incertains suivant différentes lois de probabilité ont été introduits. Cela mène à un modèle innovant et scientifiquement prometteur. Les analyses fréquentielle et temporelle ont été élaborées en résolvant les équations aléatoires et les processus stochastiques résultants. Pour plus de précision, ce travail de thèse s'articule autour de six chapitres.

Dans le premier chapitre, représentant une introduction générale, les propriétés remarquables des nanotubes de carbone et leurs utilisations dans différents domaines ont été discutés. Une large étude bibliographique a été présentée afin de couvrir un grand spectre d'études élaborées dans ce domaine. L'accent a été mis sur les modèles d'élasticité non locale de poutres et de coques utilisés et sur les phénomènes statiques et dynamiques étudiés dans le cadre de cette thèse. La quantité des travaux récemment publiés sur ces nanostructures montre l'intérêt et la portée technologique grandissants de ce type de structures et matériaux.

Le deuxième chapitre présente la modélisation et la simulation numérique du comportement vibratoire des nanotubes en carbone soumis aux conditions aux bords généralisés. Ces conditions permettent d'une part d'unifier le formalisme lié aux conditions aux bords et d'autre part de mieux approximer les conditions aux bords expérimentales. Une analyse analytique du comportement vibratoire des nano tubes en carbone a été développée et présentée. Les résultats obtenus présentent les effets du paramètre non local (e_0a) sur les fréquences propres et sur la stabilité des modes supérieurs associés. Cela montre qu' à partir d'une certaine valeur de (e_0a), la structure devient instable par flutter. L'effet des conditions aux bords sur la zone d'instabilité a aussi été élucidé. L'analyse vibratoire de ce type de structures a été effectuée et les résultats obtenus ont été comparés aux résultats numériques de la littérature.

Dans le troisième chapitre, la modélisation du comportement vibratoire propre à basses, moyennes et hautes fréquences des nano tubes en carbone mono feuillets (CNT) a été élaborée en se basant sur les modèles de Timoshenko et de Bernoulli et sur la théorie de l'élasticité non locale. De nouveaux modèles pour les fréquences propres et modes associés ont été développés pour les moyennes et hautes fréquences. Les modes obtenus, dans ce travail, sont numériquement stables à tous les ordres et peuvent être utilisés comme une base pour l'analyse modale dans une large bande de fréquences. Les effets du paramètre non local sur les fréquences propres et sur la stabilité des modes supérieurs associés ont été analysés.

Le quatrième chapitre traite l'analyse dynamique des nanotubes en carbone mono et multi- feuillets à écoulements fluide. Une formulation mathématique modélisant l'interaction fluide-structure a été obtenue en considérant un fluide stationnaire et instationnaire. Le comportement dynamique des nanotubes en carbone a été modélisé par une équation aux dérivées partielles complexes et sa résolution numérique nécessite des méthodes bien adaptées. Vu les avantages de la méthode quadrature différentielle, cette méthode a été adaptée en domaine fréquentiel pour la résolution numérique en espace. Déférents type de conditions aux bords ont été considérés et selon la vitesse d'écoulement, les modes complexes et fréquences associées ont été obtenus. Les instabilités dynamiques, représentées par la variation des fréquences complexes ($1^{ière}$, $2^{ème}$, etc) en fonction de la vitesse d'écoulement, ont été profondément analysées. Les effets des paramètres physiques et géométriques des nanotubes en carbone sur l'instabilité par divergence et par flutter due à la vitesse statique du fluide ainsi que sur l'instabilité paramétrique lorsque le fluide est pulsatile ont été analysés.

Dans le cinquième chapitre, le modèle de coques non linéaires de Donnell et la théorie de l'élasticité non locale ont été utilisés pour la mise au point de la modélisation et simulation numérique des instabilités dynamiques des nanotubes tubes en carbones multi feuillets à écoulement fluide interne. La force d'interaction fluide-structure dans le cas d'un cylindre ainsi que l'interaction de van der Wall ont été modélisées. Un système d'équations aux dérivées partielles non linéaires modélisant le comportement dynamique des NTC multi-feuillets à effets d'interactions a été obtenu. Les fréquences propres pour différentes vitesses statique d'écoulement ainsi que les effets du paramètre non local et de l'interaction de van der Waals ont été obtenues. Les effets du paramètre non local sur les vibrations non linaires des NTC ont été explicitement dérivés par le modèle complet de coques. Des nanotubes cylindriques mono et multi feuillets à écoulement interne ont été considérés. L'analyse vibratoire linéaire et non linaire ainsi que la propagation d'onde du système ont été étudiées. Les effets de la température et du paramètre non local sur la propagation d'onde ont été analysés.

Due à la taille des nanotubes en carbone, les paramètres physiques et géométriques sont très sensibles. Dans la littérature, des données très dispersées des paramètres ont été utilisées par différents auteurs. Cela a stimulé notre choix de considérer des paramètres incertains. Le chapitre six a pour objectif d'élaborer des modèles et simulations numériques pour l'analyse de l'effet incertitudes des paramètres physiques et géométriques. Vu l'effet de taille, les

paramètres des NTC intervenant dans les modèles utilisés, sont inévitablement non déterministes. Ces paramètres sont alors considérés aléatoires et pouvant suivre différentes lois de probabilité. Les comportements statiques et dynamiques des NTC sont alors modélisés par des équations aléatoires ou processus stochastiques. Bien que l'effet des paramètres aléatoires et propagation des incertitudes soient étudiés pour les structures classiques, très peu de travaux ont été publiés pour les nanotubes. Les modèles et simulations, élaborés dans ce chapitre, constituent une ébauche, scientifiquement prometteuse, pour l'analyse aléatoire du comportement dynamique des nanotubes. Les méthodes de Monté Carlo, de l'espérance conditionnelle et des polynômes de Chaos généralisés ont été utilisées pour cette fin. La méthode des paramètres aléatoires internes, récemment développée par M. Ben Said et L. Azrar a été aussi utilisée dans ce chapitre. Cette méthode permet la prise en compte d'un grand nombre de paramètres aléatoires et d'une excitation aléatoire ayant un nombre arbitraire de paramètres. L'effet des paramètres aléatoires sur les vibrations, le flambage et la stabilité dynamique a été analysé. La réponse temporelle a aussi été élaborée pour un large nombre de paramètres aléatoires.

Il est à noter que les méthodes de Monté Carlo et de l'espérance conditionnelle nécessitent un très grand temps de calcul et d'espace mémoire et que les méthodes des polynômes de Chaos ne peuvent être utilisées efficacement que pour très peu de paramètres aléatoires. La méthode des paramètres aléatoires internes basés sur les polynômes de chaos généraux permet de surmonter cette difficulté et d'analyser les effets d'un grand nombre de paramètres aléatoires. Les modèles et simulations numériques, présentés dans ce chapitre, ouvrent un champ d'étude prometteur sur les nanostructures.

Finalement, quelques conclusions ont été présentées dans le septième chapitre afin de résumer les principaux résultats développés et définir les perspectives de poursuite des travaux de recherche présentés ici.

Mots-clés: Nanostructures, nanotubes de carbone, modélisation, instabilité dynamique, paramétrique, vibration, divergence, flutter, poutres, coques, Euler-Bernoulli, Timochenko, stochastique, interaction fluide-structure, van der Waals, paramètre aléatoires, Monté Carlo, polynôme de Chaos, méthode de quadrature différentielle.

ABSTRACT

In recent years, Carbon NanoTube (CNT), have attracted growing interest and attention of many scientists around the world. This stems from their outstanding structural, mechanical, thermal, optical and electronic properties. These exceptional properties make the CNTs very unique materials with a whole range of promising and practical applications. These nano-objects are placed at the forefront of innovation in nanotechnology and especially in NEMS (Nano-Electro-Mechanical-Systems). This gives rise to an intense research activity leading to further miniaturization and taking advantage of physical phenomena occurring at nano levels. The exceptional structural, electrical and mechanical properties of CNT make them potential candidates for the design of new multifunctional and ultra-resistant composite materials. On top of their excellent mechanical properties, CNT possess high electronic transport properties that make them potential candidates for the creation of new generations of transistors, diodes, sensors, actuators, nano-oscillators etc. The dynamic analysis of these structures is essential for their use in miniaturized and advanced technologies.

The main objectives of this thesis are the development mathematical models and numerical simulations for vibration, dynamic and parametric instabilities problems of Carbon NanoTubes and CNT conveying fluid. There are two types of carbon nanotube: single walled carbon nanotube (SWCNT) and multi-walled carbon nanotubes (MWVNTs). Analytical and numerical procedures based on the differential quadrature method are elaborated in this thesis for the static and dynamic behaviors of carbon nanotubes. Based on the nonlocal elasticity theory and beams and shells models as well as on the fluid-structure and van der Waals interactions, mathematical modeling and numerical simulation of transverse vibrations and dynamic and parametric instabilities are developed. Due to its numerical advantages, the differential quadrature method is adopted for the numerical resolution in space domain. For time domain, various methods have been used. Vibration of carbon nanotubes is analyzed at low, higher and very higher frequency ranges. Models for eigenfrequencies and associated eigenmodes are elaborated based on the nonlocal Euler-Bernoulli and Timoshenko models.

For the nanotubes conveying fluid, the frequency and time domains are considered. The instability analyses have been performed with respect to the considered influencing parameters based on analytical and numerical procedures with an emphasis on complex modes. The effects of the nonlocal parameter, the fluid pulsation, the fluid viscosity, the viscoelastic coefficient and the thermal on the dynamic behaviors of the CNT-fluid system are

analyzed. Various types of instabilities such as divergence, flutter and parametric instabilities as well as their interactions are analyzed. For the sensitivity analysis of the physical and geometrical parameters of carbon nanotubes, random parameters following various probability laws are considered. This leads to innovative and promising random models. The frequency and time analyses are developed by solving the resulting random equations and stochastic process. For more detail, this thesis revolves around six chapters.

In the first chapter, representing a general introduction, the remarkable properties of carbon nanotubes and their applications in various fields are discussed. A broad literature review was given covering a wide range of studies carried out in this area. Emphasis has been placed on the nonlocal elasticity theory and the used beams and shells models as well as on the static and dynamic behaviors studied in this thesis. The number of recently published work on these nanostructures shows clearly the growing interest and technological scope of this type of structures and materials.

The nonlocal and the general boundary conditions effects on the vibration frequencies are studied in the second chapter. It was demonstrated that the nonlocal parameter, e_0a/L, has a strong effect and the clamped-free CNT may flutter at critical values of e_0a/L. This instability limit can be used as a limit for prediction values of the small length scale.

This chapter is a journal paper entitled “Length scale effect analysis on vibration behavior of single walled Carbon NanoTubes with arbitrary boundary conditions”. It is published in “Revue de Mécanique Appliquée et Théorique, Vol. 2 pages 475-484, 2011”.

In chapter three, the vibration characteristics of single walled CNT based on the nonlocal elasticity, Timoshenko and Euler-Bernoulli beam theories at small, higher and very higher levels are studied. The analytical and numerical solutions, based on the differential quadrature method, are performed. The higher and very higher frequencies and associated eigenmodes are obtained for various boundary conditions.

This chapter is a journal paper entitled “Analytical and numerical modeling of higher order free vibration characteristics of single walled Carbon NanoTubes” submitted to the international journal Physica E, 2014

In chapter four, vibration, dynamic and parametric instabilities of CNT conveying pulsating fluid are analyzed based on the nonlocal elasticity, differential quadrature method,

fluid interaction and Euler-Bernoulli beam theory. The multimode approach has been formulated based on the numerically computed eigenmodes, for dynamic and parametric instabilities. The influences of the fluid-velocity, the nonlocal parameter, the viscosity, the viscoelastic coefficient as well as the thermal effects on the dynamic behaviors and flow-induced structural instability of CNTs are studied. Various types of instabilities such as divergence, flutter and parametric instabilities and their interactions are investigated.

This chapter is a journal paper entitled "Numerical modeling of dynamic and parametric instabilities of single-walled carbon nanotubes conveying pulsating and viscous fluid" submitted to Composite Structures, 2014.

In chapter five, the nonlinear Donnell shell model and the nonlocal elasticity theory are used for linear and nonlinear free vibration and dynamic instability analyses of multi-walled CNTs conveying fluid. The van der Waals (vdW) interactions between two layers of carbon nanotube as well as the fluid-shell interaction are investigated. The free vibration and the flow velocity-frequency dependence are analyzed with respect to various physical and material parameters. The obtained results showed a strong dependence between the fluid-velocity and the frequency of MWCNTs. The effect of the van der Waals interaction between tubes is discussed and results show that the van der Waals interaction and the length scale effects may significantly influence the stability of multi-walled CNT. For the nonlinear free vibration of MWCNT, the amplitude-frequency dependences are obtained by harmonic balance method. The influences of nonlocal parameters, the vdW force and the thermal effects are discussed.

A part of this chapter is a journal paper titled "Dynamics Instability Analysis of Multi-Walled Carbon Nanotubes Conveying Fluid"
Published in the journal Advanced Materials Research, Vol. 682, pp 153-160, 2013.

Chapter six aims to develop numerical models and simulations of the uncertainty effects of physical and geometrical parameters. Given the size effect, the parameters associated to CNT models are inevitably non deterministic. These parameters are then considered random and their uncertainty effects can be approximated by different probability density laws. The static and dynamic behaviors of CNTs are then modeled by random equations or stochastic processes.

Note that there is a big lack of literature on the parameters uncertainty effects on the dynamic and static behaviors of CNT. Only very few work is available in the open literature. The

models and simulations developed in this chapter are an outline, scientifically promising, for random analysis of the dynamic behavior of nanotubes. Monte-Carlo, conditional expectation methods as well as the internal random coefficients method are used. The internal random coefficients method recently developed by Ben Said and L. Azrar; is adopted in this chapter. This method allows considering a large number of random parameters and a random excitation with an arbitrary number of parameters. The effects of random parameters on vibration, buckling and dynamic instability are analyzed. The time responses are also developed for a wide number of random parameters. It should be noted that the methods of Monte-Carlo and conditional expectation require very large computation time and memory space and the methods of polynomials chaos can be used efficiently for very few random parameters. The method of internal random coefficients, based on the general polynomials chaos, overcomes this problem and is used here to analyze the effects of a large number of random parameters. The numerical examples, developed in this chapter, have proved the applicability and effectiveness of these methods.

Chapter six is a journal paper entitled "Parameters uncertainty effects on the dynamic behavior of fluid conveying carbon nanotubes under a random excitation" will be submitted to an international journal 2014.

Keywords: Nanostructure, carbon nanotube, modeling, dynamic instability, parametric, vibration, divergence, flutter, beams, shell, Euler-Bernoulli, Timoshenko, stochastic, fluid-structure interaction, van der Waals, random parameters, Monte-Carlo, polynomials chaos, differential quadrature method.

TABLE OF CONTENTS

List of Tables

List of Figures

Chapter 1:

General introduction

1 Carbon NanoTubes presentation

Carbon NanoTubes have been discovered for the first time in 1991 by Sumio Iijima [1] and in 1993 in their single-walled form [2]. Due to their phenomenal mechanical and electronic properties, carbon nanotube structures have attracted a great deal of attention from both industrial technology and academia. The prediction of characteristics and behaviors analyses of these nanomaterials and structures are the most challengeable topics in recent years.

1.1 Description

There are two types of carbon nanotubes: single-walled nanotubes (SWCNT) and multi-wall (MWCTs) (Figure 1.1). The single-walled nanotubes are made of a single graphitic wall, while the multi-walled nanotubes comprise graphitic several walls. We can see a multiwall nanotube as threading several concentric single-walled nanotubes with the interlayer spacing between adjacent nanotubes, approximately equal to the interplants distance of graphite (about 0.34 nm). Mono or multi-walled nanotubes, are usually arranged parallel to each other according to a two-dimensional array of triangular mesh, and held together by van der Waals interactions. Generally, “most researchers have adopted the equilibrium interlayer spacing between adjacent nanotubes (about 0.34 nm) as the representative thickness of SWCNTs combined with a Young’s modulus of about 1 TPa”.

CNTs are recently used on reinforcements for various structures, field emission, chemical sensing, energy storage, sensors, actuators, transistors, memories and other Nanoelectronic devices.

The discovery of SWCNT and MWCNTs where the walls can be clearly seen (Figure 1.1) using an arc-discharge method, has stimulated many research activities in science and engineering and many researches are recently focused on the carbon nanostructures and their applications. This is due in large part to the small size, low density, high stiffness, high strength and excellent electronic properties.

A scanning electron microscopy (SEM) image of carbon nanotubes grown by arc-discharge is shown in Figure 1.2 (a). The web-like structure consists of nanotube bundles. Every bundle or rope in Figure 1.2 (a) is formed by 20–100 single walled nanotubes, as can be seen in the high-resolution transmission electron microscope picture in part (b) of the figure. In such a bundle the tubes are packed in a two-dimensional hexagonal lattice. (c) Water-assisted CVD-grown carbon nanotubes of high purity and length. The nanotube mat is shown next to the head of a matchstick. (d) A patterned substrate allows the growth of carbon nanotubes in predefined places as shown in this SEM picture [3,4].

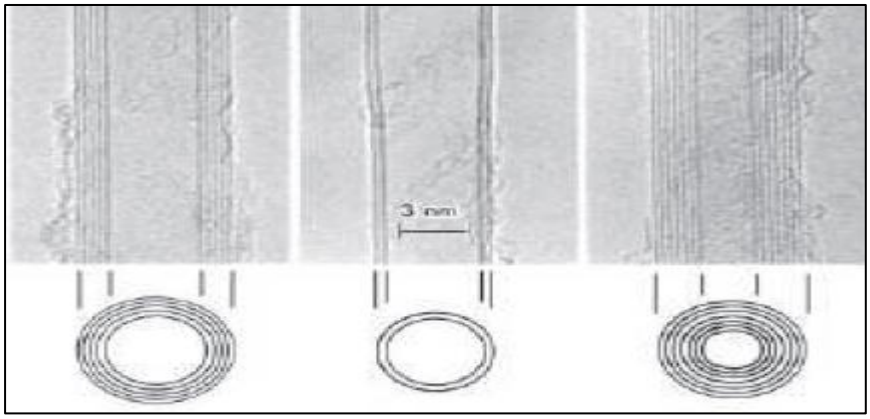

Figure 1.1 High-resolution images of a single-walled and a multiwalled carbon nanotube, [1]

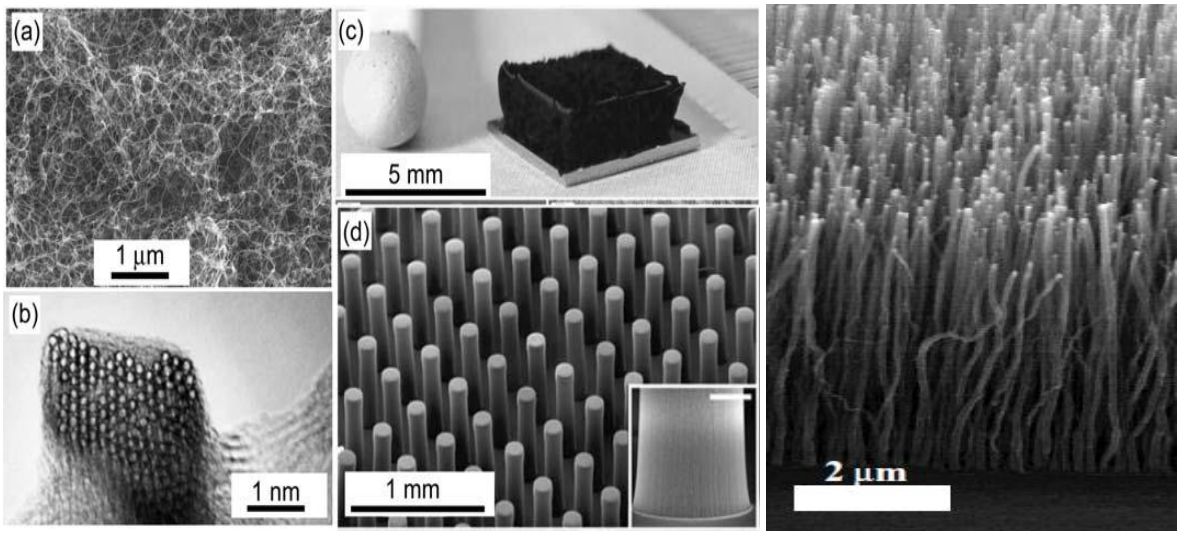

Figure 1.2 High-resolution scanning microscopy images of a single-walled bundles, [3,4,5]

The diameter and helicity of a defect-free SWNT are uniquely characterized by the vector $C_h = ma_1 + na_2 \equiv (m,n)$ that connects crystallographically equivalent sites on a two-dimensional graphene sheet, where a_1 and a_2 are the graphene lattice vectors and n and m are

integers. The carbon nanotube can be obtained by cutting a tiny strip out of a graphene sheet and rolling it up into a cylinder. This procedure is shown in (Fig. 1,3). In the laboratory, carbon nanotubes grow from carbon plasma by adding metal catalysts. The chiral vector dictates the geometric arrangement of the nanotube and there exist three distinct possible classifications. The names given for the three classes are armchair, in which *n* is equal to *m*; zigzag, where *m* is equal to 0; and helical, in all other cases, as illustrated below in Figure 1.4 [6].

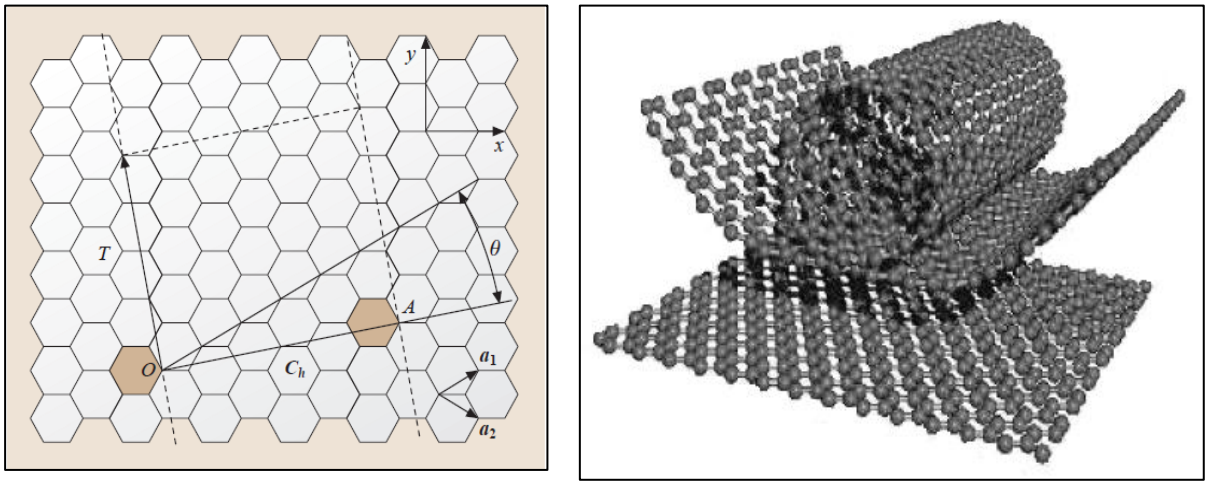

Figure 1.3 Sketch of the way to make a single-wall carbon nanotube, starting from a graphene sheet. The parameters that define the nanotube structure when the sheet is 'rolled' (chiral angle θ, chiral vector C_h figure 1.3, basis vectors a_1 and a_2) are indicated in the figure [6]

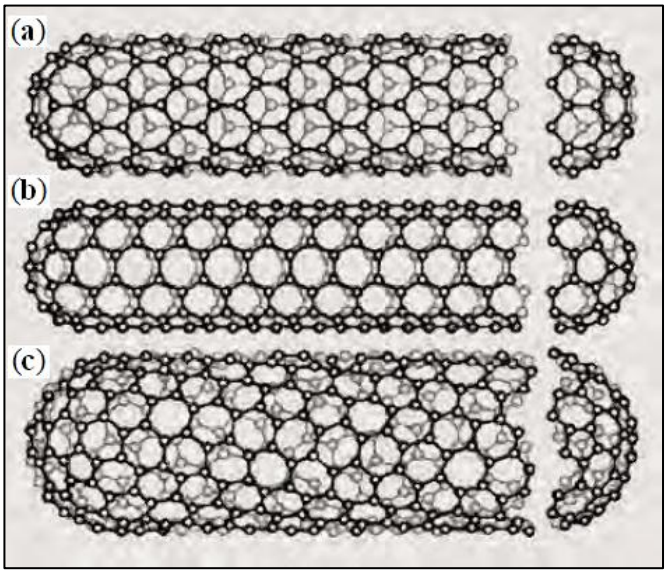

Figure 1.4.Three different SWNT structures; (a) a zig-zag-type nanotube, (b) anarmchair-type nanotube, (c) chiral, adapted from reference [6].

The various ways to roll graphene into tubes are therefore mathematically defined by the vector of helicity C_h, and the angle of helicity θ, as follows: [7]

$$OA=C_h = ma_1 + na_2 \tag{1.1}$$

$$a_1 = \frac{a\sqrt{3}}{2}x + \frac{a}{2}y \text{ and } a_2 = \frac{a\sqrt{3}}{2}x - \frac{a}{2}y$$

where a = 2.46Å is the graphene lattice constant [8] and $\cos\theta = \frac{2n+m}{2\sqrt{n^2+m^2+mn}}$

where *n* and *m* are the integers of the vector ***OA*** considering the unit vectors $\boldsymbol{a}_1$ and $\boldsymbol{a}_2$.

The diameter of a tube is related to the chiral vector by

$$d = \frac{|Ch|}{\pi} = \frac{a_{CC}}{\pi}\sqrt{3(n^2+m^2+nm)} \tag{1.2}$$

where

$$\underset{(\text{Graphite})}{1.41\text{A}^\circ} \le a_{CC} \le \underset{(C_{60})}{1.44\text{A}^\circ}$$

The chiral angle is allowed to vary between $0° \le \theta° \le 30°$; all other ranges of θ are equivalent to this interval because of the hexagonal symmetry of graphene. A chiral angle of $0°$ and $30°$ corresponds to tubes with a particular high symmetry, as we discuss later. They are called zigzag $(\theta = 0°)$ and armchair tubes $(\theta = 30°)$.

1.2 Different forms of CNTs

Based on the number of layers, CNTs can be divided into two distinct groups. Single-walled carbon nanotubes (SWCNTs) are those with a single layer of carbon atoms. Multi-walled carbon nanotubes (MWCNTs) have more than one layer and can be thought of as a number of concentric SWCNTs where the smaller nanotubes are embedded inside the larger ones. In 1985 Kroto et al. [9] discovered a new kind of carbon, the so called fullerenes. These are ball-like molecules which consist of e.g. 60 carbon atoms [10]. Later, similar configurations with a different number of atoms were discovered. For the discovery of the fullerenes Kroto, Smalley and Curl obtained the Nobel Prize for Chemistry in 1996.

Figures 1.5 and 1.6 summarize the classifications described above.

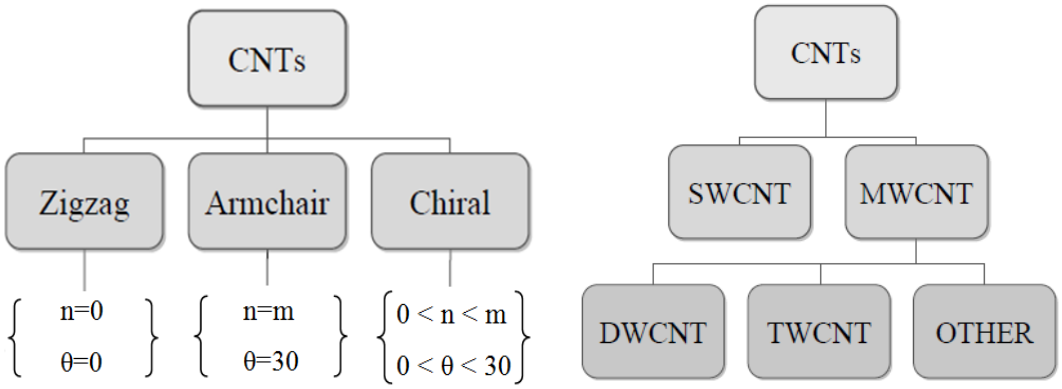

Figure 1.5 Classification of different carbon nanotube structures

According to the m, n structural parameters values, SWCNTs can be a metal, semiconductor or small-gap semiconductor [11-13]. When n=m, the CNTs are metallic. If n–m, is a multiple of three, the CNTs present an extremely small band gap and at room temperature they have metallic behavior. For other intermediate values of n–m the behavior is that of a semiconductor with a given band gap [13].

This extreme sensitivity of electronic properties on structural parameters is one of the most important aspects of nanotubes that make them very unique.

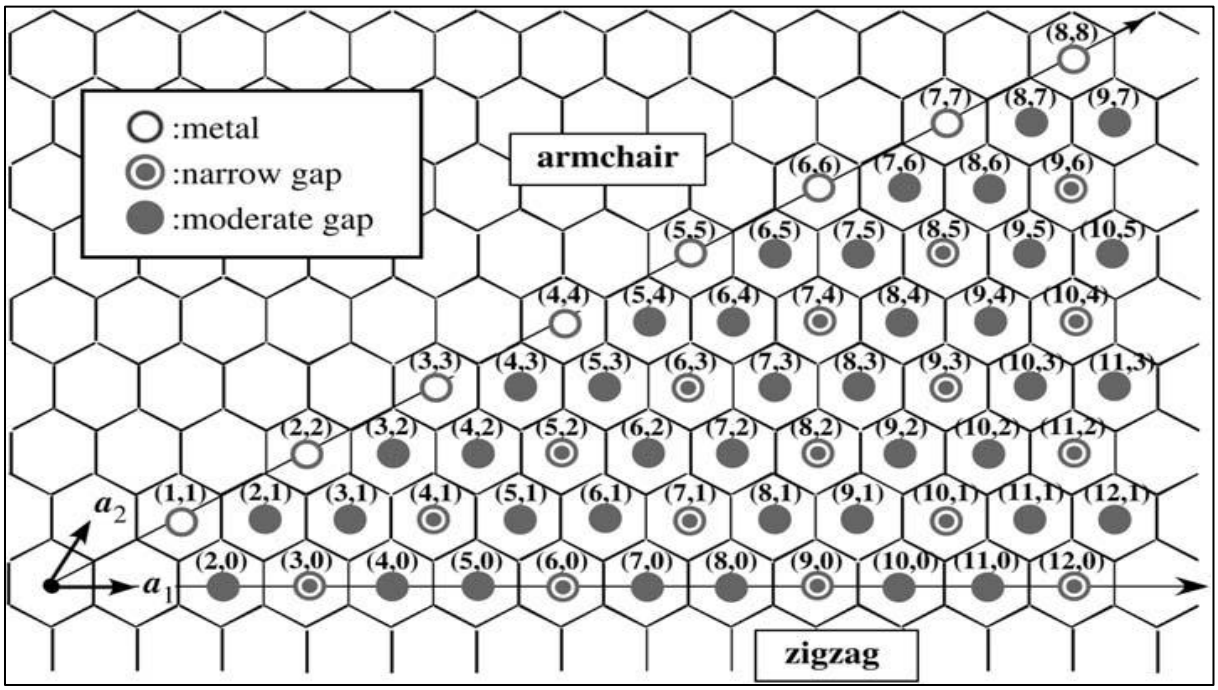

Figure 1.6 Circumferential vector map of carbon nanotubes and their electronic transport properties.

Electronic band structure calculations predict that the (n,m) indices determine the metallic or semiconducting behavior of SWNTs figure1.5. Zigzag (n,0) SWNTs should have two distinct types of behavior: the tubes will be metals when n/3 is an integer, and otherwise semiconductors. As ch rotates away from (n,0), chiral (n,m) SWNTs are possible with electronic properties similar to the zigzag tubes; that is, when (2n+m)=3 is an integer the tubes are metallic, and otherwise semiconducting. The gaps of the semiconducting (n,0) and (n,m) tubes should depend inversely on diameter.

1.3 Mechanical characteristics

Few even tried experimental investigations, it was found that Young modulus of MWNTs has mean value of 1.8 TPa with a variation from 0.40 to 4.15 TPa [14]. Krishnem et al [15] observed the vibration of SWNT and obtained the Young's modulus ranged from 0.90 to 1.70 TPa. Wang et al.[16] conducted bending tests on cantilevered tubes using atomic force microscopy and calculated the modulus to be of 1.28 TPa. Poncharal et al. [17] observed the static and dynamic mechanical deflections of cantilevered MWNTs and a modulus of about 1.0 TPa is obtained. [18,19].

Table 1.1 Values of Young's modulus for different chiralities using molecular dynamic simulation [20].

(n, m)	Diameter (nm)	Young's modulus (GPa)	(n, m)	Diameter (nm)	Young's modulus (GPa)	(n, m)	Diameter (nm)	Young's modulus (GPa)
Armchair			Zigzag			Chiral		
(8,8)	10.848	934.960	(14,0)	10.960	939.032	(12,6)	12.428	927.671
(10,10)	13.560	935.470	(17,0)	13.390	938.553	(14,6)	13.917	921.616
(12,12)	16.272	935.462	(21,0)	16.441	936.936	(16,8)	16.571	928.013
(14,14)	18.984	935.454	(24,0)	18.789	934.201	(18,9)	18.642	927.113
(16,16)	21.696	939.515	(28,0)	21.921	932.626	(20,12)	21.921	904.353
(18,18)	24.408	934.727	(31,0)	24.269	932.598	(24,11)	24.269	910.605
(20,20)	27.120	935.048	(35,0)	27.401	933.061	(30,8)	27.165	908.792

Table 1.1 Lists the values of Young's modulus of armchair, zigzag, chiral SWCNTs with different tube diameters. The values of Young's modulus are different.

The Young's and shear modulus and Poisson's ratio of SWCNTs can be defined as: [21]

$$E_{Nanotube} = \frac{\sigma}{\varepsilon} = \frac{\frac{P}{\pi D_0 h}}{\frac{\Delta L}{L_0}} = \frac{PL_0}{\pi D_0 h \Delta L} \tag{1.3}$$

$$G_{Nanotube} = \frac{TL_0}{\theta J_0},\ J_0 = \frac{\pi}{2}\left[\left(\frac{D_0 + h}{2}\right)^4 - \left(\frac{D_0 - h}{2}\right)^4\right] \tag{1.4}$$

$$\nu_{Nanotube} = -\frac{\varepsilon_c}{\varepsilon},\quad \varepsilon_c = \frac{D - D_0}{D_0} \tag{1.5}$$

Where P, T, L_0, D_0, D, h, θ, J_0 denote the total force and torque applied, length, diameter before and after deformation and wall thickness of SWCNTs, angular displacement, and polar moment of area, respectively.

Experiments are performed with bending by Atomic Force microscopic, AFM, to determine the elastic modulus. Coupling an AFM experiments and an electron microscope were used to measure the tensile strength of various types of nanotubes (figure 1.7). [22]

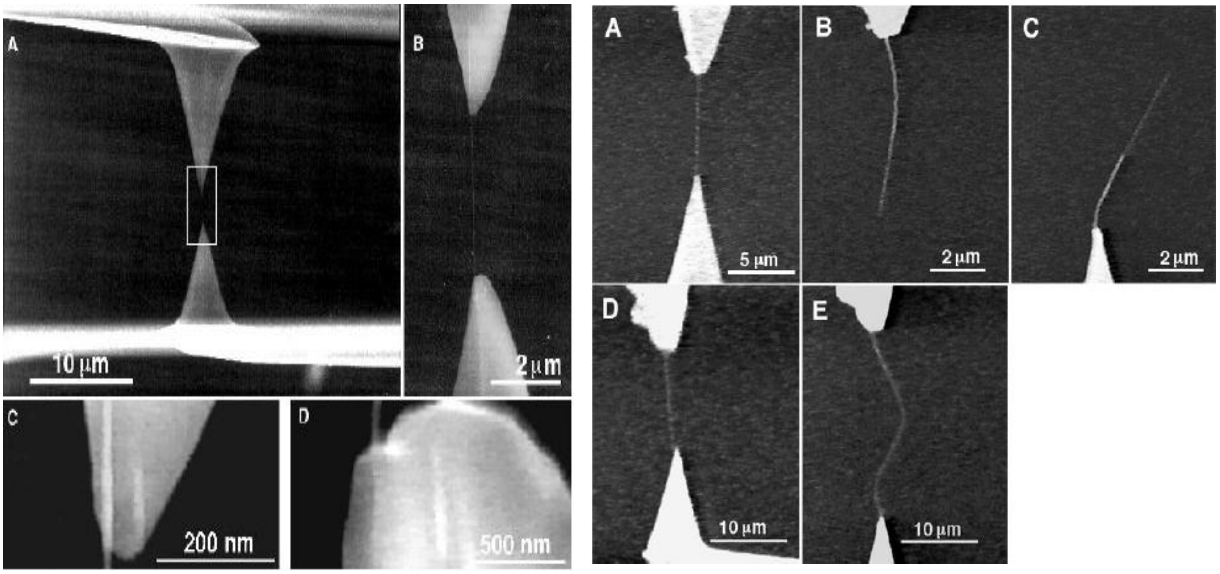

Figure 1.7 Single walled CNT traction test by the atomic force microscopic Yu et al. [22].

References [14, 22] demonstrate that the CNT mechanical and electrical are very hard to predict accurately. Due to the lower scale, the predictions are done with a large vibration.

These vibrations, that may be considered noise or random, have to be considered in the models analysis and simulations.

1.4 Different utilizations

Carbon nanotubes have advanced in the general interest and found their way into several textbooks. On the electronic states see the books by Javey and Kong [23], Bharat Bhushan [24,25] for a recent overview of Integrated Circuits and Systems Rivas et al. [26] used carbon nanotube in electrochemical sensors, Stefano Bianco [27], Saito and Zettl [28] and Christofer Hierold [29], the application of carbon nanotube in condensed material science. Nanoelectronic application devices have been extensively explored since the demonstration of the first carbon nanotube transistors [30-33].

1.4.1 Nano composites

Various uses of nanotubes are possible such as in composite structure. An interesting application for carbon nanotubes is mechanical reinforcements and composites [15], figure 1.8. High-quality SWNTs are attractive for transistors. The developments in carbon nanotube are supported by recent methods for precise high density CNT film and memory.

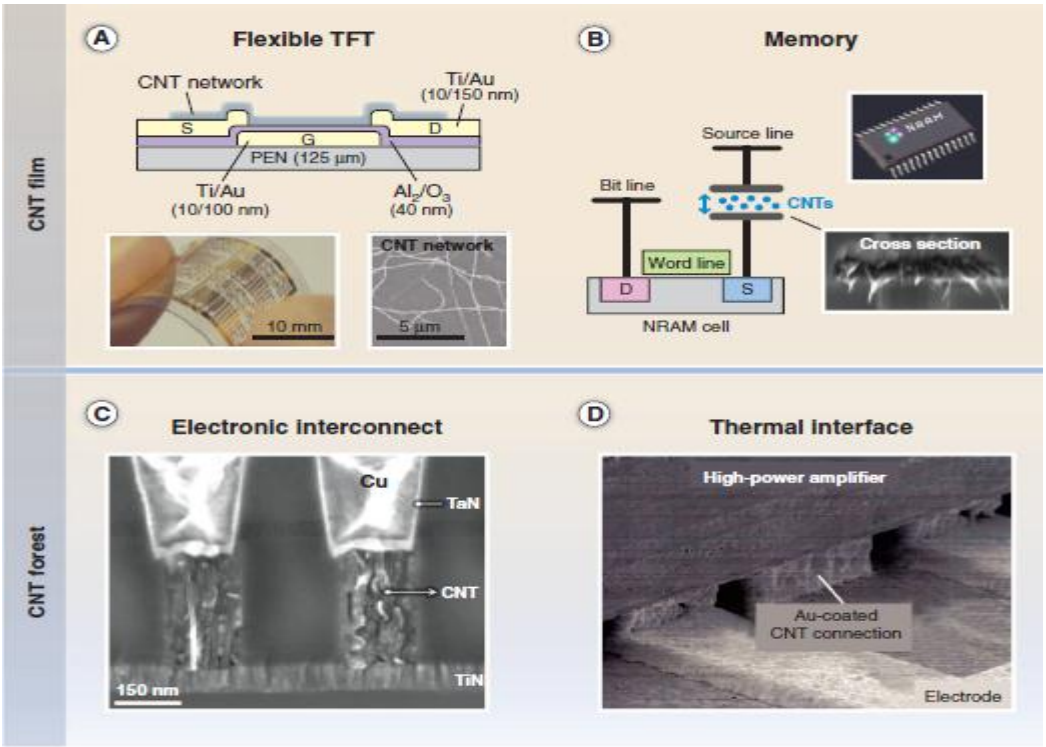

Figure 1.8. Selected CNT applications in microelectronics. (A) Flexible TFTs using CNT networks deposited by aerosol CVD. (B) CNT-based nonvolatile random access memory

(NRAM) cell fabricated by using spin-coating and patterning of a CMOS-compatible CNT solution. (C) CMOS-compatible 150-nm vertical interconnects developed by Imec and Tokyo Electron Limited. (D) CNT bumps used for enhanced thermal dissipation in high power amplifiers. [27]

Since 2006, worldwide CNT production capacity has increased at least 10-fold, and the annual number of CNT-related journal publications and issued patents continues to grow (Fig. 1.9). [27]

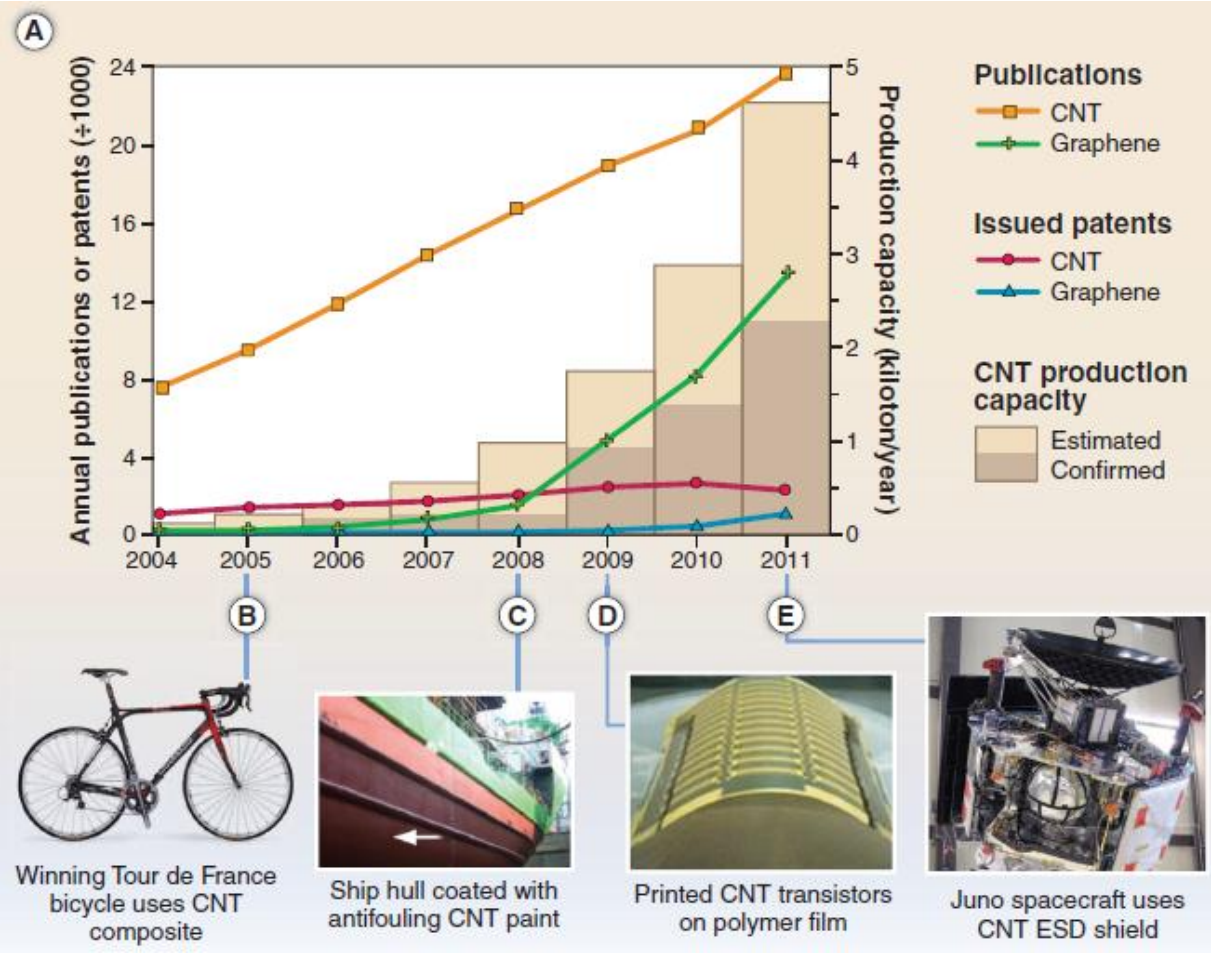

Figure 1.9 Trends in CNT research and commercialization. (A) Journal publications and issued worldwide patents per year, along with estimated annual production capacity. (B to E) Selected CNT related products: composite bicycle frame, antifouling coatings, printed electronics and electrostatic discharge shielding [27]

1.4.2 Microsystems Applications

The mechanical, electronic, and thermal properties of nanotubes suggest many applications and disruptive technologies.

IBM has recently demonstrated a 12 transistor ring oscillator can be fabricated onto the side of an individual CNT [34]. An image of the 18 μm long circuit is seen below in Figure 1.10 with a detail image showing the CNT.

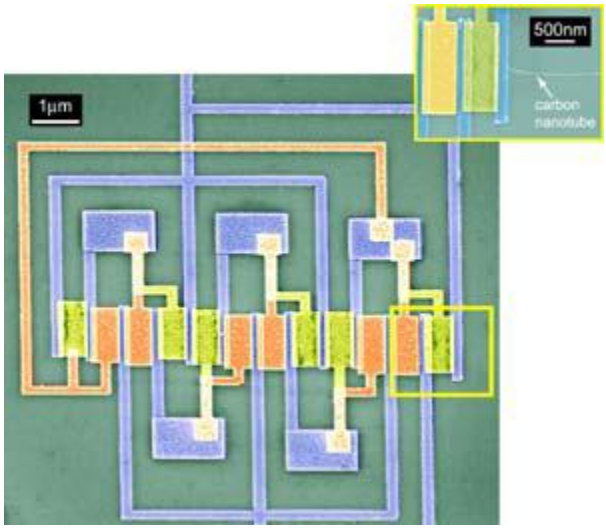

Figure 1.10 IBM produced ring oscillator consisting of 12 transistors built onto the side of an individual CNT [34]. The arrangement of the device allows it to test the speed at which the CNT based transistors are capable of switching.

1.4.3 Emission display

Another application of CNTs is their use as a field emission display material in displays and monitors. Samsung has developed a 38 inch working prototype model and in Austin, Texas based Applied Nanotech has developed a 22 inch model. The prototype nanotube emission display (NED) as seen below in Figure 1.11 was made by Motorola Labs [35].

Figure 1.11 Nanotube emitting display made by Motorola Labs [35].

The use of CNTs as field emitters have the potential to make display panels millimeters thin and economical to manufacture. A number of review articles on specialized topics have been published.

2. Carbon NanoTubes mathematical modeling

There are two major computational mathematical procedures available for static and dynamic analysis of carbon nanostructures such as Nanorods, nanobeams, nanoplates, nanotubes and nanoshells. These procedures are namely the molecular dynamic simulation (MD) and the continuum based approaches.

2.1. Molecular dynamics

In the modern nanotechnology age, microscopic analysis methods are indispensable in order to generate new functional materials and investigate physical phenomena on a molecular level. These methods treat the constituent species of a system, such as molecules and fine particles. Macroscopic and microscopic quantities of interest are derived from analyzing the behavior of these species. There are several text books in which this technique is presented in detail [36-38]. This subsection contains a brief description of the DM method. The temporal evolution of particles in interaction is obtained in the molecular dynamic by the numerical solution of classical equations of motion.

$$\frac{\partial r_i(t)}{\partial t} = v_i(t); \tag{1.6}$$

$$\frac{\partial v_i(t)}{\partial t} = \frac{f_i(t)}{m_i} \tag{1.7}$$

$$f_i(t) = \frac{\partial}{\partial r_i} V(r_1, r_2, ..., r_N) \tag{1.8}$$

$$r_i(t + \Delta t) = r_i(t) + v_i(t)\Delta t + \frac{f_i(t)}{2m_i}(\Delta t)^2 \tag{1.9}$$

where $r_i(t)$ and $v_i(t)$ denote the position and the velocity of the ith particle at time t.

m_i is the mass of the ith particle, $f_i(t)$ is the force acting on the particle.

The velocities is given by

$$v_i(t+\Delta t) = v_i(t) + \frac{f_i(t+\Delta t) + f_i(t)}{2m_i}\Delta t \tag{1.10}$$

Let us consider the two-dimensional motion of N argon atoms on a network of dimension L×L. The potential of interaction u between two atoms in the gas separated by a distance r is given by the Lennard –Jones [39]

$$u = 4\varepsilon\left[\left(\frac{\sigma}{r}\right)^{12} - \left(\frac{\sigma}{r}\right)^{6}\right] \tag{1.11}$$

where σ and ε are the Lennard-Jones parameters given by ε = 0.0556 kcal. mole^{-1} and σ = 0.34 nm respectively for this case.

The force exerted on the atom i by atom k is:

$$f_{k,j} = -\frac{du}{dr} = \frac{24\varepsilon}{r_{ki}}\left[2\left(\frac{\sigma}{r_{ki}}\right)^{13} - \left(\frac{\sigma}{r_{ki}}\right)^{7}\right] \tag{1.12}$$

The equations of motion of the atom i are given by:

$$\frac{d^2x_i}{dt^2} = a_{x,i} = \frac{1}{m}\sum_{k\neq i} f_{k,j}\frac{x_i - x_k}{r_{ki}}; \quad \frac{d^2y_i}{dt^2} = a_{y,i} = \frac{1}{m}\sum_{k\neq i} f_{k,j}\frac{y_i - y_k}{r_{ki}} \tag{1.13}$$

The numerical Verlet algorithm given by equations

$$x_{i,n+1} = 2x_{i,n} - x_{i,n-1} + (\Delta t)^2 a_{x,i,n}, \qquad y_{i,n+1} = 2y_{i,n} - y_{i,n-1} + (\Delta t)^2 a_{y,i,n} \tag{1.14}$$

The associated velocities are given by:

$$v_{x,i,n} = \frac{x_{i,n+1} - x_{i,n-1}}{2\Delta t}, \quad v_{x,i,n} = \frac{y_{i,n+1} - y_{i,n-1}}{2\Delta t} \tag{1.15}$$

The maximum separation in the x direction between two particles is only L/2. Similarly, the maximum separation in the y direction between two particles is only L/2. This can be realized as follows:

If $(x_{ij} > L/2)$ then $x_{ij} = x_{ij} - L$, if $(x_{ij} < -L/2)$ then $x_{ij} = x_{ij} + L$

If $(y_{ij} > L/2)$ then $y_{ij} = y_{ij} - L$, if $(y_{ij} < -L/2)$ then $y_{ij} = y_{ij} + L$

To demonstrate how to use molecular dynamics simulation to evaluate the mechanical properties of nanocomposites, the work by Adnan et al. [40] using molecular dynamics

simulation to investigate the effect of filler size on elastic properties of polyer nanocomposites can be followed. The elastic mechanical properties of carbon nanotube can be predicted by molecular dynamic approach by Wan and Delale [41]. The vibration of single walled carbon nanotube and graphene sheets using molecular dynamic simulation based finite element method are studied [42,43]. Sbai et al [44-45] developed modeling and simulation of vibrational breathing-like modes in individual multiwalled carbon nanotubes and analyzed the size effect on the Raman active modes. The vibration analysis of CNT has been elaborated by many authors [46-50].

The investigation of dynamic behavior of CNTs has been the subject of numerous experimental, molecular dynamic and continuum elastic modeling studies. Since controlled experiments and nanoscales are difficult and molecular atom numbers of about 10^9 by the scale and cost of computation, the continuum mechanics methods are often used to investigate some physical problems in the nanoscale.

2.2. Continuum mechanics approaches

In 1996, Yakobson et al. [51] showed using MD simulations that all the buckling patterns displayed by the molecular-dynamics simulations could be predicted by the continuum shell model. Subsequently, continuums models have been used to study the mechanical behavior of CNTs by a number of researchers and many research work have been published recently example in bending, buckling and vibration. Ghasemi et al. [52] studied analytical solution of buckling and post-buckling of multi-walled carbon nanotubes conveying fluid. Nuttawit and Variddhi [53] studied the elastic foundation on bending, buckling and vibration of carbon nanotube-reinforced composite beams. Zhang et al [54] used nonlocal elasticity to show the small-scale effects on buckling of MWCNTs under axial compression and radial pressure [55]. The vibration of CNTs conveying fluid is studied by [56-58], the vibration of the nano-plate [59-61]. Many other research works will be cited in the following sub-sections.

2.2.1. Local elasticity

The local elasticity is based on the continuum mechanics and classically used to study the behaviors of thin and thick structures as well as the 3D elasticity problems in solid and fluid mechanics. Many numerical methods are developed based on the local elasticity theory such as finite deference and finite element methods. The local elasticity theory is mainly based on the Hook's law, the general expression of the strains are given by:

$$\varepsilon = \frac{1+\upsilon}{E}\sigma + \frac{\upsilon}{E} tr(\sigma) I_d ; \tag{1.16}$$

where I_d is the identity tensor , $tr(\sigma)$ the trace of σ. Conversely, the relationship expressing the stress to strain as a function of the coefficients Lamé (κ, γ) is:

$$\sigma = 2\kappa\varepsilon + \gamma tr(\varepsilon) I_d \tag{1.17}$$

The relationship between shear modulus, Young's modulus, and Poisson's ratio is given as:

$$G = \frac{E}{2(1+\upsilon)} \tag{1.18}$$

The elastic parameters and the Lame's coefficients are related by:

$$\gamma = \frac{\upsilon E}{(1+\upsilon)(1-2\upsilon)}; \ \kappa = \frac{E}{2(1+\upsilon)} \tag{1.19}$$

The stress and strain tensors relationship can be expressed for isotropic materials by Hooke's law in the matrix form:

$$\begin{Bmatrix} \sigma_{xx} \\ \sigma_{yy} \\ \sigma_{zz} \\ \sigma_{yz} \\ \sigma_{zx} \\ \sigma_{xy} \end{Bmatrix} = \begin{bmatrix} 2\kappa+\gamma & \gamma & \gamma & 0 & 0 & 0 \\ \gamma & 2\kappa+\gamma & \gamma & 0 & 0 & 0 \\ \gamma & \gamma & 2\kappa+\gamma & 0 & 0 & 0 \\ 0 & 0 & 0 & \kappa & 0 & 0 \\ 0 & 0 & 0 & 0 & \kappa & 0 \\ 0 & 0 & 0 & 0 & 0 & \kappa \end{bmatrix} \begin{Bmatrix} \varepsilon_{xx} \\ \varepsilon_{yy} \\ \varepsilon_{zz} \\ \varepsilon_{yz} \\ \varepsilon_{zx} \\ \varepsilon_{xy} \end{Bmatrix} \tag{1.20}$$

In a case of two-dimensional loading, the constitutive law is found in a simplified and condensed form.

For 2D plane stress problems:

$$\begin{Bmatrix} \sigma_{xx} \\ \sigma_{yy} \\ \sigma_{xy} \end{Bmatrix} = \frac{E}{1-\upsilon^2} \begin{bmatrix} 1 & \upsilon & 0 \\ \upsilon & 1 & 0 \\ 0 & 0 & \dfrac{1-\upsilon}{2} \end{bmatrix} \begin{Bmatrix} \varepsilon_{xx} \\ \varepsilon_{yy} \\ 2\varepsilon_{xy} \end{Bmatrix} \tag{1.21}$$

For 2D plane strain problems:

$$\begin{Bmatrix} \sigma_{xx} \\ \sigma_{yy} \\ \sigma_{xy} \end{Bmatrix} = \frac{E}{(1+\upsilon)(1-2\upsilon)} \begin{bmatrix} 1-\upsilon & \upsilon & 0 \\ \upsilon & 1-\upsilon & 0 \\ 0 & 0 & \frac{1-2\upsilon}{2} \end{bmatrix} \begin{Bmatrix} \varepsilon_{xx} \\ \varepsilon_{yy} \\ 2\varepsilon_{xy} \end{Bmatrix} \tag{1.22}$$

The constitutive relation can be found in many standard books of elasticity or related topics. More general formulation are available for orthotropic and composite elastic materials.
It has to be noted that at small length scales, the use of the classical continuum mechanics or local elasticity for the analysis of nanostructures such as carbon nanotubes will lead to erroneous results. Therefore, the usage of non-classical continuum theories, including internal material and structural length scale parameters are more adapted.

2.2.2. Nonlocal elasticity modeling

Elastic high frequency waves show dispersive characteristics which are not considered in classical theory of elasticity and also ignore the long range intermolecular forces. Therefore, Eringen, proposed a nonlocal theory of micro orphic continua extending his previous works to improve the classical continuum mechanics for granular and fibrous solids.

Based on Eringen's theory, the constitutive equation for a linear homogenous nonlocal elastic body is given by the following integral equation [62,63]:

$$\sigma_{kl,k} + \rho(f_l - \ddot{u}_l) = 0 \tag{1.23}$$

$$\sigma_{kl}(x) = \int_V \alpha(|x-x'|,\tau)\sigma^c_{kl}(x')dv(x') \tag{1.24}$$

$$\sigma^c_{kl}(x') = \lambda\varepsilon_{rr}(x')\delta_{kl} + 2\mu\varepsilon_{kl}(x') \tag{1.25}$$

$$\varepsilon_{kl}(x') = \frac{1}{2}\left(\frac{du_k(x')}{dx'_l} + \frac{du_l(x')}{dx'_k}\right) \tag{1.26}$$

where σ_{kl}, $\varepsilon_{kl,}$ ρ, f_l and u_l are the stress tensor, the strain tensor, mass density, body force density and displacement vector, respectively. $\sigma^c_{kl}(x')$ and $\varepsilon_{kl}(x')$ are the classical stress and strain tensors at any point x', which is related by the Lamé constants λ and μ, and δ is Kronecker delta.. The nonlocal modulus is given by in the following kernel function:

$$\alpha = \alpha(|x-x'|,\tau),\ \tau = \frac{e_0 a}{l} \tag{1.27}$$

where e_0 is a constant appropriate to the material, a is internal characteristic length, l is length, τ is a dimensionless length scale and $|x - x'|$ is the Euclidean distance between x and x'.

It has to be noted that the stress-strain relation, obtained from this model, is given in an integral equation form and not in an algebraic form as in the local theory. Also note that the kernel function α depend on the material constants and internal characteristic length.

When the stress and strain are considered for a nanotube, the classical Hooke's law is replaced by a nonlocal stress-strain relation given in the following partial differential form:

$$(1 - \tau^2 l^2 \nabla^2)\sigma_{kl} = \sigma_{kl}^c \tag{1.28}$$

Where ∇^2 is the Laplace operator

The nonlocal elasticity theory has been used by a large number of researches to study size-effects on the mechanical response of carbon nanotubes. The considered shapes of CNT are beams, plates or cylinders. The previous tensors σ_{kl} and ε_{kl} will be specified for the considered nanostructures.

2.2.3. Beam models

For slender nanotubes, L/h > 10, the beam model combined with the nonlocal elasticity theory can be used. The main used models for slender nanotube are the Euler Bernoulli and Timoshenko nonlocal beam theories.

The performance of any CNT-based nanostructure is dependent on the mechanical properties of constituent CNTs such as their vibration frequencies, buckling loads, and deformations under different loadings. Vibrations of single and multi-walled nanotubes have been studied by many researchers using different beam theories. For multi-walled carbon nanotubes, inner and outer tubes are generally modeled as individual elastic beams interacting by van der Waals forces.

2.2.3.1. Euler-Bernoulli

Based on the Euler-Bernoulli beam theory, the displacement components along the axial x and transverse z directions are denoted by u_x and u_z respectively:

$$u_x = u(x,t) - z\frac{\partial w}{\partial x};\;\; u_y = 0;\;\; u_z = w(x,t) \tag{1.29}$$

where u and w are the middle plane (z=0) components and t is time. The axial strains are:

$$\varepsilon_{xx} = \frac{\partial u}{\partial x} - z\frac{\partial^2 w}{\partial x^2}; \tag{1.30}$$

Based on the nonlocal elasticity theory [62, 63, 68], the nonlocal stress tensors, resultant axial force N and moment M are obtained by the following differential equations:

$$\sigma_{xx} - (e_0 a)^2 \frac{\partial^2 \sigma_{xx}}{\partial x^2} = E\varepsilon_{xx}; \tag{1.31}$$

$$N_{xx} - (e_0 a)^2 \frac{\partial^2 N_{xx}}{\partial x^2} = EI\frac{\partial u}{\partial x};\;\; M_{xx} - (e_0 a)^2 \frac{\partial^2 M_{xx}}{\partial x^2} = -EI\frac{\partial^2 w}{\partial x^2} \tag{1.32}$$

where

$$(A, I) = \int_A (1, z^2) dA; N = \int_A \sigma_{xx} dA;\; M = \int_A \sigma_{xx} z dA;$$

$$m_0 = \int_A \rho dA = \rho A;\; m_2 = \int_A \rho z^2 dA = \frac{\rho A h^2}{12} \tag{1.33}$$

The differential equations of the motion of the nonlocal Euler-Bernoulli beam theory are given by:

$$\frac{\partial N_{xx}}{\partial x} + f - m_0 \frac{\partial^2 u}{\partial t^2} = 0 \tag{1.34}$$

$$\frac{\partial^2 M_{xx}}{\partial x^2} + q - \frac{\partial}{\partial x}\left(N_{xx}\frac{\partial w}{\partial x} \right) = m_0 \frac{\partial^2 u}{\partial t^2} - m_2 \left(\frac{\partial^4 w}{\partial x^2 \partial t^2} + \frac{\partial^4 w}{\partial y^2 \partial t^2} \right) \tag{1.35}$$

A large number of authors are based on this model to study the behavior of CNT. Adali [64] studied the vibrational principles for transversely vibrating multiwalled carbon nanotubes based on nonlocal Euler-Bernoulli beam model. Natsuki et al. [65], studied the resonant vibration of double-walled carbon nanotubes based on Euler–Bernoulli beam model and Winkler spring model. Yoon et al. [66] calculated frequencies and associated mode shapes of noncoaxial isolated multi-walled carbon nanotubes. Ouakkasse and Azrar [67], used integral equation formulation for flutter instabilities of Timoshenko beams under non conservative loads.

2.2.3.2. Nonlocal Timoshenko model

The displacement of the Timoshenko beam theory is given by:[61]

$$u_x = u(x,t) - z\phi(x,t);\;\; u_y = 0;\; u_z = w(x,t) \tag{1.36}$$

Where ϕ denotes the rotation of the cross section, u and w are the middle plane (z=0) components and t is time. The axial strains and the nonlocal strains are given by:

$$\varepsilon_{xx} = \frac{\partial u}{\partial x} - z\frac{\partial \phi}{\partial x};\;\; \varepsilon_{xz} = \frac{1}{2}\left(\frac{\partial w}{\partial x} + \phi\right); \tag{1.37}$$

$$\sigma_{xx} - (e_0 a)^2 \frac{\partial^2 \sigma_{xx}}{\partial x^2} = E\varepsilon_{xx};\;\; \sigma_{xz} - (e_0 a)^2 \frac{\partial^2 \sigma_{xz}}{\partial x^2} = 2G\varepsilon_{xz} \tag{1.38}$$

Based on these equations, the nonlocal resultant axial force N, moment M and shear force Q are obtained by the following differential equations.

$$N_{xx} - (e_0 a)^2 \frac{\partial^2 N_{xx}}{\partial x^2} = EI\frac{\partial u}{\partial x} \tag{1.39}$$

$$M_{xx} - (e_0 a)^2 \frac{\partial^2 M_{xx}}{\partial x^2} = EI\frac{\partial \phi}{\partial x} \tag{1.40}$$

$$Q_{xx} - (e_0 a)^2 \frac{\partial^2 Q_{xx}}{\partial x^2} = kAG\left(\frac{\partial w}{\partial x} + \phi\right) \tag{1.41}$$

in which

$$N = \int_A \sigma_{xx} dA, \quad M = \int_A z\,\sigma_{xx} dA, \qquad Q = ks\int_A \sigma_{xz} dA \tag{1.42}$$

Based on the nonlocal Timoshenko beam theory, the equations of motion are given by the following partial differential equations:

$$\frac{\partial Q}{\partial x} + q = m_0 \frac{\partial^2 w}{\partial t^2}, \tag{1.43}$$

$$\frac{\partial M}{\partial x} - Q = m_2 \frac{\partial^2 \psi}{\partial t^2}, \tag{1.44}$$

Based on these equation, the moment M and shear force Q are given by:

$$M = EI\frac{\partial \phi}{\partial x} + (e_0 a)^2\left[-q + \frac{\partial}{\partial x}\left(N^T \frac{\partial w}{\partial x}\right) + m_0 \frac{\partial^2 w}{\partial t^2} + m_2 \frac{\partial^3 \phi}{\partial x \partial t^2}\right] \tag{1.45}$$

$$Q = kAG\left(\frac{\partial w}{\partial x} + \phi\right) + (e_0 a)^2\left[-q + \frac{\partial}{\partial x}\left(N^T \frac{\partial w}{\partial x}\right) + m_0 \frac{\partial^2 w}{\partial t^2}\right] \tag{1.46}$$

A large number of authors are based on this model to study the behavior of CNT under non conservative loads Timoshenko beam theory was also applied in the free vibration analysis of multi-walled carbon nanotubes [68-71].

2.2.4. Nonlocal Plate mode

Many of the carbon based nanostructure for example nanotube Fullerenes, Nanorings are viewed as deformed graphene sheet these kinds of structure can be modeled by the so-called nonlocal plate theory. Various plate theories are used in the open literature. In this sub-section only the love Kirchhoff plate theory is used.

Based on the Love-Kirchhoff plate theory, the displacements u_x, u_y, u_z of a plate are given by:

$$u_x = u(x,y,t) - z\frac{\partial w}{\partial x};\ \ u_y = v(x,y,t) - z\frac{\partial w}{\partial y};\ \ u_z = w(x,y,t) \tag{1.47}$$

where u, v and w are the displacements in the x, y and z directions respectively.

The linear strains associated with these displacements are expressed as:

$$\varepsilon_{xx} = \frac{\partial u}{\partial x} - z\frac{\partial^2 w}{\partial x^2};\ \varepsilon_{yy} = \frac{\partial v}{\partial x} - \frac{\partial^2 w}{\partial y^2};\ \varepsilon_{xy} = \frac{1}{2}\left(\frac{\partial u}{\partial x} + \frac{\partial v}{\partial x} - 2z\frac{\partial^2 w}{\partial x \partial y}\right);$$
$$\varepsilon_{zz} = 0;\ \varepsilon_{xx} = 0;\ \varepsilon_{yz} = 0 \tag{1.48}$$

Based on the Eringen's theories the nonlocal plane stress constitutive relation for a nonlocal plate is written as:

$$\begin{Bmatrix}\sigma_{xx}\\ \sigma_{yy}\\ \sigma_{xy}\end{Bmatrix} - (e_0 a)^2\nabla^2\begin{Bmatrix}\sigma_{xx}\\ \sigma_{yy}\\ \sigma_{xy}\end{Bmatrix} = \begin{bmatrix} E/(1-\upsilon^2) & \upsilon E/(1-\upsilon^2) & 0\\ \upsilon E/(1-\upsilon^2) & E/(1-\upsilon^2) & 0\\ 0 & 0 & 2G\end{bmatrix}\begin{Bmatrix}\varepsilon_{xx}\\ \varepsilon_{yy}\\ \varepsilon_{xy}\end{Bmatrix} \tag{1.49}$$

where E, G and υ are the elastic modulus, shear modulus and Poisson's ratio respectively. Based on these equations the resultants moments are given by the following partial differential equations:

$$M_{xx} - (e_0 a)^2\nabla^2 M_{xx} = -D\left(\frac{\partial^2 w}{\partial x^2} + \upsilon\frac{\partial^2 w}{\partial y^2}\right) \tag{1.50a}$$

$$M_{yy} - (e_0 a)^2\nabla^2 M_{yy} = -D\left(\frac{\partial^2 w}{\partial y^2} + \upsilon\frac{\partial^2 w}{\partial x^2}\right) \tag{1.50b}$$

$$M_{xy} - (e_0 a)^2\nabla^2 M_{xy} = -D(1-\upsilon)\frac{\partial^2 w}{\partial x \partial y} \tag{1.50c}$$

where $D = Eh^3/12(1-\upsilon^2)$ denoted the bending rigidity of the plate.

Equations of motion are given by the following partial differential equations:

$$\frac{\partial N_{xx}}{\partial x} + \frac{\partial N_{xy}}{\partial y} - m_0 \frac{\partial^2 u}{\partial t^2} = 0 \tag{1.51a}$$

$$\frac{\partial N_{yy}}{\partial y} + \frac{\partial N_{xy}}{\partial x} - m_0 \frac{\partial^2 v}{\partial t^2} = 0 \tag{1.51b}$$

$$\frac{\partial^2 M_{xx}}{\partial y^2} + 2\frac{\partial M_{xy}}{\partial x \partial y} + \frac{\partial^2 M_{yy}}{\partial y^2} + \frac{\partial}{\partial x}\left(N_{xx} \frac{\partial w}{\partial x} \right) + \frac{\partial}{\partial y}\left(N_{yy} \frac{\partial w}{\partial y} \right) + \frac{\partial}{\partial x}\left(N_{xy} \frac{\partial w}{\partial y} \right) + \frac{\partial}{\partial y}\left(N_{xy} \frac{\partial w}{\partial x} \right)$$
$$= m_0 \frac{\partial^2 w}{\partial t^2} - m_2 \left(\frac{\partial^4 w}{\partial x^2 \partial t^2} + \frac{\partial^4 w}{\partial y^2 \partial t^2} \right) \tag{1.51c}$$

$$\text{where } m_0 = \int_{-h/2}^{h/2} \rho dz; \quad m_2 = \int_{-h/2}^{h/2} \rho h^2 dz \tag{1.52}$$

and h is the thickness of the plate.

Classical and first order shear deformable thin plate theories were reformulated by many authors. Abdoun et al [72-75] studied the forced vibration analyses of viscoelastic beams, plate and shells by an asymptotic numerical method for nanoplates. To cite only few ones, Pradhan and Phadikar [76] used the nonlocal theory of elasticity and the Navier's approach to investigate the vibration of simply supported double-layered graphene sheets. Murmu and Pradhan [77] used the nonlocal elasticity theory on the vibration of graphene sheets embedded in elastic medium. Jomehzadeh and Saidi [78] and Arash and Wang [79] are also used nonlocal elasticity to simulate graphitic sheets.

2.2.5. Shell model

Shell models are the most adopted models for nanotubes and particularly for non-slender ones, there are various shell models developed for shallow, non-shallow and deep shells. The main used shell models will is presented here.

The vibration and buckling of nanotubes using continuum nonlocal shell model theory are studied by many researchers.

For a general formulation, let us consider a circular cylindrical shell of radius R with the cylindrical coordinate system (x, z, θ), the longitudinal coordinate $x \in [0; L]$, circumferential coordinate $\theta \in [0; 2\pi]$ and radial coordinate $z \in [-h/2; +h/2]$. The displacements of an arbitrary point of coordinates (x, θ) on the mid-surface of the shell are denoted by u, v and w, in the longitudinal, circumferential and radial directions, respectively.

The governing equations of motion for a homogeneous isotropic elastic shell, using the linear three-dimensional theory of elasticity in cylindrical coordinates can be obtained. For thin shells, various models have been observed and applied for the static and dynamic analysis of shells. Based on the continuum mechanics these models can be also used to analyze the static and dynamic behavior of CNT.

For the thin shell model, the effects of transverse shear deformations are usually neglected in the simplified models. The strain components ε_x, ε_θ and $\gamma_{x\theta}$ at an arbitrary point of the shell are given by: [80]

$$\varepsilon_{xx} = \frac{\partial u}{\partial x} + \frac{1}{2}\left(\frac{\partial w}{\partial x}\right)^2 + \frac{1}{2}\beta^2 - z\frac{\partial^2 w}{\partial x^2}, \tag{1.53a}$$

$$\varepsilon_{\theta\theta} = \frac{1}{R}\left(\frac{\partial v}{\partial \theta} + w\right) + \frac{1}{2}\beta^2 + \frac{1}{2}\beta_\theta{}^2 + z\left(\frac{1}{R}\frac{\partial \beta_\theta}{\partial \theta}\right) \tag{1.53b}$$

$$\varepsilon_{x\theta} = \frac{1}{R}\frac{\partial u}{\partial \theta} + \frac{\partial v}{\partial x} - \beta_\theta\frac{\partial w}{\partial x} + z\left(\frac{\partial^2 w}{\partial x \partial \theta} + \frac{\partial \beta_\theta}{\partial x} + \frac{1}{R}\beta\right) \tag{1.53c}$$

where β_θ is the rotation in the direction perpendicular to the $R\theta - z$ plane, and β is the rotation in the direction perpendicular to the $R\theta - x$ plane.

Based on the nonlocal shell theory, the constitutive equations of the carbon nanotube are given by the following partial differential equations:

$$(1 - e_0{}^2 a^2 \nabla^2)\,\sigma_{xx} = \frac{E}{1-\upsilon^2}(\varepsilon_{xx} + \upsilon\,\varepsilon_{\theta\theta}) \tag{1.54a}$$

$$(1 - e_0{}^2 a^2 \nabla^2)\,\sigma_{\theta\theta} = \frac{E}{1-\upsilon^2}(\varepsilon_{\theta\theta} + \upsilon\,\varepsilon_{xx}) \tag{1.54b}$$

$$(1 - e_0{}^2 a^2 \nabla^2)\,\sigma_{x\theta} = \frac{E}{2(1+\upsilon)}\varepsilon_{x\theta} \tag{1.54c}$$

$$(1 - e_0{}^2 a^2 \nabla^2)\,\sigma_{x\theta} = \frac{E}{2(1+\upsilon)}\varepsilon_{\theta x} \tag{1.54d}$$

where E, υ, a and e_0 are Young's modulus, Poisson's ratio of carbon nanotubes, the internal characteristic lengths and the constant appropriate to each material respectively. ∇^2 is the Laplace operator and σ_{xx} and $\sigma_{\theta\theta}$ are respectively the normal stress in the x and the y directions and $\sigma_{x\theta}$ is the shear stress on the $x\theta$ plane of the middle surface. Associated with the middle surface deformation are the middle surface force resultants, which are given by:

$$N_{xx} = \int_{-h/2}^{h/2} \sigma_{xx} dz, \quad N_{\theta\theta} = \int_{-h/2}^{h/2} \sigma_{\theta\theta} dz, \quad N_{x\theta} = \int_{-h/2}^{h/2} \sigma_{x\theta} dz, \quad N_{\theta x} = \int_{-h/2}^{h/2} \sigma_{\theta x} dz, \tag{1.55}$$

$$M_{xx} = \int_{-h/2}^{h/2} \sigma_{xx} z\, dz, \; M_{\theta\theta} = \int_{-h/2}^{h/2} \sigma_{\theta\theta} z\, dz, \; M_{x\theta} = \int_{-h/2}^{h/2} \sigma_{x\theta} z\, dz, \; M_{\theta x} = \int_{-h/2}^{h/2} \sigma_{\theta x} z\, dz \tag{1.56}$$

The governing equations of motion of the single-walled carbon nanotubes conveying fluid are:

$$\frac{\partial N_{xx}}{\partial x} + \frac{1}{R}\frac{\partial N_{x\theta}}{\partial \theta} - \rho h \frac{\partial^2 u}{\partial t^2} = 0 \tag{1.57a}$$

$$\frac{\partial N_{x\theta}}{\partial x} + \frac{1}{R}\frac{\partial N_{\theta\theta}}{\partial \theta} + \frac{Q_\theta}{R} - \rho h \frac{\partial^2 v}{\partial t^2} = 0 \tag{1.57b}$$

$$\frac{\partial Q_x}{\partial x} + \frac{1}{R_i}\frac{\partial Q_\theta}{\partial \theta} - \frac{N_{\theta\theta}}{R_i} - \rho h \frac{\partial^2 w}{\partial t^2} = \Pi \tag{1.57c}$$

$$Q_x = \frac{\partial M_{xx}}{\partial x} + \frac{1}{R}\frac{\partial M_{\theta x}}{\partial \theta}; \tag{1.57d}$$

$$Q_\theta = \frac{\partial M_{x\theta}}{\partial x} + \frac{1}{R}\frac{\partial M_{\theta\theta}}{\partial \theta} \tag{1.57e}$$

where Π is the flow pressure, this parameters will be explicitly given in next section.

It should be noted that this model leads to nonlinear partial differential equations some simplification shell models will be reviewed here.

2.2.5.1. Love shell model

Based on Love's model the first approximation assumptions:

- The shell thickness *h* is small with respect to the radius of curvature *R* of the mid-plane.
- Strains are small.
- The transverse normal stress is small.
- The Kirchhoff–Love kinematic hypothesis, in which it is assumed that the normal to the undeformed middle surface remains straight and normal to the mid-surface after deformation, and undergoes no thickness stretching.

According to Love shell model, the strain components ε_x, ε_θ and $\varepsilon_{x\theta}$ at an arbitrary point of the shell are given by:

This model has been used in [81], for vibration of single walled CNT and multiwalled CNT. Liew and Wang [82] studied wave propagation in carbon nanotubes via elastic shell theories.

$$\varepsilon_{xx} = \frac{\partial u}{\partial x} - z\frac{\partial^2 w}{\partial x^2}, \tag{1.58a}$$

$$\varepsilon_{\theta} = \frac{1}{R}\left(\frac{\partial v}{\partial \theta} + w\right) - z\frac{\partial^2 w}{R^2 \partial \theta^2} \tag{1.58b}$$

$$\varepsilon_{x\theta} = \frac{1}{R}\frac{\partial u}{\partial \theta} + \frac{\partial v}{\partial x} - 2z\frac{\partial^2 w}{R\partial x \partial \theta} \tag{1.58c}$$

The non-coaxial linear vibration between the carbon chain are studied by Hu et al. [83]. Buckling of Carbon Nanotubes is reviewed by Hiroyuki Shima [84], Yan et al. [85] studied the small scale effect on the buckling behaviors of triple-walled carbon nanotubes (TWCNTs) with the initial axial stress under the temperature field.

2.2.5.2. Donnell shell model

For this model, the effects of transverse shear deformations are neglected, the rotations β and β_θ have the simplified form:

$$\beta_\theta = -\frac{1}{R}\frac{\partial w}{\partial \theta}; \quad \beta = 0 \tag{1.59}$$

The strain components ε_x, ε_θ and $\gamma_{x\theta}$ at an arbitrary point of the shell are given by: [86-90,142]

$$\varepsilon_{xx} = \frac{\partial u}{\partial x} + \frac{1}{2}\left(\frac{\partial w}{\partial x}\right)^2 - z\frac{\partial^2 w}{\partial x^2}, \tag{1.60a}$$

$$\varepsilon_{\theta\theta} = \frac{1}{R}\left(\frac{\partial v}{\partial \theta} + w\right) + \frac{1}{2}\left(\frac{1}{R}\frac{\partial w}{\partial \theta}\right)^2 - z\frac{1}{R^2}\frac{\partial^2 w}{\partial \theta^2} \tag{1.60b}$$

$$\varepsilon_{x\theta} = \frac{1}{R}\frac{\partial u}{\partial \theta} + \frac{\partial v}{\partial x} + \frac{1}{R}\frac{\partial w}{\partial \theta}\frac{\partial w}{\partial x} \tag{1.60c}$$

The governing dynamic equations are given by the following partial differential equations:

$$\frac{\partial^2 u}{\partial x^2} + \frac{\upsilon}{R}\frac{\partial w}{\partial x} + \frac{(1-\upsilon)}{2R}\frac{\partial^2 u}{\partial \theta^2} + \frac{(1-\upsilon)}{2R}\frac{\partial^2 v}{\partial \theta \partial x} + \mu^2\left(\frac{\partial^4 u}{\partial x^4} + \frac{\upsilon}{R}\frac{\partial^3 w}{\partial x^3}\right) + \frac{\mu^2(1+\upsilon)}{2R}\frac{\partial^4 v}{\partial \theta \partial x^3}$$
$$+ \frac{\mu^2(1-\upsilon)}{2R^2}\left(\frac{\partial^4 u}{\partial \theta^2 \partial x^2} + \frac{1}{R^2}\frac{\partial^4 u}{\partial \theta^4} + \frac{1}{R}\frac{\partial^4 v}{\partial \theta^3 \partial x}\right) - \rho_S\frac{(1-\upsilon^2)}{E}\frac{\partial^2 u}{\partial t^2} = 0, \tag{1.61a}$$

$$\frac{1}{R^2}\frac{\partial^2 v}{\partial\theta^2}+\frac{1}{R^2}\frac{\partial w}{\partial\theta}+\frac{\mu^2}{R^3}\left(\frac{1}{R}\frac{\partial^4 v}{\partial\theta^4}+\frac{1}{R}\frac{\partial^3 w}{\partial\theta^3}+\upsilon\frac{\partial^4 u}{\partial\theta^3\partial x}\right)+\frac{\mu^2(1-\upsilon)}{2}\left(\frac{\partial^4 u}{R\partial\theta\,\partial x^3}+\frac{\partial^4 v}{\partial x^4}+\right.$$
$$\left.\frac{1}{R^3}\frac{\partial^4 u}{\partial\theta^3\partial x}+\frac{1}{R^2}\frac{\partial^4 v}{\partial\theta^2\partial x^2}\right)+\frac{(1-\upsilon)}{2}\left(\frac{1}{R}\frac{\partial^2 u}{\partial\theta\,\partial x}+\frac{\partial^2 v}{\partial x^2}\right)-\frac{D(1-\upsilon^2)}{EhR^2}\left(\frac{1}{R^2}\frac{\partial^3 w}{\partial\theta^3}+\frac{1}{R^2}\frac{\partial^2 v}{\partial\theta^2}+\upsilon\frac{\partial^3 w}{\partial x^2\partial\theta}\right)$$
$$-\frac{D(1-\upsilon^2)\mu^2}{EhR^4}\left(\frac{1}{R^2}\frac{\partial^5 w}{\partial\theta^5}+\frac{1}{R^2}\frac{\partial^4 v}{\partial\theta^4}+\upsilon\frac{\partial^5 w}{\partial x^2\partial\theta^3}\right)-\frac{D(1-\upsilon^2)(1-\upsilon)}{EhR^2}\left(\frac{\partial^3 w}{\partial\theta\,\partial x^2}+\frac{1}{2}\frac{\partial^2 v}{\partial x^2}\right)+\frac{\upsilon}{R}\frac{\partial^2 u}{\partial\theta\,\partial x}$$
$$-\frac{D(1-\upsilon^2)(1-\upsilon)\mu^2}{EhR^2}\left(\frac{\partial^5 w}{\partial\theta\,\partial x^4}+\frac{1}{2}\frac{\partial^4 v}{\partial x^4}+\frac{1}{R^2}\frac{\partial^5 w}{\partial\theta^3\partial x^2}+\frac{1}{2R^2}\frac{\partial^4 v}{\partial\theta^2\partial x^2}\right)-\rho_S\frac{(1-\upsilon^2)}{E}\frac{\partial^2 v}{\partial t^2}=0, \qquad (1.61b)$$

$$-\frac{1}{R^2}\frac{\partial v}{\partial\theta}-\frac{2D(1-\upsilon^2)(1-\upsilon)}{EhR^2}\left(\frac{\partial^4 w}{\partial x^2\partial\theta^2}+\frac{1}{2}\frac{\partial^3 v}{\partial x^2\partial\theta}\right)-\frac{2D(1-\upsilon^2)(1-\upsilon)\mu^2}{EhR^2}\left(\frac{\partial^6 w}{\partial x^4\partial\theta^2}+\frac{1}{2}\frac{\partial^5 v}{\partial x^4\partial\theta}+\frac{1}{R^2}\frac{\partial^6 w}{\partial x^2\partial\theta^4}\right.$$
$$\left.+\frac{1}{2R^2}\frac{\partial^5 v_i}{\partial x^2\partial\theta^3}\right)-\frac{\upsilon}{R}\frac{\partial u}{\partial x}-\frac{D(1-\upsilon^2)\mu^2}{EhR^2}\left(\frac{1}{R^4}\frac{\partial^6 w}{\partial\theta^6}+\frac{1}{R^4}\frac{\partial^5 v}{\partial\theta^5}+\frac{\upsilon}{R^2}\frac{\partial^6 w}{\partial\theta^4\,\partial x^2}\right)-\frac{w}{R^2}-\frac{D(1-\upsilon^2)\mu^2}{Eh}\left(\frac{\partial^6 w}{\partial x^6}\right.$$
$$\left.+\frac{\upsilon}{R^2}\frac{\partial^5 v}{\partial\theta\,\partial x^4}+\frac{\upsilon}{R^2}\frac{\partial^6 w}{\partial x^4\partial\theta^2}\right)-\frac{D(1-\upsilon^2)}{EhR^2}\left(\frac{1}{R^2}\frac{\partial^4 w}{\partial\theta^4}+\frac{1}{R^2}\frac{\partial^3 v}{\partial\theta^3}+\upsilon\frac{\partial^4 w}{\partial\theta^2\partial x^2}\right)-\frac{\mu^2}{R^3}\left(\frac{1}{R}\frac{\partial^3 v}{\partial\theta^3}+\frac{1}{R}\frac{\partial^2 w}{\partial\theta^2}+\upsilon\frac{\partial^3 u}{\partial\theta^2\partial x}\right)$$
$$-\frac{D(1-\upsilon^2)}{Eh}\left(\frac{\partial^4 w}{\partial x^4}+\frac{\upsilon}{R^2}\frac{\partial^3 v}{\partial\theta\,\partial x^2}+\frac{\upsilon}{R^2}\frac{\partial^4 w}{\partial x^2\partial\theta^2}\right)-\rho_S\frac{(1-\upsilon^2)}{E}\frac{\partial^2 w}{\partial t^2}=\frac{(1-\upsilon^2)\Pi_1}{Eh}, \qquad (1.61c)$$

Simplified Donnell's shell theory was used to obtain explicit formulas for the radially dominated natural frequencies and mode shapes of double and triple-walled carbon nanotubes with various radii and number of tubes [86] and fluid-filled multi-walled carbon nanotubes by Yan et al. [87]. Donnell's shell theory was also used by Sun and Liu [88, 89] for the vibration of multi-walled carbon nanotubes subject to axial and pressure loadings. The small size on dispersion characteristics of wave in carbon nanotubes are studied by Xie et al. [90].

2.2.5.3. Sanders shell model

In the Sanders shell theory, these two rotations have the exact and complete form [91]

$$\beta_\theta=\frac{1}{R}\left(v-\frac{\partial w}{\partial\theta}\right);\quad \beta=\frac{1}{2}\left(\frac{\partial v}{\partial x}-\frac{\partial w}{R\partial\theta}\right) \qquad (1.62)$$

The strain components ε_x, ε_θ and $\gamma_{x\theta}$ at an arbitrary point of the shell are given by:

$$\varepsilon_{xx}=\frac{\partial u}{\partial x}+\frac{1}{2}\left(\frac{\partial w}{\partial x}\right)^2+\frac{1}{8}\left(\frac{\partial v}{\partial x}-\frac{\partial w}{R\partial\theta}\right)^2-z\frac{\partial^2 w}{\partial x^2}, \qquad (1.63a)$$

$$\varepsilon_{\theta\theta} = \frac{1}{R}\left(\frac{\partial v}{\partial \theta} + w\right) + \frac{1}{8}\left(\frac{\partial v}{\partial x} - \frac{\partial w}{R\partial \theta}\right)^2 + \frac{1}{2R^2}\left(v - \frac{\partial w}{\partial \theta}\right)^2 + z\frac{1}{R^2}\frac{\partial}{\partial \theta}\left(v - \frac{\partial w}{\partial \theta}\right) \quad (1.63b)$$

$$\varepsilon_{x\theta} = \frac{1}{R}\frac{\partial u}{\partial \theta} + \frac{\partial v}{\partial x} - \frac{1}{R}\left(v - \frac{\partial w}{\partial \theta}\right)\frac{\partial w}{\partial x} + z\left(\frac{\partial^2 w}{\partial x \partial \theta} + \frac{\partial \beta_\theta}{\partial x} + \frac{1}{2R}\left(\frac{\partial v}{\partial x} - \frac{\partial w}{R\partial \theta}\right)\right) \quad (1.63c)$$

A linearized form of this model has been used in [91] for the buckling behavior of single walled CNT. Silvestre et al. [91], Donnell and Sanders shell models are used to study the buckling of single-walled carbon nanotubes.

2.2.5.4. Flugge's shell model

For the Flugge's shell theory, the constitutive relation between stresses and strains for a homogeneous and isotropic material can be expressed by Hooke's law by: [83, 85]

$$\left(1-(e_0 a)^2\nabla^2\right)\sigma_{xx} = \frac{E}{1-\upsilon^2}(\varepsilon_{xx} + \upsilon\,\varepsilon_{\theta\theta}) \quad (1.64a)$$

$$\left(1-(e_0 a)^2\nabla^2\right)\sigma_{\theta\theta} = \frac{E}{1-\upsilon^2}(\varepsilon_{\theta\theta} + \upsilon\,\varepsilon_{xx}) \quad (1.64b)$$

$$\left(1-(e_0 a)^2\nabla^2\right)\sigma_{\theta x} = \frac{E}{2(1+\upsilon)}\varepsilon_{x\theta} \quad (1.64c)$$

$$\left(1-(e_0 a)^2\nabla^2\right)\sigma_{x\theta} = \frac{E}{2(1+\upsilon)}\varepsilon_{x\theta} \quad (1.64d)$$

In this case the resultant force can be written as :

$$N_{xx} = \int_{-h/2}^{h/2}\sigma_{xx}\left(1+\frac{z}{R}\right)dz, \quad N_{\theta\theta} = \int_{-h/2}^{h/2}\sigma_{\theta\theta}dz, \quad N_{x\theta} = \int_{-h/2}^{h/2}\sigma_{x\theta}\left(1+\frac{z}{R}\right)dz, \quad (1.65a)$$

$$M_{xx} = -\int_{-h/2}^{h/2}\sigma_{xx}\left(1+\frac{z}{R}\right)z\,dz;\; M_{\theta\theta} = -\int_{-h/2}^{h/2}\sigma_{\theta\theta}z\,dz;\; M_{x\theta} = -\int_{-h/2}^{h/2}\sigma_{x\theta}\left(1+\frac{z}{R}\right)z\,dz;$$

$$M_{\theta x} = -\int_{-h/2}^{h/2}\sigma_{\theta x}z\,dz \quad (1.65b)$$

The vibrations and buckling of nanotubes using continuum nonlocal shell theory are studied by many researchers Wang et al [92] used Flügge's shell theory to calculate frequencies and associated modes of multi-walled carbon nanotubes of different innermost radii. The wave propagation of single and multiwalled CNT has been investigated by Wang and Varadan [93] The presented shell models are adopted by various authors for static and dynamic behaviors of single walled and multi walled CNT. Various numerical methods are developed based on these models. A review of the more used ones is given bellow.

3. Used numerical methods

Based on the previous continuum models, various numerical methods have been used of the analysis of CNT. A large variety of research works are now available in the open literature on the buckling, vibration, thermoelastic behaviors of CNT as well as in fluid–CNT interaction and magnetic-CNT interactions. The most used numerical methods are cited here.

3.1 Finite difference method

The finite difference method has been widely used for vibration and buckling analysis of various structures. Recently Ansari et al. [94,95] studied the sixth-order compact finite difference method for free vibration analysis of Euler-Bernoulli beams. Shu et al. [96], proposed the free vibration analysis of plates. Karamooz Ravari et al. [97], used the finite difference method to analyze the buckling of rectangular nanoplates.

3.2 Finite Element method

Finite element method (FEM) is a powerful numerical method for solving structural problems in 1-D, 2-D and 3-D domains. Many industrial codes such as ABAQUS, ANSYS, and NASTRON etc are elaborated and well used for academic and industrial problems.

A finite element model based on nonlocal elasticity is also presented by Ansari et al. [98]. Vibrations of single and multi-walled carbon nanotubes were studied by many others researchers using the frame finite element models in the molecular structural mechanics approach [99, 100]. Pisano et al. [101] used the finite element method in 2D nonlocal elastic problems and in 2D nonhomogeneous nonlocal elastic problems by Aurora et al. [102]. The free vibration analysis of single walled and multiwalled carbon nanotubes are studied in [103-105].

3.3 Meshless method

Meshless method is in a large expansion and under adaptation to many academic and engineering problems. There are various types of Meshless methods that are elaborated for numerical solutions of differential and partial differential equations. This method is used by many authors such as in hydrodynamics [106], Biomechanics [107,108]. This method is reviewed by Nguyen et al [109]. Kiani [110] used this method to solve the flexural vibrations of double-walled carbon nanotubes. Ansari and Arjangpay [111] using the meshless local Petrov–Galerkin method for studying the vibration and buckling characteristics of single-walled carbon nanotubes

3.4 Difference quadrature method

The Differential Quadrature method (DQM) is a numerical technique for solving differential, and partial differential equations. It is an efficient method for rapid solution in one or multiple dimensions. Unlike conventional methods such as Finite Difference and Finite Element methods, the DQM requires less grid points and then less computer time and storage to obtain acceptable accuracy. Successful applications of the DQM in many engineering problems have been demonstrated by numerous researches (see for instance [112,113]). The DQM, akin to the conventional integral quadrature method, approximates the derivative of a function at any location by a linear summation of all the functional values along a mesh line. The key procedure in the DQ application lies in a determination of the weighting coefficients [112].

As this numerical method will be used for numerical solutions in this thesis, some mathematical developments are given here. This method has some numerical advantages related to the previous methods. These advantages motivate our choice of this method for numerical solutions.

The continuous solution is approximated by functional values at discrete points. The following Chebyshev-Gauss-Lobatto quadrature points are usually used.

$$y_i = \frac{1}{2}\left[1-\cos\left(\frac{i-1}{N-1}\pi\right)\right] \text{ for } i = 1,2,3,.....,n \tag{1.66}$$

where $y_i = \frac{x_i}{L}$ and n is the number of grid points in the domain [0, 1].

For a function $f(y)$, DQ approximation of the mth order derivative at the ith point is given by:

$$f(y) = \sum_{j=1}^{n} l_j(y) f(y_j) \tag{1.67-a}$$

$$\frac{d^m}{dy^m}\begin{Bmatrix} f(y_1) \\ f(y_2) \\ \vdots \\ f(y_n) \end{Bmatrix} = H_{ij}^m \begin{Bmatrix} f(y_1) \\ f(y_2) \\ \vdots \\ f(y_n) \end{Bmatrix}, \; i, j = 1,2,...,n \tag{1.67-b}$$

in which $l_j(y)$ are the Lagrange interpolation polynomials and H_{ij}^m represent the weighting coefficients given by [112-113].

$$f(y_i) = \frac{G(y)}{(y - y_i)G_1(y_i)}, \ for\, i = 1,2,...,n \qquad (1.67-c)$$

$$G(y) = \prod_{j=1}^{n}(y - y_i) \qquad (1.67-d)$$

$$G_1(y_i) = \prod_{j=1,\, j\neq i}^{n}(y - y_i), \ for\ i, j = 1,2,...,n \qquad (1.67-e)$$

$$H_{ij}^1 = \frac{G_1(y_i)}{(y_i - y_j)G_1(y_i)} \ \ for\ i, j = 1,2,...,n;\ i \neq j \qquad (1.67-f)$$

$$H_{ii}^1 = -\sum_{\substack{j=1 \\ j\neq i}}^{n} H_{ij}^1 \qquad (1.67-g)$$

The higher derivative, mth, can be calculated as:

$$H_{ij}^m = m\left(H_{ij}^1 H_{ii}^{m-1} - \frac{H_{ij}^{m-1}}{x_i - x_j} \right) \qquad for\, i = 1,2,...,n,\ j \neq i \qquad (1.67-h)$$

$$H_{ii}^m = -\sum_{\substack{j=1 \\ j\neq i}}^{n} H_{ij}^m \qquad (1.67-i)$$

The differential quadrature method was first developed by Shu [112,113], the authors used this method to solve the linear and nonlinear problems. Krowiak [114] studied analyze the vibration of plates. Janghorban and Zare [115] investigated the free vibration analysis of functionally graded single walled carbon nanotubes with variable thickness by differential quadrature method. Yas and Samadi [116] studied free vibration and buckling of nanocomposite Timoshenko beams reinforced by SWCNTs resting on an elastic foundation. Nonlinear free vibration analysis of single and multi-walled carbon nanotubes using nonlocal Timoshenko beam theory are used in [117,118]. Arani et al. [119] studied nonlinear viscose flow induced nonlocal vibration and instability of embedded DWCNC via DQM.

Based on the presented continuum models and numerical methods, buckling, vibrations, parametric instability as well as many order static and dynamic behaviors of CNT have been studied. The focus is done here on the main CNT behaviors, studied in this thesis.

4. Fluid conveying carbon nanotubes

Carbon nanotubes (CNT) conveying fluid have become ones of the most important structures in nanotechnology. They may be used at micro or nano-levels for fluid storage, fluid transport, drug delivery, micro-resonator, molecular reactors as well as for many nano-fluidic

device applications. In such applications, the dynamic characteristics, such as natural frequencies, eigenmodes, stability, critical flow velocity and parametric instability zones are of considerable interest.

During the last years, a significant amount of research has been elaborated for the dynamic behavior of CNT.

A reviews paper on pipes conveying fluid and the vibration of CNT and their composites has been published by Ibrahim [120, 121] and Gibson et al. [122]. Paidoussis [123] studied the vibration and instability of pipe conveying fluid. Amabili [124] studied the nonlinear vibrations and stability of shells and plates. The flexural vibrations of microscale pipes conveying fluid by considering the size effects of micro-flow and micro-structure is studied by Wang et al. [125]. The nonlocal, viscosity and some system parameters effects on the stability of CNT conveying pulsation fluid are studied by Liang and Su [126].

As the fluid conveying CNT behaviors is mainly studied on the beam and shell theories, the considered fluid-structure interaction force models are reviewed here.

4.1 Fluid-beams interaction forces

The internal fluid is approximated as a flow, all points of the fluid having a velocity V relative to the beam. This is a reasonable approximation for a fully developed turbulent flow profile. The inertia force exerted by the internal flow on the pipe, can be written as: [123]

$$f_{\text{int}} = -\rho_f \left.\frac{\partial^2 w}{\partial^2 t}\right|_{x=V_0 t} \tag{1.68}$$

where ρ_f is the fluid mass per unit length, V_0 is the flow velocity, w is transverse displacement. The total acceleration of the fluid mass can be decomposed into a local, Coriolis and centrifugal acceleration:

$$\begin{aligned}
\rho_f \left.\frac{\partial^2 w}{\partial t^2}\right|_{x=V_0 t} &= \rho_f \left\{ \frac{d}{dt}\left(\frac{\partial w}{\partial t} + \frac{\partial w}{\partial x}\frac{dx}{dt} \right)\Bigg|_{x=Vt} \right\} \\
&= \rho_f \left\{ \frac{d}{dt}\left(\frac{\partial w}{\partial t} + V\frac{\partial w}{\partial x} \right)\Bigg|_{x=Vt} \right\} \\
&= \rho_f \left\{ \frac{\partial^2 w}{\partial t^2} + 2V\frac{\partial^2 w}{\partial t \partial x} + V^2\frac{\partial^2 w}{\partial x^2} \right\}
\end{aligned} \tag{1.69}$$

This fluid-Beam interaction force model has been used by many authors for tubes conveying fluid instability.

4.2 Fluid-shell interaction forces

Shells coupled to the flowing fluids are widely used in engineering. The fluid is considered as incompressible and irrotational. The irrotationality property is the condition for the existence of a scalar potential function ψ . The potential ψ consists of two components: one due to the mean flow associated with the undisturbed flow velocity V in the axial direction, and the unsteady component ψ associated with the functionally graded shell motion. The potential ψ may be written as [124]

$$\psi = -Vx + \varphi \tag{1.70}$$

The potential of the unsteady component φ satisfies the Laplace equation as follows

$$\nabla^2\varphi = \frac{\partial^2\varphi}{\partial x^2} + \frac{\partial^2\varphi}{\partial r^2} + \frac{1}{r}\frac{\partial\varphi}{\partial r} + \frac{1}{r^2}\frac{\partial^2\varphi}{\partial\theta^2} = 0, \tag{1.71}$$

The perturbation pressure exerted on the wall of functionally graded shell is expressed as

$$P = \rho_f\left(\frac{\partial\varphi}{\partial t} + V\frac{\partial\varphi}{\partial x}\right)_{r=R} \tag{1.72}$$

The interface condition between fluid and shell wall is written as

$$\left(\frac{\partial\varphi}{\partial r}\right)_{r=R} = \left(\frac{\partial w}{\partial t} + V\frac{\partial w}{\partial x}\right) \tag{1.73}$$

The potential φ is expressed as

$$\varphi = f(t)\tilde{\varphi}(x)\tilde{\psi}(r)\sin(n\theta) \tag{1.74}$$

where n represents the number of circumferential waves. Substituting Eq. (1.74) into Eq. (1.71) gives

$$\frac{\partial^2\tilde{\varphi}(x)}{\partial x^2}\tilde{\psi}(r) + \frac{\partial^2\tilde{\psi}(r)}{\partial r^2}\tilde{\varphi}(x) + \frac{1}{r}\frac{\partial\tilde{\psi}(r)}{\partial r}\tilde{\varphi}(x) - \frac{n^2}{r^2}\tilde{\psi}(r)\tilde{\varphi}(x) = 0 \tag{1.75}$$

which can be separated into the following Bessel and harmonic differential equations:

$$\begin{cases} \dfrac{\partial^2\tilde{\psi}(r)}{\partial r^2} + \dfrac{1}{r}\dfrac{\partial\tilde{\psi}(r)}{\partial r} - \left(\dfrac{n^2}{r^2} + k^2\right)\tilde{\psi}(r) = 0 \\ \dfrac{\partial^2\tilde{\varphi}(x)}{\partial x^2} + k^2\tilde{\varphi}(x) = 0 \end{cases} \tag{1.76}$$

Utilizing the condition that the potential φ must be finite at $r = 0$, and the interface conditions a particular solution of Eq. (1.76) is given by

$$\tilde{\psi}(r) = cI_n(\lambda_m r); \qquad \lambda_m = \frac{m\pi}{L}; \tag{1.77}$$

where $\lambda_m = m\pi/L$, m represents the number of axial half waves and c is a constant, I_n is the modified Bessel function of the first kind of order n, which is expressed as

$$I_n(\lambda_m r) = \sum_{k=0}^{+\infty} \frac{1}{k!\Gamma(n+k+1)} \left(\frac{r}{2}\right)^{2k+n} \tag{1.78}$$

Utilizing Eqs. (1.73), (1.74) and (1.78), the potential φ is expressed as

$$\varphi = \frac{I_n(kr)}{I_n^{'}(kr)_{r=R}} \left(\frac{\partial w}{\partial t} + V\frac{\partial w}{\partial x}\right) \tag{1.79}$$

Substituting Eq. (1.79) into Eq. (1.73), the following shell-fluid interaction force is obtained.

$$\Pi = \rho_f \frac{I_n(k\,R)}{k\,I_n'(k\,R)} \left\{ \frac{\partial^2 w}{\partial t^2} + 2V\frac{\partial^2 w}{\partial x \partial t} + V^2 \frac{\partial^2 w}{\partial x^2} \right\}, \tag{1.80}$$

5. Van der Waals interaction

As the van der Waals interaction (vdW) is the main interaction force when considering multiwalled carbon nanotube an emphasis on this interaction force is presented in this subsection. The Van der Waals energy, due to the interatomic interaction, can be described by Lennard-Jones's pair potential V_{IJ} [127]

$$\mathrm{V_{ij}}(\bar{\mathrm{d}}) = 4\varepsilon\left[\left(\frac{\sigma}{\bar{\mathrm{d}}}\right)^{12} - \left(\frac{\sigma}{\bar{\mathrm{d}}}\right)^{6}\right] \tag{1.81}$$

where, $\bar{\mathrm{d}}$ is the distance between interacting atoms.

The vdW force F is obtained by taking the derivative of the Lennard-Jones pair potential, i.e.

$$\mathrm{F}(\bar{\mathrm{d}}) = -\frac{\mathrm{dV_{ij}}(\bar{\mathrm{d}})}{\mathrm{d}\bar{\mathrm{d}}} = \frac{24\varepsilon}{\sigma}\left[2\left(\frac{\sigma}{\bar{\mathrm{d}}}\right)^{13} - \left(\frac{\sigma}{\bar{\mathrm{d}}}\right)^{7}\right] \tag{1.82}$$

The Lennard-Jones model provides a smooth transition between (a) the attractive force of an approaching pair of atoms from a certain distance and (b) the repulsive force when the distance of the interacting atoms becomes less than the sum of their contact radii.

It should be noted that we are only interested in the infinitesimal deformation of CNT. Thus, the vdW force can be estimated by the Taylor expansion to the first-order around the equilibrium position, i.e. [128]

$$F(\bar{d}) = F(\bar{d}) + -\frac{dF(\bar{d}_0)}{d\bar{d}}\left(\bar{d} - \bar{d}_0\right)$$
$$= \frac{24\varepsilon}{\sigma}\left[2\left(\frac{\sigma}{\bar{d}_0}\right)^{13} - \left(\frac{\sigma}{\bar{d}_0}\right)^{7}\right] - \frac{24\varepsilon}{\sigma^2}\left[26\left(\frac{\sigma}{\bar{d}_0}\right)^{14} - 7\left(\frac{\sigma}{\bar{d}_0}\right)^{8}\right]\left(\bar{d} - \bar{d}_0\right) \quad (1.83)$$

where $\bar{d}_0$ is the initial distance between atoms of different tubes.

The vdW force exerted on any atom on a tube can be estimated by summing all forces between the atom and all atoms on the other tube.

To simplify the calculations, we consider the CNT as a continuum cylindrical shell and note that each carbon atom corresponds to the area of $9a^2/4\sqrt{3}$ [129]. Thus, the integration of Eq. (1.89) over the entire CNT leads to an analytical representation for the initial pressure p_{ij} caused by the vdW interaction: [128]

$$p_{ij} = \left(\frac{4\sqrt{3}}{9a^2}\right)^2 \frac{24\varepsilon}{\sigma}\int_{-\pi}^{\pi}\int_{-L/2}^{L/2}\left[2\left(\frac{\sigma}{\bar{d}_0}\right)^{13} - \left(\frac{\sigma}{\bar{d}_0}\right)^{7}\right]R_j\,dx\,d\theta$$
$$= \left[\frac{2048\varepsilon\sigma^{12}}{9a^4}\sum_{k=0}^{5}\frac{(-1)^k}{2k+1}\binom{5}{k}E_{ij}^{12} - \frac{1024\varepsilon\sigma^6}{9a^4}\sum_{k=0}^{2}\frac{(-1)^k}{2k+1}\binom{2}{k}E_{ij}^{6}\right]R_i \quad (1.84)$$

where a = 1.42 A ° is the C–C bond length, R_j is the radius of the j^{th} layer, and the subscripts i and j denote the ith and jth layers, respectively. The pressure increment due to the buckling jump is given by:

$$p_{ij} = -\left(\frac{4\sqrt{3}}{9a^2}\right)^2 \frac{24\varepsilon}{\sigma^2}\int_{-\pi}^{\pi}\int_{-L/2}^{L/2}\left[26\left(\frac{\sigma}{\bar{d}_0}\right)^{14} - 7\left(\frac{\sigma}{\bar{d}_0}\right)^{8}\right]\left(\bar{d} - \bar{d}_0\right)R_j\,dx\,d\theta$$
$$= \left[\frac{1001\pi\varepsilon\sigma^{12}}{3a^4}E_{ij}^{13} - \frac{1120\pi\varepsilon\sigma^6}{9a^4}E_{ij}^{7}\right]R_j(w_i - w_j) \quad (1.85)$$

where E_{ij}^{6}, E_{ij}^{7}, E_{ij}^{12} and E_{ij}^{13} are the elliptical integrals defined by:

$$E_{ij}^{m} = (R_i + R_j)^{-m}\int_0^{\pi/2}\frac{d\theta}{[1 - K_{ij}\cos(\theta)]^{m/2}} \quad (1.86)$$

where m is an integer and

$$K_{ij} = \frac{4R_iR_j}{(R_i + R_j)^2} \quad (1.87)$$

The infinitesimal deflection between two layers, the net pressure due to the Van der Waals interaction can be expressed as:

$$R_i(x,\theta) = -\sum_{j=1}^{i-1} p_{ij} + \sum_{j=i+1}^{N} p_{ij} + \sum_{j=1}^{N} \Delta p_{ij}(x,\theta) \tag{1.88}$$

where p_{ij} is the initial uniform vdW pressure contribution to the ith layer from the jth layer prior to buckling, N is the total number of layers of the multi-walled CNT, and Δp_{ij} is the pressure increment that is exerted on the ith layer from the jth layer, N is the total number of layers of the multi-walled CNT. As only infinitesimal buckling is considered, Δp_{ij} is assumed to be linearly proportional to the buckling deflection between two layers, i.e.

$$\Delta p_i(x,\theta) = \sum_{j=!}^{N} c_{ij}(w_i - w_j) = w_i \sum_{j=1}^{N} c_{ij} - \sum_{j=1}^{N} c_{ij}\, w_j \tag{1.89}$$

Comparing Eqs. (1.85) and (1.89) we have:

$$c_{ij} = \left[\frac{1001\pi\varepsilon\sigma^{12}}{3a^4}\, E_{ij}^{13} - \frac{1120\pi\varepsilon\sigma^{6}}{9a^4}\, E_{ij}^{7} \right] R_j \tag{1.90}$$

Eq. (1.90) furnishes the mathematical expression for the interaction coefficient cij that models the vdW forces in a multi-walled CNT, where each tube has been treated as an individual cylindrical shell continuum. This refined vdW model captures the effects of all layers, not just those between two adjacent layers and allows analyzing the multi walled carbon nanotubes.

6. Mathematical modeling of static behavior of CNT

6.1 Buckling of beam's CNT

The buckling instability can be resulted from various types of loads such as compressive load, thermal load. Elfelsoufi and Azrar [130,131], studied buckling, flutter and vibration analyses of beams by integral equation formulations. Sudak studied the column buckling of MWCNTs using nonlocal continuum mechanics [132]. Other researchers have used nonlocal elasticity to study CNT vibrations [133,134] and the propagation of waves in CNTs [135-137].

6.1.1 Axial compressive load

Based on the nonlocal Euler Bernoulli beam theory, the differential equation governing the transverse buckling behavior is:

$$\frac{d^2}{dx^2}\left(EI \frac{d^2 w}{dx^2} \right) + \frac{d}{dx}\left(\tilde{N} \frac{dw}{dx} \right) - (e_0 a)^2 \frac{d^2}{dx^2}\left\{ \frac{d}{dx}\left(\tilde{N} \frac{dw}{dx} \right) \right\} = 0 \tag{1.91}$$

Based on the nonlocal Timoshenko beam theory, the differential system governing the transverse buckling behavior is:

$$\frac{d}{dx}\left\{kAG\left(\frac{dw}{dx}+\phi\right)\right\}-\frac{d}{dx}\left(\tilde{N}\frac{dw}{dx}\right)-(e_0a)^2\frac{d^2}{dx^2}\left\{-\frac{d}{dx}\left(\tilde{N}\frac{dw}{dx}\right)\right\}=0 \tag{1.92}$$

$$\frac{d}{dx}\left(EI\frac{d\phi}{dx}\right)-kAG\left(\frac{dw}{dx}+\phi\right)=0 \tag{1.93}$$

where $\tilde{N}$ is the axial force.

6.2 **Buckling of cylindrical CNT.**

The buckling and post buckling can be used by many authors for plate and shells. To cite only few ones, Azrar et al [138] used an asymptotic-numerical method to compute the post buckling behavior of elastic plates and shells. For carbon nanotube, Salehi-Khojin and Jalili [139] proposed buckling of boron nitride nanotube reinforced piezoelectric polymeric composites subject to combined electro-thermo-mechanical loadings.

Based on the Donnell shell model, the partial differential equation convening the buckling behavior of cylindrical shell is: [85]

$$\frac{\partial}{\partial x}\left(\frac{\partial M_{xx}}{\partial x}+\frac{1}{R}\frac{\partial M_{\theta x}}{\partial \theta}\right)+\frac{1}{R}\frac{\partial}{\partial \theta}\left(\frac{\partial M_{x\theta}}{\partial x}+\frac{1}{R}\frac{\partial M_{\theta\theta}}{\partial \theta}\right)-\frac{N_{\theta\theta}}{R}-\tilde{N}\frac{\partial^2 w}{\partial x^2}=0 \tag{1.94}$$

6.2.1 **Thermal loads**

The buckling behavior can also be resulted from thermal load. The constitutive equations of the thermal loads using nonlocal shell theory are given by: [85]

$$\sigma_{xx}-(e_0a)^2\frac{\partial^2\sigma_{xx}}{\partial x^2}=\frac{E}{1-\upsilon^2}(\varepsilon_{xx}+\upsilon\,\varepsilon_{\theta\theta})-\frac{E\alpha_1}{1-\upsilon}T \tag{1.95a}$$

$$\sigma_{\theta\theta}-(e_0a)^2\frac{\partial^2\sigma_{\theta\theta}}{R^2\partial\theta^2}=\frac{E}{1-\upsilon^2}(\varepsilon_{\theta\theta}+\upsilon\varepsilon_{xx})-\frac{E\alpha_2}{1-\upsilon}T \tag{1.95b}$$

$$\sigma_{x\theta}-(e_0a)^2\left(\frac{\partial^2\sigma_{x\theta}}{\partial x^2}+\frac{\partial^2\sigma_{x\theta}}{R^2\partial\theta^2}\right)=\frac{E}{1-\upsilon}\varepsilon_{x\theta} \tag{1.95c}$$

$$N_{xx}-(e_0a)^2\frac{\partial^2 N_{xx}}{\partial x^2}=K(\varepsilon_{xx}+\upsilon\varepsilon_{\theta\theta})-\frac{Eh\alpha_1}{1-\upsilon}T \tag{1.96a}$$

$$N_{\theta\theta}-(e_0a)^2\frac{\partial^2 N_{\theta\theta}}{R^2\partial\theta^2}=K(\varepsilon_{\theta\theta}+\upsilon\,\varepsilon_{xx})-\frac{Eh\alpha_2}{1-\upsilon}T \tag{1.96b}$$

$$N_{x\theta}-(e_0a)^2\left(\frac{\partial^2 N_{x\theta}}{\partial x^2}+\frac{\partial^2 N_{x\theta}}{R^2\partial\theta^2}\right)=K(1-\upsilon)\varepsilon_{x\theta} \tag{1.96c}$$

$$M_{xx}-(e_0a)^2\frac{\partial^2 M_{xx}}{\partial x^2}=-D\left(\frac{\partial^2 w}{\partial x^2}+\frac{\upsilon}{R^2}\frac{\partial^2 w}{\partial \theta^2}\right)-\frac{Eh\alpha_1}{1-\upsilon}T\int_{-\frac{h}{2}}^{\frac{h}{2}}Tzdz \tag{1.97a}$$

$$M_{\theta\theta}-(e_0a)^2\frac{\partial^2 M_{\theta\theta}}{R^2\partial \theta^2}=-D\left(\frac{\partial^2 w}{R^2\partial \theta^2}+\upsilon\frac{\partial^2 w}{\partial x^2}\right)-\frac{Eh\alpha_2}{1-\upsilon}T\int_{-\frac{h}{2}}^{\frac{h}{2}}Tzdz \tag{1.97b}$$

$$M_{x\theta}-(e_0a)^2\left(\frac{\partial^2 M_{x\theta}}{\partial x^2}+\frac{\partial^2 M_{x\theta}}{R^2\partial \theta^2}\right)=-D(1-\upsilon)\frac{\partial^2 w}{R\partial x\partial \theta} \tag{1.97c}$$

where T is the temperature field applied to the shell. The constitutive equations of the thermal buckling behavior are given by:

$$Q_x=\frac{\partial M_{xx}}{\partial x}+\frac{1}{R}\frac{\partial M_{x\theta}}{\partial \theta}; \tag{1.98a}$$

$$Q_\theta=\frac{\partial M_{x\theta}}{\partial x}+\frac{1}{R}\frac{\partial M_{\theta\theta}}{\partial \theta} \tag{1.98b}$$

$$\frac{\partial Q_x}{\partial x}+\frac{1}{R}\frac{\partial Q_\theta}{\partial \theta}+\frac{N_{\theta M}+N_{\theta T}}{R^2}\frac{\partial^2 w}{\partial \theta^2}+\frac{N_{\theta M}+N_{\theta T}}{R}+\frac{\partial^2 f}{R\partial x^2}+\left(N_{xM}+N_{xT}\right)\frac{\partial^2 w}{\partial x^2}=0 \tag{1.98c}$$

Analytical and numerical methods can be used to solve the previous equations analyzing the buckling behaviors of CNT. Buckling loads and associated buckling modes can be obtained.

7. Vibration

The development of electromechanical devices and systems at the micrometer and nanometer scale are increases. These developments have led to new families of devices and sensors that require consideration electrostatic and viscous damping, viscous fluid damping, van der Waals attractive forces, and the size and location of masses, such as vibrating cantilever beam mass sensors, piezoelectric beam energy harvesters, carbon nanotube oscillators, and vibrating cantilever beam sensors for atomic force microscopes. Thus, with the introduction of these sub millimeter systems, the range of applications and factors has been increased resulting in a renewed interest in the field of the vibrations of nano and micro systems.

Modeling and analyzing of nanosystems are ones of the main goals of this thesis. The most used models for vibration analysis to CNT are beam models and shell models.

7.1 Vibration of CNT-Beam

Based on the nonlocal Euler Bernoulli beam theory, the partial differential equation of the transverse vibration behavior under axial load $\tilde{N}$ is: [69]

$$\frac{\partial^2}{\partial x^2}\left(EI\frac{\partial^2 w}{\partial x^2} \right)+\frac{\partial}{\partial x}\left(\tilde{N}\frac{\partial w}{\partial x} \right)-(e_0 a)^2\frac{\partial^2}{\partial x^2}\left\{ \frac{\partial}{\partial x}\left(\tilde{N}\frac{\partial w}{\partial x} \right)+m_0\frac{\partial^2 w}{\partial t^2} \right\}+m_0\frac{\partial^2 w}{\partial t^2}=0 \qquad (1.99)$$

Based on the nonlocal Timoshenko beam theory, the partial differential system governing the natural vibration of CNT under axial load $\tilde{N}$ are:

$$\frac{\partial}{\partial x}\left\{ kAG\left(\frac{\partial w}{\partial x}+\phi \right) \right\}-\frac{\partial}{\partial x}\left(\tilde{N}\frac{\partial w}{\partial x} \right)-(e_0 a)^2\frac{\partial^2}{\partial x^2}\left\{ -\frac{\partial}{\partial x}\left(\tilde{N}\frac{\partial w}{\partial x} \right) \right\}+m_0\left(\frac{\partial^2 w}{\partial t^2}-(e_0 a)^2\frac{\partial^4 w}{\partial x^2\partial t^2} \right)=0 \qquad (1.100)$$

$$\frac{\partial}{\partial x}\left(EI\frac{\partial \phi}{\partial x} \right)-kAG\left(\frac{\partial w}{\partial x}+\phi \right)=0 \qquad (1.101)$$

7.2 Vibration of cylindrical-CNT.

Based on the linearized Donnell shell model, the partial differential equations convening the transverse vibration behavior of cylindrical CNT under axial load $\tilde{N}$ are: [85,90]

$$\frac{\partial N_{xx}}{\partial x}+\frac{1}{R}\frac{\partial N_{x\theta}}{\partial \theta}-\rho h\frac{\partial^2 u}{\partial t^2}=0 \qquad (1.102a)$$

$$\frac{\partial N_{x\theta}}{\partial x}+\frac{1}{R}\frac{\partial N_{\theta\theta}}{\partial \theta}+\frac{1}{R}\left(\frac{\partial M_{x\theta}}{\partial x}+\frac{1}{R}\frac{\partial M_{\theta\theta}}{\partial \theta} \right)-\rho h\frac{\partial^2 v}{\partial t^2}=0 \qquad (1.102b)$$

$$\frac{\partial}{\partial x}\left(\frac{\partial M_{xx}}{\partial x}+\frac{1}{R}\frac{\partial M_{\theta x}}{\partial \theta} \right)+\frac{1}{R}\frac{\partial}{\partial \theta}\left(\frac{\partial M_{x\theta}}{\partial x}+\frac{1}{R}\frac{\partial M_{\theta\theta}}{\partial \theta} \right)-\frac{N_{\theta\theta}}{R}-\tilde{N}\frac{\partial^2 w}{\partial x^2}-\rho h\frac{\partial^2 w}{\partial t^2}=p \qquad (1.102c)$$

where p represents the van der Wall force. ρ is the mass density of carbon nanotube

Analytical and numerical methods can be used to solve the previous partial differential equation for vibration behaviors of CNT, natural frequencies and associated eigenmodes can be obtained.

The wave propagation and dispersion have been studied by many authors based on these models [90]

8. Dynamic instability behaviors

The dynamic instability behaviors can be resulted in structures subjected to non-conservative loads such us non conservative charge, wind fluid, sol-structure interaction, fluid structure interaction and so on. Based on Euler-Bernoulli beam model and integral equation formulation, this behavior has been analyzed by El Felsoufi and Azrar [140,141] and by Ouakkasse and Azrar [67] based on Timoshenko beam model. This behavior will be deeply analyzed in this thesis based on the fluid-CNT interaction.

The dynamic deflection and vibration of elastic carbon nanotube structures conveying fluid have been an interesting subject to many researchers. This is recently one of the most

important subjects in the areas of fluid structure interaction. The pipes conveying fluid are the typical structural examples of the structure. There are several excellent and comprehensive survey papers, in this topic notably Paidoussis [123], Amabili [124]

9. Parameters uncertainty

The prediction of the parameters uncertainty effects and the propagation of the uncertainties are presently a big challenge in many engineering problems. When the parameters are subjected to significant uncertainties, the accuracy of the predicted results will be inevitably altered.

In nanostructures such as CNT, the physical and geometrical parameters are inevitably uncertain. It can be seen from table 1.1 that various values are suggested for the Young modulus Moreover, in the open literature, different values are used by various authors for CNT parameters adopted in the available models. This dispersion in the CNT parameters values is deeply motivating our research work on the parameters uncertainty effects on the dynamic behaviors of CNT.

9.1 Random model

For a SWCNT in the circular cylindrical shape, the tube section A, inertia moment I, fluid mass m_f, the tube mass m_t are given by:

$$A=\left[\left(R+\frac{h}{2}\right)^2+\left(R-\frac{h}{2}\right)^2\right],\ I=\frac{\pi}{4}\left[\left(R+\frac{h}{2}\right)^4+\left(R-\frac{h}{2}\right)^4\right],$$

$$m_f=\rho_f\pi\left(R-\frac{h}{2}\right)^2,\ m_t=\rho_s\pi A, \tag{1.103}$$

All these parameters may be uncertain; this uncertainty effect can strongly affect the output results. These parameters can be assumed to be in the forms:

$$\begin{aligned} &E=E_0+\xi_1E_1;\ R=R_0+\xi_2R_1;\ h=h_0+\xi_3h_1;\ L=L_0+\xi_4L_1\\ &c=c_0+\xi_5c_1;\ \vartheta=\vartheta_0+\xi_6\vartheta_1;\ a=a_0+\xi_7a_1;\ e_0=e_0^1+\xi_8e_1^1\\ &\rho_f=\rho_0^f+\xi_9\rho_1^f;\ \rho_s=\rho_0^s+\xi_{10}\rho_1^s;\ V=V_0+\xi_{11}V_1;\ \delta=H \end{aligned} \tag{1.104}$$

where $E_0, R_0, h_0, L_0, c_0, \vartheta_0, a_0, e_0^1, \rho_0^f, \rho_0^s$ and V_0 are mean values.

$E_1, R_1, h_1, L_1, c_1, \vartheta_1, a_1, e_1^1, \rho_1^f, \rho_1^s$ and V_1 are the standard deviations and $\xi_1, \xi_2, ..., \xi_n$ are the random coefficients that may follow distribution laws.

Based on these assumptions, all the models presented in this thesis will be stochastic partial differential equations. For numerical solution of the resulting stochastic equations, well adapted numerical methods are needed.

9.2 Numerical random methods

In this subsection, the classical and well used methods are presented

9.2.1 Monte-Carlo method

For decades, Monte Carlo has been mainstream technique for random algebraic, differential and partial differential equations. This method is often used to solve problems with uncertainty parameters [145] as well as to a wide range of stochastic problems. The main limitation of this method is that it is very computationally expensive.

Even with this limitation, the Monte Carlo method is still the most popular numerical method. To give a clear overview on this method, let us consider the random differential equation:

$$C_2(\xi_1, \xi_1,...,\xi_n)\,\ddot{U} + C_1(\xi_1, \xi_1,...,\xi_n)\,\dot{U} + C_0(\xi_1, \xi_1,...,\xi_n)\,U = F(t, \xi_1, \xi_1,...,\xi_n) \qquad (1.105)$$

with initial conditions.

where $\xi_1, \xi_1,...,\xi_n$ are the random parameters. The coefficients C_j and the excitation F are then random and depending on the random parameters $\xi_1, \xi_1,...,\xi_n$

to solve the random differential equation (1.111) by the Monte Carlo method, let us denote the random vector $\tilde{\omega} = (\xi_1, \xi_2,...,\xi_n)$ and define sequence of observations $\tilde{\omega}_k = (x_{k1}, x_{k2},,..., x_{kn})$ for k=1 to N, where N is a defined integer and x_{kj} are the random numbers

For each observation $\tilde{\omega}_k$ let us put

$$C_{ik} = C_i(\tilde{\omega}_k) \text{ and } F_k(t, \tilde{\omega}_k) \quad i = 0,1,2 \qquad (1.106)$$

The coefficients C_{ik} and F_k are then deterministic and the random differential equation (1.111a) is reduced to a sequence of deterministic differential equations.

$$\begin{cases} C_{2k}\,\ddot{U} + C_{1k}\,\dot{U} + C_{0k}\,U = F_k(t) & \text{for k=1 to N} \\ + \textit{initial condition} \end{cases} \qquad (1.107)$$

These equation can be solved by classical method such us Runge-Kutta method.

The solution of these dynamical systems is denoted by U_k. The mean and the standard deviation of the random dynamical system (1.107) is approximated by:

$$\begin{cases} \bar{\mathrm{U}}(\mathrm{t})=\dfrac{1}{\mathrm{n}}\sum_{k=1}^{N} U_{\mathrm{k}}(\mathrm{t}) \\ \sigma_V(t)=\sqrt[2]{\left(\dfrac{1}{\mathrm{N}}\sum_{k=1}^{N} U_k^2(\mathrm{t})\right)-\left(\bar{\mathrm{U}}(\mathrm{t})\right)^2} \end{cases} \tag{1.108}$$

9.2.2 Polynomial Chaos

In the recent years, polynomial chaos expansions have received much attention as a promising numerical method in solving random or stochastic differential and partial differential equations.

Polynomial chaos (PC) is a non-sampling-based method to determine evolution of uncertainty in dynamical system, when there is probabilistic uncertainty in the system parameters. This method was first introduced by Norbert Wiener [147, 148] where Hermite polynomials were used to model stochastic processes with Gaussian random variables. This method was generalized for various continuous and discrete distributions using orthogonal polynomials and the L2 convergence in the corresponding Hilbert functional space. The generalized polynomial chaos were introduced leading to the consideration of non-Gaussian random variables. [149,150] stochastic finite element methods have been elaborated by many authors [151, 152]. More recently, the polynomial chaos expansions have been coupled with the component mode synthesis methods for stochastic dynamic problems by Sarsri et al [153].

The Monte Carlo and polynomial chaos methods will be used in this thesis for parameters uncertainty effects on the dynamic behaviors of CNT.

10. Conclusion

Based on the above introduction and literature survey, it is seen that CNTs can be used for many applications and utilized as the potential building blocks in nano-electro-mechanical systems, NEMS. The remarkable properties of carbon nanotubes and their applications in various fields are discussed. The number of recently published work on these nanostructures shows clearly the growing interest and technological scope of this type of structures and materials.

Different analytical models and numerical simulations and have been described and their application to the dynamic behavior of CNTs. An emphasis has been made on the continuum models that have excited much interest due to their computational efficiency and ease of use. The nonlocal elasticity theory combined with the beam and shell models are deeply described as well as the static and dynamic behaviors studied in this thesis

References

[1] S. Iijima: Helical microtubules of graphitic carbon, Nature 354, 56, pp. 115:122, 1991

[2] S. Iijima and T. Ichihashi, Single-shell carbon nanotubes of 1-nm diameter. Nature, Volume 363, 1993, pages 603–605.

[3] A. Thess, R. Lee, P. Nikolaev, H. Dai, P. Petit, J. Robert, C. Xu, Y. H. Lee, S. G. Kim, A. G. Rinzler, D. T. Colbert, G. E. Scuseria, D. Tomanek, J. E. Fischer, R. E. Smalley: Crystalline ropes of metallic carbon nanotubes, Science 273, 122, 123, 1996

[4] K. Hata, D. N. Futaba, K. Mizuno, T. Namai, M. Yumura, S. Iijima: Water assisted highly efficient synthesis of impurity-free single-walled carbon nanotubes, Science 306, 1362 (2004) 123, 124

[5] M. Meyyappan, L. Delzeit, A. Cassell and D. Hash, Carbon nanotube growth by PECVD:a review, Plasma Sources Sci. Technol. 12, pp. 205‑216, 2003

[6] B. Bhushan, Springer handbook of nanotechnology, 2 end edition, Springer Berlin Heidelberg New York, Springer Science Business Media, Inc. 2007

[7] R. Bacon, Growth structure and properties of graphite whiskers. Journal of Applied Physics, volume 31, 1960, pages 283–290.

[8] W. Krätschmer, L. D. Lamb, K. Fostiropoulos and D. R. Huffman, Solid C60: a new form of carbon. Nature, volume 347, 1990, pages 354–358.

[9] H. W. Kroto, J. R. Heath, S. C. O'Brian, R. F. Curl, R. E. Smalley, C-60 - Buckminsterfullerene, Nature 381 (1985) 162.

[10] M. S. Dresselhaus, G. Dresselhaus and P. C. Eklund. Science of Fullerenes and Carbon Nanotubes, Academic Press, San Diego Boston New York London Sydney Tokyo Toronto, University of Kentucky Kentucky, 1995

[11] N. Hamada, S. Sawada and A. Oshiyama, New one-dimensional conductors: Graphitic microtubules, Phys. Rev. Lett. 68, 1579 (1992).

[12] H. Dai, Carbon Nanotubes: Synthesis, Integration, and Properties. Acc. Chem. Res. 2002, 35, 1035-1044.

[13] E. T. Thostenson, Z. Ren and T. W. Chen, Advances in the science and technology of carbon nanotubes and their composites: a review, Composites Science and Technology 2001, 61, 1899-1912.

[14] M. M. J. Treacy, T.W. Ebbesen, J.M. Gibson, Exceptionally high Young's modulus observed for individual carbon nanotubes, Nature 381, 678 (1996)

[15] A. Krishmen, E. Dujardin, T.W. Ebbesen, P.N. Yianilos, M.M.J. Treacy, Young's modulus of single-walled nanotubes, Phys. Rev. Lett. 58, 14013 (1998).

[16] E.W. Wong, P.E. Sheehan, C.M. Lieber, Nanobeam Mechanics: Elasticity, Strength, and Toughness of Nanorods and Nanotubes, Science, 277, 1971 (1997)

[17] A. Poncharal, D. M. Parks, M. C. Boyce, Mechanics of deformation of single- and multi-wall carbon nanotubes, Journal of the Mechanics and Physics of Solids 52 (2004) 789 – 821

[18] P. Poncharal, Z. L. Wang, D. Ugarte and W. A. D. Heer, Electrostatic Deflections and Electromechanical Resonances of Carbon Nanotubes, Science, 283(5407), pp. 1513–1516, 1999

[19] H. Hu, L. Onyebueke and A. Abatan , Characterizing and Modeling Mechanical Properties of Nanocomposites-Review and Evaluation , Journal of Minerals & Materials Characterization & Engineering, Vol. 9, No.4, pp.275-319, 2010
[20] W. X. Bao, C. C. Zhu and W. Z. Cui, Simulation of Young's modulus of single-walled carbon nanotubes by molecular dynamics, Physica B 352, pp. 156-63, 2004
[21] X. Chen and G. Cao, A structural mechanics study of single-walled carbon nanotubes generalized from atomistic simulation, Nanotechnology 17, pp. 1004–1015, 2006
[22] M. F. Yu, O. Lourie, M. J. Dyer, K. Moloni, T. F. Kelly and R. S. Ruoff ,Strength and Breaking Mechanism of Multiwalled Carbon Nanotubes Under Tensile Load, Science 287, 637-640, 2000
[23] A. Javey and J. Kong, Carbon Nanotube Electronics, LLC, 233 Spring Street, New York, NY 10013, USA. 2009
[24] B. Bhushan, Nanotribology and Nanomechanics; Measurement Techniques and Nanomechanics, Springer-Verlag Berlin Heidelberg, New York, Volume 1, 2011
[25] B. Bhushan, Springer handbook of nanotechnology, 2 end edition, Springer Berlin Heidelberg New York, Springer Science Business Media, Inc. 2007
[26] G. A. Rivas, M. D. Rubianes, M. L. Pedano, N. F. Ferreyra, G. Luque and S. A. Miscoria, Carbon nanotubes: A new alternative for electrochemical sensors, Nanotechnology science and technology series, Nova Science Publishers, Inc. 2009
[27] S. Bianco, Carbon nanotubes-from research to applications, Published by InTech Janeza Trdine 9, 51000 Rijeka, Croatian, 2011
[28] S. Saito and A. Zettl, Carbon Nanotubes; Quantum Cylinders of Graphene, Elsevier Radarweg 29, PO Box 211, 1000 AE Amsterdam, The Netherlands Linacre House, Jordan Hill, Oxford OX2 8DP, UK, 2008
[29] C. Hierold, Carbon Nanotube Devices, Properties, Modeling, Integration and Applications, Advanced Micro & Nanosystems, Volume 8, 2008 Wiley-Vch Verlag GmbH & Co. KGaA, Weinheim
[30] R. Martel, T. Schmidt, H. R. Shea, T. Hertel, and P. Avouris, "Single- and multiwall carbon nanotube field-effect transistors," Applied Physics Letters, vol. 73, pp. 2447-2449, 1998.
[31] S. J. Tans, A. R. M. Verschueren, and C. Dekker, "Room-temperature transistor based on a single carbon nanotube," Nature, vol. 393, pp. 49-52, 1998.
[32] C. Chen and Y. Zhang, Nanowelded Carbon Nanotubes, From Field-Effect Transistors to Solar Microcells, Springer Heidelberg Ordrecht London NewYork, 2009
[33] Q. Cao, H.-S. Kim, N. Pimparkar, J. P. Kulkarni, C. Wang, M. Shim, K. Roy, M. A. Alam and J. A. Rogers, Medium-scale carbon nanotube thin-film integrated circuits on flexible plastic substrates. Nature, 454 (2008) 495–500.
[34] Z. Chen, J. Appenzeller, Y.-M. Lin, P. Soloman, P. Avouris, J. Sippel-Oakley, A. Rinzler, J. Tang, and S. Wind, "An Integrated Logic Circuit Assembled on a Single Carbon Nanotube," Science, 2005.
[35] B. F. Coll, K. A. Dean, E. Howard, S. V. Johnson, M. R. Johnson, and J. E. Jaskie, "Nano-emissive display technology for large-area HDTV," Journal of the Society for Information Display, vol. 14, pp. 477-485, 2006.

[36] M. C. G. Lim and Z. W. Zhong, Carbon Nanotubes as Nanodelivery Systems, Springer Singapore Heidelberg New York Dordrecht London, 2013.
[37] M. Griebel, S. Knapek and G. Zumbusch, Numerical Simulation in Molecular Dynamics, Springer-Verlag Berlin Heidelberg 2007.
[38] N. E. Henriksen and F. Y. Hansen, Theories of Molecular Reaction Dynamics, the Microscopic Foundation of Chemical Kinetics, Oxford University Press Inc., New York 2008.
[39] F. Cuadros, I. Cachadina and W. Ahumada, Determination of Lennard J ones Interaction Parameters using a new procedure, Molecular engineering 6, pp. 319-325, 1996
[40] A. Adnan, C.T. Sun, H. Mahfuz A molecular dynamics simulation study to investigate the effect of filler size on elastic properties of polymer nanocomposites, Composites Science and Technology, Vol. 67, pp. 348–356. 2007
[41] H. Wan and F. Delale A structural mechanics approach for predicting the mechanical properties of carbon nanotubes, Meccanica, Vol. 45, pp. 43-51, 2010
[42] R.D. Firouz-Abadi, A.R. Hosseinian, Free vibrations of single-walled carbon nanotubes in the vicinity of a fully constrained graphene sheet, Computational Materials Science, Vol. 53, pp. 12–17, 2012
[43] A Shakouri, T Y Ng and R M Lin A new REBO potential based atomistic structural model for graphene sheets, Nanotechnology 22, 295711 pp.1-8, 2011
[44] K Sbai, A Rahmani, H Chadli and J-L Sauvajol, Modeling and simulation of vibrational breathing-like modes in individual multiwalled carbon nanotubes, Physica E 56, p. 312-318, 2014
[45] K Sbai, A Rahmani, H Chadli and J-L Sauvajol, Finite-size effect on the Raman-active modes of double-walled carbon nanotubes, J. Phys.: Condens. Matter 20, 015204, 2008
[46] R Chowdhury, S Adhikari, F Scarpa and M I Friswell, Transverse vibration of single-layer graphene sheets, J. Phys. D: Appl. Phys. 44, 205401, pp.1-11, 2011
[47] R. Ansari, R. Gholami and S. Ajori ,Torsional Vibration Analysis of Carbon Nanotubes Based on the Strain Gradient Theory and Molecular Dynamic Simulations, J. Vib. Acoust. 135, pp. 1-6, 2013
[48] Y. Y. Zhang, C. M.Wang and V. B. C. Tan, Assessment of Timoshenko beam models for vibrational behavior of single-walled carbon nanotubes using molecular dynamics, Adv. Appl. Math. Mech., Vol. 1, No. 1, pp. 89-106 (2009)
[49] S. I. Yengejeh, J. M. P. Q. Delgado, A. G. Barbosa de Lima and A. Öchsner, Numerical simulation of the vibration behavior of curved carbon nanotubes, Advances in Materials Science and Engineering, Vol. 2014, pp. 1- 9, 2014
[50] J. W. Yoon and H. J. Hwang, A Molecular Dynamics Study on Cantilevered (3,3)(8,8)(13,13), Triple-Walled Carbon-Nanotube Resonators, Journal of the Korean Physical Society, Vol. 56, , pp. 66-69, 2010
[51] B. I., Yakobson, C. J., Brabec and J. Berhole, Nanomechanics of Carbon Tubes: Instabilities beyond Linear Range. J. Physical Review Letters, 76, pp. 2511-2514, 1996.
[52] A. Ghasemi, Morteza Dardel, Mohammad Hassan Ghasemi, mohammad Mehdi Barzegari, Analytical of buckling and post-buckling of fluid conveying multi-walled carbon nanotubes, J. Applied mathematical modeling 37, pp. 4972-4992, 2013

[53] N. Wattanasakulpong, Variddhi Ungbhakorn, Analytical solutions for bending, buckling and vibration responses of carbon nanotube-reinforced composite beams resting on elastic foundation, Computational Materials Science 71, pp. 201–208, 2013

[54] Y. Q. Zhang, G. R. Liu and J. S. Wang, Small-scale effects on buckling of multiwalled carbon nanotubes under axial compression, J. Physical Review B,70, pp. 205-430, 2004

[55] Y. Q. Zhang, G. R. Liu and X. Han, Effect of small length scale on elastic buckling of multi-walled carbon nanotubes under radial pressure, J. Physics Letters A, 349, pp. 370-376, 2006

[56] H. L. Lee, Win-Jin Chang, Vibration analysis of a viscous-fluid-conveying single-walled carbon nanotube embedded in an elastic medium, Physica E 41, 529-532, 2009

[57] W .J. Chang and H. L. Lee, Free vibration of a single-walled carbon nanotube containing a fluid flow using the Timoshenko beam model, Physics Letters A, Vol. 373, pp. 982–985, 2009

[58] T. P. Chang, M. F. Liu, Small scale effect on flow-induced instability of double-walled carbon nanotubes, European Journal of Mechanics - A/Solids, Vol. 30, pp. 992–998, 2011

[59] K. M. Liew, X. Q. He, S. Kitipornchai, Predicting nanovibration of multi-layered graphene sheets embedded in an elastic matrix, Acta Materialia 54, pp. 4229–4236, 2006

[60] S.C. Pradhan, J .K. Phadikar, Nonlocal elasticity theory for vibration of nanoplates, Journal of Sound and Vibration, Vol. 325, pp. 206–223, 2009

[61] R. Aghababaei, J. N. Reddy, Nonlocal third-order shear deformation plate theory with application to bending and vibration of plates, Journal of Sound and Vibration, Vol. 326, pp. 277–289, 2009

[62] A. C. Eringen, On differential equation of nonlocal elasticity and solution, J. Appl. Phys. 1983, pp. 4703-4710.

[63] A. C. Eringen and DGB Edelen, On nonlocal elasticity, Int. J. Eng. Science10, 1972, pp. 233–248

[64] S. Adali, Viriational principles for transversely vibrating multiwalled carbon nanotubes based on nonlocal Euler-Bernoulli beam model, Nano Letters Vol. 9, N. 5, 1737-1741.???

[65] T. Natsuki, X. W. Lei, Q. Q. Ni and M. Endo, Free vibration characteristics of double-walled carbon nanotubes embedded in an elastic medium, Physics Letters, Section A: General, Atomic and Solid State Physics, 374, pp. 2670-2674 , 2010

[66] J. Yoon, C. Q. Ru, and A. Mioduchowski, Noncoaxial resonance of an isolated multiwall carbon nanotube," Physical Review B - Condensed Matter and Materials Physics, 66(23), pp. 2334021-2334024, 2002

[67] N. Ouakkasse et L. Azrar 'Integral equation formulation for flutter instabilities of Timoshenko beams under non conservative loads' International Journal of Mathematics and Statistics, Spring 2009, Volume 4, Number S09, pp 134-144, 2009

[68] J. Yoon, C. Q. Ru and A. Mioduchowski, Terahertz vibration of short carbon nanotubes modeled as Timoshenko beams, Journal of Applied Mechanics, Transactions ASME, 72, pp. 10-17, 2005

[69] J. N. Reddy and S. D. Pang, Nonlocal continuum theories of beams for the analysis of carbon nanotubes, J. Appl. Phys. 103, 023511, 2008

[70] C. M. Wang, V. B. C. Tan and Y. Y. Zhang, Timoshenko beam model for vibration analysis of multi-walled carbon nanotubes," Journal of Sound and Vibration, 294, pp. 1060-1072, 2006

[71] M. Aydogdu, Vibration of multi-walled carbon nanotubes by generalized shear deformation theory, International Journal of Mechanical Sciences, 50, pp. 837-844, 2008

[72] F. Abdoun, L. Azrar and E.M. Daya. Damping and forced vibration analyses of viscoelastic shells. International Journal for Computational Methods in Engineering Science and Mechanics, volume 11, pp. 109 – 122, 2010.

[73] F. Abdoun, L. Azrar, E.M. Daya, and M. Potier-Ferry. Forced vibrations of sandwich viscoelastic beams and plates by an Asymptotic Numerical Method. Computers & Structures 87, 91-100. 2009.

[74] F. Abdoun, Modélisation numérique par éléments finis et contrôle des vibrations des structures à couches viscoélastique et piézoélectriques, Thesis of doctorat Abdelmalek Essaadi University, FST, Tanger, 19 Juillet 2010

[75] Azrar, L., Benamar, R., Potier-Ferry, M., 1999. An asymptotic-numerical method for large amplitude free vibrations of thin elastic plates. Journal of Sound and Vibration 220 (4), 695–727.

[76] S. C. Pradhan and J. K. Phadikar, Nonlocal elasticity theory for vibration of nanoplates, Journal of Sound and Vibration, 325, pp. 206-223, 2009

[77] T. Murmu and S. C. Pradhan, Vibration analysis of nano-single-layered graphene sheets embedded in elastic medium based on nonlocal elasticity theory, Journal of Applied Physics, 105, 2009

[78] E. Jomehzadeh and A. R. Saidi, A study on large amplitude vibration of multilayered graphene sheets, Computational Materials Science, 50, pp. 1043-1051. 2011

[79] B. Arash and Q. Wang, Vibration of single- and double-layered graphene sheets, Journal of Nanotechnology in Engineering and Medicine, 2, 2011

[80] Y. Yan , W.Q. Wang, L.X. Zhang , Nonlocal effect on axially compressed buckling of triple-walled carbon nanotubes under temperature field, Applied Mathematical Modelling, Vol. 34, pp. 3422–3429, 2010

[81] A. E. H. LOVE, A treatise on the mathematical theory of elasticity, Volume II, Cambridge: at the university press, 1893

[82] K. M. Liew, Q. Wang, Analysis of wave propagation in carbon nanotubes via elastic shell theories, International Journal of Engineering Science, Vol. 45, pp. 227–241, 2007

[83] Z. L. Hu, X. M. Guo and C. Q. Ru, The effects of an inserted linear carbon chain on the vibration of a carbon nanotube, Nanotechnology 18, 485712, pp. 1-7, 2007

[84] Hiroyuki Shima, Buckling of Carbon Nanotubes: A State of the Art Review, Materials Vol. 5, pp. 47-84, 2012

[85] Y. Yan , W. Q. Wang and L. X. Zhang , Nonlocal effect on axially compressed buckling of triple-walled carbon nanotubes under temperature field, Applied Mathematical Modelling, 34, pp.3422-3429. 2010

[86] X. Q. He, M. Eisenberger and K. M. Liew, The effect of van der Waals interaction modeling on the vibration characteristics of multiwalled carbon nanotubes, J. Appl. Phys. 100, 124317, 2006

[87] Y. Yan , W.Q. Wang, , L.X. Zhang, Noncoaxial vibration of fluid-filled multi-walled carbon nanotubes, Applied Mathematical Modelling, Vol. 34, pp. 122–128, 2010
[88] C. Sun and K. Liu, Vibration of multi-walled carbon nanotubes with initial axial loading, Solid State Communications, 143, pp. 202-207, 2007
[89] C. Q. Sun and K. X. Liu, Vibration of multi-walled carbon nanotubes with initial axial force and radial pressure," Journal of Physics D: Applied Physics, 42, 2009
[90] G. Q. Xie, X. Han, S.Y. Long, Effect of small size on dispersion characteristics of wave in carbon nanotubes, J. Solid and structures 44, 1242-1255, 2007.
[91] N. Silvestre, C.M. Wang, Y.Y. Zhang, Y. Xiang, Sanders shell model for buckling of single-walled carbon nanotubes with small aspect ratio, Composite Structures, Vol. 93, pp. 1683–1691, 2011
[92] C. Y. Wang, C. Q. Ru and A. Mioduchowski, Free vibration of multiwall carbon nanotubes, Journal of Applied Physics, 97, pp. 1-11. 2005
[93] Q. Wang and V. K. Varadan, Application of nonlocal elastic shell theory in wave propagation analysis of carbon nanotubs, J. Smart Mater. Stuct. 16, 2007, pp. 178-190.
[94] R. Ansari, R. Gholami, K. Hosseini, A sixth-order compact finite difference method for free vibration analysis of Euler-Bernoulli beams, Math. Sciences, Vol. 5, pp. 307-320, 2011
[95] R. Ansari, K. Hosseini, A. Darvizeh, B. Daneshian, A sixth-order compact finite difference method for non-classical vibration analysis of nanobeams including surface stress effects, Applied Mathematics and Computation, Vol. 219, pp. 4977–499, 2013
[96] C. Shu, W.X. Wu, H. Ding, C.M. Wang, Free vibration analysis of plates using least-square-based finite difference method, Comput. Methods Appl. Mech. Engrg. 196, pp.1330–1343, 2007
[97] M. R. Karamooz Ravari, S. Talebi , A. R. Shahidi, Analysis of the buckling of rectangular nanoplates by use of finite-difference method, J Mecanica, pp. 1-15, 2014
[98] R. Ansari, R. Rajabiehfard and B. Arash, Nonlocal finite element model for vibrations of embedded multi-layered graphene sheets, Comput. Materials Science, 49, pp. 831-838, 2010
[99] C. W. Fan, Y. Y. Liu and C. Hwu, Finite element simulation for estimating the mechanical properties of multi-walled carbon nanotubes, Applied Physics A: Materials Science and Processing, 95, pp. 819-831, 2009
[100] A. Sakhaee-Pour, M. T. Ahmadian and A. Vafai, Vibrational analysis of single-walled carbon nanotubes using beam element, Thin-Walled Structures, 47, pp. 646-652, 2009
[101] A. A. Pisano , A. Sofi, P. Fuschi, Nonlocal integral elasticity: 2D finite element based solutions, International Journal of Solids and Structures, Vol. 46, , pp. 3836–3849, 2009
[102] A. A. Pisano, A. Sofi, P. Fuschi, Finite element solutions for nonhomogeneous nonlocal elastic problems, Mechanics Research Communications, Vol. 36, pp. 755–761, 2009
[103] M. Hemmatnezhad and R. Ansari, Finite element formulation for the free vibration analysis of embedded double-walled carbon nanotubes based on nonlocal Timoshenko beam theory, Journal of Theoretical and Applied Physics 7,pp 1-10, 2013
[104] S. Prabhu, Shubrajit Bhaumik and B. K. Vinayagam, Finite element modeling and analysis of zigzag and armchair type single wall carbon nanotube, Journal of Mechanical Engineering Research Vol. 4(8), pp. 260-266, December 2012

[105] S. K. Georgantzinos, N. K. Anifantis, Vibration analysis of multi-walled carbon nanotubes using a spring‐mass based finite element model, Computational Materials Science 47, 168‐177, 2009.
[106] G. R. Liu, M. B. Liu, Smoothed particle hydrodynamics: a meshfree particle method. World Scientific, Singapore, 2003.
[107] Jorge Belinha, Meshless Methods in Biomechanics, Springer Cham Heidelberg New York Dordrecht London, Volume 16, 2014.
[108] G.R. Liu, Meshfree Methods, Moving Beyond the Finite Element Method, CRC Press, Taylor and Francis Group Boca Raton London New York, 2010.
[109] V. P. Nguyen, T. Rabczuk, S. Bordas and M. Duflot, Meshless methods: A review and computer implementation aspects, Mathematics and Computers in Simulation Vol.79, pp. 763–813, 2008.
[110] K. Kiani, A nonlocal meshless solution for flexural vibrations of double-walled carbon nanotubes, Applied Mathematics and Computation 234, pp. 557–578, 2014
[111] R. Ansari, A. Arjangpay, Nanoscale vibration and buckling of single-walled carbon nanotubes using the meshless local Petrov–Galerkin method, Physica E: Low-dimensional Systems and Nanostructures, Vol. 63, 283–292, 2014
[112] C. Shu, H. Du, A generalized approach for implementing general boundary conditions in the GDQ free vibration analysis of plates, International Journal of Solids and Structures Vol. 34, pp. 837–846, 1997
[113] C. Shu, Differential Quadrature and its Application in Engineering, Springer, London, 2000.
[114] A. Krowiak, Methods based on the differential quadrature in vibration analysis of plates, journal of theoretical and applied mechanics, 46, pp. 123-139, 2008.
[115] M. Janghorban , A. Zare, Free vibration analysis of functionally graded carbon nanotubes with variable thickness by differential quadrature method, Physica E, Vol.43, pp. 1602–1604, 2011
[116] M. H. Yas, N. Samadi, Free vibrations and buckling analysis of carbon nanotube-reinforced composite Timoshenko beams on elastic foundation, International Journal of Pressure Vessels and Piping 98, 119-128, 2012
[117] J. Yang, L.L. Ke , S. Kitipornchai , Nonlinear free vibration of single-walled carbon nanotubes using nonlocal Timoshenko beam theory, J. Physica E 42, 1727-1735, 2010.
[118] L. L. Ke, Y. Xiang , J. Yang, S. Kitipornchai, Nonlinear free vibration of embedded double-walled carbon nanotubes based on nonlocal Timoshenko beam theory, Computational, Materials Science, Vol. 47 , pp. 409–417, 2009
[119] A. G. Arani, R. Kolahchi, S. Haghighi, A. A. Mosallaie Barzoki, Nonlinear viscose flow induced nonlocal vibration and instability of embedded DWCNC via DQM, Journal of Mechanical Science and Technology , Vol. 27, pp. 21-31, 2013
[120] R. A. Ibrahim, Overview of Mechanics of Pipes Conveying Fluids—Part I: Fundamental Studies, J. Pressure Vessel Technol. 132, 034001, pp. 1-32 2010
[121] R. A. Ibrahim, Mechanics of Pipes Conveying Fluids—Part II: Applications and Fluid elastic Problems, Journal of Pressure Vessel Technology, 133 / 024001-1, 2011.
[122] R. F Gibson, E. O, Ayorind and Y. F Wen, Vibration of carbon nanotubes and their composites: A review, Composites Sciences and Technology 67, pp. 1-28, 2007.

[123] M. P. Paidoussis, Fluid-structure interactions; slender structures and axial flow, vol. 1, Academic Press, San Diego London New York Boston,1998

[124] M. Amabili, Nonlinear Vibrations and Stability of Shells and Plates, Cambridge University Press, New York, 2008

[125] L. Wang, H.T. Liu, Q. Ni, Y. Wu, Flexural vibrations of microscale pipes conveying fluid by considering the size effects of micro-flow and micro-structure, International Journal of Engineering Science 71, pp. 92–101, 2013.

[126] F. Liang, Y. Su, Stability analysis of a single-walled carbon nanotube conveying pulsating and viscous fluid with nonlocal effect, Applied Mathematical Modelling, 37, pp. 6821–6828, 2013

[127] L. A. Girifalco, Interaction potential for C60 molecules. Journal of Physical Chemistry 95, pp. 5370–5371, 1991.

[128] X. Q. He, Sritawat Kitipornchai, C.M. Wang, K.M. Liew, Modeling of van der Waals force for infinitesimal deformation of multi-walled carbon nanotubes treated as cylindrical shells, International Journal of Solids and Structures, Vol.42, pp. 6032–6047, 2005

[129] R. Saito, G. Dresselhaus and M. S. Dresselhaus, Physical Properties of Carbon Nanotubes. Imperial College Press, London, 1998.

[130] Z. Elfelsoufi and L. Azrar 'Buckling, flutter and vibration analyses of beams by integral equation formulations' Computers & Structures, Volume 83, Issues 31-32, December 2005, Pages 2632-2649

[131] Z. Elfelsoufi, Vibrations, Flambage et Instabilités statique et dynamique des poutres par la Méthode des Equations Intégrales, PhD thesis of Abdelmalek Essaadi University, FST, Tanger, 23 juin 2005

[132] L. J. Sudak, Column buckling of multiwalled carbon nanotubes using nonlocal continuum mechanics, J. Appl. Phys. 94, pp. 7281-7287, 2003

[133] Y. Q. Zhang, G. R. Liu, and X. Y. Xie, Free Transverse Vibrations of Double-Walled Carbon Nanotubes using a Theory of Nonlocal Elasticity, Phys. Rev. B, 71, pp. 195404. 2005,

[134] Q. Xie, X. Han and S.Y. Long, Effect of small size on dispersion characteristics of wave in carbon nanotubes, J. Solid and structures 44, 1242-1255, 2007.

[135] Q. Wang, G. Zhou and K. Lin, Scale Effect on Wave Propagation of Double-Walled Carbon Nanotubes, International Journal of Solids and Structures, 43, pp. 6071-6084, 2006

[136] Y. G. Hu, K. Liew, Q. Wang, X. He and B. Yakobson, Nonlocal Shell Model for Elastic Wave Propagation in Single-and Double-Walled Carbon Nanotubes, Journal of the Mechanics and Physics of Solids, 56, pp. 3475-3485, 2008

[137] Q. Wang, Wave Propagation in Carbon Nanotubes Via Nonlocal Continuum Mechanics," Journal of Applied Physics, 98, pp. 124301, 2005

[138] L. Azrar, B. Cochelin, N. Damil, M. Potier-Ferry, An asymptotic-numerical method to compute the post buckling behavior of elastic plates and shells, International Journal for Numerical Methods in Engineering (36), pp. 1251–1277, 1993.

[139] A. Salehi-Khojin and N. Jalili, Buckling of boron nitride nanotube reinforced piezoelectric polymeric composites subject to combined electro-thermo-mechanical loadings, Composites Science and Technology, Vol. 68, pp. 1489–1501, 2008

[140] Z. El Felsoufi and L. Azrar, Stability analyses of cantilevered damped beams submitted to a subtangential follower force by integral equation formulations. Cahier de l'Université Abdelmalek Essaâdi, pp 52-63, 2006

[141] Z. El Felsoufi and L. Azrar 'Integral equation formulation and analysis of the dynamic stability of damped beams subjected to sub tangential follower forces' Journal of Sound and Vibration; Vol. 296, pp. 690-713,2006

[142] A. Azrar, L. Azrar, A. Aljinaidi, M. Hamadiche, Dynamics Instability Analysis of Multi-Walled Carbon Nanotubes Conveying Fluid, J. Advanced Materials Research, ISSN 1022-6680, Vol. 682 , p 153-160, Trans Tech Publications Ltd, 2013

[143] T. Ragab and C. Basaran, The prediction of the effective charge number in single-walled carbon nanotubes using Monte Carlo simulation, CARBON, 4 9, pp. 425-434, 2011

[144] M. D. Spiridonakos and S. D. Fassois , Non-stationary random vibration modeling and analysis via functional series time-dependent ARMA (FS-TARMA) models – A critical survey, Mechanical Systems and Signal Processing 47 pp.175–224, 2014

[145] B. N. Singh, A. K. S. Bisht, M. K. Pandit, K. K. Shukla, Nonlinear free vibration analysis of composite plates with material uncertainties: A Monte Carlo simulation approach, Journal of Sound and Vibration 324, 126–138, 2009

[146] M. Shinozuka, Monte Carlo solution of structural dynamics, Int. J. Computer. Structural, 2 pp. 855- 874, 1972

[147] N. Wiener, The homogeneous chaos, Amer. J. Math, 60, pp. 897-936, 1938

[148] N. Wiener, Nonlinear Problems in Random Theory, MIT Press, Cambridge, 1958

[149] D. Xiu and G. E. Karniadakis, The Wiener-Askey polynomial chaos for stochastic differential equations, SIAM, J. Sci. Comput. 24, pp. 619-644, 2002

[150] D. Xiu, Numerical methods for stochastic computations a spectral method approach, Princeton University Press, 2010.

[151] R. G. Ghanem, Pol D. Spanos , Stochastic finite elements: a spectral approach, Springer-Verlag, 1991

[152] M. Kleiber, T. D. Hien, The stochastic finite element method, Ed, John, Wiley, 1992.

[153] D. Sarsri, L. Azrar, A. Jebbouri, A. El Hami, Component mode synthesis and polynomial chaos expansions for stochastic frequency functions of large linear FE models, Computers and Structures, 89 (2011) 346-356

Chapter II:

Length scale effect analysis on vibration behavior of single walled Carbon NanoTubes with arbitrary boundary conditions

ABSTRACT

In this paper the small length scale effects on the vibration behaviors of single walled Carbon Nano Tubes (CNT) are modeled and numerically evaluated based on the nonlocal elasticity theory and the Timoshenko beam model. Generalized boundary conditions are considered in order to take into account a more realistic and a wide range of boundary conditions. The lower as well as higher natural frequencies and associated eigenmodes can be obtained by numerically solving the presented generalized transcendental nonlinear algebraic equation. The effect of the used translational and the rotational spring constants on the vibration frequencies and mode shapes of the CNT are addressed. It is demonstrated that the small scale effect can lead to an unstable behaviors of flutter type for cantilever CNT. The coalescence of pair eigenmodes is addressed at critical length scales and these critical values are decreased by increasing the mode number.

This work has been published

Title: Length scale effect analysis on vibration behavior of single walled Carbon NanoTubes with arbitrary boundary conditions

Authors: A. Azrar.; L. Azrar.; A.Aljinaidi.

Journal: Revue de Mécanique Appliquée et Théorique, Vol. 2 pages 475-484, **2011**.

1. Introduction

Carbon NanoTubes (CNTs) have become one of the most promising material and appear to possess extraordinary physical properties. Many applications of CNTs have been reported, such as in atomic force microscopes (AFMs), sensors, actuators, resonators, nano oscillators and field emission devices. To realize the potential benefits of CNTs a fundamental understanding of nano-structured material is required in order to develop reliable constitutive models for various design purposes. The modeling for CNT is classified into two main categories. The first one is mainly based on atomistic and molecular dynamics simulations. The second one is the continuum modeling, including local and nonlocal beam or shell theories. Successful works have been concluded with continuum modeling, such as nonlocal elasticity and mechanical property investigation of CNTs [1-5]. These papers indicate that the small length scales would have significant influences and the nonlocal continuum model can effectively capture these influences in the study of nanostructures.

The Euler-Bernoulli and Timoshenko beams models combined with nonlocal elasticity theory are often used for the analysis of CNT beam like flexural motions, but for CNT in which the radial and/or circumferential displacements have more or less effects, the nonlocal elastic shell theory is more adapted. The wave propagation of single and multi walled CNT has been investigated by Wang and Varadan [6] and Mitra and Gopalakrishan [7] based on the nonlocal shell theory. An assessment of the continuum beam and shell models in the buckling prediction of CNT is provided by Zhang [8] on the basis of molecular dynamic simulation results as well as on some published results. It was demonstrated that the accuracy of the beam and shell models depends on the CNT's aspect ratios (Length/diameter, L/d) and diameter. For large aspect ratio (L/d >10) the beam model is largely enough. But for short CNT with large diameter the nonlocal shell models are more adapted.

Vibrations of CNTs are of considerable importance in a number of mechanical devices and occur during certain manufacturing processes of nanocomposites. So, there are considerable motivation for studying vibration characteristics of CNTs. Gibson et al [1], Benzair et al [9] and Civalek et al [10], among others, discussed the free vibration and bending analyses of CNTs based on the nonlocal continuum model. Azrar et al [11] developed higher order free vibration characteristics of single walled carbon nanoTubes based on the nonlocal Timoshenko and Bernoulli beam models. The mathematical development and numerical predictions based on these two models have been deeply analyzed with respect to aspect ratios

and small length scale Adali [12] and Kucuk et al. [13] elaborated variational principles of CNTs based on Bernoulli and Timoshenko models. Pin Lu et al. [14] studied the dynamic properties of flexural beam using the nonlocal elasticity model. Yoon et al. [15] developed the vibration of double walled short carbon nanotubes of small aspect ratios modeled by the Timoshenko model and neglecting the nonlocal effect and using the classical boundary conditions. The vibration analyses of classical beams under generalized boundary conditions are addressed by Li [16, 17] using the Bernoulli model and by Arboleda-Monsalve et al [18] using the Timoshenko model. In this paper the vibration characteristics of CNT under arbitrary boundary conditions based on the Timoshenko model and the nonlocal elasticity theory are investigated. The main target of the present work is to investigate the length small scale and the generalized boundary conditions effects on the eigenfrequencies and eigenmodes as well as on the instability of these nanostructures.

2. Mathematical formulation

Let us consider a slender single walled carbon nanotube of length L, diameter d and thickness h under arbitrary boundary conditions described by translational and rotational springs at both ends. This allows describing the more realistic boundary conditions and covering the classical boundary conditions by simply specifying the spring constants. The nonlocal elasticity theory combined with the Timoshenko beam model is adopted.

2.1. Constitutive and governing dynamic equations

Based on the nonlocal elasticity theory, developed by Eringen [2,3], the constitutive equation for a linear homogenous nonlocal elastic body is given by the following integral equation:

$$\sigma_{ij}(x) = \int_V \alpha(|x - x'|, \tau) C_{ijkl} \varepsilon_{kl}(x') dV(x'), \tag{2.1}$$

$$\varepsilon_{kl} = (u_{k,l} + u_{l,k}) / 2 \tag{2.2}$$

in which $\alpha(|x-x'|,\tau)$ is the nonlocal kernel function, which incorporates the nonlocal effect at the reference point x produced by local strain point at the source x' into the constitutive equations $\tau = e_0 a / L$ in which $a \, and \, L$ are internal and external characteristic lengths and e_0 is a constant appropriate to each material. C_{ijkl} is the elastic modulus tensor, $\sigma_{ij} \; and \; \varepsilon_{ij}$ are the stress and the strain tensors. The nonlocal kernel function α depends on the internal and external characteristics lengths. Various approximate models of nonlocal elasticity can be

obtained by specifying the kernel function α. This leads to a constitutive equation in an integral from. For practical reasons, the following differential constitutive equations for one dimensional case with Timoshenko hypothesis and small deflection are adopted [2,3].

$$\sigma_{xx} - (e_0 a)^2 \frac{\partial^2 \sigma_{xx}}{\partial x^2} = E\varepsilon_{xx}, \tag{2.3}$$

$$\sigma_{xz} - (e_0 a)^2 \frac{\partial^2 \sigma_{xz}}{\partial x^2} = G\gamma_{xz}, \tag{2.4}$$

where $\sigma_{xx}, \sigma_{xz}, \varepsilon_{xx}$, γ_{xz}, E and G are the nonlocal stress tensors, axial and transverse shear strains, Young modulus and shear modulus respectively. The displacement components along the axial x and transverse z directions are denoted by U and W respectively:

$$U(x,z,t) = u(x,t) - z\psi(x,t), \quad W(x,z,t) = w(x,t) \tag{2.5}$$

where ψ denotes the rotation of the cross section, u and w are the middle plane (z=0) components and t is time. The axial strains are:

$$\varepsilon_{xx} = \varepsilon_{xx}^0 + z\frac{\partial \psi}{\partial x},\ \varepsilon_{xx}^0 = \frac{\partial u}{\partial x}, \quad \gamma_{xz} = \frac{\partial w}{\partial x} + \psi, \tag{2.6}$$

Based on these equations, the nonlocal resultant axial force N, moment M and shear force Q are obtained by the following differential equations.

$$N - (e_0 a)^2 \frac{\partial^2 N}{\partial x^2} = EA\varepsilon_{xx}^0, \tag{2.7}$$

$$M = (e_0 a)^2 \frac{\partial^2 M}{\partial x^2} + EI\frac{\partial \psi}{\partial x}, \tag{2.8}$$

$$Q = (e_0 a)^2 \frac{\partial^2 Q}{\partial x^2} + ksAG\left(\frac{\partial w}{\partial x} + \psi\right), \tag{2.9}$$

$$\text{in which} \quad N = \int_A \sigma_{xx} dA, \quad M = \int_A z\sigma_{xx} dA, \qquad Q = ks\int_A \sigma_{xz} dA \tag{2.10}$$

where ks is the factor of shear depending on the shape of the cross section A.

The equations of motion for the transversely vibration of CNT is given by:

$$\frac{\partial V^T(x,t)}{\partial x} + q(x,t) = m_0 \frac{\partial^2 w(x,t)}{\partial t^2}, \tag{2.11}$$

$$\frac{\partial M(x,t)}{\partial x} - V^T(x,t) = m_2 \frac{\partial^2 \psi(x,t)}{\partial t^2}, \tag{2.12}$$

Where $q(x,t)$ is the transverse excitation force per unit length. For a constant cross section, the mass inertia m_0 and m_2 are defined by: $m_0 = \int_A \rho dA = \rho A$; $m_2 = \int_A \rho z^2 dA = \rho A \frac{h^2}{12}$,

where ρ, h, and A are the mass density of the material, the tube thickness and the cross section area respectively. Using the previous equations, the following moment and shear forces are obtained.

$$M = EI\frac{\partial \psi}{\partial x} + (e_0 a)^2\left[m_2\frac{\partial^3 \psi}{\partial x \partial t^2} + m_0\frac{\partial^2 w}{\partial t^2} - q\right], \tag{2.13}$$

$$V^T = ksAG\left(\psi + \frac{\partial w}{\partial x}\right) + (e_0 a)^2\left[m_0\frac{\partial^3 w}{\partial x \partial t^2} - \frac{\partial q}{\partial x}\right], \tag{2.14}$$

where I is the second moment depending on the considered shape of the cross section.

Substituting Eqs. (2.13) and (2.14) into (2.11) and (2.12) one obtains the partial differential system governing the dynamic behavior of undamped CNTs.

$$\begin{cases} EI\dfrac{\partial^2 \psi}{\partial x^2} - ksAG\left(\dfrac{\partial w}{\partial x} + \psi\right) = m_2\dfrac{\partial^2}{\partial t^2}\left[\psi - (e_0 a)^2\dfrac{\partial^2 \psi}{\partial x^2}\right], \\ ksAG\dfrac{\partial}{\partial x}\left(\dfrac{\partial w}{\partial x} + \psi\right) + q - (e_0 a)^2\dfrac{\partial^2 q}{\partial x^2} = m_0\dfrac{\partial^2}{\partial t^2}\left[w - (e_0 a)^2\dfrac{\partial^2 w}{\partial x^2}\right], \end{cases} \tag{2.15}$$

Recall that the classical local Timoshenko beam model is recovered when the parameter e_0 is set to zero. The vibration analysis of the CNT will be based on these equations.

3. Free vibration modeling

For linear free vibrations, let us assume that.

$$w(x,t) = W(x)e^{i\omega t}, \qquad \psi(x,t) = \Psi(x)e^{i\omega t} \text{ and } \qquad q(x,t) = 0, \tag{2.16}$$

where ω is the natural vibration frequency parameter. The substitution of Eqs. (2.16) into (2.15) leads to the following coupled differential equations.

$$\begin{cases} EI\dfrac{d^2\Psi}{dx^2} - ksAG\left(\dfrac{dW}{dx} + \Psi\right) + m_2\omega^2\left[\Psi - (e_0 a)^2\dfrac{d^2\Psi}{dx^2}\right] = 0, \\ ksAG\dfrac{d}{dx}\left(\dfrac{dW}{dx} + \Psi\right) + m_0\omega^2\left[W - (e_0 a)^2\dfrac{d^2 W}{dx^2}\right] = 0, \end{cases} \tag{2.17}$$

The coupled differential system (2.17) can be reduced to the following uncoupled fourth order differential equations [11].

$$p\frac{d^4W}{dx^4}+q\frac{d^2W}{dx^2}-rW=0 \qquad or \qquad p\frac{d^4\Psi}{dx^4}+q\frac{d^2\Psi}{dx^2}-r\Psi=0 \tag{2.18}$$

$$\text{where} \quad p=\left(EI-(e_0a)^2m_2\omega^2\right)\left(1-\frac{(e_0a)^2m_0\omega^2}{ksAG}\right); \tag{2.19}$$

$$q=m_0\omega^2\left(\Omega_0+(e_0a)^2\right)+m_2\omega^2\left(1-2\frac{(e_0a)^2m_0\omega^2}{ksAG}\right);\ r=m_0\omega^2\left(1-\frac{m_2\omega^2}{ksAG}\right); \tag{2.20}$$

Based on the characteristic equation of (2.18), the following simplified frequency equation is obtained when the rotary mass inertia m_2 is neglected [11].

$$\omega_0=\alpha^2\left[\frac{EI}{m_0}\left(\frac{1}{(1+\Omega_0\alpha^2)\,(1+(e_0a)^2\alpha^2)}\right)\right]^{1/2}, \tag{2.21}$$

$$\text{where} \quad \alpha^2=\frac{q+\sqrt{q^2+4pr}}{2p}, \qquad if \quad pr>0, \qquad \Omega_0=\frac{EI}{ksAG}, \tag{2.22}$$

$$\beta^2=\frac{\alpha^2}{1+\left(\Omega_0+(e_0a)^2\right)\alpha^2)}, \tag{2.23}$$

Note that α and β depend nonlinearly on the frequency ω. The associated eigenmodes deflection, moment and shear force are given by:

$$W(x)=A_1\sin(\alpha x)+A_2\cos(\alpha x)+A_3\sinh(\beta x)+A_4\cosh(\beta x) \tag{2.24}$$

$$M^T(x)=-EI\left(Q^4(\Omega_0+(e_0a)^2)W(x)+(1-Q^4\Omega_0(e_0a)^2)\frac{d^2W(x)}{dx^2}\right) \tag{2.25}$$

$$V^T(x)=-EI\left(Q^4(\Omega_0+(e_0a)^2)\frac{dW(x)}{dx}+(1-Q^4\Omega_0(e_0a)^2)\frac{d^3W(x)}{dx^3}\right) \tag{2.26}$$

where the unknown frequency parameter $Q=\sqrt{\omega_0\sqrt{\rho A/EI}}$ and the arbitrary constants A_i are determined by the considered boundary conditions.

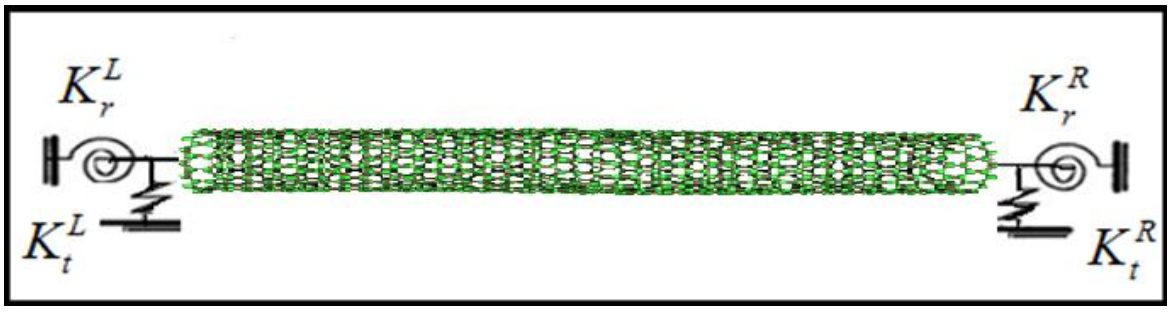

Figure 2.1 Beam elastically restrained at both ends.

For more realistic boundary conditions, the following generalized ones are considered:

$$M^T(0) - K_r^L \frac{dW(0)}{dx} = 0 \quad (2.27)$$

$$V^T(0) + K_t^L\ W(0)\ = 0 \quad (2.28)$$

$$M^T(L) + K_r^R \frac{d\,w(L,t)}{dx} = 0 \quad (2.29)$$

$$V^T(L,t) - K_t^R\ w(L,t)\ = 0 \quad (2.30)$$

where K_r^L, K_t^L *and* K_r^R, K_t^R are the translational and the rotational spring constants at the left and right ends of the CNT at x=0 and x=L (see figure 2.1). Equations (2.27-2.30) represent a set of generalized boundary conditions. The classical boundary conditions can be simply obtained as special cases when the stifnesses of the springs take some extreme values such as zero and infinity. For example, the clamped-clamped boundary condition can be easily obtained by assuming that at each end the translational and rotational spring constants are extremely large. Using equations (2.24-2.26) and the boundary conditions (2.27-2.30), one obtains the following algebraic system.

$$\begin{bmatrix} \mathrm{U}_1\alpha & K_t^L & \mathrm{U}_2\beta & K_t^L \\ -K_r^L\alpha & \mathrm{U}_1 & -K_r^L\beta & \mathrm{U}_2 \\ \left[\mathrm{U}_1\alpha\cos(\alpha)\right. & \left[-K_t^R\cos(\alpha)\right. & \left[\mathrm{U}_2\beta\cosh(\beta)\right. & \left[\mathrm{U}_2\beta\sinh(\beta)\right. \\ \left.-K_t^R\sin(\alpha)\right] & \left.-\mathrm{U}_1\alpha\sin(\alpha)\right] & \left.-K_t^R\sinh(\beta)\right] & \left.-K_t^R\cosh(\beta)\right] \\ \left[\mathrm{U}_1\sin(\alpha)\right. & \left[\mathrm{U}_1\cos(\alpha)\right. & \left[\mathrm{U}_2\sinh(\beta)\right. & \left[\mathrm{U}_2\cosh(\beta)\right. \\ \left.+K_r^R\alpha\cos(\alpha)\right] & \left.-K_r^R\alpha\sin(\alpha)\right] & \left.+K_r^R\beta\cosh(\beta)\right] & \left.+K_r^R\beta\sinh(\beta)\right] \end{bmatrix} \begin{bmatrix} A_1 \\ A_2 \\ A_3 \\ \\ A_4 \end{bmatrix} = \begin{bmatrix} 0 \\ 0 \\ 0 \\ \\ 0 \end{bmatrix}$$

in which U_1, U_2 are given by:

$$U_1 = -\alpha^2(1-(e_0a)^2Q^4\Omega_0)+(\Omega_0+(e_0a)^2)Q^4;$$

$$U_2 = \beta^2(1-(e_0a)^2Q^4\Omega_0)+(\Omega_0+(e_0a)^2)Q^4;$$

After some mathematical developments the following nonlinear algebraic transcendental equation is obtained:

$$F(\omega_n)=A+B\cos(\alpha_n)\cosh(\beta_n)+C\sin(\alpha_n)\sinh(\beta_n)+D\cos(\alpha_n)\sinh(\beta_n)+E\sin(\alpha_n)\cosh(\beta_n)=0 \quad (2.31)$$

where:

$$A = \alpha\beta((U_1^2 + K_r^L K_t^L)(U_2^2 + K_r^R K_t^R)+(U_2^2 + K_r^L K_t^L)(U_1^2 + K_r^R K_t^R));$$

$$B = 2\alpha\beta U_1U_2((K_r^R K_t^L - K_r^R K_t^R + K_t^R K_r^L - K_r^L K_t^L) - U_1U_2)$$
$$- \alpha\beta(K_r^R K_t^L + K_t^R K_r^L)(U_1^2+U_2^2)+ K_r^R K_t^R K_t^L\,\alpha\,(U_1 - U_2 - 2K_r^L\,\beta);$$

$$C = (K_r^R K_r^L(\alpha\beta)^2 - K_t^R K_t^L)(U_1 - U_2)^2 - (U_1U_2(U_1U_2 + (K_r^R K_t^R + K_r^L K_t^L)) + K_r^R K_t^R K_r^L K_t^L)(\alpha^2 - \beta^2);$$

$$D=((K_t^R - K_t^L)(U_1U_2 + K_r^R K_r^L \beta^2) - ((K_r^R - K_r^L) U_1 U_2\beta^2 - K_t^R K_r^L K_t^L))\alpha(U_2 - U_1);$$

$$E =(K_t^R - K_t^L)(U_1 U_4 (U_1 - U_2) + K_r^R K_r^L \alpha^2\beta(U_2 - U_1)) + (K_r^R - K_r^L)(U_1U_2 \alpha^2\beta (U_1 - U_2) - (U_1 - U_2) K_t^R K_t^L \beta);$$

This formulation allows one to get the natural frequencies with respect to the considered physical and material parameters. The numerical solutions of this equation are obtained by the Newton-Raphson algorithm. It is to be noted that when the small scale parameter $e_0a=0$, the characteristic equation is reduced to its classical from with generalized boundary conditions. The resulting mode deflection and rotation shapes are given by:

$$W(x)=G_1\sin(\alpha x)+G_2\cos(\alpha x)+G_3\sinh(\beta x)+\cosh(\beta x); \quad (2.32)$$

$$\psi(x)=S_{11}(G_1\cos(\alpha x)-G_2\sin(\alpha x))-S_{22}(G_3\cosh(\beta x)-\sinh(\beta x)); \quad (2.33)$$

where:

$$G_1 =\Big[\sinh(\beta)(U_1(U_2^2\beta^2 + K_t^L K_t^R) - K_t^L K_t^R U_2 + K_r^L K_t^L U_2\beta^2) - \cosh(\beta)(U_1\beta(K_t^L + K_t^R)U_2 - K_t^L \beta U_2^2 + K_r^L K_t^L K_t^R \beta) + K_t^R \beta\cos(\alpha)(U_2^2 + K_r^L K_t^L) + U_1\alpha\beta\sin(a)(U_2^2 + K_r^L K_t^L)\Big] / \Big[\beta\sin(\alpha)(K_r^L U2 U_1\alpha^2 - K_r^L U_1^2\alpha^2 + K_t^R U_2U_1 + K_r^L K_t^L K_t^R) - \alpha\beta\cos(\alpha)(U_1^2U_2 + K_r^L K_t^L U_1 + K_r^L K_t^R U_1 - K_r^L K_t^R U_2) - K_t^R \alpha\sinh(\beta)(U_1^2 + K_r^L K_t^L) + U_2\alpha\beta\cosh(\beta)(U_1^2 + K_r^L K_t^L)\Big];$$

$$G_2 =-\Big[\cosh(\beta)(\alpha(K_r^L K_t^L U_2\beta + K_r^L K_t^R U_2\beta) + U_1\alpha(U_2^2\beta - K_r^L K_t^R \beta)) - \sinh(\beta)(\alpha(K_r^L U_2^2\beta^2 + K_r^L K_t^L K_t^R) + U_1\alpha(K_t^R U2 - K_r^L U_2\beta^2)) + K_t^R \beta\sin(\alpha)(U_2^2 + K_r^L K_t^L) - U_1 a\beta\cos(a)(U_2^2 + K_r^L K_t^L)\Big] / \Big[\beta\sin(\alpha)(K_r^L U_2U_1\alpha^2 - K_r^L U_1^2\alpha^2 + K_t^R U_2U_1 + K_r^L K_t^L K_t^R) - \alpha\beta\cos(\alpha)(U_1^2U_2 + K_r^L K_t^L U_1 + K_r^L K_t^R U_1 - K_r^L K_t^R U_2) - K_t^R \alpha\sinh(\beta)(U_1^2 + K_r^L K_t^L) + U_2\alpha\beta\cosh(\beta)(U_1^2 + K_r^L K_t^L)\Big];$$

$$G_3 =-(K_t^R\cosh(\beta) - ((U_1U_2 + K_r^L K_t^L)(K_t^R\cos(\alpha) - U_1\alpha\sin(\alpha)))/(U_1^2 + K_r^L K_t^L) + U_2\beta\sinh(\beta) - (K_t^L(U_1 - U_2)(K_t^R\sin(\alpha) + U_1\alpha\cos(\alpha)))/(\alpha(U_1^2 + K_r^L K_t^L)))/(K_t^R\sinh(\beta) + (K_r^L\beta(U_1 - U_2)(K_t^R\cos(\alpha) - U_1\alpha\sin(\alpha)))/(U_1^2 + K_r^L K_t^L) + U_2\beta\cosh(\beta) - ((K_r^L K_t^L\beta + U_1U_2\beta)(K_t^R\sin(\alpha) + U_1\alpha\cos(\alpha)))/(\alpha(U_1^2 + K_r^L K_t^L)));$$

$$S_{11} = \frac{-\alpha}{1+\Omega_0\alpha^2} \quad \text{and} \quad S_{22} = \beta\frac{\left(\Omega_0 + (e_0a)^2\right)\alpha^2 + 1}{1 + (e_0a)^2\alpha^2}$$

Equations (2.31-2.33) give the mathematical modeling of the free vibration of CNT under generalized boundary conditions. The small as well as the higher order natural frequencies and associated eigenmodes can be obtained by numerically solving the considered general transcendental equation using the Newton Raphson algorithm. The small length scale as well as the generalized boundary conditions effects on the eigenfrequencies and eigenmodes can be analyzed.

4. Numerical results and discussions

Numerical results are presented using effective properties of carbon nanotubes. The following geometrical and material properties are used.

$\rho = 2300\,kg/m^3,\ E = 1000\,Gpa,\ \nu = 0.19,\ G = 420Gpa,\ \ d = 1\times10^{-9}\,m,$

$h = 0.34\times10^{-9}\,m,\quad A = 7.85\times10^{-19}\,m^2,\quad I = \dfrac{\pi d^4}{64} = 4{,}91\times10^{-38}\,m^4,$

$ks = 0.877,\quad \Omega_0 = EI/ks\,AG,\quad a = 1.5\times10^{-9}\,m,\quad L = 20\,a,$

Based on the above mathematical formulations, various type of boundary conditions can be considered by simply choosing the considered stiffness constants $K_r^L\ K_t^L, K_r^R\ K_t^R$. In table 2.1, the first four eigenvalues associated to different values of the nonlocal parameters e_0a/L and various stiffnesses of the translational and rotational springs for slender CNT ($d/L=10^{-4}$) are presented. These results are compared to those obtained by Lu et al. [14] for clamped and clamped-free CNT. For this slender CNT the Bernoulli and Timoshenko models lead to the same results. In table 2.2, short CNT (d/L=0.1) is considered and the associated first fourth natural frequencies are given. These frequencies are decreasing by increasing the small scale effect e_0a/L except for clamped free boundary conditions. For C-F CNT, complex eigenvalues are obtained at critical values of the scale length e_0a/L. For the sake of clarity, curves are presented for some cases. Figure 2.2 shows the frequency parameters corresponding to the first to the 22^{th} eigenmodes for a cantilever CNT with respect to the nonlocal parameter e_0a/L. It can be seen that the frequency parameters decrease by increasing of the nonlocal parameter e_0a/L and increase by increasing of the mode number. Exception is on the first order frequency parameter of cantilever CNT which is shown to be slightly increasing with e_0a/L. It is found from this figure that the nonlocal parameters affect greatly the dynamic properties of the cantilever CNT. Therefore, a reasonable choice of the value of the parameter e_0a/L is crucial to assure the validity of the nonlocal model and the vibration stability of the nanostructure. This shows that the instability at higher modes can occur very early than at the

first and second with respect to the small scale parameter. It can be seen that the 1st and 2nd modes shapes coalesce when $e_0a/L=0.62$, and the 3tr and 4th coalesce when $e_0a/L=0.42$. Figures 2.3-a, 2.3-b show the variation of the modes 1 and 2 (a) modes 3 and 4 (b) of a C-F CNT at various nonlocal parameters e_0a/L. Figure 2.4 shows the variations of the eigenfrequency parameter associated to the first fourth modes shapes for a CNT with the nonlocal parameter e_0a/L for various translational and rotational springs. The coalescence of pair eigenmodes is addressed at critical length scales and these critical values are decreased by increasing the mode number and increased while we get far from cantilever conditions in term of the translational and rotational springs $K_t^R and\ K_r^R$.

5. Conclusion

In this paper, the effect of the small scale length parameter on the vibration frequencies and associated mode shapes of single walled CNTs with arbitrary boundary conditions is addressed. In order to take into account the shear effect the Timoshenko model is used. The generalized boundary conditions are considered to account for a more realistic and a large wide of boundary conditions. It is demonstrated that the small scale length parameter has a prominent effect and particularity for clamped-free CNT. The C-F CNT will flutter at critical values of e_0a/L. This instability limit can be used as a limit for prediction values of the small length scale. This unstable behavior may also be observed for other non-classical boundary conditions. Results show that when nonlocal effect increases the frequencies decrease or coalesce for certain types of boundary conditions. In such case the dynamic behavior of the nanostructure is unstable.

REFERENCES

[1] R.F Gibson, E.O, Ayorind and Y.F Wen, Vibration of carbon nanotubes and their composites: A review, Composites Sciences and Technology 67, 2007, pp. 1-28.

[2] A.C. Eringen, On differential equation of nonlocal elasticity and solution, J. Appl. Phys. 54, 1983, pp. 4703-4710.

[3] A.C. Eringen and DGB Edelen, On nonlocal elasticity, Int. J. Eng. Science10, pp. 233–248

[4] J. Peddieson, R. Buch Anan and R. P. Mc Nitt, Application of nonlocal continuum models to nanotechnology, Int. J. Eng. Sci, 41, 2003, pp. 305-312.

[5] L. J. Sudak, Column bukling of multiwalled carbon nanotubes using nonlocal continuum mechanics, J. Appl. Phys. 94, 2003, pp. 7281-7287.

[6] Q. wang and V. K. Varadan, Application of nonlocal elastic shell theory in wave propagation analysis of carbon nanotubs, J. Smart Mater. Stuct. 16, 2007, pp. 178-190.

[7] M. Mitra and S. Goplakishnan, wave propagation in multi-walled carbon nanotube, J. computational Materials Science, 45, 2009, pp. 411-418.

[8]Y. Y. Zhang, C. M. Wang, W. H. Duhan, Y. Xiang and Z. Zong, assessment of continuum mechanics models in predicting buckling strains of single-walled carbon nanotubes, Nanotechnology 20, 2009, pp 1-8.

[9] A. Benzair, A. Tounsi, A. Besseghier, H. Heireche, N. Moulay and L. Boumia, The thermal effect on vibration of single-walled carbon nanotubes using nonlocal Timoshenko beam theory, J. Phys. D: Applied Physics 41(2008) 225404 pp 1-10.

[10] Ö. Civalek, Ç. Demir and B. Akgöz, Free vibration and bending analyses of cantilever microtubules based on nonlocal continuum model, Mathematical and Computational Applications., Vol. 15, No. 2, 2010, pp. 289-298.

[11] A. Azrar, L. Azrar and A. A. Aljinaidi, Higher order free vibration characteristics of single walled Carbon NanoTubes, submitted to Physica E. 2013.

[12] S. Adali, Variational Principles for transversely vibrating multiwalled carbon nanotubes based on nonlocal Euler-Bernoulli beam model, Nano Letters V. 9, No. 5, 2009, pp. 1737-1741.

[13] I. Kucuk, I.S. Sadek and S. Adali, Variational principles for multiwalled carbon nanotubes undergoing vibrations based on nonlocal Timoshenko beam theory, Journal of Nanomaterials, 2010, pp. 1-7.

[14] Pin Lu, H. P Lee, C. Lu, P. Q. Zhang, Dynamic properties of flexural beam using a nonlocal elasticity model, Journal of Applied Physics 99, 2006, 073510 pp 1-9.

[15] J. Yoon, C. Q. Ru, and A. Mioduchowski, Terahertz vibration of short carbon nanotubes modeled as Timoshenko beams, J. Appl. Mechanics Vol. 72, 2005, pp. 10-17.

[16] W. L. Li, Free vibrations of beams with general boundary conditions, Journal of Sound and vibration (2000) 237(4), pp 709-725

[17] W. L. Li, Comparison of Fourier sine and cosine series expansions for beams with arbitrary boundary conditions, Journal of Sound and vibration (2002) 255(1), pp 185-194

[18] L. G. Arboleda-Monsalve, D. G. Zapata-Medina and J. D. Aristizabal-Ochoa, Timoshenko beam-column with generalized end conditions on elastic foundation: Dynamic-stiffness matrix and load vector, Journal of Sound and Vibration 310 (2008) pp 1057–1079.

Table 2.1 The first four the eigenvalues with different nonlocal parameters e_0a/L for various stiffnesses of the translational and rotational springs with $d/L=10^{-4}$

		$K_r^L = K_t^L = 10^9$ $K_r^R = K_t^R = 10^9$ Clamped-clamped		$K_r^L = K_t^L = 10^9$ $K_r^R = K_t^R = 10^3$	$K_r^L = K_t^L = 10^9$ $K_r^R = K_t^R = 10^2$	$K_r^L = K_t^L = 10^9$ $K_r^R = K_t^R = 10$	$K_r^L = K_t^L = 10^9$ $K_r^R = K_t^R = 0$ Clamped-free	
		[14]	present	present	present	present	present	[14]
$e_0a/L=0$	n=1	4.7300	4.7300	4.6205	3.8403	2.7147	1.8751	1.8751
	n=2	7.8532	7.8532	7.2846	5.8130	5.3349	4.6941	4.6941
	n=3	10.9956	10.9956	9.5661	8.6871	8.3661	7.8548	7.8548
$e_0a/L=0.2$	n=1	4.2766	4.2766	4.2294	3.7096	2.6512	1.8919	1.8920
	n=2	6.0352	6.0352	5.9242	4.9223	4.5746	4.1924	4.1925
	n=3	7.3840	7.3840	7.1855	6.3256	6.2204	6.0674	6.0674
$e_0a/L=0.4$	n=1	3.5923	3.5923	3.5809	3.3855	2.4973	1.9543	1.9543
	n=2	4.5978	4.5978	4.5690	3.9731	3.6659	3.3456	3.3456
	n=3	5.4738	5.4738	5.4499	4.7951	4.7391	4.8370	4.8370
$e_0a/L=0.5$	n=1	3.3153	3.3153	3.3089	3.1956	2.4070	2.0219	2.0219
	n=2	4.1561	4.1561	4.1357	3.6572	3.3386	2.9433	2.9433
	n=3	4.9328	4.9328	4.9210	4.3562	4.3060	_	_

Table 2.2 The first four order eigenvalues with different nonlocal parameters e_0a/L for various stiffnesses of the translational and rotational springs with $d/L=10^{-1}$.

		$K_r^L = K_t^L = 10^9$ $K_r^R = K_t^R = 10^9$	$K_r^L = K_t^L = 10^9$ $K_r^R = K_t^R = 10^3$	$K_r^L = K_t^L = 10^9$ $K_r^R = K_t^R = 10^2$	$K_r^L = K_t^L = 10^9$ $K_r^R = K_t^R = 10$	$K_r^L = K_t^L = 10^9$ $K_r^R = K_t^R = 0$
$e_0a/L=0$	n=1	4.6812	4.5805	3.8285	2.7098	1.8745
	n=2	7.5691	7.1117	5.6994	5.2426	4.6416
	n=3	10.2187	9.1376	8.2617	7.9987	7.5717
$e_0a/L=0.2$	n=1	4.2002	4.1599	3.6877	2.6436	1.8926
	n=2	5.7206	5.5609	4.8079	4.4717	4.1160
	n=3	6.6986	6.6266	5.9599	5.8713	5.7501
$e_0a/L=0.4$	n=1	3.5029	3.4638	3.3379	2.4885	1.9525
	n=2	4.3355	4.3185	3.8834	3.5713	3.2741
	n=3	4.9347	4.9266	4.5097	4.4402	4.4198
$e_0a/L=0.5$	n=1	3.2265	3.2217	3.1361	2.3934	2.0178
	n=2	3.9156	3.9037	3.5772	3.2516	2.8848
	n=3	4.4410	4.4369	4.1001	4.0220	_

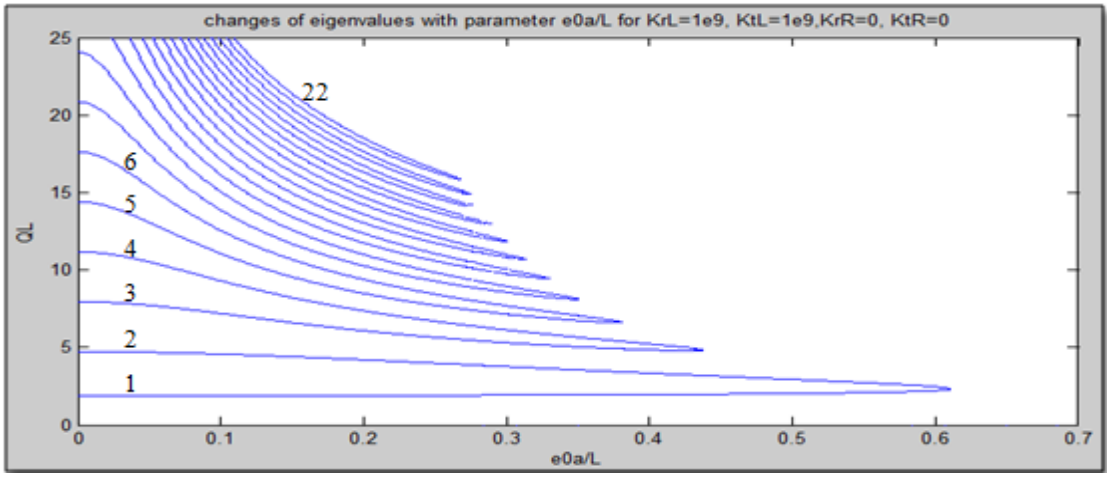

Figure 2.2 Small length scale (e_0a/L) effect on the frequency parameters $Q_jL = L\sqrt{\omega_j\sqrt{\rho A/EI}}$ of a cantilever single walled CNT for j=1, 22 ($K_r^L = K_t^L = 10^9$, $K_r^R = K_t^R = 0$ *and* $d/L = 10^{-1}$)

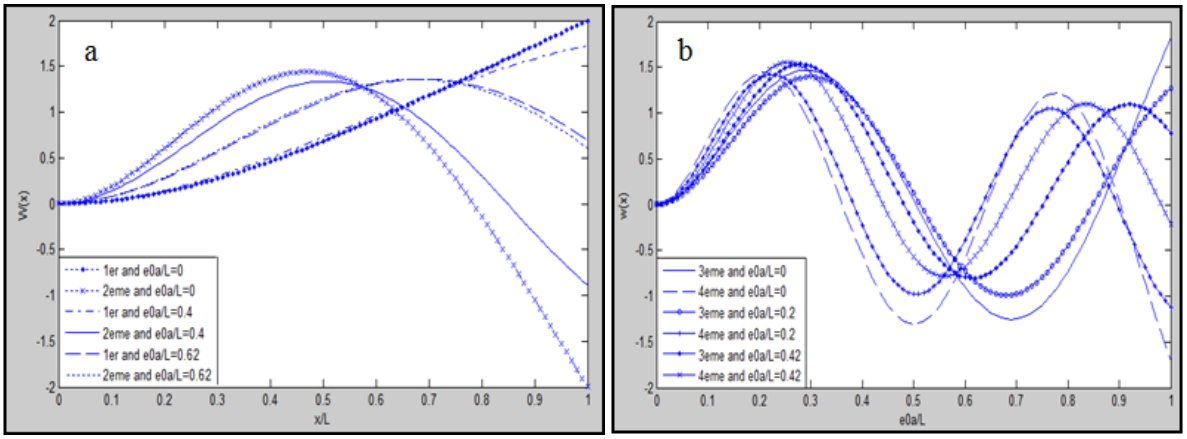

Figure 2.3 Modes 1 and 2 (a) modes 3 and 4 corresponding to different nonlocal parameters e_0a/L of a C-F CNT (K_r^R*and* $K_t^R = 0$, $K_r^L = K_t^L = 10^9$ *and* $d/L = 10^{-1}$)

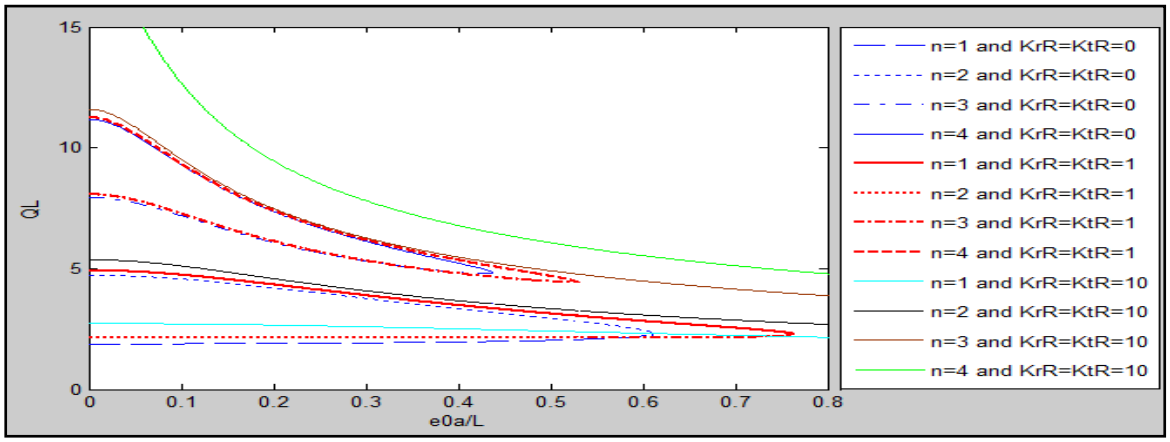

Figure 2.4 Variations of eigenfrequency with parameters Q_iL with respect to e_0a/L associated to various values of K_r^R*and* K_t^R of a SWCNT with ($K_r^L = K_t^L = 10^9$, $d/L = 10^{-1}$)

Chapter III:

Analytical and numerical modeling of higher order free vibration characteristics of single walled Carbon NanoTubes

ABSTRACT

In this paper analytical and numerical investigations of small, higher and asymptotic order vibration eigenmodes and natural eigenfrequencies of single walled Carbon Nano Tubes (CNT) are elaborated. The analytical modeling is based on the nonlocal elasticity theory and two beam models and the numerical simulation is based on the differential quadrature method (DQM). As carbon nanotubes are usually submitted to higher frequencies, the investigations of their higher order vibration characteristics are prominent. Due to numerical instability, the common analytical forms of eigenmodes can be only used for the first twelve modes or so. New mathematical models for very higher eigenmodes and associated eigenfrequencies of CNT with various boundary conditions are developed based on Timoshenko and Bernoulli beam models. The obtained eigenmodes are well conditioned and numerically stable at all orders and can be used as a basis for modal analysis at any required frequency range. Based on the differential quadrature method the free vibration characteristics are numerically obtained at small and higher orders for Timoshenko and Bernoulli models. The analytically and numerically obtained results are well compared at small, higher and very higher frequency orders. The small scale effects on the lower as well as on the higher natural frequencies and eigenmodes are analyzed for various CNT boundary conditions.

This work has been submitted to publication in Journal Physica E 2014
Title: Analytical and numerical modeling of higher order free vibration characteristics of single walled Carbon NanoTubes

Authors: **A. Azrar, L. Azrar & A. Aljinaidi**

1. Introduction

Carbon nanotubes (CNT) are among the most promising new materials for the design and development of nanoelectro-mechanical systems (NEMS). This is due on one hand to their excellent electronic and mechanical properties; on the other hand to the significant progress that has been made in the last few years in modeling and fabrication of carbon nanostructures. Vibrations of CNT are of considerable importance in a number of nanomechanical devices such as sensors, actuators, higher frequency resonators, nano oscillator and field emission devices. Introduced by the use of ultrasonic, microwaves or other higher frequencies, wave propagations are widely used for nanotubes dispersion in resin matrix materials of nanocomposites. So, there are considerable motivations for studying vibration characteristics of CNT at lower and higher frequencies. To the best authors' knowledge there is no published research work on higher vibrations characteristics of CNT.

Mechanical behaviors of CNTs including vibrational behavior have been the subject of numerous recent studies. A review paper on vibration of CNT and their composites has been published by Gibson et al. [1]. Eringen's nonlocal elasticity [2,3] allows one to account for the small scale effect that is very significant when dealing with micro and nanostructures. From the work of Peddieson et al. [4] and Sudak [5], using Eringen's nonlocal model, several studies have been devoted to different mechanical behaviours of beams, plates and shells on the nanoscale. Thus, the nonlocal theory of elasticity has been used to investigate the static and dynamic behaviours of nanobeams and CNT by many authors such as Sudak [5], Wang and Varadan [6], Benzair et al. [7], Reddy and Pang [8], Zhen and Fang [9], Murmu and Pradhan [10], Narendar and Gopalakrishnan [11]. These papers indicate that the small length scales would have significant influences and the nonlocal continuum model can effectively capture these influences in the study of nanostructures.

Vibration analysis of both single and double walled carbon nanotubes (SWCNT, DWCNT) considering the small-scale effect by the nonlocal continuum mechanics is presented by Wang and Varadan [6]. The thermal effect on vibration of CNT has been elaborated by Benzair et al. [7]. It was concluded that at low and room temperature the critical axial stress for infinitesimal vibration of a SWCNT increases as the value of temperature change increases, while at high temperature the critical axial stress decreases as the value of temperature change increases. Murmu and Paradhan [10] studied the thermal stability effect on a SWCNT embedded in an elastic medium based on nonlocal elasticity theory without considering fluid

flow. Narendar and Gopalakrishnan [11] and Cai and Wang [12] showed that only the nonlocal elastic Timoshenko beam model is able to predict the decrease in phase velocities of wave propagation in a CNT. Adali [13] developed a variational principle for transversely vibrating of multi walled CNT based on the nonlocal Euler-Bernoulli beam model and Kucuk et al. [14] based on the Timoshenko model. Lu et al. [15] proposed the dynamic properties of flexural beams using a nonlocal elasticity model.

Arash and Ansari [16] used nonlocal shell model for vibration characteristics of single walled CNTs with different boundary conditions. Yoon et al. [17] developed the vibration of double walled short carbon nanotubes of small aspect ratios modeled by the Timoshenko model and neglecting the nonlocal effect. Civalek et al [18] used the nonlocal and Bernoulli beam theories for free vibration analysis of microtubules and Loya et al [19] for cracked nanobeams. Length scale effect analysis on vibration behavior of single walled Carbon NanoTubes with generalized various boundary conditions have been elaborated by Azrar et al [20, 21]. Pradhan and Murmu [22], studied the application of nonlocal elasticity and DQM in the flapwise bending vibration of a rotating nanocantilever. Janghorban et al [23] proposed the free vibration analysis of functionally graded carbon nanotubes with variable thickness by differential quadrature method. Narendar [24] used the differential quadrature based nonlocal flap wise bending vibration analysis of rotating nanotube with consideration of transverse shear deformation and rotary inertia. Shu developed the differential quadrature ant its application in engineering [25].

However, so far, high frequency vibrations have not been studied sufficiently and there are no reported papers for CNT vibrations at higher orders. Therefore, investigation of higher eigenmodes and eigenfrequencies of CNT are of interest from both practical and theoretical viewpoints. The aim of this paper is to investigate analytically and numerically the vibration characteristics of CNT at higher and very higher frequency orders. The Timoshenko and Bernoulli beam models are combined with the nonlocal elasticity theory. New explicit relationships of eigenmodes and associated eigenfrequencies are given for various boundary conditions at lower and very higher orders. The developed higher order eigenmodes are numerically stable. Based on the differential quadrature method, numerical investigations are elaborated for small as well as for very higher frequency orders. The small scale and the aspect ratio effects on the eigenfrequencies and eigenmodes are analyzed.

2. Mathematical formulation

For the vibration analysis of single walled carbon nanotubes the Timoshenko beam model combined with nonlocal beam theory is adopted. The Euler-Bernoulli beam model is also used here as a special case. The transverse and rotation eigenmodes as well as the corresponding natural frequencies relationships associated to various boundary conditions are elaborated at small and at very higher orders.

The deformations of the considered carbon nanotubes are assumed in the x-z plane and the displacement components along the axial x and transverse z directions are denoted by U and W respectively:

$$U(x,z,t) = u(x,t) - z\psi(x,t), \quad W(x,z,t) = w(x,t) \tag{3.1}$$

where ψ denotes the rotation of the cross section, u and w are the middle plane (z=0) components and t is time. The axial strains are:

$$\varepsilon_{xx} = \varepsilon_{xx}^0 + z\frac{\partial \psi}{\partial x},\ \varepsilon_{xx}^0 = \frac{\partial u}{\partial x}, \quad \gamma_{xz} = \frac{\partial w}{\partial x} + \psi, \tag{3.2}$$

in which γ_{xz} denotes the transverse shear strain.

Note that in large length scales, the classical continuum models are sufficient and give accurate computational results for material and structural systems. But, when the length scales are of level such as in nano-materials or nano devices the so called nonlocal continuum mechanics proposed by Eringen [2,3] are more adapted. Recently, many researchers applied Eringen's theory to the nano-scales structures such as single walled and multiple walled carbon nanotubes and showed that the small length scales have significant influences in the stability, static and dynamic behaviors of nanostructures.

The nonlocal mechanics pretends that the stress tensor at a reference point x in a body depends not only on the strain tensor at the point x, as in the classical local elasticity theory, but also on the strain tensor at all other points 'x' of this body. Based on this theory, the constitutive equation for a linear homogenous nonlocal elastic body is given by the following integral equation: [2,3]

$$\sigma_{ij}(x) = \int_V \alpha(|x - x'|, \tau) C_{ijkl} \varepsilon_{kl}(x') dV(x'), \tag{3.3}$$

$$\varepsilon_{kl} = (u_{k,l} + u_{l,k})/2 \tag{3.4}$$

in which $\alpha(|x - x'|, \tau)$ is the nonlocal kernel function , C_{ijkl} is the elastic modulus tensor and ε_{kl} is the strain tensor. To use the integral formulation (3.3) the kernel function α has to be

known. The nonlocal kernel α depends on the internal and external characteristics lengths and its explicit expression is hard to be obtained [2,3]. For practical reasons, the following differential constitutive equations for one dimensional case are adopted [2,3].

$$\sigma_{xx} - (e_0 a)^2 \frac{\partial^2 \sigma_{xx}}{\partial x^2} = E\varepsilon_{xx}, \tag{3.5}$$

$$\sigma_{xz} - (e_0 a)^2 \frac{\partial^2 \sigma_{xz}}{\partial x^2} = G\gamma_{xz}, \tag{3.6}$$

where $\sigma_{xx}, \sigma_{xz}, e_0$, a, E and G are the nonlocal stress tensors, a constant appropriate to each material, an internal characteristic length, Young modulus and the shear modulus respectively. Based on these equations, the nonlocal resultant axial force N, moment M and shear force Q are obtained by the following differential equations.

$$N - (e_0 a)^2 \frac{\partial^2 N}{\partial x^2} = EA\varepsilon_{xx}^0, \tag{3.7}$$

$$M = (e_0 a)^2 \frac{\partial^2 M}{\partial x^2} + EI\frac{\partial \psi}{\partial x}, \tag{3.8}$$

$$Q = (e_0 a)^2 \frac{\partial^2 Q}{\partial x^2} + ksAG(\frac{\partial w}{\partial x} + \psi), \tag{3.9}$$

in which

$$N = \int_A \sigma_{xx} dA, \quad M = \int_A z\,\sigma_{xx} dA, \qquad Q = ks\int_A \sigma_{xz} dA \tag{3.10}$$

Where ks is the factor of shear depending on the shape of the cross section A. For a constant cross section, the mass inertia m_0, m_2 are defined by:

$$m_0 = \int_A \rho dA = \rho A\,; \quad m_2 = \int_A \rho z^2\, dA = \rho A\frac{h^2}{12}, \tag{3.11}$$

Where ρ is the mass density of the material. Based on Timoshenko beam theory, the equations of motion are:

$$\frac{\partial Q}{\partial x} + q = m_0 \frac{\partial^2 w}{\partial t^2}, \tag{3.12}$$

$$\frac{\partial M}{\partial x} - Q = m_2 \frac{\partial^2 \psi}{\partial t^2}, \tag{3.13}$$

Where $q(x,t)$ is the transverse excitation force per unit length. Using these equations of motion, the following moment and shear force are obtained.

$$M = EI\frac{\partial \psi}{\partial x} + (e_0 a)^2\left[m_2 \frac{\partial^3 \psi}{\partial x \partial t^2} + m_0 \frac{\partial^2 w}{\partial t^2} - q \right], \tag{3.14}$$

$$Q = ksAG\left(\psi + \frac{\partial w}{\partial x} \right) + (e_0 a)^2\left[m_0 \frac{\partial^3 w}{\partial x \partial t^2} - \frac{\partial q}{\partial x} \right], \tag{3.15}$$

Substituting Eqs. (3.14) and (3.15) into (3.12) and (3.13) one obtains the partial differential system governing the dynamic behavior of the undamped CNT.

$$\begin{cases} EI\dfrac{\partial^2 \psi}{\partial x^2} - ksAG\left(\dfrac{\partial w}{\partial x} + \psi \right) = m_2 \dfrac{\partial^2}{\partial t^2}\left[\psi - (e_0 a)^2 \dfrac{\partial^2 \psi}{\partial x^2} \right], & (3.16) \\ ksAG\dfrac{\partial}{\partial x}\left(\dfrac{\partial w}{\partial x} + \psi \right) + q - (e_0 a)^2 \dfrac{\partial^2 q}{\partial x^2} = m_0 \dfrac{\partial^2}{\partial t^2}\left[w - (e_0 a)^2 \dfrac{\partial^2 w}{\partial x^2} \right], & (3.17) \end{cases}$$

For the sake of comparative study, the Euler-Bernoulli beam equations are given in the Appendix A.

Recall that the local Timoshenko and Bernoulli beam models are recovered when the small parameter e_0 is set to zero. As the aim of this paper is the development of mathematical formulations of the higher vibration eigenmodes and frequencies of the CNT the lower order vibration characteristics have been quickly formulated for the sake of clarity.

3. Analytical analysis

3.1 Lower orders free vibration characteristics

For linear free vibrations, let us assume that.

$$w(x,t) = W(x)e^{i\omega t}, \qquad \psi(x,t) = \Psi(x)e^{i\omega t} \text{ and } \qquad q(x,t) = 0, \tag{3.18}$$

where ω is the natural vibration frequency parameter. The substitution of Eq. (3.18) into (3.16 -3.17) leads to the following coupled differential equations.

$$\begin{cases} EI\dfrac{d^2 \Psi}{dx^2} - ksAG\left(\dfrac{dW}{dx} + \Psi \right) + m_2 \omega^2 \left[\Psi - (e_0 a)^2 \dfrac{d^2 \Psi}{dx^2} \right] = 0, \\ ksAG\dfrac{d}{dx}\left(\dfrac{dW}{dx} + \Psi \right) + m_0 \omega^2 \left[W - (e_0 a)^2 \dfrac{d^2 W}{dx^2} \right] = 0, \end{cases} \tag{3.19}$$

The differential system (3.19) is reduced to the following uncoupled forth order differential equations.

$$p\frac{d^4 W}{dx^4} + q\frac{d^2 W}{dx^2} - rW = 0 \qquad or \qquad p\frac{d^4 \Psi}{dx^4} + q\frac{d^2 \Psi}{dx^2} - r\Psi = 0 \tag{3.20}$$

where

$$p = \left(EI - (e_0 a)^2 m_2 \omega^2\right)\left(1 - \frac{(e_0 a)^2 m_0 \omega^2}{ksAG}\right); \tag{3.21}$$

$$q = m_0 \omega^2 \left(\Omega_0 + (e_0 a)^2\right) + m_2 \omega^2 \left(1 - 2\frac{(e_0 a)^2 m_0 \omega^2}{ksAG}\right); \tag{3.22}$$

$$r = m_0 \omega^2 \left(1 - \frac{m_2 \omega^2}{ksAG}\right); \tag{3.23}$$

For separate solutions of the characteristic equation, the general solution of (3.20) can be written in the form:

$$W(x) = \sum_{i=1}^{4} a_i e^{\lambda_i x} \tag{3.24}$$

where $\lambda_i^2 = \dfrac{-q \pm \sqrt{q^2 + 4pr}}{2p}$ (3.25)

The associated frequency equation is given by:

$$\mathrm{A}\omega^4 - \mathrm{B}\omega^2 + R = 0; \tag{3.26}$$

$$\mathrm{A} = \frac{m_0 m_2}{ksAG}\left((e_0 a)^2 \alpha^2 + 1\right)^2; \tag{3.27}$$

$$\mathrm{B} = (e_0 a)^2 (m_2 + \Omega_0 m_0)\alpha^4 + \left(m_0(\Omega_0 + (e_0 a)^2) + m_2\right)\alpha^2 + m_0; \quad \Omega_0 = \frac{EI}{ksAG}; \quad R = EI\alpha^4; \tag{3.28}$$

$$\alpha^2 = \frac{q + \sqrt{q^2 + 4pr}}{2p}, \qquad \beta^2 = \frac{-q + \sqrt{q^2 + 4pr}}{2p} \quad if \quad q^2 + 4pr > 0 \tag{3.29-a}$$

$$\alpha^2 + \beta^2 = \frac{\sqrt{q^2 + 4pr}}{p} \tag{3.29-b}$$

The solutions of (3.26) are classically given by:

$$\omega_1^2 = \frac{\mathrm{B} - \sqrt{\mathrm{B}^2 - 4\mathrm{A}R}}{2\mathrm{A}}, \qquad \omega_2^2 = \frac{\mathrm{B} + \sqrt{\mathrm{B}^2 - 4\mathrm{A}R}}{2\mathrm{A}}; \tag{3.30}$$

When the rotary mass inertia m_2 is neglected, the following simplified frequency equation is obtained.

$$\omega_0 = \sqrt{\frac{R}{\mathrm{B}}} = \alpha^2 \left[\frac{EI}{m_0}\left(\frac{1}{(1 + \Omega_0 \alpha^2)\,(1 + (e_0 a)^2 \alpha^2)}\right)\right]^{1/2}, \tag{3.31}$$

$$\beta^2 = \alpha^2 \left(\frac{1}{1 + \left(\Omega_0 + (e_0 a)^2\right)\alpha^2)}\right), \tag{3.32}$$

The associated deflection and rotation eigenmodes are given by:

$$W(x) = a_1 \sin(\alpha x) + a_2 \cos(\alpha x) + a_3 \sinh(\beta x) + a_4 \cosh(\beta x) \tag{3.33}$$

$$\Psi(x) = S_{11}\left(a_1 \cos(\alpha x) - a_2 \sin(\alpha x)\right) - S_{22}\left(a_3 \cosh(\beta x) + a_4 \sinh(\beta x)\right) \tag{3.34}$$

$$\textit{where} \qquad S_{11} = \frac{-\alpha}{1+\Omega_0\alpha^2} \tag{3.35}$$

$$S_{22} = \beta\frac{\left(\Omega_0 + (e_0a)^2\right)\alpha^2 + 1}{1+(e_0a)^2\alpha^2} \tag{3.36}$$

in which the arbitrary constants a_i are determined by the considered boundary conditions.

3.1.1 Simply supported case

For simply supported boundary conditions, the following conditions have to be satisfied at x=0 and x=L.

$$W = 0, \quad and \quad M = EI\frac{d\Psi}{dx} - (e_0a)^2\omega^2\left[m_2\frac{d\Psi}{dx} + m_0W\right] = 0, \tag{3.37}$$

After some mathematical developments, the resulting mode shapes are:

$$W_n(x) = a_n\sin(\alpha_n x), \qquad \Psi_n(x) = a_nS_{11}\cos(\alpha_n x), \qquad \alpha_n = n\pi/L, \tag{3.38}$$

where a_n is an arbitrary constant. The associated natural frequencies are given by:

$$\text{if } m_2 = 0, \qquad \omega_n = \left(\frac{n\pi}{L}\right)^2\left[\frac{EI}{m_0}\left(\frac{1}{(1+\Omega_0(n\pi/L)^2)\,(1+(e_0a)^2(n\pi/L)^2)}\right)\right]^{1/2}, \tag{3.39}$$

$$\textit{if } m_2 \neq 0, \quad \omega_n^{\,2} = \Big\{(e_0a)^2(m_2+\Omega_0m_0)(n\pi/L)^4 + m_0(\Omega_0+(e_0a)^2) + m_2 + m_0$$
$$\pm\Big(\left[(e_0a)^2(m_2+\Omega_0m_0)(n\pi/L)^4 + m_0(\Omega_0+(e_0a)^2) + m_2 + m_0\right]^2$$
$$-4\left[(e_0a)^4m_0m_2\left(\frac{n\pi}{L}\right)^4 + 2(e_0a)^4m_0m_2\left(\frac{n\pi}{L}\right)^2 + m_0m_2\right]\Omega_0\left(\frac{n\pi}{L}\right)^4\Big)^{1/2}\Big\}\Big/\Big\{2\Big(\frac{(e_0a)^4m_0m_2}{ksAG}\left(\frac{n\pi}{L}\right)^4$$
$$+\frac{2(e_0a)^4m_0m_2}{ksAG}(n\pi/L)^2 + \frac{m_0m_2}{ksAG}\Big)\Big\} \tag{3.40}$$

3.1.2 Clamped-Clamped case C-C

When the two edges of the beam are clamped, the four boundary conditions are

$$W(0) = \Psi(0) = 0; \quad W(L) = \Psi(L) = 0, \tag{3.41}$$

The resulting mode shapes are given by:

$$W_n(x) = a_n\left[\cos(\alpha_n x) - \cosh(\beta_n x) + \Gamma_{n\,CC}\left(\sin(\alpha_n x) + \frac{S_{11}}{S_{22}}\sinh(\beta_n x)\right)\right], \tag{3.42}$$

$$\Psi_n(x) = a_nS_{11}\left[\frac{S_{22}}{S_{11}}\sinh(x\beta_n) - \sin(\alpha_n x) + \Gamma_{n\,CC}\left(\cos(\alpha_n x) - \cosh(\beta_n x)\right)\right], \tag{3.43}$$

$$\Gamma_{n\,CC} = \frac{S_{22}\left(\cosh\,(\beta_n L) - \cos(\alpha_n L)\right)}{S_{22}\sin(\alpha_n L) + S_{11}\sinh(\beta_n L)}, \tag{3.44}$$

where (α_n, β_n), verify the following transcendental equation:

$$2 - 2\cos(\alpha_n L)\,\cosh\,(\beta_n L) + \left(\frac{S_{11}}{S_{22}} - \frac{S_{22}}{S_{11}}\right)\sin(\alpha_n L)\sinh(\beta_n L) = 0 \tag{3.45}$$

Note that α_n and β_n are related and depend nonlinearly on ω_n.

3.1.3 Clamped simply-supported case C-S

For clamped simply supported conditions, one has to verify

$$W(0) = 0; \qquad \Psi(0) = 0; \quad W(L) = 0 \;\; and \;\; M(L) = 0; \tag{3.46}$$

The resulting mode shapes are given by:

$$W_n(x) = a_n\left[\cos(\alpha_n x) - \cosh\,(\beta_n x) + \Gamma_{n\,CS}\left(\sin(\alpha_n x) + \frac{S_{11}}{S_{22}}\sinh(\beta_n x)\right)\right], \tag{3.47}$$

$$\Psi_n(x) = a_n S_{11}\left[\frac{S_{22}}{S_{11}}\sinh(x\beta_n) - \sin(\alpha_n x) + \Gamma_{n\,CS}\left(\cos(\alpha_n x) - \cosh\,(\beta_n x)\right)\right], \tag{3.48}$$

$$\Gamma_{n\,CS} = \frac{S_{22}\left(\cosh\,(\beta_n L) - \cos(\alpha_n L)\right)}{\left(S_{22}\beta_n \sin(\alpha_n L) + S_{11}\alpha_n \sinh(\beta_n L)\right)} \tag{3.49}$$

where (α_n, β_n), verify the following transcendental equation:

$$S_{22}\tan(\alpha_n L) + S_{11}\tanh(\beta_n L) = 0 \tag{3.50}$$

3.1.4 Cantilever beams C-F

For a cantilever beam, the considered clamped free boundary conditions are:

$$W(0) = 0; \qquad \Psi(0) = 0; \quad Q(L) = 0 \quad and\, M(L) = 0; \tag{3.51}$$

This leads to the following mode shapes:

$$W_n(x) = a_n\left[\cos(\alpha_n x) - \cosh\,(\beta_n x) + \Gamma_{n\,CF}\left(\sin(\alpha_n x) + \frac{S_{11}}{S_{22}}\sinh(\beta_n x)\right)\right], \tag{3.52}$$

$$\Psi_n(x) = a_n S_{11}\left[S_{22}/S_{11}\sinh(x\beta_n) - \sin(\alpha_n x) + \Gamma_{n\,CF}\left(\cos(\alpha_n x) - \cosh\,(\beta_n x)\right)\right], \tag{3.53}$$

$$\Gamma_{n\,CF} = \frac{S_{22}\left(\beta_n{}^2\cos(\alpha_n L) + \alpha_n{}^2\cosh\,(\beta_n L)\right)}{\left(S_{11}\alpha_n{}^2\sinh(\beta_n L) - S_{22}\beta_n{}^2\sin(\alpha_n L)\right)}, \tag{3.54}$$

where (α_n, β_n) verify the following transcendental equation:

$$\begin{aligned} &S_{22}\beta_n{}^3 - S_{11}\alpha_n{}^3 + \alpha_n\beta_n\left(\alpha_n S_{22} - \beta_n S_{11}\right)\cos(\alpha_n L)\cosh\,(\beta_n L) \\ &-\alpha_n\beta_n\left(\alpha_n S_{11} + \beta_n S_{22}\right)\sin(\alpha_n L)\sinh(\beta_n L) = 0, \end{aligned} \tag{3.55}$$

The natural frequencies corresponding to the considered boundary conditions can be obtained by solving numerically the associated transcendental equations. Note that these equations are nonlinear on α_n and have infinite solutions. The numerical solutions are obtained here by the Newton-Raphson algorithm. The previous relationships allow one to investigate the lower order free vibration characteristics of CNTs and to analyze the small scale effects on it.

Let us note that the natural frequencies and the corresponding eigenmodes can be accurately obtained for small orders (1 to 12) using the previous relationships. But, for higher orders (more than 12) the eigenmodes are ill conditioned in the vicinity of (x=L) and can not be obtained accurately using the previous equations except for S-S boundary conditions.

For CNT, the higher order eigenfrequencies and eigenmodes are of big interest. Nanometer scale higher frequency resonators and oscillators are critical components of many nano-electro-mechanical systems (NEMS). Analytical relationships of higher order frequencies and associated eigenmodes are very useful for the design of these emerging materials and devices. For accurate solutions at higher orders, the following mathematical models are developed herein.

3.2 Higher orders vibration characteristics

For simply supported boundary conditions very higher eigenmodes and eigenfrequencies can be explicitly obtained. But, for the other boundary conditions, some mathematical regularizations are needed in other to get numerically stable eigenmodes. Mathematical models are elaborated here for Timoshenko and Euler Bernoulli Beam models.

3.2.1 Timoshenko model

3.2.1.1 Clamped-clamped CNT

The associated mode shape functions of clamped–clamped CNT based on Timoshenko model are given by equation (3.42-3.43). It has to be noted that when the order n is large the coefficient α_n is large too and then the hyperbolic functions become very large when x is near to the border L. This leads to ill conditioned eigenmodes. The resulting disturbing effect can be overcome by using some approximations for large n. Equation (3.44) is rewritten as

$$\Gamma_{n\,CC} = \Lambda_{n\,CC} + S_{22}/S_{11}, \tag{3.56}$$

where

$$\Lambda_{n\,CC} = -\frac{\cos(\alpha_n L) + S_{22}/S_{11}\sin(\alpha_n L) - e^{(-\beta_n L)}}{\sin(\alpha_n L) + S_{11}/S_{22}\sinh(\beta_n L)}, \tag{3.57}$$

using these equations, the eigenmode given in (3.42) is rewritten as:

$$W_n(x) = a_n\left\{\cos(\alpha_n x) + \Gamma_{n\,CC}\,\sin(\alpha_n x) - e^{(-\beta_n x)} + \Lambda_{n\,CC}\,\frac{S_{11}}{S_{22}}\sinh(\beta_n x)\right\}, \tag{3.58}$$

This new form of $W_n(x)$ is an exact solution for the n^{th} mode shape.

By making some simplifications, Eq. (3.58) can be modified so that it is numerically well-conditioned for very large n. For this goal, the following mathematical equations are used

$$\Lambda\frac{S_{11}}{S_{22}}\sinh(\beta_n x) = -\frac{\cos(\alpha_n L) + S_{22}/S_{11}\sin(\alpha_n L) - e^{(-\beta_n L)}}{2\sin(\alpha_n L)/\left(e^{(\beta_n L)} - e^{-(\beta_n L)}\right) + S_{11}/S_{22}}\frac{S_{11}}{S_{22}}\frac{e^{(\beta_n x)} - e^{-(\beta_n x)}}{e^{(\beta_n L)} - e^{-(\beta_n L)}} \tag{3.59}$$

Based on these equations, the following new deflection and rotation eigenmodes relationships are obtained.

$$\hat{W}_n(x) = a_n\left\{\cos(\alpha_n x) + \Gamma_{nCC}\sin(\alpha_n x) - e^{-(\beta_n x)} - \frac{\cos(\alpha_n L) + S_{22}/S_{11}\sin(\alpha_n L) - e^{(-\beta_n L)}}{2\sin(\alpha_n L)/\left(e^{(\beta_n L)} - e^{-(\beta_n L)}\right) + S_{11}/S_{22}}\frac{S_{11}}{S_{22}}\frac{e^{(\beta_n x)} - e^{-(\beta_n x)}}{e^{(\beta_n L)} - e^{-(\beta_n L)}}\right\} \tag{3.60}$$

$$\hat{\Psi}_n(x) = a_n S_{11}\left\{\Gamma_{nCC}\cos(\alpha_n x) - \sin(\alpha_n x) - S_{22}/S_{11}e^{(-\beta_n x)} + \frac{\cos(\alpha_n L) + S_{22}/S_{11}\sin(\alpha_n L) - e^{(-\beta_n L)}}{2\sin(\alpha_n L)/\left(e^{(\beta_n L)} - e^{(-\beta_n L)}\right) + S_{11}/S_{22}}\frac{e^{(\beta_n x)} + e^{(-\beta_n x)}}{e^{(\beta_n L)} - e^{(-\beta_n L)}}\right\} \tag{3.61}$$

where

$$\beta_n = \Upsilon\left(\frac{1}{1+\mathrm{X}_n}\right)^{1/2} = \Upsilon\left(1 + \sum_{k=1}^{N}\frac{1}{k!}\left(\prod_{j=0}^{k-1}\left(-\frac{1}{2} - j\right)\right)\mathrm{X}_n{}^k\right) + o(X_n{}^N) \tag{3.62}$$

$$\Upsilon = \left(\frac{1}{\Omega_0 + (e_0 a)^2}\right)^{1/2};\ \text{and}\ \mathrm{X}_n = \left(\frac{1}{\left(\Omega_0 + (e_0 a)^2\right)\alpha_n}\right); \tag{3.63}$$

For large n, α_n is large and then X_n tends to zero. The power series expansion (3.62) can be truncated at a required order which leads to an approximate value of β_n.

These new relationships are considered here to be the higher order vibrations eigenmodes models for clamped-clamped Timoshenko CNT.

Note that by letting e_0=0, the higher order clamped-clamped beam's eigenmodes based on Timoshenko beam theory are obtained.

To get $\hat{W}_n(x)$ and $\hat{\Psi}_n(x)$ as well as the associated eigenfrequencies, the coefficients α_n and β_n have to be obtained. Using the previous mathematical developments, the transcendental equation (3.45) is rearranged as:

$$-2+\left(\cos(\alpha_n L)-\frac{1}{2}\left(\frac{S_{11}}{S_{22}}-\frac{S_{22}}{S_{11}}\right)\sin(\alpha_n L)\right)e^{\beta_n L}+\left(\cos(\alpha_n L)+\frac{1}{2}\left(\frac{S_{11}}{S_{22}}-\frac{S_{22}}{S_{11}}\right)\sin(\alpha_n L)\right)e^{-\beta_n L}=0 \quad (3.64)$$

The numerical solution of this nonlinear algebraic equation allows one to get the higher order α_n and then the C-C CNT natural frequencies.

Asymptotic C-C case.

Based on some mathematical developments the asymptotic eigenmodes and frequencies are obtained. For very large n the asymptotic coefficients α_n and β_n are explicitly given by:

$$\alpha_n \approx \frac{n\pi}{L};\ \ \beta_n \approx \Upsilon=\left(\frac{1}{\Omega_0+(e_0 a)^2}\right)^{1/2}; \quad (3.65)$$

These new relationships allow one to get α_n at very higher orders without any numerical computation. This asymptotic value can be used in equation (3.31) in order to get the associated very higher natural frequencies.

The very higher other eigenmodes for clamped-clamped CNT are then given by:

$$\hat{W}_n(x)=a_n\left\{\cos(\alpha_n x)+\Gamma_{nCC}\sin(\alpha_n x)-e^{-(\Upsilon x)}\right.$$
$$\left.-\frac{\cos(\alpha_n L)+S_{22}/S_{11}\sin(\alpha_n L)-e^{(-\Upsilon L)}}{2(S_{22}/S_{11})\sin(\alpha_n L)/\left(e^{(\Upsilon L)}-e^{-(\Upsilon L)}\right)+1}\frac{e^{(\Upsilon x)}-e^{-(\Upsilon x)}}{e^{(\Upsilon L)}-e^{-(\Upsilon L)}}\right\} \quad (3.66)$$

$$\hat{\Psi}_n(x)=a_n S_{11}\left\{\Gamma_{nCC}\cos(\alpha_n x)-\sin(\alpha_n x)-S_{22}/S_{11}e^{(-\Upsilon x)}\right.$$
$$\left.+\frac{\cos(\alpha_n L)+S_{22}/S_{11}\sin(\alpha_n L)-e^{(-\Upsilon L)}}{2\sin(\alpha_n L)/\left(e^{(\Upsilon L)}-e^{(-\Upsilon L)}\right)}\frac{e^{(\Upsilon x)}+e^{(-\Upsilon x)}}{e^{(\Upsilon L)}-e^{(-\Upsilon L)}}\right\} \quad (3.67)$$

$$\text{where}\quad \Gamma_{n\,CC}=\frac{S_{22}\left(\cosh(\Upsilon L)-\cos(\alpha_n L)\right)}{S_{22}\sin(\alpha_n L)+S_{11}\sinh(\Upsilon L)}, \quad (3.68)$$

3.2.2 Clamped-simply supported CNT.

Based on the same mathematical developments, the Timoshenko higher eigenmodes associated to clamped-simply supported CNT are given by the following relationships.

$$\hat{W}_n(x) = a_n \left(\cos(\alpha_n x) + \Gamma_{n\,CS}\ \sin(\alpha_n x) - e^{(-\beta_n x)} \right.$$
$$\left. + \frac{\cos(\alpha_n L) + S_{22}/S_{11} \sin(\alpha_n L) + (\alpha_n/\beta_n)^2 e^{(-\beta_n L)}}{-2\sin(\alpha_n L)/\left(e^{(\beta_n L)} - e^{-(\beta_n L)}\right) + (\alpha_n/\beta_n)^2 S_{11}/S_{22}} \frac{S_{11}}{S_{22}} \frac{e^{(\beta_n x)} - e^{-(\beta_n x)}}{e^{(\beta_n L)} - e^{-(\beta_n L)}} \right), \tag{3.69}$$

$$\hat{\Psi}_n(x) = a_n S_{11} \left(\Gamma_{n\,CS}\ \cos(\alpha_n x) - \sin(\alpha_n x) - \frac{S_{22}}{S_{11}} e^{(-\beta_n x)} \right.$$
$$\left. - \frac{\cos(\alpha_n L) + S_{22}/S_{11} \sin(\alpha_n L) + (\alpha_n/\beta_n)^2 e^{(-\beta_n L)}}{-2\sin(\alpha_n L)/\left(e^{(\beta_n L)} - e^{-(\beta_n L)}\right) + (\alpha_n/\beta_n)^2 S_{11}/S_{22}} \frac{e^{(\beta_n x)} + e^{-(\beta_n x)}}{e^{(\beta_n L)} - e^{-(\beta_n L)}} \right), \tag{3.70}$$

Using similar mathematical development as for the C-C case, equation (3.50) is rearranged as:

$$\left(\tan(\alpha_n L) + \frac{S_{11}}{S_{22}} \right) e^{(\beta_n L)} + \left(\tan(\alpha_n L) - \frac{S_{11}}{S_{22}} \right) e^{-(\beta_n L)} = 0 \tag{3.71}$$

For large n, this equation has to be numerically solved to get first the related α_n and β_n and then the associated natural frequencies.

Asymptotic C-S case.

For very higher orders the asymptotic coefficients α_n are explicitly given by:

$\alpha_n = n\pi / L;$

The corresponding eigenmodes are :

$$\hat{W}_n(x) = a_n \left(\cos(\alpha_n x) + \Gamma_{n\,CS}\ \sin(\alpha_n x) - e^{(-\Upsilon x)} \right.$$
$$\left. + \frac{\cos(\alpha_n L) + S_{22}/S_{11} \sin(\alpha_n L) + (\alpha_n/\Upsilon)^2 e^{(-\Upsilon L)}}{-2(S_{22}/S_{11})\sin(\alpha_n L)/\left(e^{(\Upsilon L)} - e^{-(\Upsilon L)}\right) + (\alpha_n/\Upsilon)^2} \frac{e^{(\Upsilon x)} - e^{-(\Upsilon x)}}{e^{(\Upsilon L)} - e^{-(\Upsilon L)}} \right), \tag{3.72}$$

$$\hat{\Psi}_n(x) = a_n S_{11} \left(\Gamma_{n\,CS}\ \cos(\alpha_n x) - \sin(\alpha_n x) - \frac{S_{22}}{S_{11}} e^{(-\Upsilon x)} \right.$$
$$\left. - \frac{\cos(\alpha_n L) + S_{22}/S_{11} \sin(\alpha_n L) + (\alpha_n/\Upsilon)^2 e^{(-\Upsilon L)}}{-2\sin(\alpha_n L)/\left(e^{(\Upsilon L)} - e^{-(\Upsilon L)}\right) + (\alpha_n/\Upsilon)^2 S_{11}/S_{22}} \frac{e^{(\Upsilon x)} + e^{-(\Upsilon x)}}{e^{(\Upsilon L)} - e^{-(\Upsilon L)}} \right), \tag{3.73}$$

where $$\Gamma_{n\,CS} = \frac{S_{22}\left(\cosh(\Upsilon L) - \cos(\alpha_n L)\right)}{\left(S_{22}\beta_n \sin(\alpha_n L) + S_{11}\alpha_n \sinh(\Upsilon L)\right)} \tag{3.74}$$

3.2.3 Cantilever CNT.

Based on the same mathematical manipulations, the following higher eigenmodes associated to cantilever CNTs are given by the following relationships.

$$\hat{W}_n(x) = a_n \left(\cos(\alpha_n x) + \Gamma_{n\,CF}\ \sin(\alpha_n x) - e^{(-\beta_n x)} \right.$$
$$\left. + \frac{\cos(\alpha_n L) + S_{22}/S_{11} \sin(\alpha_n L) - \left(\alpha_n/\beta_n\right)^2 e^{(-\beta_n L)}}{-2\sin(\alpha_n L)/\left(e^{(\beta_n L)} - e^{-(\beta_n L)}\right) + \left(\alpha_n/\beta_n\right)^2 S_{11}/S_{22}} \frac{S_{11}}{S_{22}} \frac{e^{(\beta_n x)} - e^{-(\beta_n x)}}{e^{(\beta_n L)} - e^{-(\beta_n L)}} \right), \tag{3.75}$$

$$\hat{\Psi}_n(x) = a_n S_{11} \left(\Gamma_{n\,CF}\ \cos(\alpha_n x) - \sin(\alpha_n x) - \frac{S_{22}}{S_{11}} e^{(-\beta_n x)} \right.$$
$$\left. - \frac{\cos(\alpha_n L) + S_{22}/S_{11} \sin(\alpha_n L) + \left(\alpha_n/\beta_n\right)^2 e^{(-\beta_n L)}}{-2\sin(\alpha_n L)/\left(e^{(\beta_n L)} - e^{-(\beta_n L)}\right) + \left(\alpha_n/\beta_n\right)^2 S_{11}/S_{22}} \frac{e^{(\beta_n x)} + e^{-(\beta_n x)}}{e^{(\beta_n L)} - e^{-(\beta_n L)}} \right), \tag{3.76}$$

The associated higher order transcendental equation is given by:

$$\beta_n{}^3 - \frac{S_{11}}{S_{22}} \alpha_n{}^3 + \frac{1}{2} \left(\alpha_n{}^2 \beta_n \left(1 - \frac{\beta_n}{\alpha_n} \frac{S_{11}}{S_{22}} \right) \cos(\alpha_n L) - \alpha_n{}^2 \beta_n \left(\frac{S_{11}}{S_{22}} + \frac{\beta_n}{\alpha_n} \right) \sin(\alpha_n L) \right) e^{(\beta_n L)}$$
$$+ \frac{1}{2} \left(\alpha_n{}^2 \beta_n \left(1 - \frac{\beta_n}{\alpha_n} \frac{S_{11}}{S_{22}} \right) \cos(\alpha_n L) + \alpha_n{}^2 \beta_n \left(\frac{S_{11}}{S_{22}} + \frac{\beta_n}{\alpha_n} \right) \sin(\alpha_n L) \right) e^{-(\beta_n L)} = 0, \tag{3.77}$$

For large n, this nonlinear equation is solved here by the Newton Raphson algorithm to get the related α_n and β_n and then the C-F CNT eigenfrequencies.

Asymptotic C-F case.

The asymptotic coefficients α_n and the corresponding asymptotic eigenmodes are explicitly given by:

$$\alpha_n = (2n+1)\,\pi/2L$$

$$\hat{W}_n(x) = a_n \left(\cos(\alpha_n x) + \Gamma_{n\,CF}\ \sin(\alpha_n x) - e^{(-\Upsilon x)} \right.$$
$$\left. + \frac{\cos(\alpha_n L) + S_{22}/S_{11} \sin(\alpha_n L) - \left(\alpha_n/\Upsilon\right)^2 e^{(-\Upsilon L)}}{-2\left(S_{22}/S_{11}\right)\sin(\alpha_n L)/\left(e^{(\Upsilon L)} - e^{-(\Upsilon L)}\right) + \left(\alpha_n/\Upsilon\right)^2} \frac{e^{(\Upsilon x)} - e^{-(\Upsilon x)}}{e^{(\Upsilon L)} - e^{-(\Upsilon L)}} \right), \tag{3.78}$$

$$\hat{\Psi}_n(x) = a_n S_{11} \left(\Gamma_{n\,CF}\ \cos(\alpha_n x) - \sin(\alpha_n x) - \frac{S_{22}}{S_{11}} e^{(-\Upsilon x)} \right.$$
$$\left. - \frac{\cos(\alpha_n L) + S_{22}/S_{11} \sin(\alpha_n L) + \left(\alpha_n/\Upsilon\right)^2 e^{(-\Upsilon L)}}{-2\sin(\alpha_n L)/\left(e^{(\Upsilon L)} - e^{-(\Upsilon L)}\right) + \left(\alpha_n/\Upsilon\right)^2 S_{11}/S_{22}} \frac{e^{(\Upsilon x)} + e^{-(\Upsilon x)}}{e^{(\Upsilon L)} - e^{-(\Upsilon L)}} \right), \tag{3.79}$$

These higher and very higher eignemodes and the associated eigenfrequancy analytical relationships allow are one to investigate the vibration characteristics of Timoshenko CNT at very large frequency ranges. It has to be noted that in the studied cases, these new higher and

very higher eigenmodes are numerically stable and well-conditioned. They can be used as a basis for dynamic analysis of CNT at any needed frequency range.

3.3 Euler-Bernoulli model

The previous mathematical developments are also adapted here for higher order vibration characteristics of Eluler-Bernoulli beams. This leads to new analytical relationships of higher order Euler-Bernoulli eigenmodes $\hat{W}_n^E$ and associated eigenfrequencies for various CNT boundary conditions. The smaller order characteristics are recalled in the appendix. A.

3.3.1 Clamped-clamped CNT.

The associated mode shape functions of clamped–clamped CNT based on the Euler-Bernoulli model are given by equation (A.3.14). Using the same mathematical procedure as previously equation (A.15) is rewritten as:

$$\Gamma^E{}_{n\,CC} = \Lambda^E{}_{n\,CC} - \alpha_{nE}/\beta_{nE}, \tag{3.80}$$

where

$$\Lambda^E{}_{n\,CC} = -\frac{\cos(\alpha_{nE}L) - \beta_{nE}/\alpha_{nE}\sin(\alpha_{nE}L) - e^{(-\beta_{nE}L)}}{\sin(\alpha_{nE}L) - \alpha_{nE}/\beta_{nE}\sinh(\beta_{nE}L)}, \tag{3.81}$$

Using (81) and Eq. (A.14) the following eigenmodes are obtained

$$\hat{W}_n^E(x) = a_{2n}\left[\cos(\alpha_{nE}x) + \Gamma^E_{n\,CC}\,\sin(\alpha_{nE}x) - e^{(-\beta_{nE}x)} - \Lambda^E_{n\,CC}\frac{\alpha_{nE}}{\beta_{nE}}\sinh(\beta_{nE}x)\right], \tag{3.82}$$

This new form of $\hat{W}_n^E(x)$ is an exact form for the nth mode shape.

Making some mathematical simplifications, Eq. (3.81) can be modified so that it is numerically well-conditioned for large n. Let us rewrite:

$$\Lambda^E_{nCC}\frac{\alpha_{nE}}{\beta_{nE}}\sinh(\beta_{nE}x) = \frac{\left(\cos(\alpha_{nE}L) - \beta_{nE}/\alpha_{nE}\sin(\alpha_{nE}L) - e^{(-\beta_{nE}L)}\right)}{2\sin(\alpha_{nE}L)/\left(e^{(\beta_{nE}L)} - e^{-(\beta_{nE}L)}\right) - \alpha_{nE}/\beta_{nE}}\frac{\alpha_{nE}}{\beta_{nE}}\frac{e^{(\beta_{nE}x)} - e^{-(\beta_{nE}x)}}{e^{(\beta_{nE}L)} - e^{-(\beta_{nE}L)}}, \tag{3.83}$$

Additionally, equations (3.82) and (3.83) are combined to give the following new deflection eigenmodes at higher orders:

$$\hat{W}_n^E(x) = a_{2n}\left(\cos(\alpha_{nE}x) + \Gamma^E{}_{n\,CC}\,\sin(\alpha_{nE}x) - e^{(-\beta_{nE}x)}\right.$$
$$\left. + \frac{\cos(\alpha_{nE}L) - \beta_{nE}/\alpha_{nE}\sin(\alpha_{nE}L) - e^{(-\beta_{nE}L)}}{2\sin(\alpha_{nE}L)/\left(e^{(\beta_{nE}L)} - e^{-(\beta_{nE}L)}\right) - \alpha_{nE}/\beta_{nE}}\frac{\alpha_{nE}}{\beta_{nE}}\frac{e^{(\beta_{nE}x)} - e^{-(\beta_{nE}x)}}{e^{(\beta_{nE}L)} - e^{-(\beta_{nE}L)}}\right), \tag{3.84}$$

Note that by letting e_0=0, the higher order clamped-clamped beam's eigenmodes based on Euler-Bernoulli beam theory are also obtained.

Again, to get $\hat{W}_n^E(x)$ as well as the associated eigenfrequencies, the coefficients α_{nE} and β_{nE} have to be obtained. They can be obtained by numerically solving the C-C transcendental equation (A.3.16). For well conditioning at large n, equation (A.3.16) is rearranged as:

$$-2+\left(\cos(\alpha_{nE}L)+\frac{1}{2}\left(\frac{\alpha_{nE}}{\beta_{nE}}-\frac{\beta_{nE}}{\alpha_{nE}}\right)\sin(\alpha_{nE}L)\right)e^{\beta_{nE}L}$$
$$+\left(\cos(\alpha_{nE}L)-\frac{1}{2}\left(\frac{\alpha_{nE}}{\beta_{nE}}-\frac{\beta_{nE}}{\alpha_{nE}}\right)\sin(\alpha_{nE}L)\right)e^{-\beta_{nE}L}=0 \qquad (3.85)$$

where $\beta_{nE}=\Upsilon^E\left(\frac{1}{1+\mathrm{X}_n^{\ E}}\right)^{1/2}=\Upsilon^E\left(1+\sum_{k=1}^{N}\frac{1}{i!}\left(\prod_{k=0}^{k-1}\left(-\frac{1}{2}-j\right)\right)\mathrm{X}_n^{\ Ek}\right)+o(X_n^{\ EN})$.

and $\Upsilon^E=\frac{1}{(e_0a)};\ \mathrm{X}_n^{\ E}=\left(\frac{1}{(e_0a)^2\alpha_n}\right);$

The numerical solution of this nonlinear algebraic equation allows one to numerically obtain the higher order α_{nE} .

Asymptotic C-C case.

For very large n, the asymptotic coefficient α_{nE} is, in this case, explicitly given by:

$$\alpha_{nE}=n\pi/L; \qquad (3.86)$$

These new relationships allow one to get α_{nE} at higher and very higher vibration orders of the clamped CNT based on Euler- Bernoulli model.

$$\hat{W}_n^E(x)=a_{2n}\left(\cos(\alpha_{nE}x)+\Gamma^E_{\ n\,CC}\ \sin(\alpha_{nE}x)-e^{(-\Upsilon^E x)}\right.$$
$$\left.+\frac{\cos(\alpha_{nE}L)+\left(\Upsilon^E/\alpha_{nE}\right)^2-e^{(-\Upsilon^E L)}}{2\sin(\alpha_{nE}L)/\left(e^{(\Upsilon^E L)}-e^{-(\Upsilon^E L)}\right)-\left(\alpha_{nE}/\Upsilon^E\right)^3}\left(\frac{\alpha_{nE}}{\Upsilon^E}\right)\frac{e^{(\Upsilon^E x)}-e^{-(\Upsilon^E x)}}{e^{(\Upsilon^E L)}-e^{-(\Upsilon^E L)}}\right), \qquad (3.87)$$

3.3.2 Clamped-simply supported CNT.

The Euler-Bernoulli higher eigenmodes associated to clamped-simply supported CNT are given by the following relationships.

$$\hat{W}_n^E(x)=a_{2n}\left(\cos(\alpha_{nE}x)+\Gamma_{\ n\,CS}\ \sin(\alpha_{nE}x)-e^{(-\beta_{nE}x)}\right.$$
$$\left.-\frac{\cos(\alpha_{nE}L)-\beta_{nE}/\alpha_{nE}\sin(\alpha_{nE}L)+\left(\alpha_{nE}/\beta_{nE}\right)^2e^{(-\beta_{nE}L)}}{-2\sin(\alpha_{nE}L)/\left(e^{(\beta_{nE}L)}-e^{-(\beta_{nE}L)}\right)-\left(\alpha_{nE}/\beta_{nE}\right)^3}\left(\frac{\alpha_{nE}}{\beta_{nE}}\right)\frac{e^{(\beta_{nE}x)}-e^{-(\beta_{nE}x)}}{e^{(\beta_{nE}L)}-e^{-(\beta_{nE}L)}}\right), \qquad (3.88)$$

where α_{nE} are solutions of the following transcendental equations.

$$\left(\tan(\alpha_{nE}L)-\frac{\alpha_{nE}}{\beta_{nE}}\right)e^{\beta_{nE}L}+\left(\tan(\alpha_{nE}L)+\frac{\alpha_{nE}}{\beta_{nE}}\right)e^{-\beta_{nE}L}=0; \tag{3.89}$$

Asymptotic C-S case.

The asymptotic coefficient α_{nE} is explicitly given in this case by:

$$\alpha_{nE}L=(2n+1)\pi/2; \tag{3.90}$$

The associated very higher eigenmode is:

$$\hat{W}_n^E(x)=a_{2n}\left(\cos(\alpha_{nE}x)+\Gamma^E{}_{n\,CS}\,\sin(\alpha_{nE}x)-e^{(-\Upsilon^E x)}\right.$$
$$\left.-\frac{\cos(\alpha_{nE}L)-\Upsilon^E/\alpha_{nE}\sin(\alpha_{nE}L)+\left(\alpha_{nE}/\Upsilon^E\right)^2 e^{(-\Upsilon^E L)}}{-2\sin(\alpha_{nE}L)/\left(e^{(\Upsilon^E L)}-e^{-(\Upsilon^E L)}\right)-\left(\alpha_{nE}/\Upsilon^E\right)^3}\left(\frac{\alpha_{nE}}{\Upsilon^E}\right)\frac{e^{(\Upsilon^E x)}-e^{-(\Upsilon^E x)}}{e^{(\Upsilon^E L)}-e^{-(\Upsilon^E L)}}\right), \tag{3.91}$$

3.3.3 Cantilever CNT.

For the considered clamped-free boundary conditions the higher eigenmodes associated to cantilever CNT are given by the following relationships.

$$\hat{W}_n^E(x)=a_{2n}\left(\cos(\alpha_{nE}x)+\Gamma_{n\,CS}\,\sin(\alpha_{nE}x)-e^{(-\beta_{nE}x)}\right.$$
$$\left.-\frac{\cos(\alpha_{nE}L)-\beta_{nE}/\alpha_{nE}\sin(\alpha_{nE}L)-\left(\alpha_{nE}/\beta_{nE}\right)^2 e^{(-\beta_{nE}L)}}{-2\sin(\alpha_{nE}L)/\left(e^{(\beta_{nE}L)}-e^{-(\beta_{nE}L)}\right)+\left(\alpha_{nE}/\beta_{nE}\right)^3}\left(\frac{\alpha_{nE}}{\beta_{nE}}\right)\frac{e^{(\beta_{nE}x)}-e^{-(\beta_{nE}x)}}{e^{(\beta_{nE}L)}-e^{-(\beta_{nE}L)}}\right), \tag{3.92}$$

The associated higher order transcendental equation is given by:

$$(e_0a)^2\,\alpha_{nE}\beta_{nE}\sin(\alpha_{nE}L)\sinh(\beta_{nE}L)+2\cos(\alpha_{nE}L)\cosh(\beta_{nE}L)-2=0; \tag{3.93}$$

Asymptotic C-F case.

For very large n, the asymptotic coefficient α_{nE} is explicitly given by:

$$\alpha_{nE}=n\pi/L \tag{3.94}$$

and the associated eigenmode is:

$$\hat{W}_n^E(x)=a_{2n}\left(\cos(\alpha_{nE}x)+\Gamma^E{}_{n\,CS}\,\sin(\alpha_{nE}x)-e^{(-\Upsilon^E x)}\right.$$
$$\left.-\frac{\cos(\alpha_{nE}L)-\Upsilon^E/\alpha_{nE}\sin(\alpha_{nE}L)+\left(\alpha_{nE}/\Upsilon^E\right)^2 e^{(-\Upsilon^E L)}}{-2\sin(\alpha_{nE}L)/\left(e^{(\Upsilon^E L)}-e^{-(\Upsilon^E L)}\right)-\left(\alpha_{nE}/\Upsilon^E\right)^3}\left(\frac{\alpha_{nE}}{\Upsilon^E}\right)\frac{e^{(\Upsilon^E x)}-e^{-(\Upsilon^E x)}}{e^{(\Upsilon^E L)}-e^{-(\Upsilon^E L)}}\right), \tag{3.95}$$

The presented new analytical models for the CNT Timoshenko and Euler-Bernoulli higher order eigenmodes and eigenfrequencies allow one to investigate the higher order free vibration

characteristics of CNT under the considered boundary conditions. The higher order natural frequencies are obtained by numerically solving the presented nonlinear transcendental equation associated to the considered boundary conditions using the Newton-Raphson algorithm. The small scale length effects on the eigenfrequencies and eigenmodes can be analyzed. Based on these new analytical eigenmodes, the modal analysis at higher frequencies can be analyzed by selecting the needed eigenmodes and the frequency range under considerations. The Timoshenko and the Euler-Bernoulli higher order eigenmodes and eigenfrequencies of classical beam can be obtained from these analytical models by simply neglecting the small scales parameter e_0 (e_0=0).

4. Numerical analysis

For the assessment of the developed analytical models numerical investigations are also elaborated based on the differential quadrature method (DQM). Timoshenko and Euler-Bernoulli beam models are used for numerical comparisons. This method, akin to approximate the derivative of a function at any location by a linear summation of all the function values along a mesh line [25]. The procedure the DQ application lies in the determination of the weighting coefficients. The continuous solution is approximated by the functional values at discrete points. In the present paper Chebyshev-Gauss-Lobatto quadrature points are used [25]

$$y_i = \frac{1}{2}\left[1-\cos\left(\frac{i-1}{N-1}\pi\right)\right] \text{ for } i = 1,2,3,.....N, \tag{3.96}$$

where $y_i = \frac{x_i}{L}$ and N is the number of grid points in the domain [0, L].

For a function *f(y),* DQ approximation of the m^{th} order derivative at the i^{th} point is given by:

$$f(y,t) = \sum_{m=1}^{N} l_m(y) f(y_m,t) \tag{3.97-a}$$

$$\frac{d^m}{dy^m}\begin{Bmatrix} f(y_1) \\ f(y_2) \\ \vdots \\ f(y_n) \end{Bmatrix} = C_{ij}^m \begin{Bmatrix} f(y_1) \\ f(y_2) \\ \vdots \\ f(y_n) \end{Bmatrix}, \; i, j = 1,2,...,N \tag{3.97-b}$$

in which $l_m(y)$ are the Lagrange interpolation polynomials and C_{ij}^m represent the weighting coefficients given by [25].

$$f(y_1) = \frac{M(y)}{(y - y_i)M_1(y_i)}, \ for\, i = 1,2,...,n \qquad (3.97-c)$$

$$M(y) = \prod_{j=1}^{n}(y - y_j) \qquad (3.97-d)$$

$$M_1(y_i) = \prod_{j=1,\, j\neq i}^{n}(y_i - y_j), \ for\ i, j = 1,2,...,n \qquad (3.97-e)$$

$$C_{ij}^1 = \frac{M_1(y_i)}{(y_i - y_j)M_1(y_i)} \quad for\ i, j = 1,2,...,n;\ i \neq j \qquad (3.97-f)$$

$$H_{ii}^1 = -\sum_{\substack{j=1 \\ j\neq i}}^{n} H_{ij}^1 \qquad (3.97-g)$$

The higher derivative m[th] can be calculated as:

$$H_{ij}^m = m\left(H_{ij}^1 H_{ii}^{m-1} - \frac{H_{ij}^{m-1}}{x_i - x_j} \right) \qquad for\, i = 1,2,...,n,\ j \neq i \qquad (3.97-h)$$

$$H_{ii}^m = -\sum_{\substack{j=1 \\ j\neq i}}^{n} H_{ij}^m \qquad (3.97-i)$$

The discrete classical boundary conditions at x=0 and x=L using the DQ method can be written as:

$$W_1 = 0 \qquad (3.98-a)$$

$$\sum_{k=1}^{n} C_{1k}^{n0} W_k = 0 \qquad (3.98-b)$$

$$W_n = 0 \qquad (3.98-c)$$

$$\sum_{k=1}^{n} C_{nk}^{n1} W_k = 0 \qquad (3.98-d)$$

where n_0 and n_1 may be taken as either 1, 2 or 3 and $W_k = W(y_k)$. Choosing the values of n_0 and n_l can give the following classical boundary conditions:

n_0 =2; n_1 =2 simply supported

n_0 =1; n_1 =1 clamped-clamped

n_0 =1; n_1 =2 clamped-simply supported

n_0 =1; n_l =3 clamped-free

n_0 =2; n_l =3 free-free

Applying Equations (3.97) and (3.98) to equations (3.16-3.17), one obtains the following ordinary differential system:

$$\left(\sum_{k=1}^{N} C_{ik}^{2} W_k + \sum_{k=1}^{N} C_{ik}^{1} \Psi_k\right) = \zeta\,\chi\left(I_1 \ddot{W}_i - \mu^2 \sum_{k=1}^{N} C_{ik}^{2} \ddot{W}_k\right) \qquad (3.99-a)$$

$$\chi \sum_{k=1}^{N} C_{ik}^{2} \Psi_k - \left(\sum_{k=1}^{N} C_{ik}^{1} W_k + \Psi_k\right) = \xi\left(I_1 \ddot{\Psi}_i - \mu^2 \sum_{k=1}^{N} C_{ik}^{2} \ddot{\Psi}_k\right) \qquad (3.99-b)$$

where $\chi = \dfrac{EI}{KAGL^2}, \zeta = \dfrac{m_0 L^4}{EI}, \xi = \dfrac{m_2}{KAG}, \mu = \dfrac{e_0 a}{L}$ and $W_k = W(y_k),\ \Psi_k = \Psi(y_k)$

The moment and shear force given by equations (3.14) and (3.15) are rewritten as:

$$\bar{M} = \sum_{k=1}^{N} C_{ik}^{1} \Psi_k + \mu^2\left(\zeta \sum_{k=1}^{N} C_{ik}^{1} \ddot{\Psi}_k + \xi \ddot{W}_k\right) \qquad (3.100-a)$$

$$\bar{Q} = \Psi_k + \sum_{k=1}^{N} C_{ik}^{1} W_k + \mu^2 \xi \sum_{k=1}^{N} C_{ik}^{1} \ddot{W}_k \qquad (3.100-b)$$

$\bar{M}$ and $\bar{Q}$ will be used for the assumed boundary conditions.

For harmonic motion the ordinary differential system (3.99) can be written in the following eigenvalue problem:

$$\left([K] + \Omega^2 [M]\right)\{Z\} = 0 \qquad (3.101)$$

where $\{Z\}$ denotes the unknown dynamic displacement vector defined by:

$$\{Z\} = \left\{ W_i^1\ W_i^2 \cdots W_i^N \,\middle|\, \Psi_i^1\ \Psi_i^2 \cdots \Psi_i^N \right\}^T \qquad (3.102)$$

and [K] and [M] are the stiffness and mass matrices respectively.

The assumed boundary conditions can also be expressed in a matrix form as:

$$[K_B]\{Z^*\} + [K_S]\{\bar{Z}\} = 0 \qquad (3.103)$$

where $\{Z^*\} = \left\{ W_i^1, W_i^N \,\middle|\, \Psi_i^1, \Psi_i^N \right\}^T$ and $\{\bar{Z}\} = \left\{ W_i^2\ W_i^4 \cdots W_i^{N-1} \,\middle|\, \Psi_i^2\ \Psi_i^4 \cdots \Psi_i^{N-1} \right\}^T$. $[K_B]$ and $[K_S]$ are 4×4 and $4\times(2N-4)$ matrices respectively. Similarly, for harmonic motion Eq. (3.103) can be rewritten as:

$$[K_D]\{Z^*\} + [\bar{K}]\{\bar{Z}\} - \Omega^2 [\bar{M}]\{\bar{Z}\} = 0 \qquad (3.104)$$

Coupling equations (3.103) and (3.104), the final eigenvalue problem to be numerically solved is given by:

$$\left\{[\bar{K}] - [K_D][K_B]^{-1}[K_S] - \Omega^2 [\bar{M}]\right\}\{\bar{Z}\} = 0 \qquad (3.105)$$

where $[\bar{K}]$ and $[\bar{M}]$ are $(2N-4)\times(2N-4)$ matrices respectively

These matrices are formulated for Timoshenko and Euler-Bernoulli CNT models. The previously considered boundary conditions are adopted for numerical comparisons. Based on

this numerical procedure, numerical analysis of CNT free vibration at small, higher as well as very higher orders is investigated.

5. Numerical results and discussions

In this paper, analytical solutions and numerical ones based on the DQM are obtained for small, higher and very higher CNT vibration eigenmodes and associated eigenfrequencies. The numerical results are presented using effective properties of carbon nanotubes, Timoshenko and Euler-Bernoulli models. The following geometrical and material properties are used.

$\rho = 2300\,kg/m^3,\ E = 1000\,Gpa,\ \nu = 0.19,\ G = 420Gpa,\ d = 1\times10^{-9}m,$

$h = 0.34\times10^{-9}m,\quad A = 7.85\times10^{-19}m^2,\quad I = \dfrac{\pi d^4}{64} = 4{,}91\times10^{-38}m^4,$

$ks = 0.877,\quad \Omega_0 = EI/ksAG,\quad a = 1.5\times10^{-9}m,\quad L = 20\,a,$

Let us denote by $\omega^T_{n\,NL}$ *and* $\omega^E_{n\,NL}$ the nth Timoshenko and Bernoulli nonlocal frequency respectively and $\omega^T_{n\,L}$ *and* $\omega^E_{n\,L}$ the nth local frequency ones. W_n and W_{nE} denote respectively the nth eigenmode obtained by the Timoshenko and Euler-Bernoulli beam models.

Figures 3.1 show the frequency ratios $\omega^T_{n\,NL}/\omega^E_{n\,L}$ and $\omega^E_{n\,NL}/\omega^E_{n\,L}$ corresponding to the first to the 100th eigenmodes for various boundary conditions and various values of the nonlocal parameter e_0. These results are obtained by the presented analytical relationships using the Newton- Raphson algorithm. For higher modes, these frequencies tend to constant values depending on e_0. It can be seen that the frequency ratios decrease by increasing of the nonlocal parameter e_0 and the parameter n and tend to the given asymptotic values. The obtained results are similar to those obtained by Reddy and Pang [8]. Their investigation was limited to the first modes that are numerically stable. In this paper the developed methodological approach is illustrated for small, higher as well as for very higher orders S-S, C-C, C-F and C-S CNT. The small length (e_0a) effects on the Euler-Bernoulli frequency ratio $\omega^E_{n\,NL}/\omega^E_{n\,L}$ for the first twelfth modes are presented in Figures 3.2 for S-S, C-C, C-F and C-S boundary conditions. These first modes are commonly used by many authors and the same results are also obtained by Wang and Varadan [6]. It is clearly shown in these figures that the small effect is obvious for higher modes.

Numerical results, based on the DQ method, are investigated for the considered boundary conditions. Small and higher modes orders are considered and the convergence of the results is tested with respect to modes number. The obtained results for non-dimensional vibration

frequencies computed for different N nodes are shown in Tables 3.1 and 3.2. Exact analytical solutions for small orders, obtained from [15], or by our equations (3.45) and (3.55), are also given for comparison. Excellent agreement has been achieved between the presented analytical solution and the obtained numerical ones. It is seen from table 3.1 that when the grid point number reaches N=12 the DQM gives accurate predictions for the first vibration frequencies. For higher orders, large number of grid points is needed as presented in table 3.2. The presented analytical results are obtained based on the developed analytical relationships (3.45, 3.55) and (3.64, 3.77). The convergence of the DQM results to the analytical ones with respect to the grid points number N is observed in table 3.2. It has to be noted that the needed CPU time for DQM is rapidly increasing by increasing N. Various other numerical tests are elaborated for different boundary conditions and showed the assessment of the presented analytical relationships as well as the convergence of the DQM predictions with respect to grid points number.

For eigenmodes, regularized and non-regularized (classical) formulations will be used as well as the DQM numerical predictions for small and higher orders. Based on the Timoshenko beam model, regularized, classical and numerical first eleventh modes W_n (n=1, 2,…, 11) are presented in figure 3.3 for e_0=0 and C-C case. It is observed that the regularized (3.60) and DQM numerical predictions agree very well with the exact classical results (3.42). Based on these three procedures, the higher modes W_n (n=12,13,14,15) are plotted in figure 3.4. It is shown that the classical modes are numerically unstable in the vicinity of x=L, and this disturbing instability is increasing by increasing the mode number. This instability is also demonstrated in figure 3.5 for the C-C CNT models eigenmodes with e_0=0.2. Based on the Bernoulli beam model the developed classical, regularized, and numerical predictions obtained by the DQM are used and compared. The obtained results for the 12^{th} to the 15^{th} C-C beam eigenmodes (e_0=0) are presented in figure 3.6 and show instability behavior near x=L. This mode instability is more pronounced when Euler–Bernoulli model is used as clearly shown in figure 3.7 for C-C CNT. The instability of higher classical eigenmodes of C-S and C-F CNT and beams are also met and not presented here for the sake of brevity. This disturbing instability is heavily increasing by increasing the order mode number. These results demonstrate clearly the inaccuracy of the classical eigenmode formulations. The regularized and numerical DQM higher order modes (12^{th} to 24^{th}) based on Timoshenko model are presented in figure 3.8 for C-C beams (e_0=0) and in figure 3.9 for the 20^{th} to 24^{th} C-C CNT, (e_0=0.4). Figure 3.8 shows that for e_0=0 the regularized eigenmodes 12 to 24 are stable and

well-conditioned. It is clearly shown that the present regularized relationships give accurate predictions for higher order mode shapes. The regularized relationships and the DQM predictions are very well compared for various other boundary conditions at different higher others. The regularized eigenmodes are well conditioned and stable at all tested case.

The effect of the internal characteristic parameter e_0 on the uncorrected 20^{th} C-C CNT Timoshenko eigenmode is presented in figure 3.10. It is demonstrated that for e_0=0, W_{20T} is hardly unstable and this instability disappears by increasing e_0 for 0 to 1. The same stabilizing effect is observed for the 20^{th} uncorrected Euler-Bernoulli as presented in figure 3.11. Based on the presented corrected eigenmodes, the new 20^{th} C-C CNT eigenmodes corresponding to Timoshenko and Bernoulli models are presented in figures 3.12 and 3.13 for various values of e_0 (e_0= 0, 0.2, 0.4, 0.6, 0.8, 1). Different other benchmark tests are investigated and demonstrated the well-conditioning and stability of the presented eigenmodes at higher orders.

The aspect ratio d/L effect on the frequency ratio $\omega^T_{n\,NL} / \omega^E_{n\,L}$ is presented in figure 3.10 for the first to the hundredth eigenmodes of a C-C CNT (e_0= 0.33). For slender CNT, the Bernoulli and Timoshenko models lead to the same results and a large difference can be observed by increasing d/L. The Timoshenko frequencies are decreasing by increasing the aspect ratio d/L. For higher modes, the frequencies tend asymptotically to constant values depending on the e_0 and d/L for each considered boundary condition.

6. Conclusion

Based on the nonlocal elasticity theory, Timoshenko and Euler-Bernoulli beam models and the differential quadrature method the vibration characteristics of single walled CNT are modeled for small to very higher eigenmodes. New mathematical relationships for higher and very higher eigenmodes and frequencies are elaborated for CNT with various boundary conditions. The analytical and DQM numerical results are well compared at small, higher and very higher orders. The small scale effect on the frequencies and eigenmodes at small and very higher modes is deeply analyzed. The numerical instability problem, limiting the classical mode formulations, is overcome. The developed analytical relationships for eigenmodes at higher orders are well conditioned and numerically stable and can then be used as a basis for modal analysis at any required frequency range.

REFERENCES

[1] R.F Gibson, E.O, Ayorind and Y.F Wen, Vibration of carbon nanotubes and their composites: A review, Composites Sciences and Technology 67, 2007, pp. 1-28.

[2] A.C. Eringen, On differential equation of nonlocal elasticity and solution, J. Appl. Phys. 54, 1983, pp. 4703-4710.

[3] A.C. Eringen and DGB Edelen, On nonlocal elasticity, Int. J. Eng. Science10, 1972, pp. 233–248

[4] J. Peddieson, R. Buch Anan and R. P. Mc Nitt, Application of nonlocal continuum models to nanotechnology, Int. J. Eng. Sci, 41, 2003, pp. 305-312.

[5] L. J. Sudak, Column buckling of multiwalled carbon nanotubes using nonlocal continuum mechanics, J. Appl. Phys. 94, 2003, pp. 7281-7287.

[6] Q. Wang and V. K. Varadan, Vibration of carbon nanotube studied using nonlocal continuum Mechanics, Smart Mater. Struct. 15, 2006, pp. 659-666.

[7] A. Benzair, A. Tounsi, A. Besseghier, H. Heireche N. Moulay and L. Boumia, The thermal effect on vibration of single-walled carbon nanotubes using nonlocal Timoshenko beam theory, J. Appl. Phys.41, 2008, pp. 1-10.

[8] J. N. Reddy and S.D. Pang, Nonlocal continuum theory of beams for the analysis of carbon nanotubes, J. Appl. Phys.103, 2008, pp. 1-16.

[9] Y. Zhen and B. Fang, Thermal–mechanical and nonlocal elastic vibration of single-walled carbonnanotubes conveying fluid, J. Comp. Mater. Science, 2010, pp. 1–7.

[10] T. Murmu, S.C. Pradhan, Thermal effects on the stability of embedded carbon nanotubes, J. Comp. Mater. Science 47, 2010, pp. 721–726.

[11] S. Narendar, S. Gopalakrishnan, Nonlocal scale effects on wave propagation in multi-walled carbon nanotubes, J. comp. Mater. Science 47, 2009, pp. 526-538.

[12] H. Cai and X. Wang, Effect of initial stress on the transverse wave propagation in carbon nanotubes based on Timoshenko laminated beam models, Ist. of Phys. Pub. Nanoteshnology 17, 2006, pp. 45-53.

[13] S. Adali, Variational Principles for transversely vibrating multiwalled carbon nanotubes based on nonlocal Euler-Bernoulli beam model, Nano Letters V. 9, No. 5, 2009, pp. 1737-1741.

[14] I. Kucuk, I.S. Sadek and S. Adali, Variational Principles for Multiwalled Carbon Nanotubes Undergoing Vibrations Based on Nonlocal Timoshenko Beam Theory, Journal of Nanomaterials, 2010, pp. 1-7.

[15] P. Lu, H. P. Lee and C. Lu, Dynamic properties of flexural beams using a nonlocal elasticity model, Journal of Applied Physics 99, 073510, 2006, pp 1-9

[16] B. Arash, R. Ansari, Evaluation of nonlocal parameter in the vibrations of single-walled carbon nanotubes with initial strain, J. Phys. Vol. 42, 2010, pp. 2058-2064.

[17] J. Yoon, C. Q. Ru, and A. Mioduchowski, Terahertz vibration of short carbon nanotubes modeled as Timoshenko beams, J. Appl. Mechanics Vol. 72, 2005, pp. 10-17.

[18] Ö. Civalek, Ç. Demir and B. Akgöz, Free vibration and bending analyses of cantilever microtubules based on nonlocal continuum model. Mathematical and Computational Applications., Vol. 15, No. 2, 2010, pp. 289-298.

[19] J. Loya, J. López-Puente, R. Zaera, and J. Fernández-Sáez, Free transverse vibrations of cracked nano beams using a nonlocal elasticity model, Journal of Applied Physics 105, 2009, pp. 1-9.

[20] A. Azrar, L. Azrar and A. A. Aljinaidi, Length scale effect analysis on vibration behavior of single walled Carbon NanoTubes with arbitrary boundary conditions, Revue de Mécanique Appliquée et Théorique, Vol. 2 pp 475-484, 2011.

[21] A. Azrar, L. Azrar, A. A. Aljinadi and M. Hamadiche, Dynamics instability analysis of multi-walled carbon nanotubes conveying fluid, J. Advanced Materials Research Vol. 682, pp 153-160, 2013

[22] S. C. Pradhan and T. Murmu, Application of nonlocal elasticity and DQM in the flapwise bending vibration of a rotating nanocantilever, J. Physica E 42 pp 1944–1949, 2010

[23] Maziar Janghorban, Amin Zare, Free vibration analysis of functionally graded carbon nanotubes with variable thickness by differential quadrature method, J. Physica E 43 pp 1602–1604, 2011

[24] S. Narendar, Differential quadrature based nonlocal flap wise bending vibration analysis of rotating nanotube with consideration of transverse shear deformation and rotary inertia, J. Applied Mathematics and Computation 219, pp 1232–1243, 2012

[25] C. Shu, Differential Quadrature and its Application in Engineering, Spinger, London, 2000.

Appendix A

Based on the Euler-Bernoulli beam model, the associated nonlocal resultant shear force Q^E and moment M^E are given by [20]:

$$Q^E = m_2 \frac{\partial^3 w^E}{\partial x \partial t^2} - \frac{\partial}{\partial x}\left(EI \frac{\partial^2 w^E}{\partial x^2} \right) + (e_0 a)^2 \frac{\partial}{\partial x}\left(m_0 \frac{\partial^2 w^E}{\partial t^2} - m_2 \frac{\partial^4 w^E}{\partial x^2 \partial t^2} - q \right), \quad (A.3.1)$$

$$M^E = -EI \frac{\partial^2 w^E}{\partial x^2} + (e_0 a)^2 \left(-q + m_0 \frac{\partial^2 w^E}{\partial t^2} - m_2 \frac{\partial^4 w^E}{\partial x^2 \partial t^2} \right), \quad (A.3.2)$$

where w^E is the associated transverse displacement.

The associated equation of motion based on the Euler-Bernoulli beam theory is given by the following fourth order partial differential equation.

$$EI \frac{\partial^4 w^E}{\partial x^4} - (e_0 a)^2 \frac{\partial^2}{\partial x^2}\left(m_0 \frac{\partial^2 w^E}{\partial t^2} - m_2 \frac{\partial^4 w^E}{\partial x^2 \partial t^2} - q \right) + q = -m_0 \frac{\partial^2 w^E}{\partial t^2} + m_2 \frac{\partial^4 w^E}{\partial x^2 \partial t^2}, \quad (A.3.3)$$

For harmonic motion, on gets:

$$\left(EI - m_2 (e_0 a)^2 \omega^2 \right) \frac{d^4 W^E}{dx^4} + \left(m_2 \omega^2 + (e_0 a)^2 m_0 \omega^2 \right) \frac{d^2 W^E}{dx^2} - m_0 \omega^2 W^E \quad (A.3.4)$$

This equation is rewritten as:

$$p^E \frac{d^4 W^E}{dx^4} + q^E \frac{d^2 W^E}{dx^2} - r^E W^E = 0 \quad (A.3.5)$$

$$p^E = EI - (e_0 a)^2 m_2 \omega^2, \; q^E = m_2 \omega^2 + (e_0 a)^2 m_0 \omega^2, \quad r^E = m_0 \omega^2 \quad (A.3.6)$$

The associated Euler-Bernoulli frequency is simply given by:

$$\omega_E{}^2 = \alpha_E{}^4 \left(\frac{EI}{(m_0 + m_2 \alpha_E{}^2)\,(1 + (e_0 a)^2 \alpha_E{}^2)} \right), \quad (A.3.7)$$

$$\alpha_E{}^2 = \frac{q^E + \sqrt{q^{E2} + 4 p^E r^E}}{2 p^E}, \qquad \beta_E{}^2 = \frac{-q^E + \sqrt{q^{E2} + 4 p^E r^E}}{2 p^E} \quad if \quad p^E r^E > 0 \quad (A.3.8)$$

More simply, for m_2=0:

$$\omega_E{}^2 = \alpha^4 \left(\frac{EI}{m_0\,(1 + (e_0 a)^2 \alpha_E{}^2)} \right), \quad (A.3.9)$$

$$\beta_E{}^2 = \alpha_E{}^2 \left(\frac{1}{1 + (e_0 a)^2 \alpha_E{}^2} \right), \quad (A.3.10)$$

1. Simply supported CNT

For simply supported boundary conditions, one gets:

$$W_n^E(x) = a_1 \sin(\alpha_{nE} x), \qquad \alpha_{nE} = n\pi / L, \quad (A.3.11)$$

if $m_2 = 0$, $\omega_n^E = \left(\frac{n\pi}{L}\right)^2 \left(\frac{EI}{m_0 (1+(e_0 a)^2 (n\pi/L)^2)}\right)^{1/2}$, (*A*.3.12)

if $m_2 \neq 0$, $\omega_n^E = \left(\frac{n\pi}{L}\right)^2 \left(\frac{EI}{(m_0 + m_2 (n\pi/L)^2)\,(1+(e_0 a)^2 (n\pi/L)^2)}\right)^{1/2}$, (*A*.3.13)

2. Clamped-Clamped CNT

When the two edges of the beam are clamped, the resulting mode shapes are given by:

$$W_n^E(x) = a_2 \left[\cos(\alpha_{nE} x) - \cosh(\beta_{nE} x) + \Gamma^E{}_{n\,CC} \left(\sin(\alpha_{nE} x) - \frac{\alpha_{nE}}{\beta_{nE}} \sinh(\beta_{nE} x) \right) \right], \quad (A.3.14)$$

$$\Gamma^E{}_{n\,CC} = \frac{\beta_{nE} \left(\cosh(\beta_{nE} L) - \cos(\alpha_{nE} L)\right)}{\beta_{nE} \sin(\alpha_{nE} L) - \alpha_{nE} \sinh(\beta_{nE} L)}, \quad (A.3.15)$$

where (α_{nE}, β_{nE}) verify the following transcendental equation:

$$2 - 2\cos(\alpha_{nE} L)\cosh(\beta_{nE} L) - \left(\frac{\alpha_{nE}}{\beta_{nE}} - \frac{\beta_{nE}}{\alpha_{nE}}\right) \sin(\alpha_{nE} L) \sinh(\beta_{nE} L) = 0 \quad (A.3.16)$$

3. Clamped simply supported CNT

For clamped simply supported conditions, the resulting mode shapes are given by:

$$W_n^E(x) = a_2 \left[\cos(\alpha_{nE} x) - \cosh(\beta_{nE} x) + \Gamma^E{}_{n\,CS} \left(\sin(\alpha_{nE} x) - \frac{\alpha_{nE}}{\beta_{nE}} \sinh(\beta_{nE} x) \right) \right], \quad (A.3.17)$$

$$\Gamma^E{}_{n\,CS} = \frac{\beta_{nE} \left(\cosh(\beta_{nE} L) - \cos(\alpha_{nE} L)\right)}{\left(\beta_{nE}{}^2 \sin(\alpha_{nE} L) - \alpha_{nE}{}^2 \sinh(\beta_{nE} L)\right)} \quad (A.3.18)$$

where (α_{nE}, β_{nE}) verify the following transcendental equation :

$$\beta_{nE} \tan(\alpha_{nE} L) - \alpha_{nE} \tanh(\beta_{nE} L) = 0 \quad (A.3.19)$$

4. Cantilever CNT

For a cantilever CNT, the clamped free boundary conditions considered are:

$$W^E(0) = 0; \quad \frac{dW^E(0)}{dx} = 0; \quad Q^E(L) = 0; \text{ and } M^E(L) = 0; \quad (A.3.20)$$

The associated Euler-Bernoulli modes are:

$$W_n^E(x) = a_2 \left[\cosh(\beta_{nE} x) - \cos(\alpha_{nE} x) + \Gamma^E{}_{n\,CF} \left(\sin(\alpha_{nE} x) + \frac{\alpha_{nE}}{\beta_{nE}} \sinh(\beta_{nE} x) \right) \right], \quad (A.3.21)$$

$$\Gamma^E{}_{n\,CF} = \frac{\beta_{nE} \left(\beta_{nE}{}^2 \cos(\alpha_{nE} L) + \alpha_{nE}{}^2 \cosh(\beta_{nE} L)\right)}{\left(\alpha_{nE}{}^3 \sinh(\beta_{nE} L) - \beta_{nE}{}^3 \sin(\alpha_{nE} L)\right)}, \quad (A.3.22)$$

where (α_{nE}, β_{nE}) verify the following transcendental equation:

$$(e_0 a)^2 \alpha_{nE} \beta_{nE} \sin(\alpha_{nE} L) \sinh(\beta_{nE} L) + 2\cos(\alpha_{nE} L)\cosh(\beta_{nE} L) - 2 = 0, \quad (A.3.23)$$

Simply Supported- Simply Supported

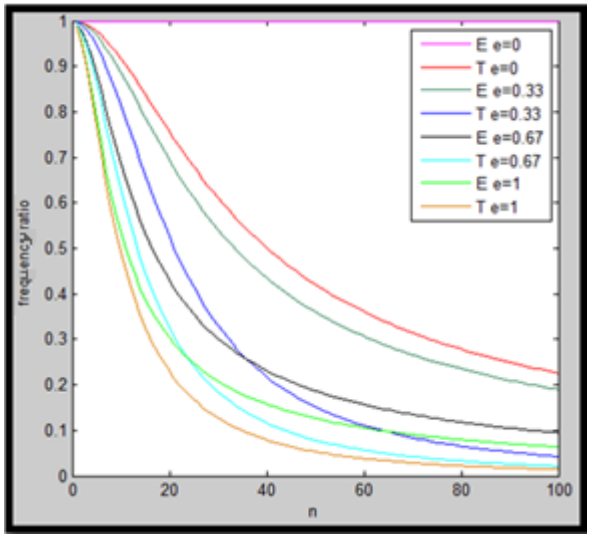

b) Clamped - Clamped

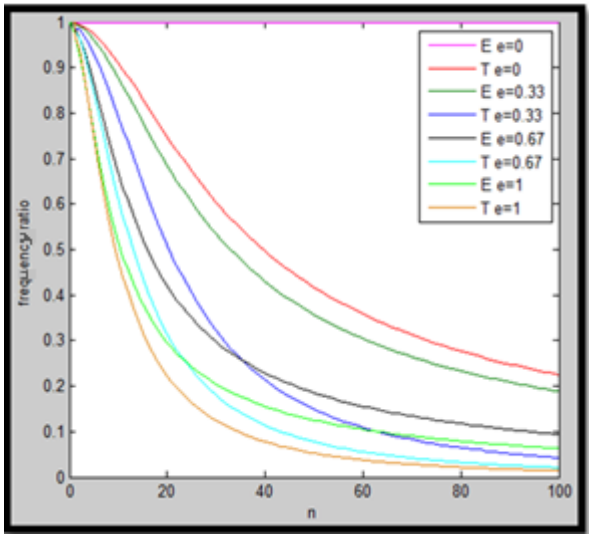

c) Clamped- free

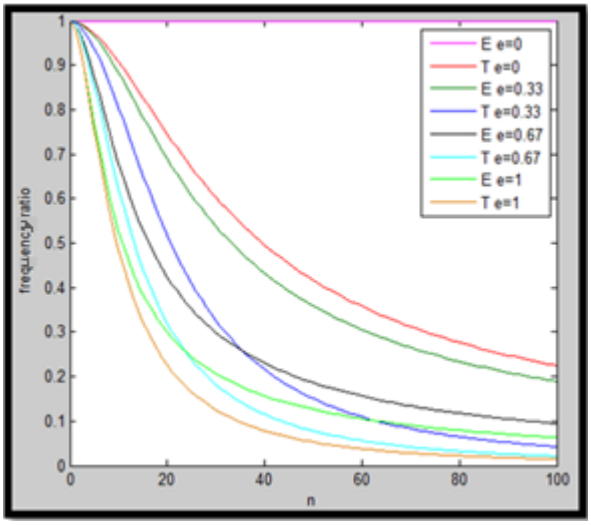

d) Clamped-Simply Supported

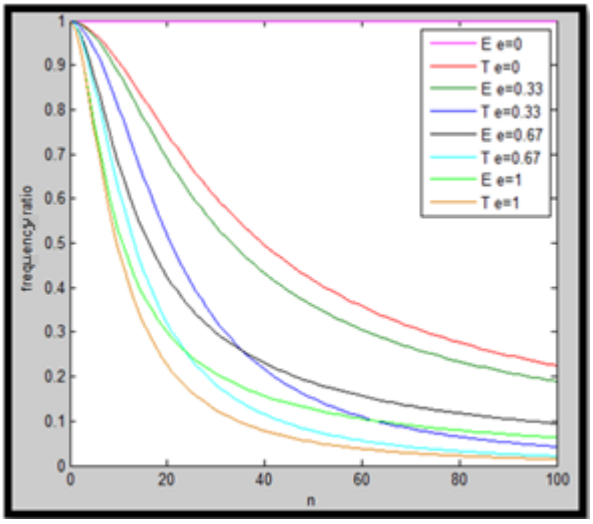

Figure 3.1 Frequency ratios $\omega^{T}_{n\,NL}/\omega^{E}_{n\,L}$ and $\omega^{E}_{n\,NL}/\omega^{E}_{n\,L}$ as a function of the order n, corresponding to S-S, C-C, S-C and C-F SWCNT for various values of the nonlocal parameter e_0

Simply Supported- Simply Supported

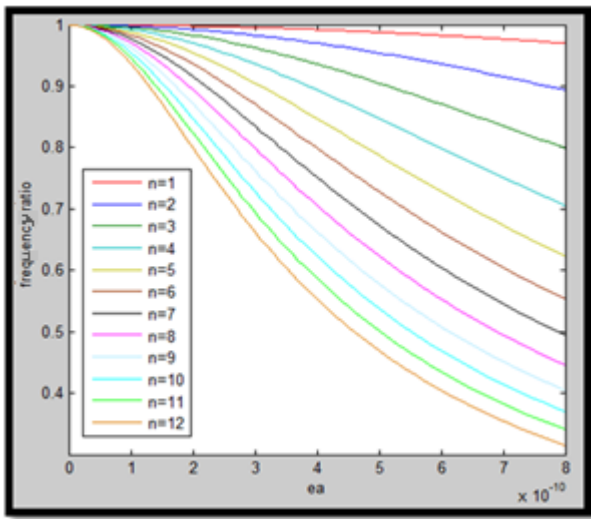

b) Clamped-clamped

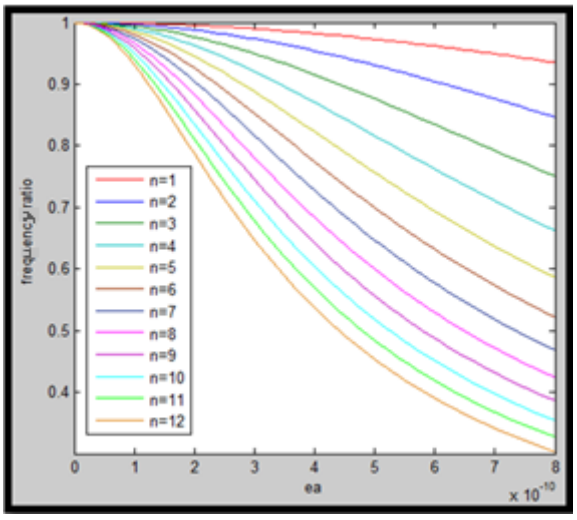

c) Clamped-Simply Supported

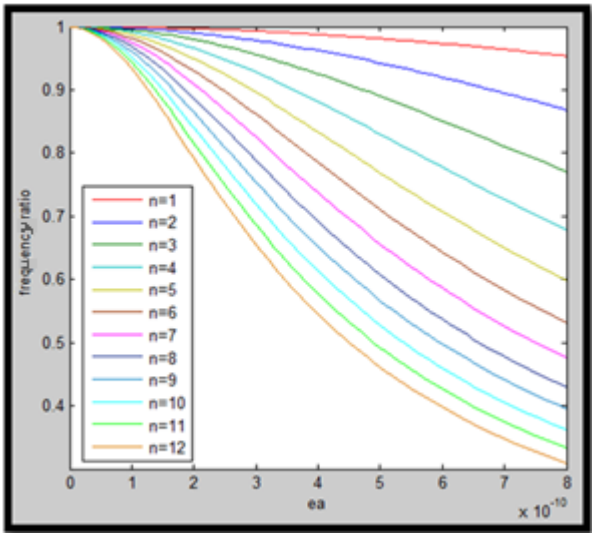

d) Clamped-Free

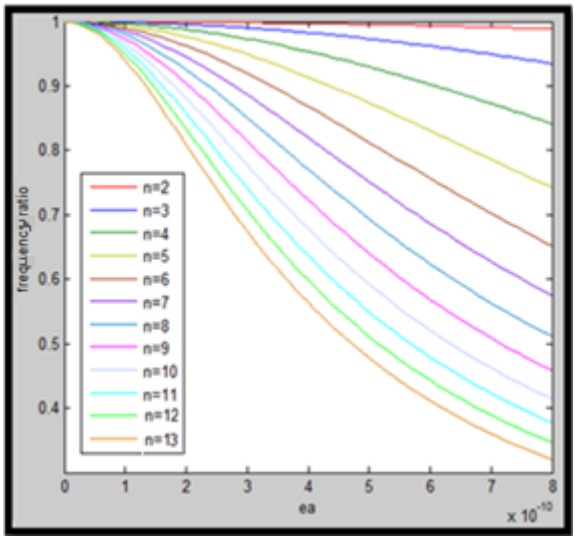

Figure 3.2 Small length scale (e_0a) effect on the frequency ratio $\omega^E_{n\,NL} / \omega^E_{n\,L}$ of a SWCNT with L=10 nm

Table 3.1 First fourth the frequency parameters $\omega_{n\ NL}^{T*}$ for clamped and cantilever nanobeams with L/d =10^{-4} obtained numerically by DQM using N nodes

e_0a/L	$\omega_{n\ NL}^{T}$	Clamped-clamped					
	n	[15]	N=8	N=12	N=15	N=20	N=30
$e_0a/L=0$	n=1	4.7300	4.7368	4.7300	4.7300	4.7300	4.7300
	n=2	7.8532	7.9717	7.8534	7.8532	7.8532	7.8532
	n=3	10.9956	10.6812	10.9863	10.9955	10.9956	10.9956
	n=4	14.1372	11.7298	14.0488	14.1399	14.1372	14.1372
$e_0a/L=0.2$	n=1	4.2766	4.2676	4.2752	4.2762	4.2766	4.2766
	n=2	6.0352	6.1116	6.0283	6.0336	6.0349	6.0352
	n=3	7.3840	6.7816	7.3569	7.3795	7.3834	7.3840
	n=4	8.4624	6.8467	8.3394	8.4576	8.4611	8.4623
e_0a/L	$\omega_{n\ NL}^{T}$	Cantilever					
	n		N=8	N=12	N=15	N=20	N=30
$e_0a/L=0$	n=1	1.8751	1.8761	1.8751	1.8751	1.8751	1.8751
	n=2	4.6941	4.6107	4.6939	4.6941	4.6941	4.6941
	n=3	7.8548	7.5400	7.8489	7.8549	7.8548	7.8548
	n=4	10.9955	11.0158	11.2010	10.9990	10.9955	10.9955
$e_0a/L=0.2$	n=1	1.8920	1.8986	1.8928	1.8917	1.8920	1.8919
	n=2	4.1925	4.0877	4.1880	4.1940	4.1922	4.1925
	n=3	6.0674	5.8157	6.0690	6.0656	6.0679	6.0672
	n=4	7.3617	7.4646	7.5376	7.3703	7.3616	7.3619

Table 3.2 Higher order frequency parameters $\omega_{n\ NL}^{T}$ obtained analytically and numerically by DQM using N nodes

e_0a/L	$\omega_{n\ NL}^{T}$	Clamped-clamped				
$e_0a/L=0.2$	n	Analytical, Eq. (64)	N=90	N=100	N=110	N=120
	n=60	30.9450	31.4477	30.8290	30.9461	30.9450
	n=70	33.3880	37.2244	34.5860	33.2404	33.4059
	n=80	35.8834	56.7734	41.2376	37.7929	35.8535
	n=90	40.9929	--	63.0971	45.2682	41.0368
	n=100	49.3407	--	--	69.4259	49.3112
	$\omega_{n\ NL}^{T}$	Cantilever				
$e_0a/L=0.2$	n	Analytical, Eq. (77)	N=90	N=100	N=110	N=120
	n=20	17.6497	17.6497	17.6497	17.6497	17.6497
	n=30	21.6508	21.6509	21.6508	21.6508	21.6508
	n=40	25.0139	25.0140	25.0139	25.0139	25.0139
	n=50	27.9731	28.0128	27.9716	27.9732	27.9732
	n=60	30.6467	--	--	--	30.6470

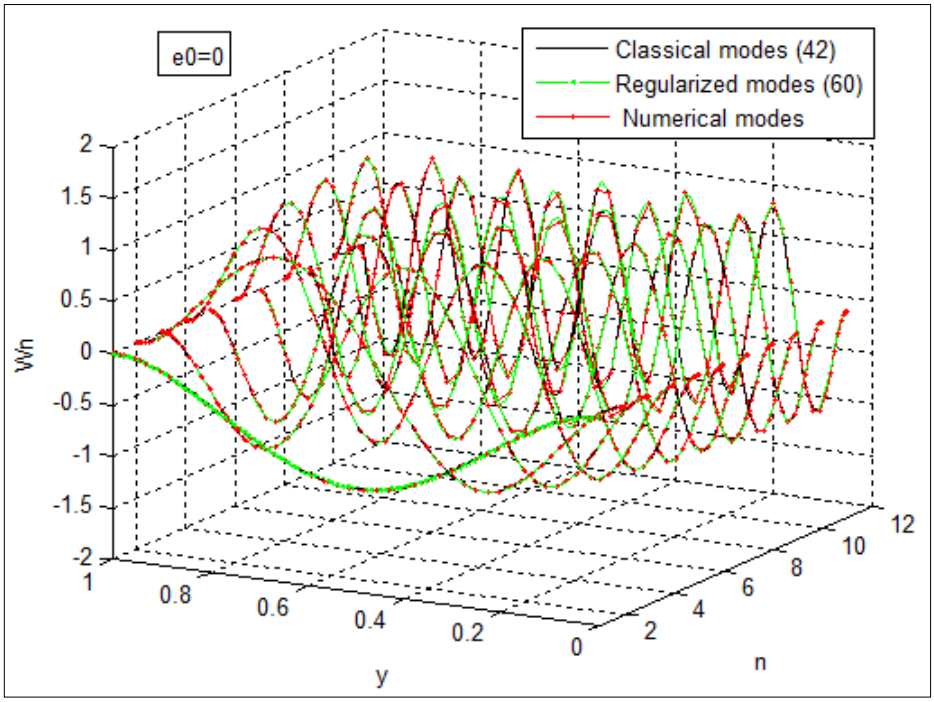

Figure 3.3 Comparison of the first eleventh Timoshenko vibration mode shapes W_n (n=1-11) predictions of a C-C CNT mass normalized for e_0=0, obtained by equations (3.42) and (3.60) and by DQM.

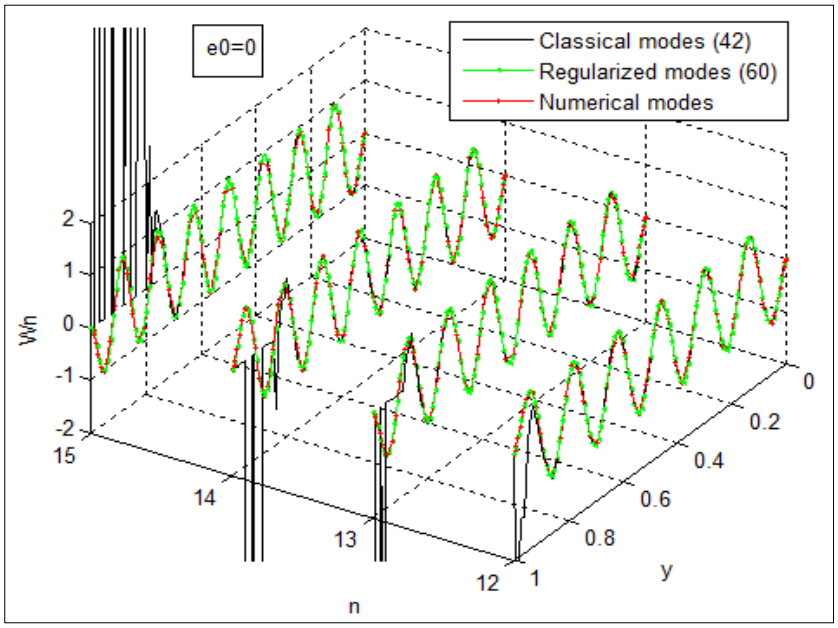

Figure 3.4 Higher vibration Timoshenko mode shapes Wn (n=12-15) of C-C CNT mass normalized for e0=0, obtained by equations (3.42) and (3.60) and by DQM.

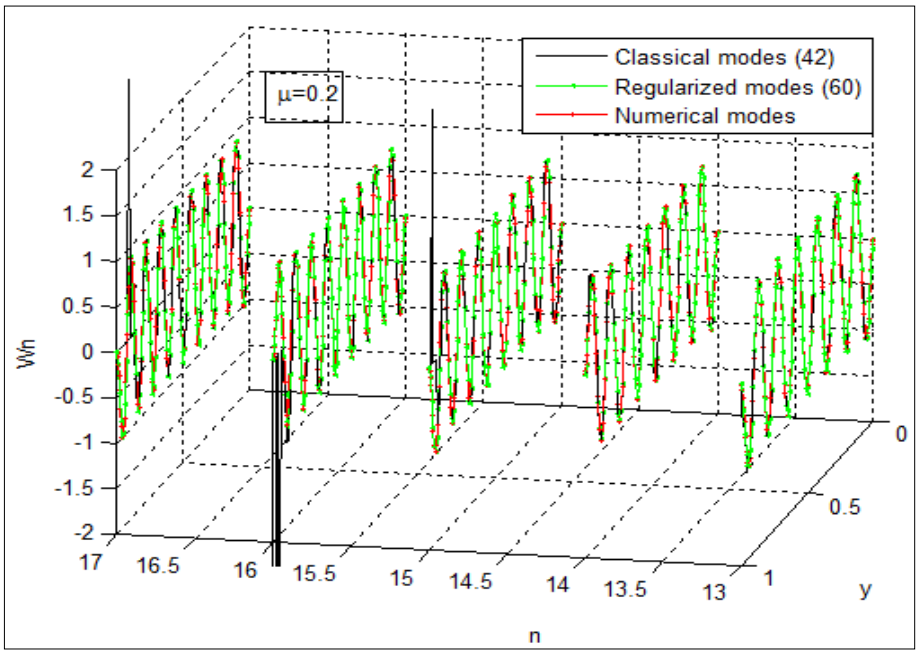

Figure 3.5 Uncorrected higher vibration Timoshenko mode shapes Wn (n=13-17) of C-C CNT mass normalized for e0=0.2, obtained by equations (3.42) and (3.60) and by DQM.

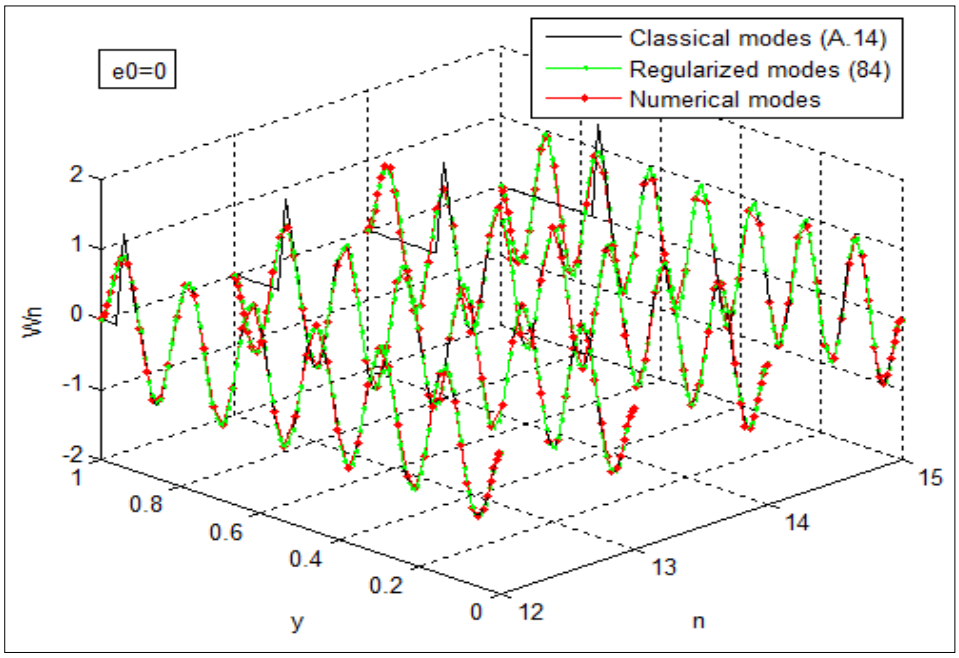

Figure 3.6 Uncorrected higher vibration Euler-Bernoulli mode shapes WnEB (n=12-15) of C-C CNT mass normalized for e0=0, obtained by equations (A.14) and (3.84) and by DQM.

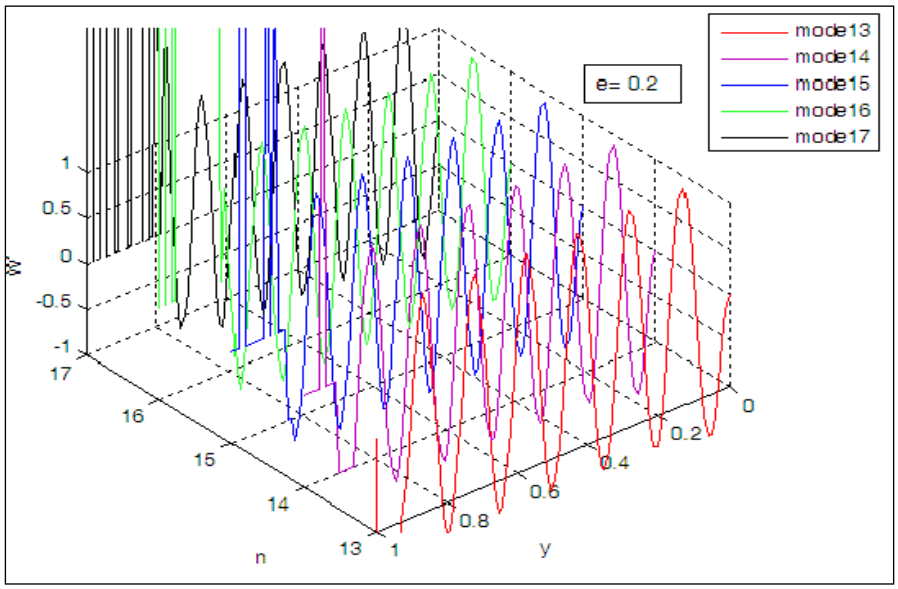

Figure 3.7 Uncorrected higher vibration Euler-Bernoulli mode shapes W_{nEB} (n=13-17) of C-C CNT mass normalized for e_0=0.2, obtained by equation (3.82)

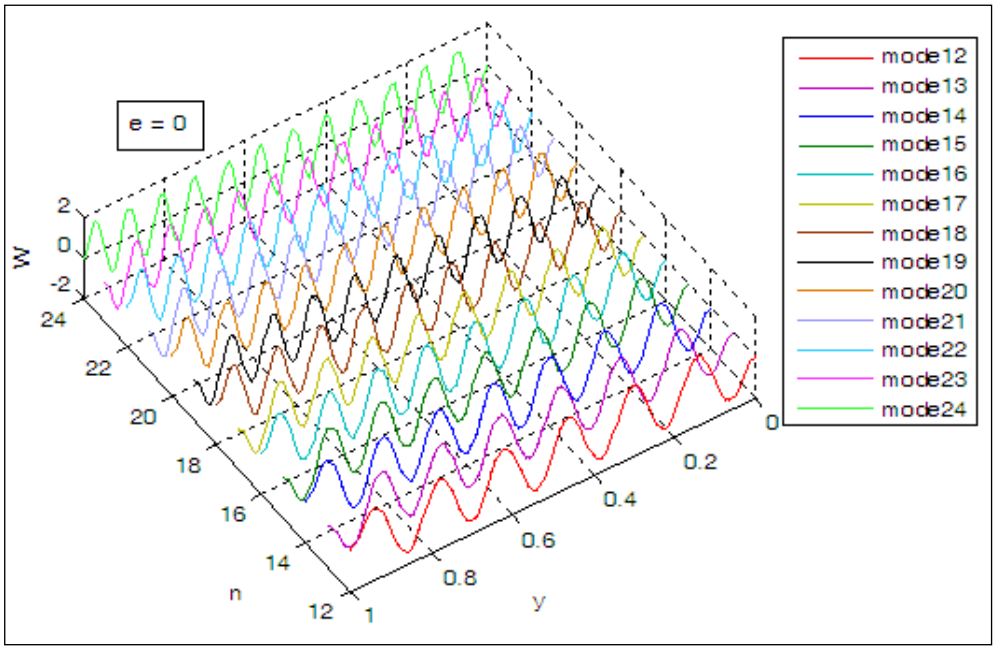

Figure 3.8 Regularized higher vibration Timoshenko mode shapes W_n (n=12 to 24) of C-C CNT mass normalized for e_0=0, obtained by equation (3.60).

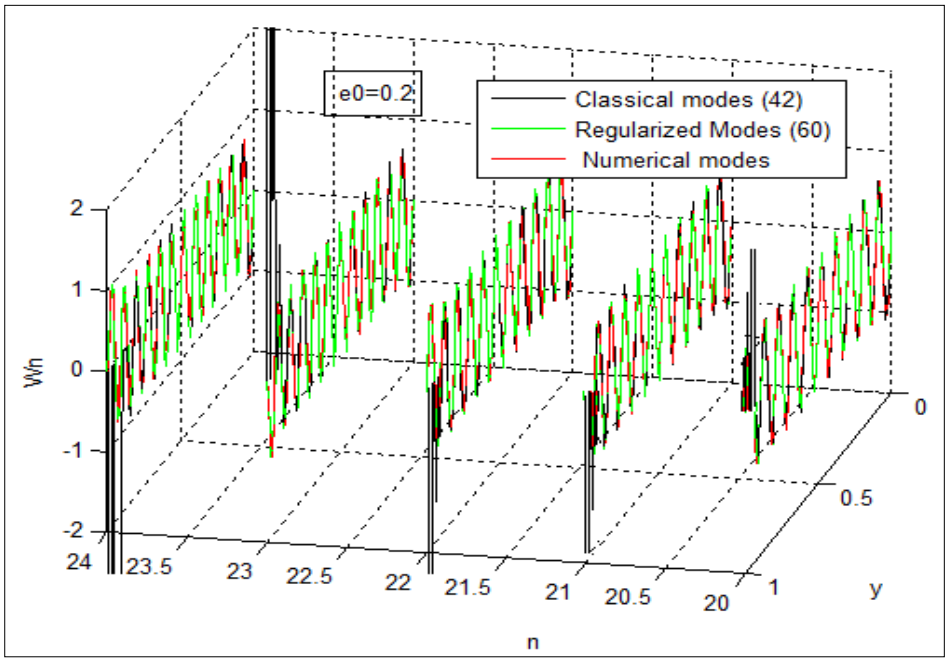

Figure 3.9 Regularized and DQM-numerical higher vibration Timoshenko mode shapes W_n (n=20-24) of C-C CNT mass normalized for e_0=0.4

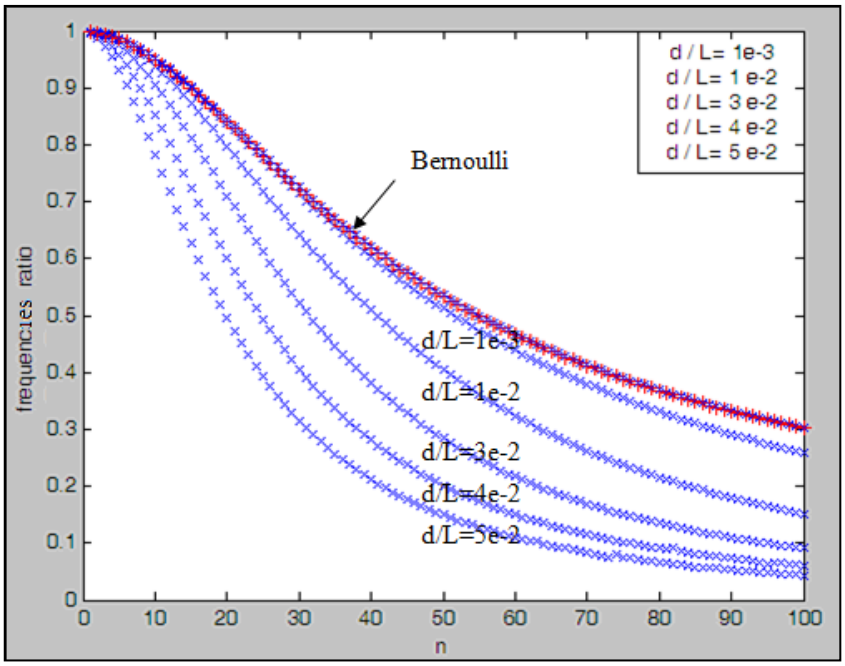

Figure 3.10 Variation of frequencies ratio $\omega^{T}_{n\,NL} / \omega^{E}_{n\,L}$ of C-C CNT with different modes n=1 to 100 for various aspect ratios d/L, (e_0=0.33)

Chapter IV:

Dynamic and parametric instabilities numerical modeling of multi-walled carbon nanotubes conveying pulsating and viscous fluid

Abstract

The dynamic and parametric instabilities of single-walled carbon nanotubes (CNTs) conveying pulsating and viscous fluid embedded in an elastic medium are modeled and numerically investigated. The partial differential equation of motion based on the nonlocal elasticity theory, Euler Bernoulli beam's model and fluid-tube interaction is given. Based on the differential quadrature method, complex eigenmodes and associated eigenfrequencies are investigated with respect to the flow velocity as well as to the other considered physical parameters. Multimodal formulation based on real and complex modes are presented in the frequency and time domains. Models are elaborated for dynamic instabilities such as divergence and flutter as well as for parametric instability behaviors. The influences of the nonlocal parameter, the fluid pulsation and viscosity, the viscoelastic coefficient and the thermal effects on the dynamic behaviors of the CNT-fluid system are analyzed. Instability boundaries and interaction between the dynamic and parametric instabilities are investigated.

This work has been submitted the international Journal: **Composite structure, 2014**

Title: **Numerical modeling of dynamic and parametric instabilities of single-walled carbon nanotubes conveying pulsating and viscous fluid**

Authors: **A. Azrar, L. Azrar and A. A. Aljinaidi**

1. Introduction

Carbon nanotubes (CNT) conveying fluid have become ones of the most important structures in nanotechnology. They may be used at micro or nano-levels for fluid storage, fluid transport, drug delivery, micro-resonator, molecular reactors as well as for many nano-fluidic device applications. In such applications, the dynamic characteristics, such as natural frequencies, eigenmodes, stability, critical flow velocity and parametric instability zones are of considerable interest. During the last years, a significant amount of research has been elaborated for the dynamic behavior of CNT. A review paper on vibration of CNT and their composites has been published by Gibson et al. [1]. Lee and Chang [2] studied the vibration analysis of a viscous fluid conveying single walled carbon nanotube embedded in an elastic medium. Wang [3] proposed the vibration analysis of fluid-conveying nanotubes with consideration of surface effects. Eringen's nonlocal elasticity [4,5] allows one to account for the small scale effect that is very significant when dealing with micro and nanostructures. Reddy [6] studied the nonlocal theories for bending, buckling and vibration of beams. Duan et al [7] proposed the development of analytical vibration solutions for microstructured beam model to calibrate length scale coefficient in nonlocal Timoshenko beams. Eringen's small length scale coefficient for buckling of nonlocal Timoshenko beam based on microstructured beam model are studied by Zhang et al [8]. Wang et al [9] proposed the calibration of Eringen's small length scale coefficient for initially stressed vibrating nonlocal Euler beams based on microstructured beam model. The finite element analysis of forced vibration for pipe conveying harmonically pulsating fluid has been studied by Seo et al. [10]. Hong et al. [11] studied the vibration of a single-walled carbon nanotube embedded in an elastic medium under a moving internal nanoparticle. Mirramezani and Mirdamadi [12] analyzed the effects of nonlocal elasticity and Knudsen number on fluid–structure interaction in carbon nanotube conveying fluid. Baohui et al. [13] used the wave method to investigate the free vibration analysis of micropipe conveying fluid. Ghavanloo et al [14] studied the vibration and instability analysis of carbon nanotubes conveying fluid and resting on a linear viscoelastic Winkler foundation. Wang et al. [15] reported the flexural vibrations of micro scale pipes conveying fluid by considering the size effects of micro-flow and micro-structure. Wang and Ni [16] proposed a reappraisal of the computational modeling of carbon nanotubes conveying viscous fluid. The thermal mechanical vibration and instability of a fluid conveying single walled carbon nanotube embedded in an elastic medium based on nonlocal elasticity theory

have been analyzed by Chang [17]. Ansari et al [18] studied the dynamic stability of embedded single walled carbon nanotube including thermal environment effects. Vibration and dynamic instability analyses of CNT are elaborated in [19,20,21] and the higher order free vibration of SWCNTs was deeply analyzed in [21]. The dynamic stability of parametrically excited linear resonant beams under periodic axial force has been recently studied by Jing et al. [22]. To the authors' knowledge, there are no studies in literature on the dynamic instability of CNT based on complex modes nor on the dynamic and parametric instabilities interactions of these structures. Therefore, numerical and analytical methodological approaches are here proposed, proving simplified models as well as theoretical and numerical insights into the dynamic and parametric instabilities and on their interactions.

In the present paper, the governing equation of motion is first derived based on the fluid-tube interaction, the nonlocal theory and the Euler Bernoulli beams' model. A numerical procedure based on the differential quadrature method and multimodal formulations have been elaborated for the dynamic and parametric instabilities of CNT conveying pulsating and viscoelastic fluid. Frequency and time domains are considered and instability analyses have been performed with respect to the considered influencing parameters based on analytical and numerical procedures with an emphasis on complex modes. The influences of the nonlocal parameter, fluid viscosity, viscoelastic coefficient, foundation of the elastic medium, thermal environment and static and dynamic velocity effects on the dynamic behaviors of the CNTs-fluid system are analyzed. Various types of instabilities such as divergence, flutter and principal parametric instabilities as well as their interaction are analyzed.

2. Mathematical modeling

The flexural vibration of a slender carbon nanotube conveying fluid and subjected to axial force, thermal loading, fluid flow and fluid pressure can be modeled based on the Euler-Bernoulli beam model by the following partial differential equation:

$$\frac{\partial Q}{\partial x} = m_t \frac{\partial^2 W}{\partial t^2} + F_e + F_T + F_f + F_p \tag{4.1}$$

where W, Q and m_t are the transverse displacement, shear force and mass of the tube per unit length respectively. F_e, F_T and F_f are the axial force, the thermal force and the force per unit of length induced by fluid flow. F_p represents a force due to the axial fluid pressure. The

momentum-balance equation for the fluid motion may be described by the Navier-Stokes equation: [16, 25]

$$\rho \frac{dU}{dt} = -\nabla P + \vartheta \nabla^2 U \tag{4.2}$$

in which $U(t) = (U_r, U_\theta, U_x)$ is the time dependent fluid velocity in the cylindrical coordinate system with components in r, θ and x directions. ρ, P and ϑ are the mass density of the internal fluid, the pressure and the viscosity of the flowing fluid.

The exerted force due to the fluid flow in the nanotube can be obtained from (4.2). At the point of the contact between the inside tube and internal fluid, their respective velocity and accelerations in the direction of flexural displacement become equal. These relationships thus can be written as: [16]

$$U_r = \frac{dW}{dt} \tag{4.3}$$

where

$$\frac{dW}{dt} = \left(\frac{\partial}{\partial t} + U_x(r) \frac{\partial}{\partial x} \right) W \tag{4.4}$$

Substituting equation (4.3) into Eq. (4.2) and using Eq. (4.4) one obtains:

$$F_f = A_f \frac{\partial p_r}{\partial r} = -m_f \left(\frac{\partial^2 W}{\partial t^2} + 2U_x \frac{\partial^2 W}{\partial x \partial t} + U_x{}^2 \frac{\partial^2 W}{\partial x^2} \right) + \vartheta A_f \left(U_x \frac{\partial^3 W}{\partial x^3} + \frac{\partial^3 W}{\partial x^2 \partial t} \right) \tag{4.5}$$

in which m_f is the mass of the fluid per unit axial length, A_f is the cross sectional area of the internal fluid respectively.

The axial resultant force due to the thermal loading, F_T, and the force due to the axial pressure exerted by the fluid, F_p, are given by [25]:

$$F_T = \frac{EA\alpha_x T}{(1-2\upsilon)} \frac{\partial^2 W}{\partial x^2}, \quad F_p = m_f \frac{dU_x}{dt} (L - x) \frac{\partial^2 W}{\partial x^2} \tag{4.6}$$

in which E, A, L, υ, α_x and T_s represent the Young modulus, tube cross sectional area, length, Poisson ratio of the CNT, thermal expansion and the temperature change respectively.

Based on the Euler-Bernoulli beam theory, the transverse shear force Q and bending moment $\bar{M}$ of the viscoelastic tube are given by [25]:

$$Q = \frac{\partial \bar{M}}{\partial x} = \left(E - \delta \frac{\partial}{\partial t} \right) I \frac{\partial^3 W}{\partial x^3} \tag{4.7}$$

and $\bar{M} = \int z \sigma_{xx} dA$

where δ is the viscoelastic coefficient of the tube.

Based on the nonlocal elasticity theory, the following differential constitutive equation for one dimensional case is adopted [4, 5, 17, 19-21].

$$\sigma_{xx} - (e_0 a)^2 \frac{\partial^2 \sigma_{xx}}{\partial x^2} = E \varepsilon_{xx}, \tag{4.8}$$

where $e_0 a$, ε_{xx} and σ_{xx} are the nonlocal parameter, the axial strain and stress on the nanotube respectively. Using equation (4.8), the moment $\bar{M}$ is obtained by the following differential equation.

$$\bar{M} - (e_0 a)^2 \frac{\partial^2 \bar{M}}{\partial x^2} = EI \frac{\partial^2 W}{\partial x^2}, \tag{4.9}$$

Combining equations (4.1) and (4.5) to (4.9), the partial differential equation of motion for a CNTs conveying fluid and subjected to the considered forces can be written as:

$$\begin{aligned}
&\left(1+\delta\frac{\partial}{\partial t}\right)EI_1\frac{\partial^4 W_1}{\partial x^4}+\left[m_f U_x^2 - N_T + m_f\frac{\partial U_x}{\partial t}(L-x)\right]\frac{\partial^2 W_1}{\partial x^2}+\left(m_f+m_1\right)\frac{\partial^2 W_1}{\partial t^2}+2m_f U_x\frac{\partial^2 W_1}{\partial x\partial t}\\
&-\vartheta A_f\left(U_x\frac{\partial^3 W_1}{\partial x^3}+\frac{\partial^3 W_1}{\partial x^2\partial t}\right)-\left(e_0 a\right)^2\left[\left(m_f+m_1\right)\frac{\partial^4 W_1}{\partial x^2\partial t^2}+\left(m_f U_x^2-N_T\right)\frac{\partial^4 W_1}{\partial x^4}+2m_f U_x\frac{\partial^4 W_1}{\partial x^3\partial t}\right]\\
&=\sum_{j=2}^{N} c_{1j}\left(W_1-W_j\right)-\left(e_0 a\right)^2\sum_{j=2}^{N} c_{1j}\left(\frac{\partial^2 W_1}{\partial x^2}-\frac{\partial^2 W_j}{\partial x^2}\right)\\
&\left(1+\delta\frac{\partial}{\partial t}\right)EI_i\frac{\partial^4 W_i}{\partial x^4}+m_i\frac{\partial^2 W_i}{\partial t^2}-\left(e_0 a\right)^2 m_i\frac{\partial^4 W_i}{\partial x^2\partial t^2}\\
&=\sum_{\substack{j=1\\ i\neq j}}^{N} c_{ij}\left(W_i-W_j\right)-\left(e_0 a\right)^2\sum_{j=2}^{N} c_{ij}\left(\frac{\partial^2 W_i}{\partial x^2}-\frac{\partial^2 W_j}{\partial x^2}\right), \qquad i=2,3,..,N-1\\
&\left(1+\delta\frac{\partial}{\partial t}\right)EI_N\frac{\partial^4 W_N}{\partial x^4}+m_N\frac{\partial^2 W_N}{\partial t^2}-\left(e_0 a\right)^2\left(K+m_N\frac{\partial^2}{\partial t^2}\right)\frac{\partial^2 W_N}{\partial x^2}+\bar{K}W_N\\
&=\sum_{j=1}^{N-1} c_{Nj}\left(W_N-W_j\right)-\left(e_0 a\right)^2\sum_{j=2}^{N} c_{Nj}\left(\frac{\partial^2 W_N}{\partial x^2}-\frac{\partial^2 W_j}{\partial x^2}\right),
\end{aligned} \tag{4.10}$$

where N_T and $\bar{K}$ are respectively the axial resultant force due to the thermal loading and the constant of the elastic medium. Note that the time and space (t, x) dependences are omitted for readability purpose. The van der Waals interaction coefficient is given by:

$$c_{ij} = \left[\frac{1001\pi\varepsilon\sigma^{12}}{3a^4} E_{ij}^{13} - \frac{1120\pi\varepsilon\sigma^{6}}{9a^4} E_{ij}^{7} \right] R_j \tag{4.11}$$

$$E_{ij}^{m} = (R_i + R_j)^{-m} \int_0^{\pi/2} \frac{d\theta}{[1 - K_{ij}\cos(\theta)]^{m/2}} \tag{4.12}$$

$$K_{ij} = \frac{4R_i R_j}{(R_i + R_j)^2} \tag{4.13}$$

In this paper, a pulsating internal axial flow is considered and the flow velocity is assumed to be harmonically fluctuating and to have the following form:

$$U_x(t) = U_0 \left[1 + \eta \cos(\Omega t)\right] \tag{4.14}$$

where U_0 is the static mean flow velocity, η is the amplitude of the harmonic fluctuation and Ω its frequency.

The following dimensionless variables and parameters are used:

$$w = \frac{W}{L}, y = \frac{x}{L}, \tau = \sqrt{\left(\frac{EI}{m_f + m_t}\right)} \frac{t}{L^2}, u = \sqrt{\frac{m_f}{EI}} L U_x, \alpha = \sqrt{\left(\frac{EI}{m_f + m_t}\right)} \frac{c}{L^2}, \mu = \frac{e_0 a}{L}, T = \frac{N_T L^2}{EI},$$

$$k = \frac{\bar{K} L^4}{EI}, N_T = -\frac{EA\alpha_x T_s}{1 - 2\upsilon}, \beta = \frac{\vartheta A}{\sqrt{EI\, m_f}}, M_r = \sqrt{\left(\frac{m_f}{m_f + m_t}\right)}, V_0 = \sqrt{\frac{m_f}{EI}} L U_0, \omega = \sqrt{\frac{(m_f + m_t)L^4}{EI}} s \tag{4.15}$$

Equation (4.10) is thus transformed into the following dimensionless partial differential equation:

$$\left(1+\alpha\frac{\partial}{\partial\tau}\right)\frac{\partial^4 w_1}{\partial y^4}+\left(u^2-T+M_r\frac{du}{d\tau}(1-y)\right)\frac{\partial^2 w_1}{\partial y^2}+2M_r u\frac{\partial^2 w_1}{\partial y\partial\tau}+\frac{\partial^2 w_1}{\partial\tau^2}-\beta\left(u\frac{\partial^3 w_1}{\partial y^3}\right.$$
$$\left.+M_r\frac{\partial^2 w_1}{\partial y^2\partial\tau}\right)-\mu^2\left(\frac{\partial^4 w_1}{\partial y^2\partial\tau^2}+\left(u^2-T\right)\frac{\partial^4 w_1}{\partial y^4}+2M_r u\frac{\partial^4 w_1}{\partial y^3\partial\tau}\right)$$
$$=\sum_{j=2}^{N}\overline{c}_{1j}\left(w_1-w_j\right)-\mu^2\sum_{j=2}^{N}\overline{c}_{1j}\left(\frac{\partial^2 w_1}{\partial y^2}-\frac{\partial^2 w_j}{\partial y^2}\right) \qquad (4.16a)$$

$$\left(1+\alpha\frac{\partial}{\partial\tau}\right)\frac{\partial^4 w_i}{\partial y^4}+\beta_i\frac{\partial^2 w_i}{\partial\tau^2}-\beta_i\mu^2\frac{\partial^4 w_i}{\partial y^2\partial\tau^2}$$
$$=\sum_{\substack{j=1\\ i\neq j}}^{N}\overline{c}_{1j}\left(w_i-w_j\right)-\mu^2\sum_{j=2}^{N}\overline{c}_{1j}\left(\frac{\partial^2 w_i}{\partial y^2}-\frac{\partial^2 w_j}{\partial y^2}\right), \qquad i=2,3,...,N-1 \qquad (4.16b)$$

$$\left(1+\alpha\frac{\partial}{\partial\tau}\right)\frac{\partial^4 w_N}{\partial y^4}+\beta_N\frac{\partial^2 w_N}{\partial\tau^2}-\mu^2\left(\beta_N\frac{\partial^4 w_N}{\partial y^2\partial\tau^2}+k\frac{\partial^2 w_N}{\partial y^2}\right)+kw_N$$
$$=\sum_{j=1}^{N-1}\overline{c}_{Nj}\left(w_N-w_j\right)-\mu^2\sum_{j=2}^{N}\overline{c}_{1j}\left(\frac{\partial^2 w_N}{\partial y^2}-\frac{\partial^2 w_j}{\partial y^2}\right), \qquad (4.16c)$$

The objective of this paper is to investigate the dynamic and parametric instability behaviors as well as their interaction of the CNT-fluid system based on the partial differential equation (4.13). The time dependent fluid velocity is considered leading to a PDE with periodically varying coefficients. Mathematical formulations based on numerical and analytical procedures are elaborated.

It should be noted that for accurate investigation of the instability of CNT conveying fluid, the used modal basis has to be carefully selected. For this aim, the parametric free vibration analysis is first deeply studied using numerical and analytical methods with respect to the fluid velocity and to the other considered parameters. Complex eigenmodes and eigenfrequencies are obtained. Based on the obtained eingenmodes and the Galerkin procedure, various modal bases are used for dynamic and parametric instability analyses.

3. Numerical procedure

3.1 Differential quadrature method

For numerical investigations of vibration, dynamic and parametric instability analyses of the considered CNT-fluid system, the differential quadrature method (DQM) is adopted here. This method, akin to approximate the derivative of a function at any location by a linear summation of all the function values along a mesh line [23,24]. The procedure DQ application lies in the determination of the weighting coefficients. The continuous solution is

approximated by functional values at discrete points. In the present paper, the following Chebyshev-Gauss-Lobatto quadrature points are used.

$$y_i = \frac{1}{2}\left[1-\cos\left(\frac{i-1}{N-1}\pi\right)\right] \text{ for } i = 1,2,3,.....,n \tag{4.17}$$

where $y_i = \frac{x_i}{L}$ and n is the number of grid points in the domain [0, 1].

For a function *f(y),* DQ approximation of the mth order derivative at the ith point is given by:

$$f(y) = \sum_{j=1}^{n} l_j(y) f(y_j) \tag{4.18}$$

$$\frac{d^m}{dy^m}\begin{Bmatrix} f(y_1) \\ f(y_2) \\ \vdots \\ f(y_n) \end{Bmatrix} = H_{ij}^m \begin{Bmatrix} f(y_1) \\ f(y_2) \\ \vdots \\ f(y_n) \end{Bmatrix},\ i, j = 1,2,...,n \tag{4.19}$$

in which $l_j(y)$ are the Lagrange interpolation polynomials and H_{ij}^m represent the weighting coefficients given by [24].

$$f(y_i) = \frac{G(y)}{(y-y_i)G_1(y_i)},\ for\, i = 1,2,...,n \tag{4.20-a}$$

$$G(y) = \prod_{j=1}^{n}(y-y_i) \tag{4.20-b}$$

$$G_1(y_i) = \prod_{j=1,\, j\neq i}^{n}(y-y_i),\ for\ i, j = 1,2,...,n \tag{4.20-c}$$

$$H_{ij}^1 = \frac{G_1(y_i)}{(y_i-y_j)G_1(y_i)}\quad for\ i, j = 1,2,...,n;\ i \neq j \tag{4.20-d}$$

$$H_{ii}^1 = -\sum_{\substack{j=1 \\ j\neq i}}^{n} H_{ij}^1 \tag{4.20-e}$$

The higher derivative, mth, can be calculated as:

$$H_{ij}^{m} = m\left(H_{ij}^{1} H_{ii}^{m-1} - \frac{H_{ij}^{m-1}}{x_i - x_j} \right) \qquad for\, i = 1,2,...,n,\ j \neq i \qquad (4.20-f)$$

$$H_{ii}^{m} = -\sum_{\substack{j=1 \\ j \neq i}}^{n} H_{ij}^{m} \qquad (4.20-g)$$

The discrete classical boundary conditions at y=0 and y=1, using the DQ method, can be written as:

$$w_1 = 0 \qquad (4.21-a)$$

$$\sum_{k=1}^{n} H_{1k}^{n0} w_k = 0 \qquad (4.21-b)$$

$$w_n = 0 \qquad (4.21-c)$$

$$\sum_{k=1}^{n} H_{nk}^{nl} w_k = 0 \qquad (4.21-d)$$

where n_0 and n_l may be taken as either 1, 2 or 3 and $w_k = w(y_k)$. is the transverse displacement of tube at point y_k. Choosing the values of n_0 and n_l can give the following classical boundary conditions: [24,25]

simply supported: n_0 =2; n_l =2

clamped-clamped: n_0 =1; n_l =1

clamped-simply supported: n_0 =1; n_l =2

clamped-free: n_0 =1; n_l =3

free-free: n_0 =2; n_l =3

Applying equations (4.20) and (4.21) to equation (4.16), one obtains the following ordinary differential system for i=1,2,…,n.

$$\sum_{k=1}^{n} H_{sk}^{4} w_k^1 + \alpha \sum_{k=1}^{n} H_{sk}^{4} \dot{w}_k^1 + \left(u^2 - T + M_r \frac{\partial u}{\partial \tau}(1-y) \right) \sum_{k=1}^{n} H_{sk}^{2} w_k^1 + \ddot{w}_s^1$$
$$+2M_r u \sum_{k=1}^{n} H_{sk}^{1} \dot{w}_k^1 - \beta \left(u \sum_{k=1}^{n} H_{sk}^{3} w_k^1 + M_r \sum_{k=1}^{n} H_{sk}^{2} \dot{w}_k^1 \right)$$
$$-\mu^2 \left[\sum_{k=1}^{n} H_{sk}^{2} \ddot{w}_k^1 + \left(u^2 - T \right) \sum_{k=1}^{n} H_{sk}^{4} w_k^1 + 2M_r u \sum_{k=1}^{n} H_{sk}^{3} \dot{w}_k^1 \right] = \sum_{j=2}^{N} \bar{c}_{1j} \left(w_s^1 - w_s^j \right) \qquad (4.22a)$$

$$\sum_{k=1}^{n} H_{sk}^{4} w_k^i + \alpha \sum_{k=1}^{n} H_{sk}^{4} \dot{w}_k^i + \beta_i \ddot{w}_s^i - \beta_i \mu^2 \sum_{k=1}^{n} H_{sk}^{2} \ddot{w}_k^i = \sum_{\substack{j=1 \\ i \neq j}}^{N} \bar{c}_{ij} \left(w_s^i - w_s^j \right), \qquad i = 2,3,...,N-1$$

$$\sum_{k=1}^{n} H_{sk}^{4} w_k^N + \alpha \sum_{k=1}^{n} H_{sk}^{4} \dot{w}_k^N + \beta_N \ddot{w}_s^N - \mu^2 \left(\beta_N \sum_{k=1}^{n} H_{sk}^{2} \ddot{w}_k^N + k \sum_{k=1}^{n} H_{sk}^{2} w_k^N \right) + k w_s^N = \sum_{j=1}^{N-1} \bar{c}_{Nj} \left(w_s^N - w_s^j \right)$$

This system can be rewritten in the following matrix from.

$$[M]\{\ddot{w}\}+[C(\tau)]\{\dot{w}\}+[K(\tau)]\{w\}=0 \qquad (4.22b)$$

where

$$[M]=\begin{bmatrix} I_1-\mu^2H^2 & 0 & \cdots & 0 \\ 0 & \beta_2\left(I_1-\mu^2H^2\right) & \ddots & \vdots \\ \vdots & \ddots & \ddots & 0 \\ 0 & \cdots & 0 & \beta_N\left(I_1-\mu^2H^2\right) \end{bmatrix}$$

$$[K]=[K_0]+[K_1]\cos(\Omega\tau)+[K_2]\cos(\Omega\tau)^2+[K_3]\sin(\Omega\tau)$$

$$[C]=[C_0]+[C_1]\cos(\Omega\tau)$$

$$[K_0]=\begin{bmatrix} K_0^1 & \tilde{c}_{12}I_1 & \cdots & \tilde{c}_{1N}I_1 \\ \tilde{c}_{21}I_1 & H^4 & \ddots & \vdots \\ \vdots & \ddots & \ddots & \tilde{c}_{(N-1)N}I_1 \\ \tilde{c}_{N1}I_1 & \cdots & \tilde{c}_{N(N-1)}I_1 & K_0^N \end{bmatrix};\ [K_1]=\begin{bmatrix} K_1^1 & 0 & \cdots & 0 \\ 0 & 0 & \ddots & \vdots \\ \vdots & \ddots & \ddots & 0 \\ 0 & \cdots & 0 & 0 \end{bmatrix};\ [K_2]=\begin{bmatrix} K_2^1 & 0 & \cdots & 0 \\ 0 & 0 & \ddots & \vdots \\ \vdots & \ddots & \ddots & 0 \\ 0 & \cdots & 0 & 0 \end{bmatrix}$$

$$[K_3]=\begin{bmatrix} K_3^1 & 0 & \cdots & 0 \\ 0 & 0 & \ddots & \vdots \\ \vdots & \ddots & \ddots & 0 \\ 0 & \cdots & 0 & 0 \end{bmatrix};\ [C_0]=\begin{bmatrix} C_0^1 & 0 & \cdots & 0 \\ 0 & 0 & \ddots & \vdots \\ \vdots & \ddots & \ddots & 0 \\ 0 & \cdots & 0 & 0 \end{bmatrix};\ [C_1]=\begin{bmatrix} C_1^1 & 0 & \cdots & 0 \\ 0 & 0 & \ddots & \vdots \\ \vdots & \ddots & \ddots & 0 \\ 0 & \cdots & 0 & 0 \end{bmatrix}$$

$$\left[K_0^1\right]=\left(1-\mu^2\left(V_0^2-T\right)\right)H^4+\left(V_0^2-T\right)H^2-\beta V_0H^3;\ \left[K_0^N\right]=H^4+k\left(I_1-\mu^2H^2\right)$$

$$\left[K_1^1\right]=2V_0^2\eta\left(H^2-\mu^2H^4\right)-\beta V_0\eta H^3;\left[K_2^1\right]=V_0^2\eta^2\left(H^2-\mu^2H^4\right);\left[K_3^1\right]=M_r\Omega V_0\eta\left(y-1\right)H^2$$

$$\left[C_0^1\right]=\alpha H^4-\beta M_rH^2+2M_rV_0\left(H^1-\mu^2H^3\right);\left[C_1^1\right]=2M_rV_0\,\eta\left(H^1-\mu^2H^3\right)$$

$$\{w\}=\left\{w_1^1\ w_2^1\ldots w_N^1, w_1^2\ w_2^2\ldots w_N^2,\ldots., w_1^N\ w_2^N\ldots w_N^N\right\}^T$$

Note that the matrices C and K dependent on time as well as on some influencing physical parameters. Numerical time response can be obtained by numerical methods such as Newmark, θ-Wilson, Runge- Kutta, etc. As the matrices K and C depend on the fluid flow velocity, considered time dependent, various types of instabilities such as divergence, flutter and parametric can occur and then may complicate the dynamic response analysis. For the sake of clarity, these types of instabilities are separately formulated.

3.2 Dynamic instability formulation

For static fluid velocity $u(t)=V_0\ (\eta=0),$ the differential system (4.22b) is then reduced to the following eigenvalue problem by assuming that $w(\tau)=W\,e^{\omega\tau}$

$$\left(\omega^2[M]+\omega[C]+[K]\right)\{W\}=0 \tag{4.23}$$

where $\{W\}$ denotes the unknown dynamic displacement vector defined by:

$$\{W\}=\left\{w_1^1\ w_2^1 \ldots w_N^1, w_1^2\ w_2^2 \ldots w_N^2, \ldots., w_1^N\ w_2^N \ldots w_N^N\right\}^T \tag{4.24}$$

and [K], [M] and [C] are the resulting stiffness, mass and damping matrices respectively.

The assumed boundary conditions can also be expressed in a matrix form using (4.21)

$$[K_B]\{W_B\}+[K_C]\{W_S\}=0 \tag{4.25}$$

where $\{W_B\}=\left\{w_1^1\ w_2^1\ w_{N-1}^1\ w_N^1, w_1^2\ w_2^2\ w_{N-1}^2\ w_N^2, \ldots., w_1^N\ w_2^N w_{N-1}^N\ w_N^N\right\}^T$ and

$\{W_S\}=\left\{w_3^1\ w_4^1 \ldots w_{n-2}^1, w_3^2\ w_4^2 \ldots w_{n-2}^2, \ldots., w_3^n\ w_4^n \ldots w_{n-1}^n\right\}^T$ $[K_B]$ and $[K_C]$ are $4n\times 4n$ and $4n\times(n^2-4n)$ matrices respectively.

Using this vector decomposition Eq. (4.23) can be rewritten as:

$$[K_D]\{W_B\}+[K_S]\{W_S\}+\left(\omega[C_S]+\omega^2[M_S]\right)\{W_S\}=0 \tag{4.26}$$

Coupling equations (4.25) and (4.26), one gets:

$$\left\{[K_S]-[K_D][K_B]^{-1}[K_C]+\omega[C_S]+\omega^2[M_S]\right\}\{W_S\}=0 \tag{4.27}$$

where $[K_S]$, $[M_S]$ and $[C_S]$ are $(n^2-4n)\times(n^2-4n)$ matrices.

This frequency dependent relation is rewritten in the following eigenvalue problem form:

$$\begin{cases}\Gamma Y=\omega Y,\\ \Gamma=\begin{pmatrix}M_s & 0\\ 0 & M_s\end{pmatrix}^{-1}\begin{pmatrix}0 & K_h\\ K_h & C_S\end{pmatrix},\ Y=\begin{Bmatrix}W_s\\ \omega W_s\end{Bmatrix},\end{cases} \tag{4.28}$$

$$K_h=[K_S]-[K_D][K_B]^{-1}[K_C]$$

By solving this eigenvalue problem, eigenmodes and associated eigenfrequencies can be numerically obtained for various types of boundary conditions. Based on this numerical procedure, real and complex eigenmodes and the associated eigenfrequencies can be obtained with respect to V_0, T and the other relevant physical parameters. As the Galerkin procedure will be based on the obtained eigenmodes, two distinct cases are considered here.

Case 1: Classical real modal basis

In this case, the free vibration analysis is done by considering V_0=T=k=α=β=Mr=0. This will lead to natural frequencies and real eigenmodes independent from V_0, T, k, β and α. These

real modes are classically used in modal vibration analysis of tubes conveying fluid. For example, for simply supported case, the eigenmodes $w_j(x) = \sin(j\pi x / L)$ are classically used by many authors. This may lead to erroneous results for dynamic instability analysis.

Case 2: General modal basis

By considering all parameters, complex eigenfrequencies and eigenmodes are resulted. These complex characteristics have been carefully computed for the considered boundary conditions. Using the numerically obtained eigenmodes, Galerkin's method can be applied for dynamic and parametric instability analyses.

4. Multi-modal formulation

For multimodal analysis, the CNT deflection can be approximated by N modes.

$$W_k(\tau) = \sum_{i=1}^{N} Z_{ki}\, q_i(\tau); \qquad k = 1, 2 \tag{4.29}$$

Where Z_i *and* $q_i(\tau)$ are the vector eigenfunctions that depend on the considered physical parameters and the generalized coordinates respectively. Equations (4.22-b) and (4.29) lead to the following time dependent differential system for j=1 to N.

$$\sum_{i=1}^{N} \left\langle M\, Z_{ki}, \bar{Z}_{kj} \right\rangle \ddot{q}_i(\tau) + \sum_{i=1}^{N} \left\langle \left[C_0 + C_1 \cos(\Omega\tau) \right] Z_{ki}, \bar{Z}_{kj} \right\rangle \dot{q}_i(\tau) +$$

$$\sum_{i=1}^{N} \left\langle \left[K_0 + K_1 \cos(\Omega\tau) + K_2 \cos^2(\Omega\tau) + K_3 \sin(\Omega\tau) \right] Z_{ki}, \bar{Z}_{kj} \right\rangle q_i(\tau) = 0 \tag{4.30}$$

where $\bar{Z}_{kj}$ stands complex conjugate of Z_{kj}.

For the dynamic response, numerical solution of the time dependent system (4.30) can be conducted based on a numerical procedure for the considered mode number. The effects of the considered parameters can be investigated.

For a deep analysis of instability behaviors of the considered CNT-fluid system, models of dynamic and parametric instability behaviors are formulated hereafter.

Static fluid case (η=0)

For the dynamic instability analysis of CNT conveying static fluid velocity, the critical fluid velocities and velocity-frequency dependence can be investigated based on equation (4.23). The time response at any static velocity level can be obtained by numerically solving the following reduced differential system.

$$[M]\{\ddot{q}_r\}+[C_0]\{\dot{q}_r\}+[K_0]\{q_r\}=0 \tag{4.31}$$

where

$$\{q\}=\left\{q_1^1\ q_1^1....q_1^N,....,q_N^1\ q_N^1....q_N^N\right\}^T$$

5. Parametric instability formulation

The parametric instability behaviors of single walled carbon nanotubes conveying pulsating fluid can be investigated at various fixed values of the influencing parameters V_0, T, k, μ and β. Here, the effects of η and Ω on the system stability are the main focuses at various velocity V_0 levels.

The generalized coordinate $q_j(\tau)$ is assumed to be periodic and is expressed in the form:

$$q_j(\tau)=\sum_{k=0}^{\bar{N}}\left\{a_k\sin\left(\frac{k\Omega\tau}{2}\right)+b_k\cos\left(\frac{k\Omega\tau}{2}\right)\right\} \tag{4.32}$$

Based on the multi-modal formulation and substituting Eq. (4.32) into equation (4.30) the following algebraic system is obtained

$$[G]\{X\}=\{0\} \tag{4.33}$$

where [G] is a $(2\bar{N}+1)\times(2\bar{N}+1)$ matrix and X is a $(2\bar{N}+1)$ vector $\{X\}=\left\{b_0,a_1,b_1,...,a_{\bar{N}},b_{\bar{N}}\right\}^T$

For the sake of clarity, the matrix G is given in the appendix A for $\bar{N}=5$. The characteristic equation of this problem, $\det(G)=0,$ allows one to get a highly nonlinear algebraic relationship on Ω given the instability boundaries. For the sake of simplicity, the characteristic equation is given for some particular simple cases.

Particular cases

The stability regions can be obtained based on the algebraic equation (4.33) by considering the required modes. Various modes and various harmonic decompositions can be considered for the required accuracy.

One-mode approach

Based on the one-mode and one-harmonic approach $(N=\bar{N}=1)$, the instability boundaries can be obtained by solving the following algebraic equation.

$$\left(\frac{\Omega}{2}\right)^4\left(1+\mu^2(H_{11}^2)^2\right)^2-\left(\frac{\Omega}{2}\right)^2\left[(\alpha_1+\alpha_4)\left(1+\mu^2(H_{11}^2)^2\right)+\alpha_2\alpha_3\right]+\alpha_1\alpha_4=0 \tag{4.34a}$$

This leads to

$$\xi_0\eta^4+(\xi_2 V_0^2\Omega^2+\zeta_0)\eta^2+\lambda\Omega^4+\gamma_2\Omega^2+\gamma_0=0 \tag{4.34b}$$

$$\eta=\pm\sqrt{\frac{-(\xi_2 V_0^2\Omega^2+\zeta_0)\mp\sqrt{\Delta}}{2\xi_0}} \tag{4.34c}$$

where

$$\Delta=(\xi_2 V_0^2\Omega^2+\zeta_0)^2-4\xi_0(\lambda\Omega^4+\gamma_2\Omega^2+\gamma_0)$$

$$\alpha_1=\frac{Y_2}{2}-\frac{Y_4}{2}+Y_6;\ \alpha_2=\frac{Y_4}{2}+Y_6;\ \alpha_3=\frac{Y_1}{2}+\frac{Y_3}{4}-\frac{Y_5}{2};\ \alpha_4=\frac{Y_1}{2}+\frac{Y_3}{4}+\frac{Y_5}{2};$$

$$\lambda=-\left(\mu^2H_{11}^2-1\right)^2/16$$

$$\xi_0=(-(1/4)(H_{11}^4)^2\mu^4-(1/4)(H_{11}^2)^2+(1/2)\mu^2H_{11}^4H_{11}^2)V_0^4;$$

$$\xi_2=(1/4)Mr^2F_{11}^2-(1/4)(H_{11}^2)^2\mu^2+(1/4)H_{11}^2-(1/2)Mr^2F_{11}H_{11}^2+(1/4)(H_{11}^2)^2Mr^2$$
$$-(1/4)\mu^2H_{11}^4+(1/4)\mu^4H_{11}^2H_{11}^4$$

$$\zeta_0=(-H_{11}^2H_{11}^4T\mu^2+(H_{11}^2)^2T-H_{11}^2H_{11}^4+(H_{11}^4)^2\mu^2)V_0^2$$

$$\gamma_0=(-(H_{11}^2)^2-(H_{11}^4)^2\mu^4+2\mu^2H_{11}^2H_{11}^4)V_0^4+2H_{11}^2H_{11}^4T-(H_{11}^2)^2T^2+(-2H_{11}^2H_{11}^4T\mu^2$$
$$+2(H_{11}^2)^2T-2H_{11}^2H_{11}^4+2(H_{11}^4)^2\mu^2)V_0^2-c_{11}^2$$

$$\gamma_2=((1/2)H_{11}^2-(1/2)(H_{11}^2)^2\mu^2-(1/2)\mu^2H_{11}^4+(1/2)\mu^4H_{11}^2H_{11}^4)V_0^2-(1/4)\alpha^2(H_{11}^4)^2$$
$$+(1/2)\beta Mr\alpha H_{11}^2H_{11}^4+(1/2)H_{11}^4+(1/2)(H_{11}^2)^2T\mu^2-(1/2)H_{11}^2T-(1/4)\beta^2Mr^2(H_{11}^2)^2-(1/2)\mu^2H_{11}^2H_{11}^4$$

Y_j are given in the Appendix A.

Two-modes approach

Based on the two-modes and one-harmonic approach $(N=2,\bar{N}=1)$, the instability boundaries associated to the first two modes can be obtained by solving the following algebraic equation.

$$\left(\frac{\Omega}{2}\right)^8\beta_8+\left(\frac{\Omega}{2}\right)^6\beta_6+\left(\frac{\Omega}{2}\right)^4\beta_4+\left(\frac{\Omega}{2}\right)^2\beta_2+\beta_0=0 \tag{4.35}$$

where the coefficients $\beta_0, \beta_2, \beta_4, \beta_6, \beta_8$ are given by:

$$\beta_0 = (S_{11}S_{14} - S_{12}S_{13})(S_{41}S_{44} - S_{43}S_{42})$$

$$\beta_2 = \frac{1}{4}(S_{12}S_{13} - S_{11}S_{14})(S_{41}m_4 + m_1S_{44}) - \frac{1}{4}(S_{11}m_4 + m_1S_{14})(S_{41}S_{44} - S_{43}S_{42}) + (S_{11}S_{23} - S_{21}S_{13})(S_{42}S_{34} - S_{32}S_{44})$$
$$+ (S_{11}S_{24} - S_{22}S_{13})(S_{32}S_{43} - S_{34}S_{41}) + (S_{21}S_{14} - S_{12}S_{23})(S_{42}S_{33} - S_{31}S_{44}) + (S_{22}S_{14} - S_{12}S_{24})(S_{31}S_{43} - S_{33}S_{41})$$

$$\beta_4 = \frac{1}{16}\left(m_1{}^2S_{14}S_{44} + S_{11}m_4^2S_{41}\right) + \frac{m_1}{4}\left(S_{24}(S_{11}S_{34} - S_{12}S_{33}) + S_{23}(S_{32}S_{44} - S_{42}S_{34}) + S_{24}(S_{34}S_{41} - S_{32}S_{43})\right.$$
$$\left. + S_{22}(S_{14}S_{33} - S_{13}S_{34})\right) + \frac{m_4m_1}{16}\left((S_{11} + S_{41})(S_{14} + S_{44}) - S_{12}S_{13} - S_{43}S_{42}\right) + \frac{m_4}{4}\left(S_{21}(S_{14}S_{31} - S_{13}S_{32})\right.$$
$$\left. S_{23}(S_{11}S_{32} - S_{12}S_{31}) + S_{21}(S_{31}S_{44} - S_{42}S_{33}) + S_{22}(S_{33}S_{41} - S_{31}S_{43})\right) + S_{22}S_{23}(S_{32}S_{33} - S_{31}S_{34})$$
$$+ S_{21}S_{24}(S_{31}S_{34} - S_{32}S_{33})$$

$$\beta_6 = \frac{-1}{64}\left((S_{11} + S_{41})m_1m_4^2 + (S_{14} + S_{44})m_4m_1{}^2\right) - \frac{1}{16}\left((S_{22}S_{33} + S_{23}S_{32})m_1m_4 + S_{24}S_{34}m_1^2 + S_{21}S_{31}m_4^2\right)$$

$$\beta_8 = \frac{1}{256}m_1^2m_4^2$$

in which:

$$S_{24} = \frac{1}{2}\left(-\left(MrV_0\eta - \beta Mr\right)H_{22}^2 + MrV_0\eta F_{22} + \alpha H_{22}^4\right);$$

$$S_{31} = \frac{1}{2}\left(MrV_0\eta F_{11} - \alpha H_{11}^4 + \left(\beta Mr - MrV_0\eta\right)H_{11}^2\right)$$

$$S_{32} = \frac{1}{2}\left(MrV_0\eta F_{21} - 2MrV_0D_{21} + 2\mu^2MrV_0H_{21}^3\right) + \frac{1}{4}\left(2MrV_0\eta D_{21} - 2\mu^2MrV_0\eta H_{21}^3\right)$$

$$S_{21} = \frac{1}{2}\left(-\left(MrV_0\eta + \beta Mr\right)H_{11}^2 + MrV_0\eta F_{11} + \alpha H_{11}^4\right)$$

$$S_{22} = \frac{1}{2}\left(MrV_0\eta F_{21} + 2MrV_0D_{21} - 2\mu^2MrV_0H_{21}^3\right) + \frac{1}{4}\left(2MrV_0\eta D_{21} - 2\mu^2MrV_0\eta H_{21}^3\right)$$

$$S_{23} = \frac{1}{2}\left(MrV_0\eta F_{12} + 2MrV_0D_{12} - 2\mu^2MrV_0H_{12}^3\right) + \frac{1}{4}\left(2MrV_0\eta D_{12} - 2\mu^2MrV_0\eta H_{12}^3\right)$$

$$S_{11} = \frac{1}{2}\left(\left(V_0^2\eta^2 - 2V_0^2\eta\right)H_{11}^2 + \left(2\mu^2V_0^2\eta - \mu^2V_0^2\eta^2\right)H_{11}^4\right) + k\,I_{11}^1 + (V_0^2 - T - \mu^2K)\,H_{11}^2 + (1 - \mu^2V_0^2)\,H_{11}^4$$

$$S_{12} = \left(\frac{1}{2}\beta V_0\eta - \beta V_0\right)H_{21}^3;\; S_{13} = \left(\frac{1}{2}\beta V_0\eta - \beta V_0\right)H_{12}^3$$

$$S_{14} = \frac{1}{2}\left(\left(V_0^2\eta^2 - 2V_0^2\eta\right)H_{22}^2 + \left(2\mu^2V_0^2\eta - \mu^2V_0^2\eta^2\right)H_{22}^4\right) + k\,I_{22}^1 + (V_0^2 - T - \mu^2k)\,H_{22}^2 + (1 - \mu^2V_0^2)\,H_{22}^4$$

$$S_{33} = \frac{1}{2}\left(MrV_0\eta F_{12} - 2MrV_0D_{12} + 2\mu^2MrV_0H_{12}^3\right) + \frac{1}{4}\left(2MrV_0\eta D_{12} - 2\mu^2MrV_0\eta H_{12}^3\right)$$

$$S_{34} = \frac{1}{2}\left(MrV_0\eta F_{22} - \alpha H_{22}^4 + \left(\beta Mr - MrV_0\eta\right)H_{22}^2\right)$$

$$S_{41} = \frac{1}{2}\left(2V_0^2\eta H_{11}^2 - 2\mu^2V_0^2\eta H_{11}^4\right) + k\,I_{11}^1 + (V_0^2 - T - \mu^2k)H_{11}^2 + (1 - \mu^2V_0^2)H_{11}^4$$

$$S_{42}=\left(-\frac{1}{2}\beta V_0\eta+2V_0^2\eta\right)H_{21}^3;\ S_{43}=\left(-\frac{1}{2}\beta V_0\eta-\beta V_0\right)H_{12}^3$$

$$S_{44}=\frac{1}{2}\left(2V_0^2\eta H_{22}^2-2\mu^2V_0^2\eta H_{22}^4\right)+k\,I_{22}^1+(V_0^2-T-\mu^2k)H_{22}^2+(1-\mu^2V_0^2)H_{22}^4$$

$$F=\left\langle y_iC_{ij}^3Z_i,\bar{Z}_j\right\rangle$$

$$m_i=I_{ii}^1-\mu^2H_{ii}^2$$

For more general cases using more eigenmodes and harmonics, a highly nonlinear algebraic equation f(Ω)=det(G)=0 will be resulted and thus has to be numerically solved.

Based on these relationships, the dynamic and parametric instability analyses can be numerically investigated. The effects of the considered physical parameters on the divergence, flutter and parametric instability zones as well as the associated time response can be numerically analyzed.

6. Analytical procedure

For the sake of accuracy and comparison, analytical procedures are elaborated for some simple cases. As various parameters such as fluid velocity, thermal effect, tube viscoelasticity and fluid velocity and viscosity are considered, the free dynamic behaviors of the CNT can be affected by all these parameters. To easily handle the effect of these parameters, it is important to obtain some associated analytical relationships. To this aim, the transverse displacement is assumed of the form:

$$W(y,\tau)=w(y)e^{i\omega\tau} \tag{4.36}$$

The complex characteristic equation associated to the main governing equation (4.16a), for a static fluid velocity $(\eta=0)$, is given for, $w(y)=e^{\lambda y}$, by:

$$\left(i\omega\alpha+1-\mu^2(V_0^{\,2}-T)\right)\lambda^4+\left(i\beta V_0-2\omega M_rV_0\ \mu^2\right)\lambda^3-\left(V_0^{\,2}-T-i\beta M_r-\mu^2(k-\omega^2)\right)\lambda^2$$

$$+2\omega M_rV_0\,\lambda+k-\omega^2=0 \tag{4.37}$$

For four distinct solutions of (4.37), the general solution associated to (4.16a) can be written in the form:

$$w(y)=A_1e^{i\lambda_1y}+A_2e^{i\lambda_2y}+A_3e^{i\lambda_3y}+A_4e^{i\lambda_4y} \tag{4.38}$$

where the arbitrary constants A_i are determined by the considered boundary conditions.

It should to be noted that the resulting frequencies and eigenmodes depend on the considered parameters such as V_0, k, α, etc and on the temperature T. This will lead to complex

eigenfrequencies and eigenmodes that may be deeply changed with respect to these parameters.

For simply supported and clamped CNT, the associated eigenmodes are given by:

$$\varphi_j(y) = A_1 e^{i\lambda_{1j}y} + A_2 e^{i\lambda_{2j}y} + A_3 e^{i\lambda_{3j}y} + A_4 e^{i\lambda_{4j}y} \tag{4.39}$$

where

$$A_2 = -\frac{(\gamma_{4j}-\gamma_{1j})e^{i\lambda_{3j}} + (\gamma_{1j}-\gamma_{3j})e^{i\lambda_{4j}} + (\gamma_{3j}-\gamma_{4j})e^{i\lambda_{1j}}}{(\gamma_{3j}-\gamma_{4j})e^{i\lambda_{2j}} + (\gamma_{4j}-\gamma_{2j})e^{i\lambda_{3j}} + (\gamma_{2j}-\gamma_{3j})e^{i\lambda_{4j}}} A_1;$$

$$A_3 = -\frac{(\gamma_{4j}-\gamma_{1j})e^{i\lambda_{2j}} + (\gamma_{1j}-\gamma_{2j})e^{i\lambda_{4j}} + (\gamma_{2j}-\gamma_{4j})e^{i\lambda_{1j}}}{(\gamma_{3j}-\gamma_{4j})e^{i\lambda_{2j}} + (\gamma_{4j}-\gamma_{2j})e^{i\lambda_{3j}} + (\gamma_{2j}-\gamma_{3j})e^{i\lambda_{4j}}} A_1;$$

$$A_4 = -(A_1 + A_2 + A_3)$$

in which $\gamma_{ij} = \lambda_{ij}$ and $\gamma_{ij} = \lambda_{ij}^2$ for clamped and simply supported boundary conditions respectively. The resulting transcendental equation is thus given by:

$$\left[e^{(\lambda_{1j}+\lambda_{2j})} + e^{(\lambda_{3j}+\lambda_{4j})}\right](\gamma_{2j}-\gamma_{1j})(\gamma_{4j}-\gamma_{3j}) + \left[e^{(\lambda_{1j}+\lambda_{3j})} + e^{(\lambda_{2j}+\lambda_{4j})}\right](\gamma_{2j}-\gamma_{4j})(\gamma_{3j}-\gamma_{1j})$$
$$+\left[e^{(\lambda_{2j}+\lambda_{3j})} + e^{(\lambda_{1j}+\lambda_{4j})}\right](\gamma_{1j}-\gamma_{4j})(\gamma_{2j}-\gamma_{3j}) = 0 \tag{4.40}$$

It has to be noted that equations (4.37) and (4.40) have to be simultaneously numerically solved in order to get the frequency and eigenmodes at required flow velocity levels. A numerical iterative-incremental procedure based on the Newton-Raphson algorithm has been elaborated for that goal. The simplified as well as the complex eigenmodes can be obtained based on this semi-analytical methodological approach.

Simplified case

The analytical formulation is more simple for α=β=Mr=0. In this case, equation (4.37) is reduced to:

$$\left(1-\mu^2(V_0^2-T)\right)\lambda^4 - \left(V_0^2 - T - \mu^2(k-\omega^2)\right)\lambda^2 + k - \omega^2 = 0 \tag{4.41}$$

and its solutions are :

$$\lambda_1 = \sqrt{\frac{\left(V_0^2 - T - \mu^2(k-\omega^2)\right) + \sqrt{\Delta}}{2\left(1-\mu^2(V_0^2-T)\right)}};\ \lambda_2 = -\lambda_1; \lambda_3 = \sqrt{\frac{\left(V_0^2 - T - \mu^2(k-\omega^2)\right) - \sqrt{\Delta}}{2\left(1-\mu^2(V_0^2-T)\right)}}; \lambda_4 = -\lambda_3$$

where: $\Delta = \left(V_0^2 - T - \mu^2(k-\omega^2)\right)^2 - 4\left(1-\mu^2(V_0^2-T)\right)\left(k-\omega^2\right)$

Equation (4.40) is also reduced to:

$$F(\omega) = (\lambda_1 - \lambda_3)^2 (e^{i(\lambda_1+\lambda_3)} + e^{-i(\lambda_1+\lambda_3)}) - (\lambda_1 + \lambda_3)^2 (e^{i(\lambda_1-\lambda_3)} + e^{-i(\lambda_1-\lambda_3)}) + 8\lambda_1\lambda_3 = 0 \quad (4.42)$$

The mode shapes $\varphi_j(y)$ can be thus classically for the considered boundary conditions by:

$$\varphi_j(y) = A_1 e^{i\lambda_{1j}y} + A_2 e^{-i\lambda_{1j}y} + A_3 e^{i\lambda_{3j}y} + A_4 e^{-i\lambda_{3j}y} \quad (4.43)$$

For more simplification k=0, in this case, equation (4.16a) can be written as:

$$\left(1 - \mu^2 (V_c^{\,2} - T)\right) \frac{d^4 w}{dy^4} + \left(V_c^{\,2} - T\right) \frac{d^2 w}{dy^2} = 0 \quad (4.44)$$

if $\left(1 - \mu^2 (V_c^{\,2} - T)\right) \neq 0$

$$\frac{d^4 w}{dy^4} + \gamma^2 \frac{d^2 w}{dy^2} = 0 \quad \gamma^2 = \frac{\left(V_c^{\,2} - T\right)}{\left(1 - \mu^2 (V_c^{\,2} - T)\right)} \quad (4.45)$$

The general solution associated to (4.45) can be written in the form:

$$w(y) = A_1 + A_2 y + A_3 \sin(\gamma y) + A_4 \cos(\gamma y) \quad (4.46)$$

For the clamped boundary condition, the transcendental equation is given by:

$$\gamma \sin\left(\frac{\gamma}{2}\right)\left(\tan\left(\frac{\gamma}{2}\right) - \frac{\gamma}{2}\right) = 0 \quad (4.47)$$

The solutions of equation (4.47) are given by:

$$\gamma = 2n\pi \quad n \in \mathbb{N} \quad or \; \gamma = [8.986; 15.451; 21.808; 28.132; 34.442; \ldots] \quad (4.48)$$

And the associated mode shapes are given by:

$$w(y) = \mathrm{A}\left(1 - \frac{\gamma(\cos(\gamma)-1)}{-\gamma+\sin(\gamma)}\, y + \frac{(\cos(\gamma)-1)}{-\gamma+\sin(\gamma)} \sin(\gamma y) - \cos(\gamma)\right) \quad (4.49)$$

For the simply supported boundary condition, the transcendental equation is given by:

$$\gamma^4 \sin(\gamma) = 0 \quad (4.50)$$

The solutions are given by:

$\gamma = n\pi \quad n \in \mathbb{N}$

and the associated mode shapes are given by:

$$w(y) = A\sin(\gamma y) \quad (4.51)$$

The critical flow velocity is given by:

$$V_c = \sqrt{\frac{\gamma^2\left(1 + \mu^2 T\right) + T}{\left(1 + \gamma^2 \mu^2\right)}} \quad (4.52)$$

A multimodal dynamic analysis can be elaborated based on the analytical modes $\varphi_j(y)$ by assuming:

$$w(y,\tau)=\sum_{j=1}^{N}\varphi_j(y)\,q_j(\tau) \tag{4.53}$$

Substituting Eqs. (4.14) and (4.39) into the main governing equation (4.16a) and integrating over [0, 1], the following second-order ordinary differential system is obtained.

$$\left[\bar{\bar{A}}-\mu^2\bar{\bar{B}}\right]\{\ddot{q}_r\}+\left[\alpha\bar{\bar{C}}+2M_rV_0\left(1+\eta\cos(\Omega\tau)\right)\bar{\bar{D}}-\beta M_r\,\bar{\bar{B}}-2\mu^2M_rV_0\left(1+\eta\cos(\Omega\tau)\right)\bar{\bar{E}}\right]\{\dot{q}_r\}$$
$$+\left[\left(V_0^2\left(1+2\eta\,\cos(\Omega\tau)+\eta^2\cos(\Omega\tau)^2\right)-T-\mu^2k+M_rV_0\eta\,\Omega\sin(\Omega\tau)\right)\bar{\bar{B}}-M_rV_0\eta\,\Omega\sin(\Omega\tau)\bar{\bar{F}}\right.$$
$$\left.+k\bar{\bar{A}}-\beta V_0\left(1+\eta\,\cos(\Omega\tau)\right)\bar{\bar{E}}+\left(1-\mu^2V_0^2\left(1+2\eta\,\cos(\Omega\tau)+\eta^2\cos(\Omega\tau)^2\right)\right)\bar{\bar{C}}\right]\{q_r\}=0 \tag{4.54}$$

where $\bar{\bar{A}},\bar{\bar{B}},\bar{\bar{C}},\bar{\bar{D}},\bar{\bar{E}}$ and $\bar{\bar{F}}$ are matrices with elements given by: (s, r=1,2,…,N).

$$\bar{\bar{A}}_{sr}=\int_0^1\varphi_r\bar{\varphi}_s dy,\ \bar{\bar{D}}_{sr}=\int_0^1\frac{d\varphi_r}{dy}\bar{\varphi}_s dy,\ \bar{\bar{B}}_{sr}=\int_0^1\frac{d^2\varphi_r}{dy^2}\bar{\varphi}_s dy,\ \bar{\bar{E}}_{sr}=\int_0^1\frac{d^3\varphi_r}{dy^3}\bar{\varphi}_s dy,$$

$$\bar{\bar{C}}_{sr}=\int_0^1\frac{d^4\varphi_r}{dy^4}\bar{\varphi}_s dy,\ \bar{\bar{F}}_{sr}=\int_0^1 y\frac{d^2\varphi_r}{dy^2}\bar{\varphi}_s\,dy$$

It should be stated that when the modal basis is available analytically, the dynamic and parametric instability analyses can be investigated based on the same procedures developed in the previous sections.

7. Numerical results and discussion

Let us note that due to the fluid velocity the dynamic instability will occur at increased static velocity V_0. This will lead to divergence and flutter instabilities. Then, even if the viscosities of the fluid and tube are disregarded, the complex eigenmodes and frequencies may occur. This paper will focus on complex eigenmodes and on the coupling dynamic and parametric instabilities with respect to static velocity and dynamic pulsation fluid. For the sake of clarity, the one-mode and two-modes approaches are used for the analysis. Based on these approaches, the first and second natural frequencies, critical flow velocity and stability regions are obtained. The time responses are computed for various instability regions.

For numerical analysis, the following material and geometrical parameters of CNT-fluid system are used. The Young's modulus of carbon nanotube is assumed to be E=1TPa with an effective thickness about h=0.34 nm. The diameter d, the mass density ρc and the aspect ratio L/d of SWCNT are 1nm, 2300 kg/m^3, and 10 respectively. The fluid inside the nanotube is

assumed to be the water with the mass density ρ_f and viscosity ϑ are 1000 kg/m3 and 1.12x103 Pa respectively [2]. Two cases of the low and high temperature are considered. At low and room temperature, the thermal expansion coefficients αx=-1.6e-6 K^{-1} and at high temperature αx=1.1e-6.K^{-1}

For comparison and validation of the presented numerical and analytical methodological approaches numerical results are presented in tables 4.1 and 4.2. The finite difference method (FDM) has been also used and programed here for numerical comparison. The details of this classic numerical approach have been omitted here. Numerical results of the three first natural frequencies of simply supported and clamped boundary conditions CNT are given for various values of V_0. Numerical results are obtained based on the DQM for point numbers N=7, 10, 15 and on the FDM for N=15, 50, 100 and presented in tables 4.1 and 4.2. The analytical results obtained based on equations (4.32, 4.35) are also given for convergence test. It is demonstrated that the DQM converges for 15 points while the finite difference method needs largely more discretization points (N=100) to converge.

Complex eigenmodes will be classically induced by the fluid and solid viscosities and particularly by the static fluid velocity V_0. The tube viscoelasticity is generally too small and thus can be neglected. To clarify the fluid viscosity and velocity effects on the CNT vibration behaviors, numerical results of the obtained eigenmodes are presented.

Figures 4.1 and 4.2 present real and imaginary parts of the first mode shape, mass normalized, of a simply supported CNT for $V_0 = 0, 1, 2, 3, 4, 5, 6, 7$ as well as the classical simplified mode "$\sin(\pi x/L)$". Note that, for these small values of V_0, $\sin(\pi x/L)$ is good enough for the real part of the first mode. The imaginary part, neglected by this classical mode, is not zero even for $V_0 = 0$ as the fluid viscosity is considered. At large V_0, the shape of the real part changes and the imaginary part is highly increased as shown in figure 4.2. The first mode of a clamped CNT at various values of V_0 is presented in figure 4.3. It is demonstrated that for small values of V_0; ($V_0 = 0, 1, 2, 3, 4, 5$) the real part is almost unchanged but there is an imaginary part that is considerably increasing with V_0. To show the effect of V_0 on the first modes a large range of values of V_0 is considered and real and imaginary parts of the first, second and third eigenmodes are presented in figures 4.4, 4.5 and 4.6 for a clamped CNT ($\beta = \alpha = Ts = K = 0$). These figures show that there is a transition of the real part of the first mode to the second one and that the imaginary parts of all modes become very significant when the static velocity V_0 exceeds a critical value. To show the coalescence behavior at a

critical fluid velocity V_0, the first and second modes are presented in figure 4.7 for clamped case.

The transition from mode to mode and the growing of imaginary parts with respect to V_0 can be explained by the frequency-velocity dependence curves giving the dynamic instability behavior of the CNT-fluid system. This dynamic behavior is investigated here based on the one and two-real-mode as well as on the complex modes approaches. Figure 4.8 demonstrates the divergence and flutter instability types for the considered simply supported and clamped CNT based on one-real mode, two-real modes and one-complex mode approaches. The real frequency parts decreases with increasing of the flow velocity V_0 up to the divergence instability (ω=0). The critical values of V_0 for the divergence instability associated to complex-mode are V_0= 3.14 for the considered simply supported CNT and V_0=6.28 for the clamped CNT (T=0, α=0). The critical values of the flutter instability are V_0=6.38 and V_0=9.01 for S-S and C-C CNT respectively.

It should to be stated that a one-real mode approach leads to erroneous results for flutter analysis but good enough for divergence detection. The predictions obtained for the dynamic instability analysis based on the two-real-modes and the one-complex mode approaches are very close for simply supported case but leads to different values for clamped case for large values of V_0.

The temperature effect on the dynamic instability of a clamped CNT predicted by a one complex-mode approach is presented in figure 4.9 and only small effects are observed.

The effects of the static fluid velocity V_0, the viscosity β, the viscoelastic parameter α, the nonlocal parameter μ and the thermal coefficient effect Ts on real and imaginary parts of the first, second and third frequencies of cantilever CNTs conveying fluid are presented in figure 4.10. This effect is more significant at higher velocities.

A parametric study with respect to all considered physical and material parameters can be easily done by the presented methodological approaches.

Figures 4.11 and 4.12 demonstrate the effects of the static fluid velocity V_0, the viscosity β, the viscoelastic parameter α, the nonlocal parameter μ and the thermal coefficient effect T_s on the instability boundaries in the principal parametric resonance based on the one- real-mode approach. In figure 4.11 the instability areas, origins of parametric instability are reduced with increase in fluid viscosity β and the viscoelastic coefficient α. It should be noted that a larger flow velocity V_0 leads to a large instability region. In figure 4.12, the effects of

the nonlocal parameter μ and the thermal coefficient T_s are presented. The parametric resonance regions move significantly backwards by increasing the nonlocal parameter μ and slightly upwards by increasing T_s.

The one and two-modes based parametric instability regions of the CNT with different values of the static flow velocity V_0 of a simply supported and clamped CNT are presented in figures 4.13, 4.14 respectively. The influences of the nonlocal parameter on the parametric frequency are presented in figure 4.13. The difference between the one and two modes predictions in stability regions are presented in figure 4.15. It is observed that the critical parametric frequency and dimensionless pulsation amplitude η associated to bifurcations point are increased when two-modes are used. The fluid viscosity β effect is demonstrated in figures 4.16. Moreover comparison between the real and the complex mode approaches are given in figure 4.17. It demonstrated that for fixed V_0 the parametric instability regions are shifted to the higher parametric frequency when the complex modes are used. For a general representation, figure 4.18 shows the parametric instability regions of the clamped CNT in three dimensions (Ω, V_0, η) based on one complex-mode. The evolutions of the parametric instability frequencies and the associated bifurcation points for different viscous parameter β are shown in figure 4.19. These analyses allow determining the stability boundaries and zones with respect to the static fluid velocity V_0 and to the other physical parameters.

To clearly demonstrate the dynamic behaviors in these regions, time responses are presented in figure 4.20 for SS CNT and in figure 4.21 for CC- CNT based on the one-real mode and two-real modes approaches. These figures show the time responses associated to various values of Ω for fixed values of V_0. It is observed that the dynamic response is very sensitive to the static velocity V_0 as well to the parameters η and Ω. The stability and instability behaviors are clearly demonstrated with respect the parametric instability zones.

8. Conclusion

Vibration, dynamic and parametric instabilities of CNT conveying pulsating fluid are analyzed based on the nonlocal elasticity fluid interaction and Euler-Bernoulli beam theory. A numerical methodological approach based on the differential quadrature method has been formulated. For comparisons in some simple cases a semi analytical procedure has been also developed. The multimode approach has been formulated based on the numerically computed eigenmodes, for dynamic and parametric instabilities. For simplified models a one-real mode,

a two-real mode and one-complex mode approaches have been developed for both types of instabilities. The inaccuracy of the one-real mode approach is demonstrated. The influences of the internal fluid velocity, the nonlocal parameter, the viscosity, the viscoelastic coefficient as well as the thermal effects on the dynamic behaviors and flow-induced structural instability of CNTs are studied. Various types of instabilities such as divergence, flutter and parametric instability and their interactions are investigated.

References

[1] R.F Gibson, E.O, Ayorind and Y.F Wen, Vibration of carbon nanotubes and their composites: A review, Composites Sciences and Technology 67, pp. 1-28, 2007.

[2] H. L. Lee and W. J. Chang, Vibration analysis of a viscous fluid conveying single walled carbon nanotube embedded in an elastic medium, J. Physica E 41, 529-532, 2009.

[3] L. Wang, Vibration analysis of fluid-conveying nanotubes with consideration of surface effects. J. Physica E 43, 437–439, 2010.

[4] A.C. Eringen, On differential equation of nonlocal elasticity and solution, J. Appl. Phys. 54, pp. 4703-4710, 1983.

[5] A.C. Eringen and DGB Edelen, On nonlocal elasticity, Int. J. Eng. Science10, pp. 233–248, 1972

[6] J.N. Reddy, Nonlocal theories for bending, buckling and vibration of beams, Int. J. Eng. Science 45, pp. 288–307, 2007

[7] W. H. Duan, N. Challamel, C. M. Wang, and Z. Ding, Development of analytical vibration solutions for microstructured beam model to calibrate length scale coefficient in nonlocal Timoshenko beams, J. Appl. Phys. 114, 104312, 2013

[8] Z. Zhang, N. Challamel, and C. M. Wang, Eringen's small length scale coefficient for buckling of nonlocal Timoshenko beam based on microstructured beam model

Citation: J. Appl. Phys. 114, 114902, 2013

[9] C. M. Wang, Z. Zhang, N. Challamel and W. H. Duan, Calibration of Eringen's small length scale coefficient for initially stressed vibrating nonlocal Euler beams based on microstructured beam model, J. Phys. D: Appl. Phys. 46, 345501, 2013

[10] Y. S. Seo, W. B. Jeong, S. H. Jeong, J. S. Oh and W. S. Yoo, Finite element analysis of forced vibration for pipe conveying harmonically pulsating fluid, J. JSEM, Series C,Vol 48, No.4, 2005.

[11] Z. Hong, D. Qing-Tian and L. Shao-Hua, Vibration of a single-walled carbon nanotube embedded in an elastic medium under a moving internal nanoparticle, J. Applied Mathematical Modelling 37, 6940–6951, 2013.

[12] M. Mirramezani and H. R. Mirdamadi, Effects of nonlocal elasticity and Knudsen number on fluid–structure interaction in carbon nanotube conveying fluid, J. Physica E 44 2005–2015, 2012.

[13] L. Baohui, G. Hangshan, L. Yongshou and Y. Zhufeng, Free vibration analysis of micropipe conveying fluid by wave method, J. Results in Physics 2, 104–109, 2012.

[14] E. Ghavanloo, F. Daneshmand and M. Rafiei , Vibration and instability analysis of carbon nanotubes conveying fluid and resting on a linear viscoelastic Winkler foundation, J. Physica E 42, 2218–2224, 2010.

[15] L. Wang, H.T. Liu, Q. Ni and Y. Wu, Flexural vibrations of microscale pipes conveying fluid by considering the size effects of micro-flow and micro-structure, J. of Engineering Science 71, 92–101, 2013.

[16] L. Wang and Q. Ni, A reappraisal of the computational modeling of carbon nanotubes conveying viscous fluid, J. Mechanics Research Communications 26, 833-837, 2009.

[17] T. P. Chang, Thermal–mechanical vibration and instability of a fluid-conveying

single-walled carbon nanotube embedded in an elastic medium based on nonlocal elasticity theory, Applied Mathematical Modelling 36, 1964–1973, 2012.

[18] R. Ansari, R. Gholami and S. Sahmani, Dynamic stability of embedded single walled carbon nanotube including thermal environment effects, J. Scientia Iranica F 19, 919-925, 2012.

[19] A. Azrar, L. Azrar, A. A. Aljinaidi and M. Hamadiche, Dynamics instability analysis of multi-walled carbon nanotubes conveying fluid. J. Advanced Materials Research Vol. 682, 153-160, 2013.

[20] A. Azrar, L. Azrar and A. A. Aljinaidi, Length scale effect analysis on vibration behavior of single walled Carbon NanoTubes with arbitrary boundary conditions. Revue de Mécanique Théorique et Appliquée, Vol. **2**, 475- 485, 2011.

[21] A. Azrar, L. Azrar and A. A. Aljinaidi, Analytical and numerical modeling of higher order free vibration characteristics of single walled Carbon NanoTubes, submitted to J. Physica E, 2014.

[22] L. Jing, F. Shang-Chun, L. Yan and G. Zhan-She, Dynamic stability of parametrically excited linear resonant beams under periodic axial force, J. Chin. Phys. B Vol.21, No. 11 110401, 2012.

[23] C. Shu, Differential Quadrature and its Application in Engineering, Spinger, London, 2000.

[24] Z. Zong and Y. Zhang, Advanced Differential Quadrature Methods, Chapman & Hall/CRC, Taylor & Francis Group, 2009.

[25] M. P. Paidoussis, Fluid-Structure Interactions: Slender Structures and Axial Flow, Vol.1, Academic Press, 1998.

Appendix A

G=

$\frac{1}{2}Y_2+Y_6$	0	0	$\frac{1}{2}(Y_1+Y_3)\Omega$	$\frac{1}{4}Y_2$	0	0	0	$\frac{1}{4}Y_2$	0	0	
0	$\frac{1}{2}Y_2-\frac{1}{2}Y_4-\frac{1}{4}M\Omega^2+Y_6$	$(\frac{1}{2}Y_1+\frac{1}{4}Y_3-\frac{1}{2}Y_5)\Omega$	0	0	$-\frac{1}{4}Y_2+\frac{1}{2}Y_4\Omega$	$-(\frac{1}{2}Y_1+\frac{3}{4}Y_3)\Omega$	0	0	$\frac{1}{4}Y_2$	0	
0	$(\frac{1}{2}Y_1+\frac{1}{4}Y_3+\frac{1}{2}Y_5)\Omega$	$\frac{1}{2}Y_4+Y_6-\frac{1}{4}M\Omega^2$	0	0	$(\frac{1}{2}Y_1+\frac{3}{4}Y_3)\Omega$	$\frac{1}{2}Y_4+\frac{1}{4}Y_2$	0	0	0	$\frac{1}{4}Y_2$	
$Y_1\Omega$	0	0	$\frac{1}{4}Y_2-M\Omega^2+Y_6$	$-\Omega Y_5$	0	0	$\frac{1}{2}Y_4$	$-(Y_1+Y_3)\Omega$	0	0	
Y_2	0	0	ΩY_5	$\frac{3}{4}Y_2+Y_6-M\Omega^2$	0	0	$(Y_1+Y_3)\Omega$	$\frac{1}{2}Y_4$	0	0	
0	$\frac{1}{2}Y_4-\frac{1}{4}Y_2$	$\frac{1}{2}Y_1-\frac{1}{4}Y_3)\Omega$	0	0	$\frac{1}{2}Y_2+Y_6-\frac{9}{4}M\Omega^2$	$-\frac{3}{2}\Omega Y_5$	0	0	$\frac{1}{2}Y_4$	$-(Y_1+\frac{5}{4}Y_3)\Omega$	
0	$(\frac{1}{4}Y_3-\frac{1}{2}Y_1)\Omega$	$\frac{1}{2}Y_4$	0	0	$\frac{3}{2}\Omega Y_5$	$\frac{1}{2}Y_2+Y_6-\frac{9}{4}M\Omega^2$	0	0	$(Y_1+\frac{5}{4}Y_3)\Omega$	$\frac{1}{2}Y_4$	
0	0	0	$\frac{1}{2}Y_4$	$\frac{1}{2}(Y_1-Y_3)\Omega$	0	0	$\frac{1}{2}Y_2+Y_6-4M\Omega^2$	$-2\Omega Y_5$	0	0	
$\frac{1}{2}Y_2$	0	0	$\frac{1}{2}Y_3\Omega-Y_1$	$\frac{1}{2}Y_4$	0	0	$2\Omega Y_5$	$\frac{1}{2}Y_2+Y_6-4M\Omega^2$	0	0	
0	$\frac{1}{4}Y_2$	0	0	0	$\frac{1}{2}Y_4$	$(\frac{1}{2}Y_1-\frac{3}{4}Y_3)\Omega$	0	0	$\frac{1}{2}Y_2$	$-\frac{5}{2}\Omega Y_5$	
0	0	$\frac{1}{2}Y_2$	0	0	$(-\frac{1}{2}Y_1+\frac{3}{4}Y_3)\Omega$	$\frac{1}{2}Y_4$	0	0	$\frac{5}{2}\Omega Y_5$	$\frac{1}{2}Y_2+Y_6-\frac{25}{4}M\Omega^2$	

where Y_i are given by :

$$Y_1 = \mathrm{Mr}\mathrm{V}_0\eta\left(F - H^2\right),$$

$$Y_2 = \mathrm{V}_0^2\eta^2\left(H^2\text{-}\mu^2H^4\right),$$

$$Y_3 = 2\mathrm{Mr}\mathrm{V}_0\eta\left(H^1\text{-}\mu^2\,H^3\right),$$

$$Y_4 = 2\mathrm{V}_0^2\eta\left(H^2\text{-}\mu^2H^4\right)\text{-}\beta\mathrm{V}_0\eta\,H^3,$$

$$Y_5 = 2\mathrm{Mr}\mathrm{V}_0\left(H^1\text{-}\mu^2H^3\right)+\alpha H^4\text{-}\beta\mathrm{Mr}H^2,$$

$$Y_6 = k\,I^1+(\mathrm{V}_0^2\text{-T-}\mu^2\mathrm{k})\,H^2+(1\text{-}\mu^2\mathrm{V}_0^2)H^4\text{-}\beta\mathrm{V}_0H^3,$$

Table 4.1 Resonant frequencies of a simply supported SWCNT for V_0= 0, 2, 4 and (μ = 0, β=0, α = 0, Ts=0)

V_0	ω	DQM			Finite difference method			Analytical
		N=7	N=10	N=15	N=15	N=50	N=100	
V_0=0	ω1	3.1490	3.1415	3.1416	3.1359	3.1411	3.1415	3.1416
	ω2	5.9207	6.2783	6.2832	6.2374	6.2791	6.2822	6.2832
	ω3	7.8871	9.6355	9.4247	9.2705	9.4108	9.4213	9.4248
V_0=2	ω1	2.7513	2.7523	2.7520	2.7453	2.7514	2.7519	2.7520
	ω2	6.1219	6.1207	6.1219	6.0747	6.1175	6.1206	6.1218
	ω3	9.5479	9.3227	9.3205	9.1647	9.3065	9.3171	9.3204
V_0=4	ω1	1.9439-1.9439i	1.9473 + 1.9473i	1.9464 - 1.9464i	1.9474 + 1.9474i	1.9465 - 1.9465i	1.9464 + 1.9464i	1.9463 - 1.9463i
	ω2	5.5630	5.5421	5.5468	5.4930	5.5418	5.5454	5.5467
	ω3	9.2757	8.9954	8.9869	8.8243	8.9722	8.9832	8.9868

Table 4.2 Resonant frequencies of a clamped-clamped SWCNT for V_0= 0, 4, 7 and (μ = 0, β=0, α = 0, Ts=0)

V_0	ω	DQM			Finite difference method			Analytical
		N=7	N=10	N=15	N=15	N=50	N=100	
V_0=0	ω1	4.7498	4.7299	4.7300	4.6875	4.7261	4.7291	4.7300
	ω2	7.6435	7.8483	7.8532	7.6999	7.8390	7.8496	7.8532
	ω3	9.3753	11.1148	10.9956	10.6334	10.9615	10.9871	10.9956
V_0=4	ω1	4.1809	4.1349	4.1354	4.0896	4.1313	4.1344	4.1354
	ω2	7.1085	7.4487	7.4543	7.2959	7.4397	7.4506	7.4543
	ω3	8.9864	10.8456	10.6968	10.3267	10.6621	10.6880	10.6968
V_0=7	ω1	1.989+1.9899i	2.2783+2.2783i	2.2769+2.2769i	2.2975+2.2975i	2.2789+2.2789i	2.2774+2.2774i	2.2769+2.2769i
	ω2	5.4779	6.3596	6.3697	6.1767	6.3523	6.3654	6.3697
	ω3	7.8852	10.230	9.9951	9.5971	9.9581	9.9857	9.9949

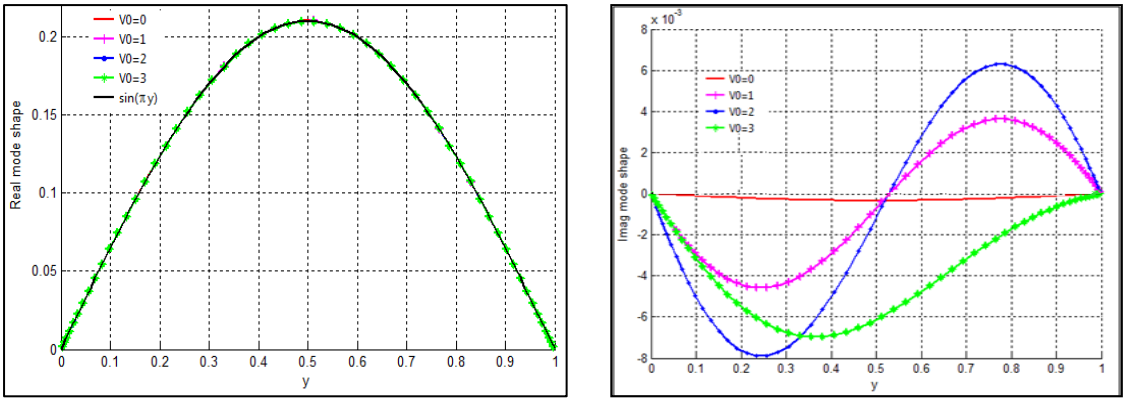

Figure 4.1 Real and imaginary parts of the first complex mode shape mass normalized of a simply-supported SWCNT at different dimensionless small flow velocities V_0, (β=0.01, α=0, μ=0.1, Ts=0.1, k=0.5)

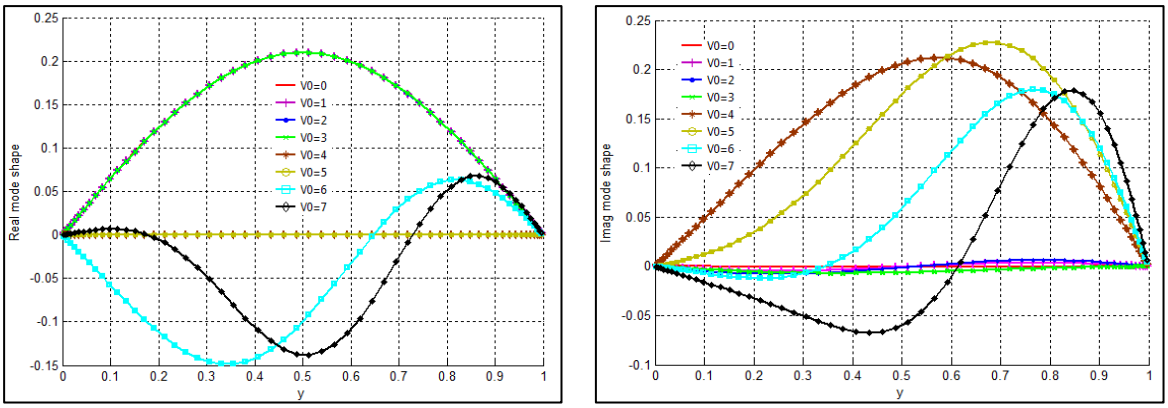

Figure 4.2 Real and imaginary parts of the first complex mode shape mass normalized of a simply-supported SWCNT at different dimensionless flow velocities V_0, (β=0.01, α=0, μ=0.1, Ts=0.1, k=0.5)

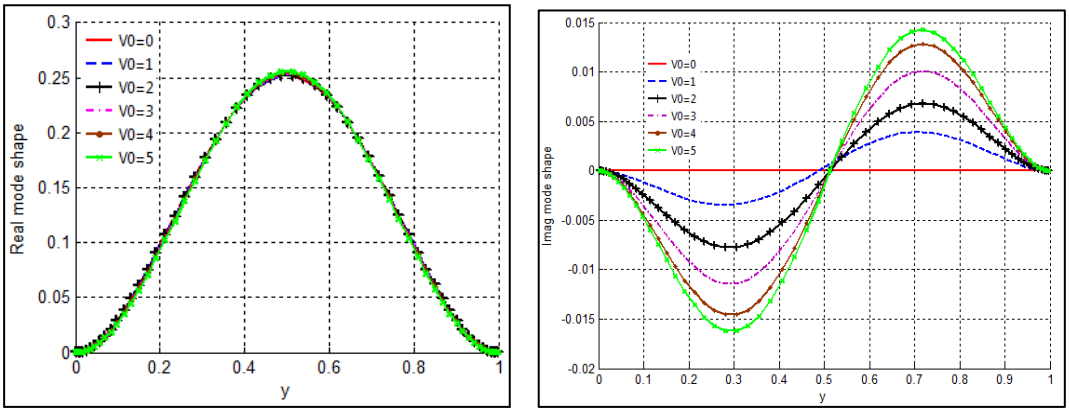

Figure 4.3 Real and imaginary parts of the first complex mode shape mass normalized of a clamped SWCNT at different dimensionless small flow velocities V_0, (β=0, α=0, Ts=0, k=0)

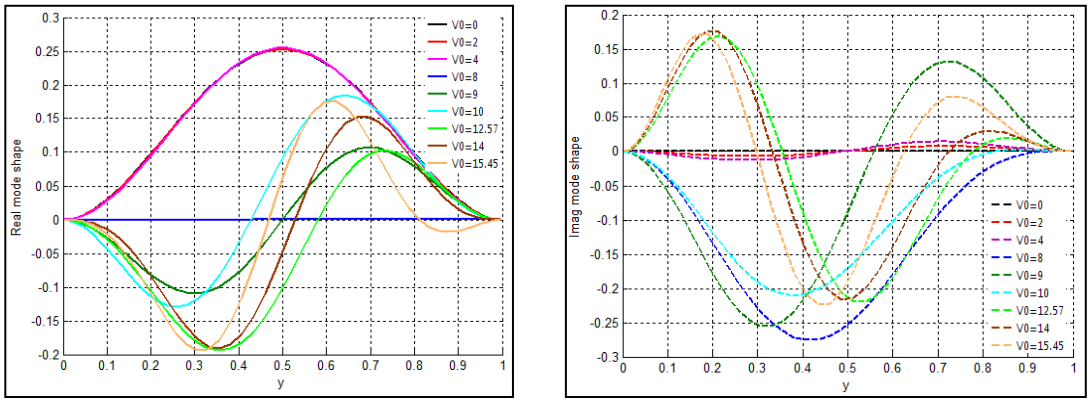

Figure 4.4 Real and imaginary parts of the first complex mode shapes mass normalized of a clamped SWCNT at different dimensionless flow velocities V_0, (β=0, α=0, Ts=0, k=0)

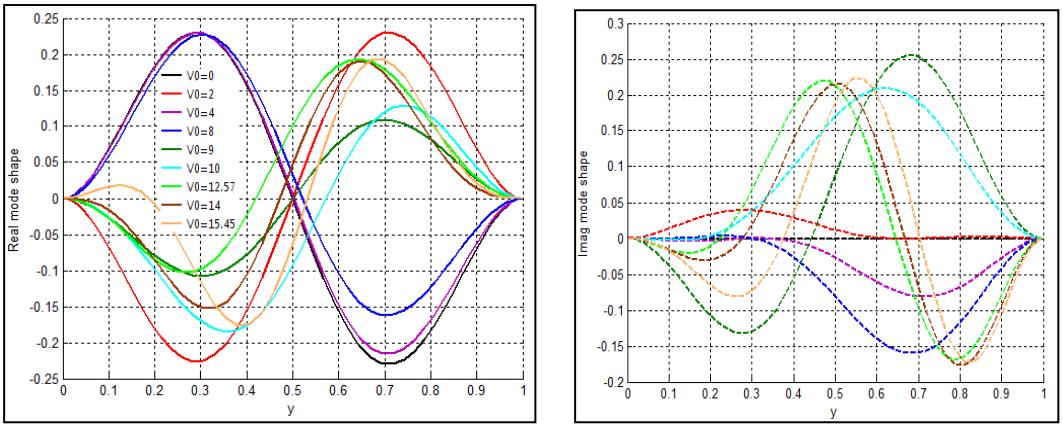

Figure 4.5 Real and imaginary parts of the second complex mode shapes mass normalized of a clamped SWCNT at different dimensionless flow velocities V_0, (β=0, α=0, μ=0, Ts=0, k=0)

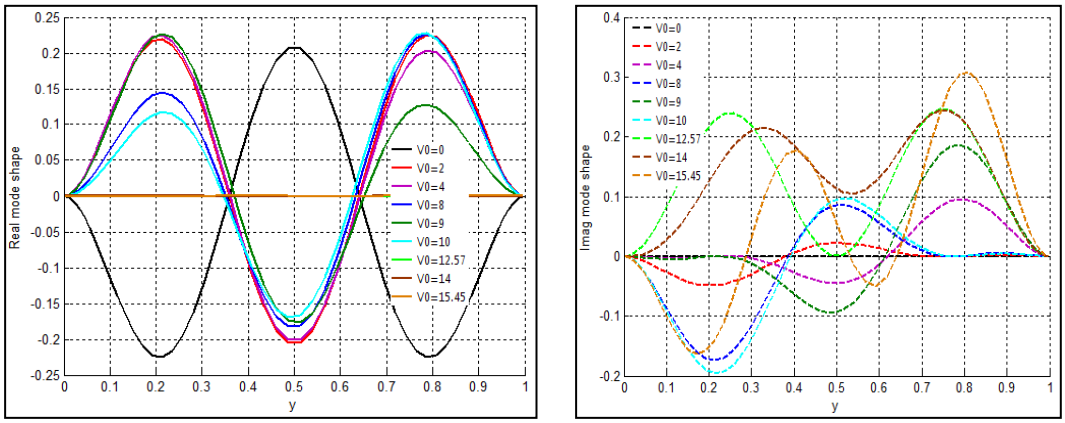

Figure 4.6 Real and imaginary parts of the third complex mode shapes mass normalized of a clamped SWCNT at different dimensionless flow velocities V_0, (β=0, α=0, μ=0, Ts=0, k=0)

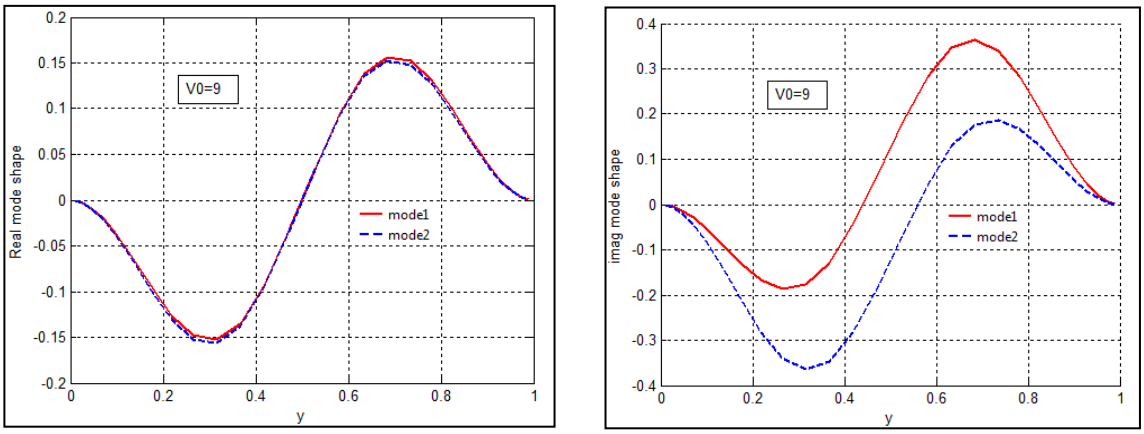

Figure 4.7 Real and imaginary parts of the first and second complex mode shapes mass normalized of a clamped SWCNT at a flow velocities V_0=9, (β=0, α=0, μ=0, Ts=0, k=0)

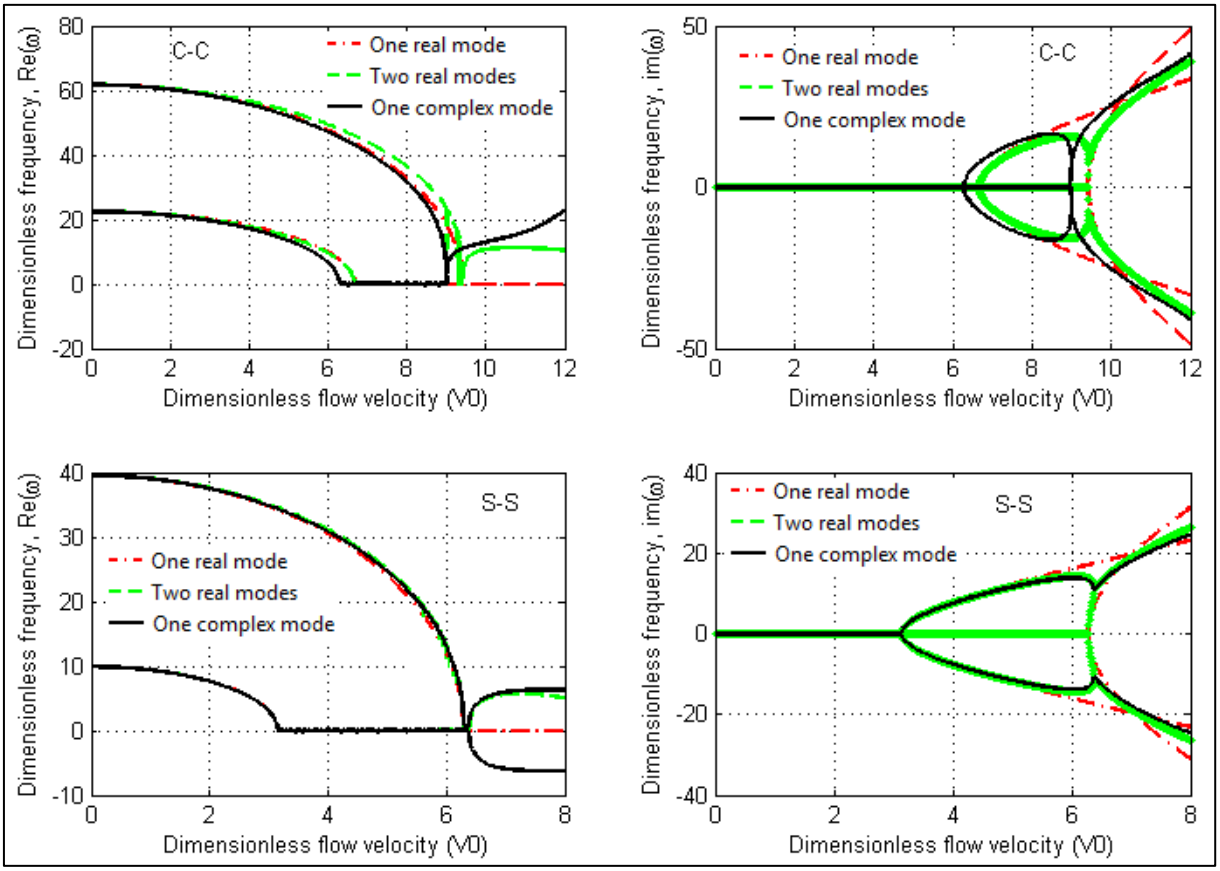

Figure 4.8. Real and imaginary parts of dimensionless frequency ω as a function of flow static velocity V0 for clamped and simply supported SWCNT based on one-complex-mode one and two-real mode approaches.

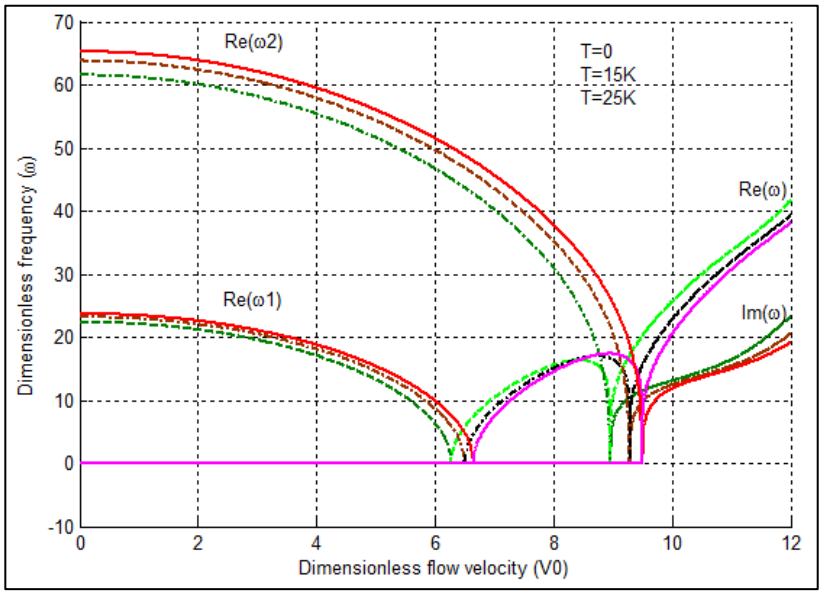

Figure 4-9 Variation of dimensionless frequency of a CC-SWCNT with flow velocity for different temperature changes in high temperature (e_0a/L= 0.05, K=0 MPa), based on the complex mode.

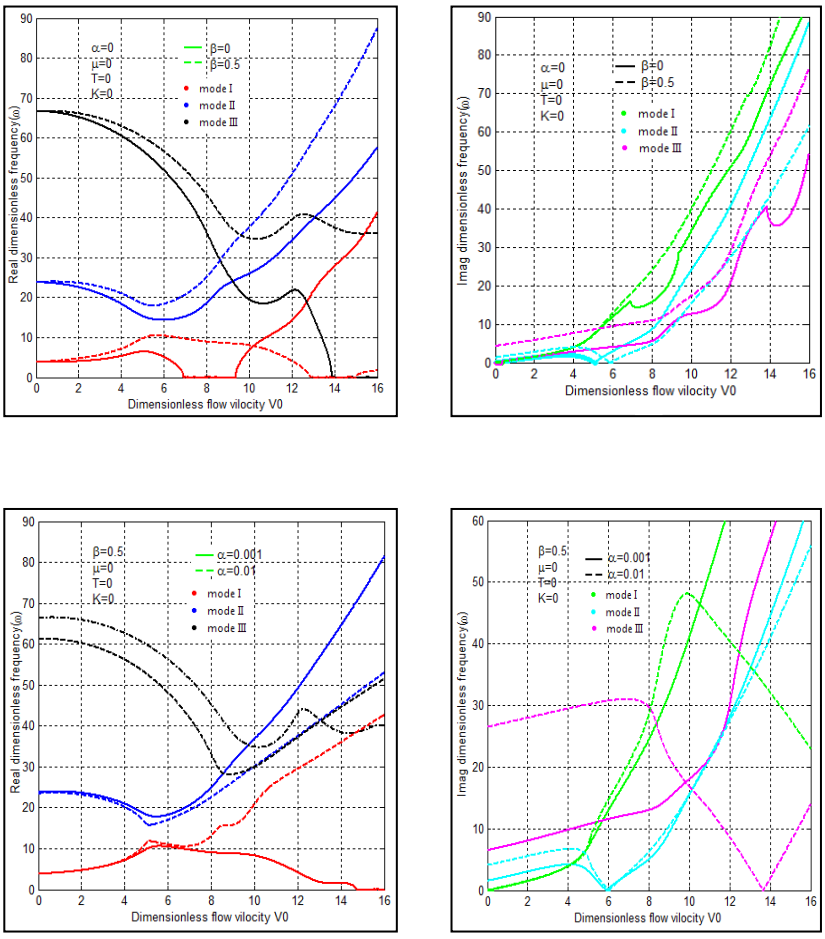

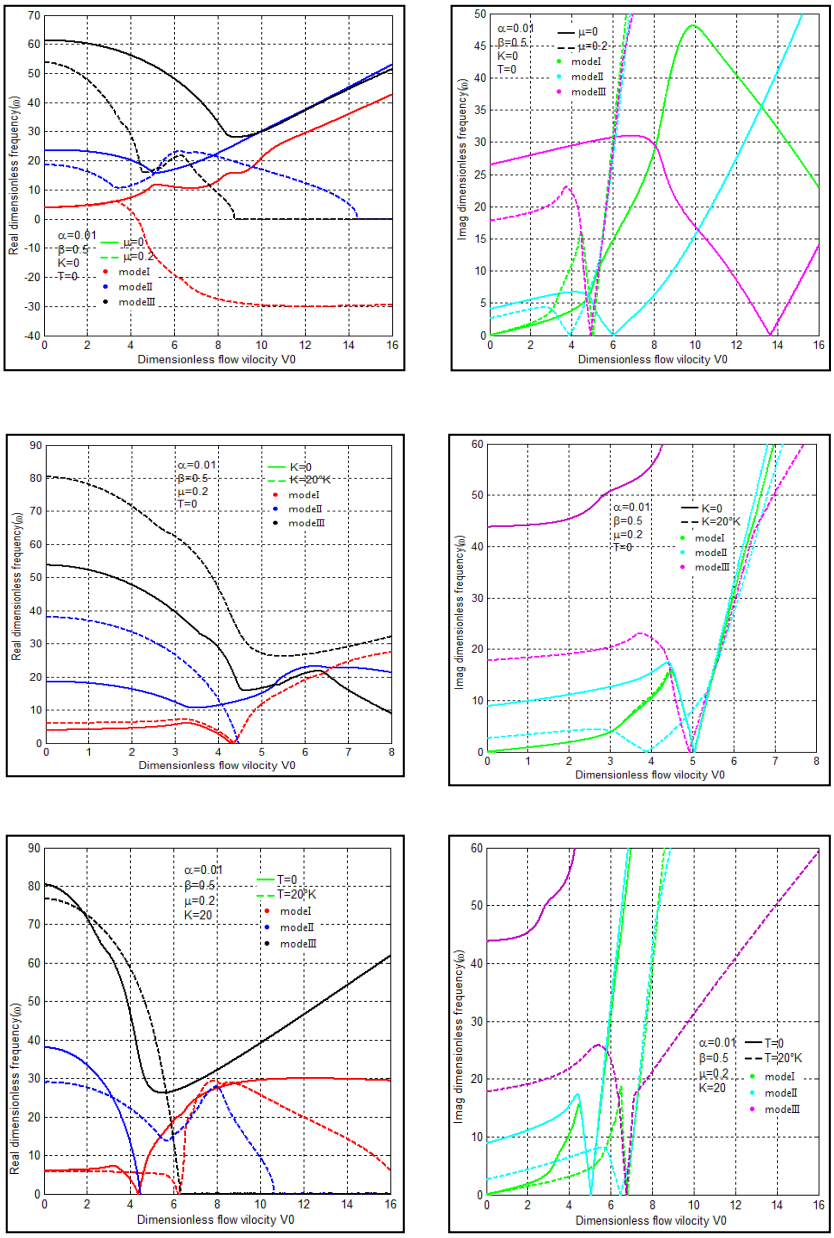

Figure 4.10 Real and imaginary dimensionless first, second and third frequency of a cantilever SWCNT with flow velocity for different physical parameters.

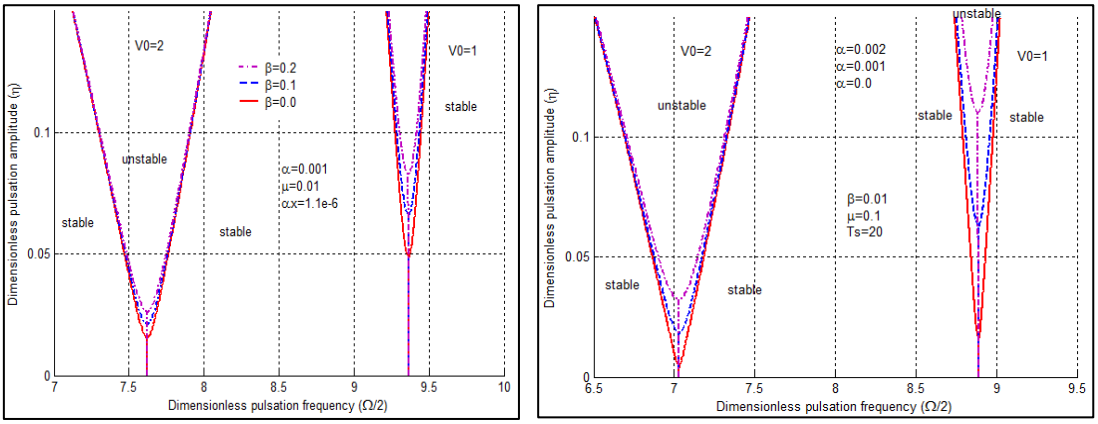

Figure 4.11 One-mode based instability regions of the CNT with different values of the viscous parameter β and viscoelastic coefficient α for a simply supported SWCNT.

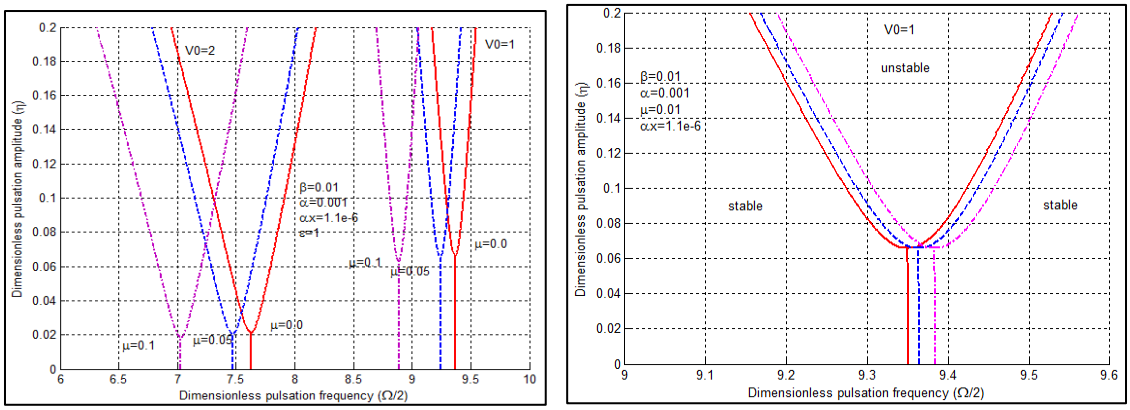

Figure 4.12 One-mode based instability regions of the CNT with different values of the nonlocal parameter μ and the thermal coefficient Ts for simply supported SWCNT.

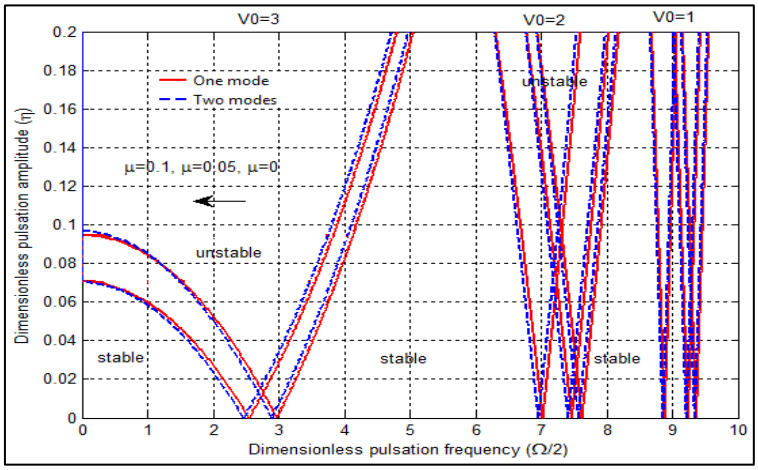

Figure 4.13 One-mode and two-modes based instability regions of a simply-supported SWCNT with different values of the static velocity V_0, (μ = 0, β = 0, α=0, T=0, k=0)

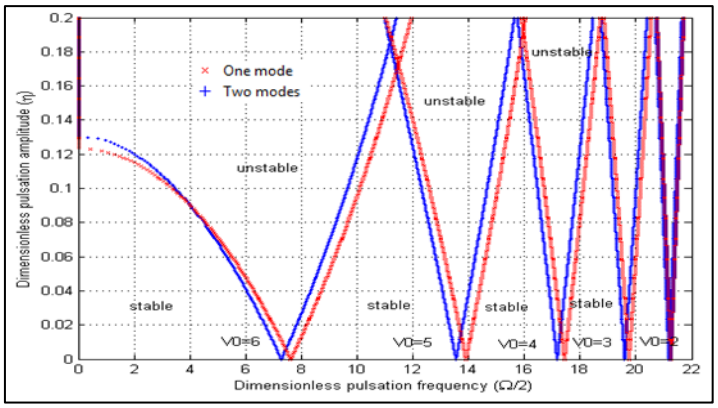

Figure 4.14 One-mode and two-modes based instability regions of a clamped SWCNT with different values of the static velocity V_0, ($\mu = 0$, $\beta = 0$, $\alpha = 0$, T=0, k=0)

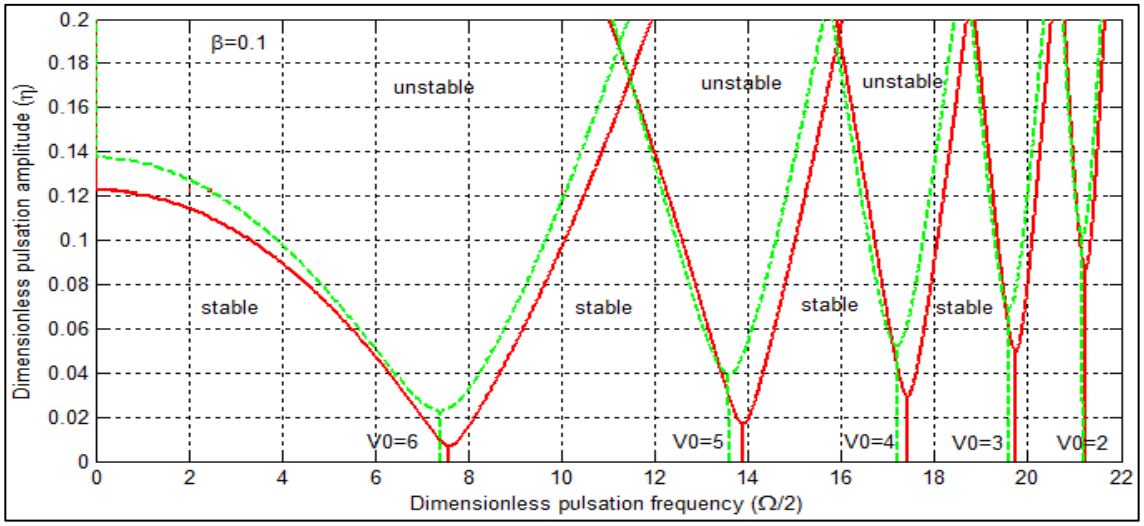

Figure 4.15 One-mode and two-modes based instability regions of a clamped SWCNT with different values of the static velocity V_0, $\beta = 0.1$, ($\mu = 0$, $\alpha = 0$, T=0, k=0)

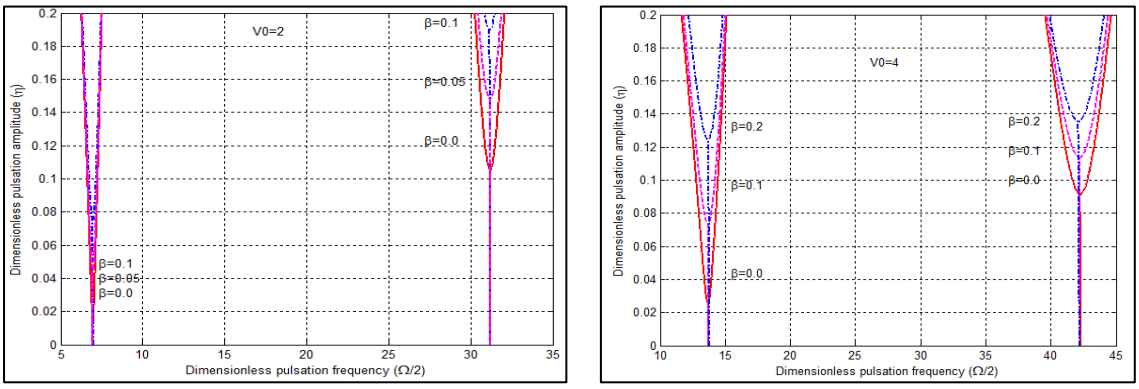

Figure 4.16 Two-modes based instability regions of the SWCNT with different values of the fluid viscosity β for simply supported (Left) and clamped (Right) boundary conditions for $\mu = 0.1$, $\alpha = 0.001$

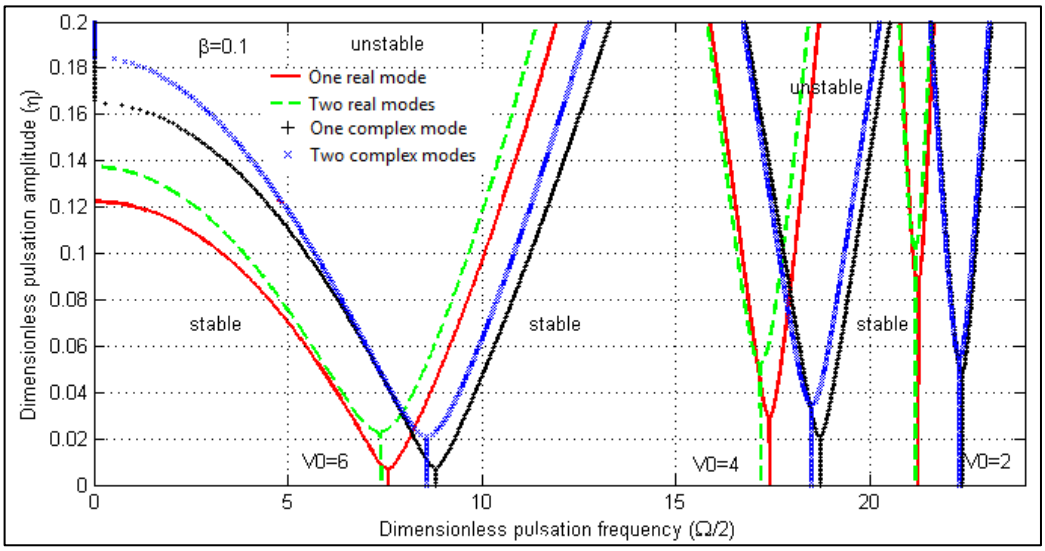

Figure 4.17 Instability regions of a clamped SWCNT with different values of the static velocity V_0 based in various modal approaches, β=0.1 and (μ = 0, α = 0, T=0, k=0)

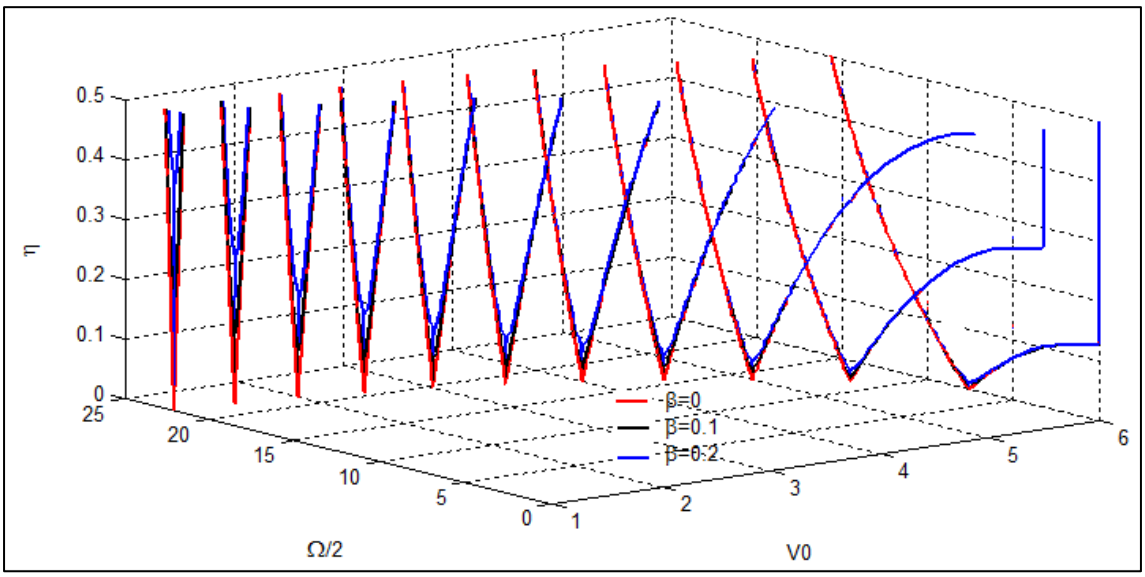

Figure 4.18 One-complex mode based parametric instability regions of a clamped SWCNT with respect to the static velocity V_0 for different values of β, (μ = 0, α = 0, T=0, k=0)

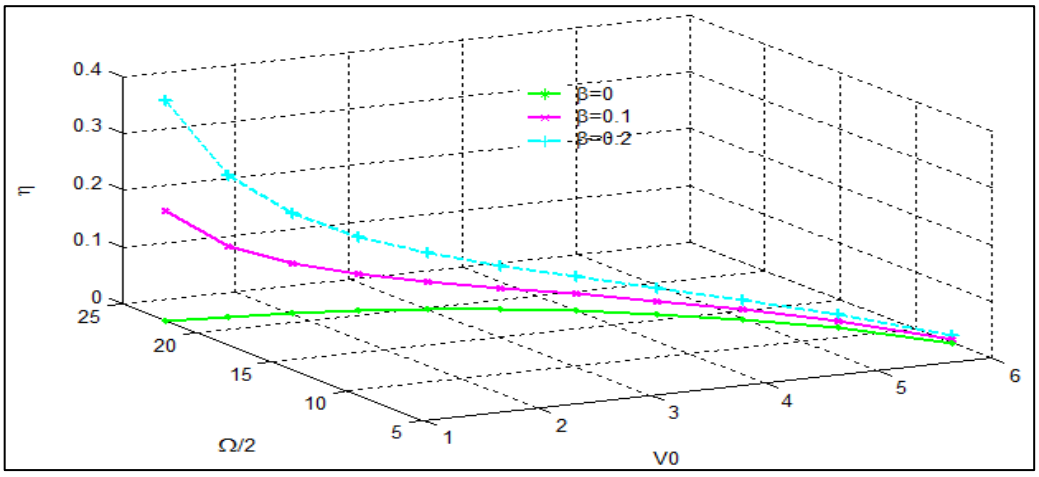

Figure 4.19 Parametric instability bifurcation points for different values of β

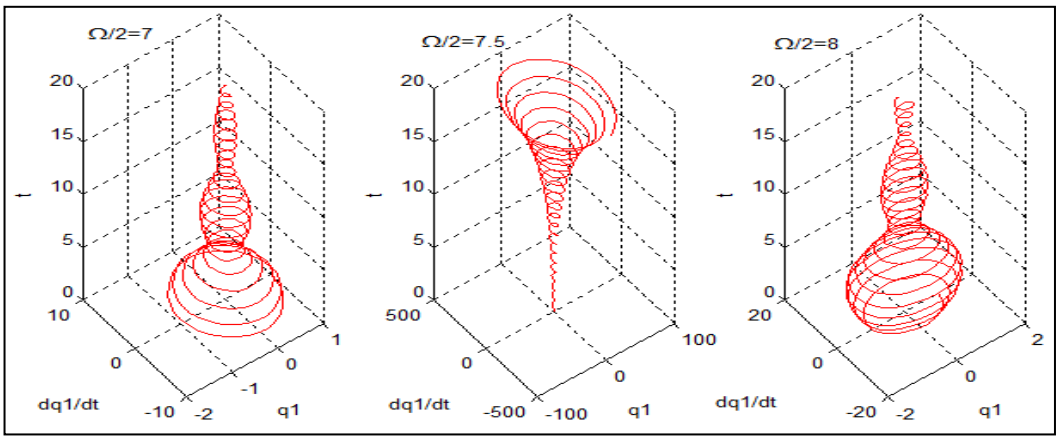

Figure 4.20 One real-mode time responses for μ = 0.1, β = 0.01, V0= 2, α = 0.001, Ts=20, η=0.1 and different values of Ω (Ω/2=7, 7.5, 8) for a simply supported SWCNT.

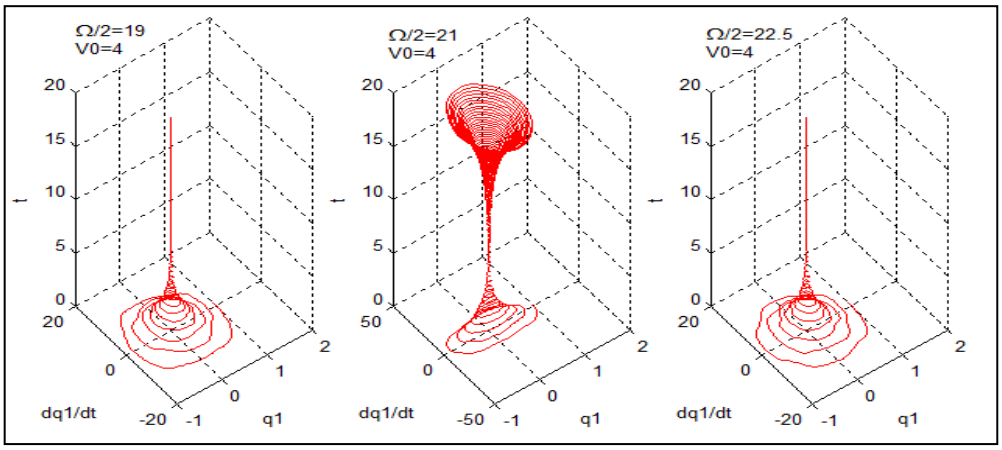

Figure 4.21 Two-mode time responses for μ = 0.1, β = 0.01, V0= 4, α = 0.001, Ts=20, η=0.14 and different values of Ω for a C-C- SWCNT.

Chapiter V:

Shells based dynamics instability and nonlinear vibration analysis of multi-walled carbon nanotubes conveying fluid

Abstract:

The dynamic instability and the nonlinear vibration of conveying fluid multi-walled carbon nanotubes (MWCNT) are analyzed. Based on the nonlocal elasticity theory, Donnell's shell model, potential flow theory and the van der Waals interaction between walls, the governing partial differential equations are formulated. Using the Galerkin procedure, the time and harmonic formulation for the transverse response of each wall are explicitly given. For linear analysis, the free vibration and the dynamic instability behavior are investigated for multiwalled CNT with respect to the considered parameters. The small scale parameter and the internal fluid interaction effects on the dynamic behaviors of the MWCNT-fluid system as well as the instabilities induced by the fluid velocity are investigated.

Using the harmonic balance method the nonlinear amplitude-frequency responses are obtained and the effects of the influencing parameters on this behavior are analyzed.

This work has been published
Title: Dynamics instability analysis of multi-walled carbon nanotubes conveying fluid
Authors: A. Azrar, L. Azrar, A. Aljinaidi & M. Hamadiche
Journal: **J. Advanced Materials Research**, ISSN 1022-6680, Vol. 682 , p 153-160, Trans Tech Publications Ltd, **2013**

1. Introduction

Cylindrical shells conveying fluid are found in numerous industrial and engineering applications. Therefore, the dynamics of shells containing flow fluid has been studied extensively. For thin shells containing fluid, dynamic instability are major problems due to many different loads, including fluid flow. Fluid flows inside carbon nanotubes (CNTs) have become an attractive research topic in recent years, and a great deal of literature has been published on topics such as the noncoaxial vibration of fluid-filled multi walled-carbon nanotubes, Yan et al [1]. Soltani et al [2] proposed nonlinear free and forced vibration analysis of a single walled carbon nanotube using shell model. There are three major categories for simulating the mechanical properties of the CNTs: experience, molecular dynamic simulation (MDS) and continuum mechanics. Considering the limited application of the MDS, continuum modeling is considered to be an appropriate method of investigating the mechanical properties of CNTs. The theory of nonlocal elasticity, Eringen [3,4], allows accounting for the small scale effect that is very significant when dealing with micro and nanostructures. He et al [5] and Yan et al [6] studied pressure dependence of the instability of multiwalled carbon nanotubes conveying fluids. Wang [7] and Yan et al [8] studied the dynamical behavior of carbon nanotubes conveying fluid. Chang and Liu [9] used small scale effect on flow induced instability of double walled carbon nanotubes. Wang et al [10] proposed the coupling vibration of fluid-filled carbon nanotubes. Dong et al [11] used the wave propagation in fluid-filled multi-walled carbon nanotubes embedded in elastic matrix. Hu et al [12] proposed the nonlocal shell model for elastic wave propagation in single and double-walled carbon nanotubes. Wang and Ni [13] discussed vibration and instability of carbon nanotubes conveying fluid. Yan et al [14] studied nonlocal effect on axially compressed buckling of triple-walled carbon nanotubes under temperature field. Vibrational analysis of fluid-filled carbon nanotubes using the wave propagation approach has been proposed by Natsuki et al [15]. The effect of small size on dispersion characteristics of wave in carbon nanotubes has been studied by Xie et al [16]. Azrar et al [17, 18] developed higher order free vibration analyses of single walled carbon nanotubes with various boundary condition types. Azrar et al [19] discussed the nonlinear vibration analysis of actively loaded sandwich piezoelectric beams with geometric imperfections. Amabili et al [20-22] studied the nonlinear vibration and stability of circular cylindrical shells conveying flowing fluid.

In this paper, the small scale effects on the flow-induced instability of MWCNTs based on Donnell's shell model are investigated. The influences of the van der Waals interactions between walls, the flow velocity and the nonlocal parameter on the natural frequencies are obtained by numerically solving the elaborated transcendental nonlinear algebraic equation. The critical flow velocity as well the divergence and flutter instability behaviors are investigated for CNT with various number of walls.

2. Mathematical formulation

Let us consider a multiwalled carbon nanotube of length L, innermost radius R_I, outermost radius R_o, diameter d and thickness h. The cylindrical coordinate system (x,θ,z) is considered where $x\in[0;L]$ is the longitudinal, $\theta\in[0;2\pi]$ is the circumferential and $z\in[-h/2;h/2]$ is the radial coordinates respectively. The fluid inside the inner tube is assumed to be ideal incompressible and the flow is driven by pressure. Based on the nonlocal shell and van der Waals models the governing partial differential equations will be given.

2.1 Nonlocal shell model

Based on the nonlinear Donnell shell theory, the strain tensors at each cylindrical wall are given:

$$\varepsilon_{xx}^{i}=\frac{\partial u_i}{\partial x}+\frac{1}{2}\left(\frac{\partial w_i}{\partial x}\right)^2-z\frac{\partial^2 w_i}{\partial x^2},$$

$$\varepsilon_{\theta\theta}^{i}=\frac{1}{R_i}\frac{\partial v_i}{\partial\theta}+\frac{w_i}{R_i}+\frac{1}{2}\left(\frac{\partial w_i}{R_i\partial\theta}\right)^2-z\frac{\partial^2 w_i}{R_i^2\partial\theta^2}$$

$$and\ \varepsilon_{x\theta}^{i}=\frac{1}{R_i}\frac{\partial u_i}{\partial\theta}+\frac{\partial v_i}{\partial x}+\frac{1}{R_i}\frac{\partial w_i}{\partial x}\frac{\partial w_i}{\partial\theta}-2z\frac{\partial^2 w_i}{\partial\theta\partial x} \tag{5.1}$$

where R_i is the radius, u_i, v_i and w_i are displacements in the (x,θ,z) directions respectively of the i^{th} wall. Based on the nonlocal theory, the temperature effects are introduced through the stress-strain relationship and the constitutive equations of CNTs are [2]

$$(1-e_0{}^2a^2\nabla^2)\,\sigma_{xx}^{i}=\frac{E}{1-\upsilon^2}(\varepsilon_{xx}^{i}+\upsilon\,\varepsilon_{\theta\theta}^{i})-\frac{E\alpha_1}{1-\upsilon}T \tag{5.2a}$$

$$(1-{e_0}^2a^2\nabla^2)\ \sigma^i_{\theta\theta}=\frac{E}{1-\upsilon^2}(\varepsilon^i_{\theta\theta}+\upsilon\,\varepsilon^i_{xx})-\frac{E\alpha_2}{1-\upsilon}T \tag{5.2b}$$

$$(1-{e_0}^2a^2\nabla^2)\ \sigma^i_{x\theta}=\frac{E}{1+\upsilon}\varepsilon^i_{x\theta} \tag{5.2c}$$

where E, ν, a and e_0 are Young's modulus, Poisson's ratio of carbon nanotubes, the internal characteristic lengths and the constant appropriate to each material respectively. ∇^2 is the Laplace operator and σ_{xx} and $\sigma_{\theta\theta}$ are respectively the normal stress in the x and the y directions and $\sigma_{x\theta}$ is the shear stress on the $x\theta$ plane of the middle surface, T is the temperature change, α_1 and α_2 are the thermal expansion coefficients in the axial and the circumferential directions, respectively. The force and moment resultants, which now include temperature effects, are given by:

$$N^i_{xx}=\int_{-h/2}^{h/2}\sigma^i_{xx}dz,\ N^i_{\theta\theta}=\int_{-h/2}^{h/2}\sigma^i_{\theta\theta}dz,\ N^i_{x\theta}=\int_{-h/2}^{h/2}\sigma^i_{x\theta}dz, \tag{5.3a}$$

$$M^i_{xx}=\int_{-h/2}^{h/2}\sigma^i_{xx}z\,dz,\ M^i_{\theta\theta}=\int_{-h/2}^{h/2}\sigma^i_{\theta\theta}z\,dz,\ M^i_{x\theta}=\int_{-h/2}^{h/2}\sigma^i_{x\theta}z\,dz \tag{5.3b}$$

the substituting of Eq (5.3) into Eq. (5.2) leads to the following nonlinear partial differential equations

$$(1-{e_0}^2a^2\nabla^2)\ N^i_{xx}=K(\varepsilon^i_{xx}+\upsilon\,\varepsilon^i_{\theta\theta})-\frac{Eh\alpha_1T}{1-\upsilon}=N_{xM}+N_{xT} \tag{5.4a}$$

$$(1-e_0^2a^2\nabla^2)\ N^i_{\theta\theta}=\frac{Eh}{1-\upsilon^2}(\varepsilon^i_{\theta\theta}+\upsilon\,\varepsilon^i_{xx})-\frac{Eh\alpha_2T}{1-\upsilon}=N_{\theta M}+N_{\theta T} \tag{5.4b}$$

$$(1-e_0^2a^2\nabla^2)\,N^i_{x\theta}=\frac{Eh}{1+\upsilon}\varepsilon^i_{x\theta} \tag{5.4c}$$

$$M^i_{xx}-(e_0a)^2\frac{\partial^2M^i_{xx}}{\partial x^2}=D\left(\frac{\partial^2w}{\partial x^2}+\frac{\upsilon}{R^2}\frac{\partial^2w}{\partial\theta^2}\right)-\frac{E\alpha_1}{1-\upsilon}\int_{-h/2}^{h/2}Tzdz \tag{5.5a}$$

$$M^i_{\theta\theta}-(e_0a)^2\frac{\partial^2M^i_{\theta\theta}}{R^2\partial\theta^2}=D\left(\frac{1}{R^2}\frac{\partial^2w}{\partial\theta^2}+\upsilon\frac{\partial^2w}{\partial x^2}\right)-\frac{E\alpha_2}{1-\upsilon}\int_{-h/2}^{h/2}Tzdz \tag{5.5b}$$

$$M^i_{x\theta}-(e_0a)^2\left(\frac{\partial^2M^i_{x\theta}}{\partial x^2}+\frac{\partial^2M^i_{x\theta}}{R^2\partial\theta^2}\right)=-D(1-\upsilon)\frac{\partial^2w}{R\,\partial x\,\partial\theta} \tag{5.5c}$$

where $K=\frac{Eh}{1-\upsilon^2}$ *and* $D=\frac{Eh^3}{12(1+\upsilon)}$, N_{xM}, N_{xT} express the membrane force caused by

mechanical loads, and $N_{\theta M}$, $N_{\theta T}$ are the membrane force caused by the thermal loads. The nonlinear governing equations of motion of the multi-walled carbon nanotubes are:

$$Q_x^i = \frac{\partial M_{xx}^i}{\partial x} + \frac{1}{R_i}\frac{\partial M_{x\theta}^i}{\partial \theta};\ Q_\theta^i = \frac{\partial M_{x\theta}^i}{\partial x} + \frac{1}{R_i}\frac{\partial M_{\theta\theta}^i}{\partial \theta} \tag{5.6a}$$

$$\frac{\partial Q_x^i}{\partial x} + \frac{1}{R_i}\frac{\partial Q_\theta^i}{\partial \theta} + \frac{N_{\theta M}^i + N_{\theta T}^i}{R_i} + \frac{N_{\theta M}^i + N_{\theta T}^i}{R_i^2} + N_{\theta M}^i \frac{\partial^2 w^i}{\partial x^2} + N_{\theta T}^i \frac{\partial^2 w^i}{\partial x^2} + \frac{1}{R_i}\frac{\partial^2 f^i}{\partial x^2}$$
$$+ \frac{\partial^2 w^i}{R_i^2 \partial \theta^2}\frac{\partial^2 f^i}{\partial x^2} + \frac{\partial^2 f^i}{R_i^2 \partial \theta^2}\frac{\partial^2 w^i}{\partial x^2} - 2\frac{\partial^2 f^i}{R_i^2 \partial x \partial \theta}\frac{\partial^2 w^i}{\partial x \partial \theta} + p_i(x,\theta) - \rho h \frac{\partial^2 w_i}{\partial t^2} - \Pi \tag{5.6b}$$

where

$$\frac{\nabla^4 f^i}{\rho h} = -\frac{w_{i,xx}}{R_i} - \frac{w_{i,\theta\theta}}{R_i^2} w_{i,xx} + \frac{w^2{}_{i,x\theta}}{R_i^2} \tag{5.7}$$

where p_i is the van der Waals force, ρ is the mass density of the carbon nanotubes. Q_x^i and Q_θ^i are the equivalent static shearing stresses of the ith wall respectively. $N_{\theta M}^0$ express the pre-stress caused by mechanical loads, N_{xT}^0, $N_{\theta T}^0$ are the pre-stress caused by the thermal loads and $f^i(x,y)$ is the stress function.

2.2 Linear dynamic instability formulations

For the dynamic instability analysis with respect to the flow velocity, this partial differential system (5.6) has to be solved. For the sake of simplicity, only equations related to the transverse displacement are retained. The dynamic governing equations of N-layered WCNTs conveying fluid are then reduced to the following partial differential system:

$$
\begin{cases}
\dfrac{w_1}{{R_1}^2}+\dfrac{(1-\upsilon^2)D}{Eh}\left(\dfrac{\partial^4 w_1}{\partial x^4}+\dfrac{2}{{R_1}^2}\dfrac{\partial^4 w_1}{\partial x^2\partial\theta^2}+\dfrac{1}{{R_1}^4}\dfrac{\partial^4 w_1}{\partial\theta^4}\right)+(e_0a)^2\left\{\dfrac{\partial^2 w_1}{{R_1}^4\partial\theta^2}\right. \\
\left.+\dfrac{(1-\upsilon^2)D}{Eh}\left(\dfrac{2-\nu}{{R_1}^2}\left(\dfrac{\partial^6 w_1}{{R_1}^2\partial x^2\partial\theta^4}+\dfrac{\partial^6 w_1}{\partial x^4\partial\theta^2}\right)+\dfrac{\partial^6 w_1}{{R_1}^6\partial\theta^6}+\dfrac{\partial^6 w_1}{\partial x^6}\right)\right\}=-\dfrac{(1-\upsilon^2)}{Eh}\left(\rho_s h\dfrac{\partial^2 w_1}{\partial t^2}-p_1+\Pi\right),\ i=1 \\
\dfrac{w_i}{{R_i}^2}+\dfrac{(1-\upsilon^2)D}{Eh}\left(\dfrac{\partial^4 w_i}{\partial x^4}+\dfrac{2}{{R_i}^2}\dfrac{\partial^4 w_i}{\partial x^2\partial\theta^2}+\dfrac{1}{{R_i}^4}\dfrac{\partial^4 w_i}{\partial\theta^4}\right) \\
+(e_0a)^2\left\{\dfrac{\partial^2 w_i}{{R_i}^4\partial\theta^2}+\dfrac{(1-\upsilon^2)D}{Eh}\left(\dfrac{2-\nu}{{R_i}^2}\left(\dfrac{\partial^6 w_i}{{R_i}^2\partial x^2\partial\theta^4}+\dfrac{\partial^6 w_i}{\partial x^4\partial\theta^2}\right)+\dfrac{\partial^6 w_i}{{R_i}^6\partial\theta^6}+\dfrac{\partial^6 w_i}{\partial x^6}\right)\right\} \\
=-\dfrac{(1-\upsilon^2)}{Eh}\left(\rho_s h\dfrac{\partial^2 w_i}{\partial t^2}-p_i\right), i=2,3,....,N
\end{cases}
\tag{5.8}
$$

For convenience, non-dimensional parameters and the following variables are used.

$$
\tilde{\alpha}=\frac{12(1-\upsilon^2)D}{Eh\,Rr^2},\ V_r=\sqrt{E/\rho_S},\quad R_r=\frac{h}{\sqrt{12}},\quad \tilde{p}_i(x,\theta)=\sum_{j=1}^{N}\tilde{c}_{ij}(\tilde{w}_i-\tilde{w}_j),
$$

$$
\tilde{R}_i=\frac{R_i}{R_r},\ \tilde{L}=\frac{L}{R_r},\ \tilde{\mu}=\frac{e_0a}{R_r},\ \tau=\frac{V_r t}{R_r},\ \tilde{x}=\frac{x}{R_r},\ \tilde{w}=\frac{w}{R_r},\ \tilde{\omega}=\frac{\omega R_r}{V_r}
$$

The following coupled differential equations are then obtained.

$$
\begin{cases}
\dfrac{\tilde{w}_1}{\tilde{R}_1^2}+\tilde{\alpha}\left(\dfrac{\partial^4\tilde{w}_1}{\partial\tilde{x}^4}+\dfrac{2}{\tilde{R}_1^2}\dfrac{\partial^4\tilde{w}_1}{\partial\tilde{x}^2\partial\theta^2}+\dfrac{1}{\tilde{R}_1^4}\dfrac{\partial^4\tilde{w}_1}{\partial\theta^4}\right)+\tilde{\mu}^2\left\{\dfrac{\partial^2\tilde{w}_1}{\tilde{R}_1^4\partial\theta^2}\right. \\
\left.+\tilde{\alpha}\left(\dfrac{2-\nu}{\tilde{R}_1^2}\left(\dfrac{\partial^6\tilde{w}_1}{\tilde{R}_1^2\partial\tilde{x}^2\partial\theta^4}+\dfrac{\partial^6\tilde{w}_1}{\partial x^4\partial\theta^2}\right)+\dfrac{\partial^6\tilde{w}_1}{\tilde{R}_1^6\partial\theta^6}+\dfrac{\partial^6\tilde{w}_1}{\partial\tilde{x}^6}\right)\right\}=-(1-\upsilon^2)\left(\dfrac{\partial^2\tilde{w}_1}{\partial\tau^2}-\dfrac{\tilde{p}_1}{\sqrt{12}}+\dfrac{\tilde{\Pi}}{\sqrt{12}}\right), i=1 \\
\dfrac{\tilde{w}_i}{\tilde{R}_i^2}+\tilde{\alpha}\left(\dfrac{\partial^4\tilde{w}_i}{\partial\tilde{x}^4}+\dfrac{2}{\tilde{R}_i^2}\dfrac{\partial^4\tilde{w}_i}{\partial\tilde{x}^2\partial\theta^2}+\dfrac{1}{\tilde{R}_i^4}\dfrac{\partial^4\tilde{w}_i}{\partial\theta^4}\right)+\tilde{\mu}^2\left\{\dfrac{\partial^2\tilde{w}_i}{\tilde{R}_i^4\partial\theta^2}\right. \\
\left.+\tilde{\alpha}\left(\dfrac{2-\nu}{\tilde{R}_i^2}\left(\dfrac{\partial^6\tilde{w}_i}{\tilde{R}_i^2\partial\tilde{x}^2\partial\theta^4}+\dfrac{\partial^6\tilde{w}_i}{\partial x^4\partial\theta^2}\right)+\dfrac{\partial^6\tilde{w}_i}{\tilde{R}_i^6\partial\theta^6}+\dfrac{\partial^6\tilde{w}_i}{\partial\tilde{x}^6}\right)\right\}=-(1-\upsilon^2)\left(\dfrac{\partial^2\tilde{w}_i}{\partial\tau^2}-\dfrac{\tilde{p}_i}{\sqrt{12}}\right), i=2,3,....,N.
\end{cases}
\tag{5.9}
$$

Where $\tilde{p}_i(x,\theta)$ is the interaction on tube *i* due tube *j* and the van der Waals interaction coefficients $\tilde{c}_{ij}$ are given by: [1]

$$
\tilde{c}_{ij}=\left[\frac{1001\pi\varepsilon\sigma^{12}}{3a^4\rho_S{V_r}^2{R_r}^{11}}\,\tilde{E}_{ij}^{13}-\frac{1120\pi\varepsilon\sigma^6}{9a^4\rho_S{V_r}^2{R_r}^5}\,\tilde{E}_{ij}^{7}\right]\tilde{R}_j \tag{5.10}
$$

where the subscripts *i* and *j* denoted the ith and jth layers, respectively, and E_{ij}^{7} and E_{ij}^{13} are the

elliptical integrals given by:

$$\tilde{E}_{ij}^{m} = (\tilde{R}_i + \tilde{R}_j)^{-m} \int_0^{\pi/2} \frac{d\theta}{[1-\tilde{K}_{ij}\cos(\theta)]^{m/2}} \quad and \quad \tilde{K}_{ij} = \frac{4\tilde{R}_i\,\tilde{R}_j}{(\tilde{R}_i + \tilde{R}_j)^2} \tag{5.11}$$

The resulting flow pressure $\tilde{\Pi}$ is given by:

$$\tilde{\Pi} = \frac{\rho_f}{\rho_s} \frac{I_n(k\tilde{R}_i)}{k\,I_n'(k\tilde{R}_i)} \left\{ \frac{\partial^2 \tilde{w}_1}{\partial \tau^2} + 2\frac{V_0}{V_r} \frac{\partial^2 \tilde{w}_1}{\partial \tilde{x}\partial \tau} + \left(\frac{V_0}{V_r}\right)^2 \frac{\partial^2 \tilde{w}_1}{\partial \tilde{x}^2} \right\}, \tag{5.12}$$

For the dynamic instability analysis, the PDE (5.9) has to be solved with respect to given flow velocity V_0, small scale parameter and other physical and material parameters. The transverse displacement of the jth tube is assumed to be in the form:

$$\tilde{w}_j = A_j e^{i(\tilde{k}x + \tilde{\omega}\tau)} \cos(n\theta) \tag{5.13}$$

where the amplitudes A_j verify the following amplitude frequency relationship:

$$\begin{aligned} &\left(a_{11} - (B_1\tilde{\omega}^2 + B_2\tilde{\omega}V_0 + B_3{V_0}^2)\right)A_1 + \frac{(1-\upsilon^2)}{\sqrt{12}} \sum_{j=1}^{N} \tilde{c}_{ij} A_j = 0, \\ &\frac{(1-\upsilon^2)}{\sqrt{12}} \sum_{j=1}^{N} \tilde{c}_{ij} A_j + \left(a_{kk} - (1-\upsilon^2)\tilde{\omega}^2\right)A_k = 0, \quad k = 2,3,....,N \end{aligned} \tag{5.14}$$

in which for $k = 1,2,3,...,N$

$$a_{kk} = \frac{1}{\tilde{R}_k^2} + \tilde{\alpha}\left(\tilde{k}^2 + \left(\frac{n}{\tilde{R}_k}\right)^2\right)^2 - \frac{(1-\upsilon^2)}{\sqrt{12}} \sum_{j=1}^{N} \tilde{c}_{kj} + \tilde{\mu}^2 \left\{ \frac{1}{\tilde{R}_k^2}\left(\frac{n}{\tilde{R}_k}\right)^2 + \tilde{\alpha}\left[(2+\upsilon)\tilde{k}^2\left(\frac{n}{\tilde{R}_k}\right)^2\left(\tilde{k}^2 + \left(\frac{n}{\tilde{R}_k}\right)^2\right) + \left(\frac{n}{\tilde{R}_k}\right)^6 + \tilde{k}^6 \right] \right\}$$

$$\text{and } B_1 = (1-\upsilon^2)\left\{1 - \frac{\rho_f}{\rho_s}\frac{1}{\tilde{k}\sqrt{12}}\frac{I_n(\tilde{k}\tilde{R}_i)}{I_n'(\tilde{k}\tilde{R}_i)}\right\}, \quad B_2 = (1-\upsilon^2)\left\{\frac{\rho_f}{V_r\rho_s}\frac{2}{\sqrt{12}}\frac{I_n(\tilde{k}\tilde{R}_i)}{I_n'(\tilde{k}\tilde{R}_i)}\right\}, \quad B_3 = (1-\upsilon^2)\left\{\frac{\rho_f}{{V_r}^2\rho_s}\frac{\tilde{k}}{\sqrt{12}}\frac{I_n(\tilde{k}\tilde{R}_i)}{I_n'(\tilde{k}\tilde{R}_i)}\right\}$$

To determine the nontrivial solutions of A_i, the following characteristic equation has to be solved.

$$\det\begin{bmatrix} a_{11} - (B_1\tilde{\omega}^2 + B_2\tilde{\omega}V_0 + B_3{V_0}^2) & \frac{(1-\upsilon^2)}{\sqrt{12}}\tilde{c}_{12} & \frac{(1-\upsilon^2)}{\sqrt{12}}\tilde{c}_{13}\cdots & \frac{(1-\upsilon^2)}{\sqrt{12}}\tilde{c}_{1N} \\ \frac{(1-\upsilon^2)}{\sqrt{12}}\tilde{c}_{21} & a_{22} - (1-\upsilon^2)\tilde{\omega}^2 & \frac{(1-\upsilon^2)}{\sqrt{12}}\tilde{c}_{23}\cdots & \frac{(1-\upsilon^2)}{\sqrt{12}}\tilde{c}_{2N} \\ \vdots & \vdots & \vdots & \vdots \\ \frac{(1-\upsilon^2)}{\sqrt{12}}\tilde{c}_{N1} & \frac{(1-\upsilon^2)}{\sqrt{12}}\tilde{c}_{N2} & \frac{(1-\upsilon^2)}{\sqrt{12}}\tilde{c}_{N3} & a_{NN} - (1-\upsilon^2)\tilde{\omega}^2 \end{bmatrix} = 0, \tag{5.15}$$

This formulation allows one to get the natural frequencies $\tilde{\omega}_i$ (i=1, 2,…, N) for N walled CNT with respect to the considered physical and material parameters. The dynamic instability

behavior related to the flow velocity can be investigated based on the presented methodological approach.

2.3 Reduced nonlinear dynamic formulation

By neglecting the axial and the circumferential displacement (u,v) a reduced partial differential system on the transverse displacements w in each wall is resulted. From Eqs. (5.5-5.7), the following nonlinear partial deferential system is obtained.

$$D\nabla^4 w_i + D(e_0 a)^2 \eta_i + \rho h \frac{\partial^2 w_i}{\partial t^2} = \frac{N^i_{\theta M} + N^i_{\theta T}}{R_i}\left(1 + \frac{1}{R_i}\frac{\partial^2 w_i}{\partial \theta^2}\right) + \left(N^i_{xM} + N^i_{xT}\right)\frac{\partial^2 w_i}{\partial x^2}$$
$$+ \frac{1}{R_i}\frac{\partial^2 f^i}{\partial x^2} + \frac{\partial^2 w_i}{R_i{}^2 \partial \theta^2}\frac{\partial^2 f^i}{\partial x^2} + \frac{\partial^2 f^i}{R_i{}^2 \partial \theta^2}\frac{\partial^2 w_i}{\partial x^2} - 2\frac{\partial^2 f^i}{R_i{}^2 \partial x \partial \theta}\frac{\partial^2 w_i}{\partial x \partial \theta} + p_i(x,\theta) - \Pi \qquad (5.16)$$

where $\eta_i = \frac{\partial^6 w_i}{\partial x^6} + \frac{\partial^6 w_i}{R_i{}^6 \partial \theta^6} + \frac{2-\upsilon}{R_i{}^2}\left(\frac{\partial^4 w_i}{\partial x^4 \partial \theta^2} + \frac{\partial^4 w_i}{R_i{}^2 \partial \theta^4 \partial x^2}\right)$

The multiwalled is assumed to be filled with a moving fluid in the inner cylinder. Based on some mathematical developments, the flow pressure Π given by: [4]

$$\Pi = \frac{\rho_f L I_n(m\pi R_1 / L)}{m\pi I'_n(m\pi R_1 / L)}\left\{\frac{\partial^2 w_1}{\partial t^2} + 2V_0\frac{\partial^2 w_1}{\partial x \partial t} + V_0{}^2\frac{\partial^2 w_1}{\partial x^2}\right\} \qquad (5.17)$$

in which ρ_f is the mass density of the fluid, I_n is the modified Bessel function of order n, prime (') is the derivative with respect to the spatial variable and V_0 is the uniform mean flow velocity of conveying fluid. The total forces can be given:

$$N^0_{ix\,M} = \frac{1}{R_i^2} f_{i,\theta\theta} = -\frac{Eh}{8}\beta_m^2 A_i^2 \cos(2n\theta),\ at\ x = 0\ \ and\ \ x = L,\ \ N^0_{ix\,T} = -\frac{Eh\alpha_1 T}{1-\upsilon} \qquad (5.18)$$

$$N^0_{i\theta\,M} = -\left(-\sum_{j=1}^{i-1} p_{ij} + \sum_{j=1+1}^{N} p_{ij}\right)R_i,\ \ N^0_{i\theta T} = -\frac{Eh\alpha_2 T}{1-\upsilon} \qquad (5.19)$$

$$p_i(x,\theta) = -\sum_{j=1}^{i-1} p_{ij} + \sum_{j=1+1}^{N} p_{ij} + \Delta p_i(x,\theta) \qquad (5.20)$$

$$p_{ij} = \left[\frac{2048\varepsilon\sigma^{12}}{9a^4}\sum_{k=0}^{5}\frac{(-1)^k}{2k+1}\binom{5}{k}E_{ij}{}^{12} - \frac{1024\varepsilon\sigma^6}{9a^4}\sum_{k=0}^{2}\frac{(-1)^k}{2k+1}\binom{2}{k}E_{ij}{}^6\right]R_i \qquad (5.21)$$

$$\Delta p_i(x,\theta) = w_i\sum_{j=1}^{N} c_{ij} - \sum_{j=1}^{N} c_{ij}\, w_j \qquad (5.22)$$

$$c_{ij} = \left[\frac{1001\pi\varepsilon\sigma^{12}}{3a^4} E_{ij}^{13} - \frac{1120\pi\varepsilon\sigma^{6}}{9a^4} E_{ij}^{7} \right] R_j \tag{5.23}$$

$$E_{ij}^{m} = (R_i + R_j)^{-m} \int_0^{\pi/2} \frac{d\theta}{[1 - K_{ij}\cos(\theta)]^{m/2}} \tag{5.24}$$

$$K_{ij} = \frac{4R_i R_j}{(R_i + R_j)^2} \tag{5.25}$$

where c_{ij} the van der Waals interaction coefficients. For the dynamic instability analysis, the PDE (5.16) has to be solved with respect to given flow velocity V_0, small scale parameter e_0 and other physical and material parameters.

It is noted that the pre-stressed boundary conditions are not satisfied locally at the two end sections. It is easy to demonstrate that the boundary conditions are globally satisfied when an integration of equation (5.18). The transverse displacement of the jth tube is assumed to be in the form [2]

$$w_i = A_i(t)\sin(n\theta)\sin(\frac{m\pi x}{L}) + \frac{n^2}{4R_i} A^2{}_i(t)\sin^2(\frac{m\pi x}{L}) \tag{5.26}$$

where m, n denoted the axial and the circumferential wave number, and A(t) is the time-dependence amplitude of the vibration. Substituting Eq. (5.26) into Eq. (5.7) and solving for particular solution, we have:

$$\frac{f_i}{\rho h} = \frac{n\beta_m^2\beta_i^2}{4(9\beta_m^2+\beta_i^2)^2} A_i^3 \sin(3\beta_m x)\sin(n\theta) + \frac{1}{32}\frac{\beta_m^2}{\beta_i^2} A_i^2 \cos(2n\theta)$$
$$- \frac{n\beta_m^2\beta_i^2}{4(\beta_m^2+\beta_i^2)^2} A_i^3 \sin(\beta_m x)\sin(n\theta) + \frac{\beta_m^2}{(\beta_m^2+\beta_i^2)^2}\frac{A_i}{R_i}\beta_m^2 \sin(\beta_m x)\sin(n\theta) \tag{5.27}$$

$$\text{where } \beta_m = m\pi/L,\ \beta_i = n/R_i \tag{5.28}$$

$$X = D\nabla^4 w_i + D(e_0 a)^2 \eta_i + \rho h \frac{\partial^2 w_i}{\partial t^2} - \frac{N_{\theta M}^i + N_{\theta T}^i}{R_i} - \frac{N_{\theta M}^i + N_{\theta T}^i}{R_i^2}\frac{\partial^2 w_i}{\partial\theta^2} - N_{xT}^i \frac{\partial^2 w_i}{\partial x^2}$$
$$- \frac{1}{R_i}\frac{\partial^2 f^i}{\partial x^2} - \frac{\partial^2 w_i}{R_i^2\partial\theta^2}\frac{\partial^2 f^i}{\partial x^2} - \frac{\partial^2 f^i}{R_i^2\partial\theta^2}\frac{\partial^2 w_i}{\partial x^2} + 2\frac{\partial^2 f^i}{R_i^2\partial x\partial\theta}\frac{\partial^2 w_i}{\partial x\partial\theta} - p_i(x,\theta) + \Pi \tag{5.29}$$

The Galerkin method is applied to project equation (5.29), where equations (5.26) and (5.27) are used and equating the result to zero, one has:

$$\int_0^L \int_0^{2\pi} X(x,\theta) Z_s(x,\theta)\, dx d\theta = 0 \tag{5.30}$$

where

$$Z_s(x,\theta)=\frac{\partial w}{\partial \theta}=\sin(n\theta)\sin(\beta_m x)+\frac{n^2}{2R_i}A_i\sin^2(\beta_m x) \tag{5.31}$$

After some mathematical developments and neglecting the viscous velocity effects, the following highly nonlinear differential equations for unknown functions $\zeta_i(t)$ in the non-dimensional form, are obtained:

$$a_i\ddot{\zeta}_i(t)+b_i\zeta_i(t)+c_i\left(\zeta_i^2\ddot{\zeta}_i(t)+\zeta_i\dot{\zeta}_i^2(t)\right)+d_i\zeta_i^3(t)+e_i\zeta_i^5(t)+\sum_{j=1}^{N}c_{ij}\zeta_j(t)$$

$$+\sum_{j=1}^{N}c_{ij}g_j\zeta_j^3(t)=0,\ i=1,2,...,N \tag{5.32}$$

$$\text{where } a_1=1+\frac{\rho_f In(n\xi_1)}{\rho n\tilde{h}\xi_1 In'(n\xi_1)},\ a_i=1,\ i=2,3,...,N \tag{5.33}$$

$$b_1=\frac{E}{\rho R_1^2}\left[\frac{\varepsilon_i(\xi_1^2+1)^2}{12(1-\upsilon^2)}-\frac{n^2R_1}{Eh}\sum_{j=2}^{N}p_{1j}+\frac{\xi_1^4}{(\xi_1^2+1)^2}-\frac{n\xi_1\tilde{V}^2In(n\xi_1)}{\tilde{h}In'(n\xi_1)}-\frac{R_1^2}{Eh}\sum_{j=2}^{N}c_{1j}-\frac{n^2\alpha_2T}{(1-\upsilon)}\right.$$
$$\left.-\frac{n^2\xi_1^2\alpha_1T}{(1-\upsilon)}-\frac{n^2\varepsilon_i}{12(1-\upsilon^2)}\mu_1^2\left[\xi_1^6+1+(2-\upsilon)\xi_1^2(\xi_1^2+1)\right]\right] \tag{5.34}$$

$$b_i=\frac{E}{\rho R_i^2}\left[\frac{\varepsilon_i(\xi_i^2+1)^2}{12(1-\upsilon^2)}-\frac{n^2}{Eh}\left(-\sum_{j=1}^{i-1}p_{ij}+\sum_{j=i+1}^{N}p_{ij}\right)R_i-\frac{R_i^2}{Eh}\sum_{j=1}^{N}c_{ij}+\frac{\xi_i^4}{(\xi_i^2+1)^2}-\frac{n^2\alpha_2T}{(1-\upsilon)}-\frac{n^2\xi_i^2\alpha_1T}{(1-\upsilon)}\right.$$
$$\left.-\frac{n^2\varepsilon_i\mu_i^2}{12(1-\upsilon^2)}\left[1+\xi_i^6+(2-\upsilon)\xi_i^2(\xi_i^2+1)\right]\right],\ i=2,..,N \tag{5.35}$$

$$c_1=\left(1+\frac{\rho_f I_n(n\xi_1)}{\rho n\tilde{h}_1\xi_1 In'(n\xi_1)}\right)\left(\frac{3\varepsilon_i}{8}\right),\ c_i=\left(\frac{3\varepsilon_i}{8}\right),\ i=2,..,N \tag{5.36}$$

$$d_1=\frac{E\varepsilon_1}{\rho R_1^2}\left[\frac{\xi_1^4}{16}-\frac{\xi_1^4}{(\xi_1^2+1)^2}+\frac{\varepsilon_1\xi_1^4}{12(1-\upsilon^2)}(1-4n^2\xi_1^2\mu^2)-\frac{\alpha_1n^2\xi_1^2T}{4(1-\upsilon)}+\frac{n\xi_1\tilde{V}^2I_n(n\xi_1)}{2\tilde{h}_1In'(n\xi_1)}\right], \tag{5.37}$$

$$d_i=\frac{E\varepsilon_i}{\rho R_i^2}\left[\frac{\xi_i^4}{16}-\frac{\xi_i^4}{(\xi_i^2+1)^2}+\frac{R_i^2}{Eh}\sum_{j=1}^{N}c_{ij}+\frac{\varepsilon_i\xi_i^4}{12(1-\upsilon^2)}(1-4n^2\xi_i^2\mu^2)-\frac{\alpha_1n^2\xi_i^2T}{4(1-\upsilon)}\right],\ i=2,...,N \tag{5.38}$$

$$e_i=\frac{3\varepsilon_i^2E\xi_i^4}{16\rho R_i^2}\left[\frac{1}{(\xi_i^2+1)^2}+\frac{1}{(9\xi_i^2+1)^2}\right],\ i=1,2,...,N \tag{5.39}$$

$$g_i=\frac{E\varepsilon_i}{\rho R_i^2}\sum_{j=1}^{N}c_{ij};\ i=1,2,...,N \tag{5.40}$$

$\xi_i = \frac{\beta_m}{\beta_i}, \tilde{h}_i = \frac{h}{R_i}, \mu_i = \frac{e_0 a}{R_i}, \varepsilon_i = \frac{n^4 h^2}{R_i^2}, \tilde{V} = \sqrt{\frac{\rho_f}{E}} V_0$ and ζ_i are the vibration amplitudes defined by:

$\zeta_i(t) = A_i(t)/h$

It has to be noted that equation (5.32) is highly nonlinear differential system and its solution necessitates well adopted methods of course in time domain, this system can be solved by classical methods such as Runge-Kutta or Newmark methods. The time response can then be obtained with respect to the considered parameters. But, in frequency domain a hard analysis is resulted in order to get the nonlinear frequency-amplitude dependence and in internal responses with respect to the influencing parameters.

The corresponding linear frequencies can readily be evaluated by neglecting the nonlinear terms in equation (5.30) and taking $\zeta_i(t) = Y_i \sin(\omega t)$ where Y_i is represent the amplitudes of the tubes, as

$$\Omega^2 = \left(\frac{b_i}{a_i} + \frac{b_i}{a_i} \sum_{j=1}^{N} c_{ij} \right); \tag{5.41}$$

For nonlinear vibration analysis, the first order harmonic leads to the following nonlinear algebraic system.

$$\begin{cases} \omega^2 \left(a_1 Y_1 + \frac{c_1}{2} Y_1^3 \right) = b_1 Y_1 + \frac{3}{4} c_1 Y_1^3 + \frac{5}{8} d_1 Y_1^5 + \frac{1}{\rho h} \sum_{j=1}^{N} c_{1j} Y_j - \frac{1}{\rho h} \sum_{j=1}^{N} c_{1j} g_j Y_j^3 \\ \omega^2 \left(a_i Y_i + \frac{c_1}{2} Y_i^3 \right) = b_i Y_i + \frac{3}{4} c_i Y_i^3 + \frac{5}{8} d_i Y_i^5 + \frac{1}{\rho h} \sum_{j=1}^{N} c_{ij} Y_j - \frac{1}{\rho h} \sum_{j=1}^{N} c_{1j} g_j Y_j^3, \ i = 2, .., N \end{cases} \tag{5.42}$$

3 Numerical results and discussions

For numerical results, the used physical and material parameters are as follows: the wall thickness. $h = 0.34nm,$ the mass density of the tube is $\rho_s = 2.3 g/cm^3,$ the mass density of the fluid

is $\rho_f = 1 g/cm^3$, the Poison's ratio $\upsilon = 0.19$, the effective bending stiffness $D = 0.85eV$, in plan stiffness $Eh = 360 J/m^2$, and the parameters used in the van der Waals interaction coefficient are:

$a = 1.42A°,\ \sigma = 3.4A°,\ \varepsilon = 2.968 meV$ and the radius $R_i = R_1 + (i-1)h,\quad i=1,2,...,N.$

In this paper, the developed methodological approach is illustrated for multi-walled CNTs and the effect of various physical and material parameters on the dynamic instability can be obtained linear dynamic analysis.

Comparisons of the numerically obtained free vibration frequencies for a three WCTs and the associated amplitude ratios A_1/A_2 are listed in table 5.1 for $e_0=0$ the some results presented in [1] than those are obtained. The first sixth natural frequencies of a six-walled carbon nanotube with and without nonlocal effect are presented in table 5.2 with different wave numbers n and m. It is observed that these frequencies decrease by increasing the innermost radius R_1 even for $e_0 a \neq 0$. The effects of the various other parameters such as n, m and the van der Waals parameters can be easily analyzed. The dynamic instability can be investigated with respect to the fluid velocity V for CNT with a chosen number of walls and the frequency-velocity dependence can be obtained for CNT with different numbers of walls. For a double walled CNT, the effect of the wave number m is shown in figure 5.1 and the effect of van der Waals interaction in figure 5.2 for R_1=11.9 nm and the ratio L/R_2=12. It is observed, in figure 5.1, that the instability type is first the divergence and the signed is flutter. By increasing V, the divergence and flutter instabilities occur and m has a strong effect on this instabilities. For the van der Waals effect, it is observed in figure 5.2 that the divergence and flutter critical velocities are increased by the van der Waals parameter. The small scale effect on the frequency-velocity dependence is presented in figure 5.3 for e_0a =0 and e_0a=0.4nm. Increasing this parameter leads to a decrease of the natural frequencies as well as the critical divergence and flutter velocities as clearly presented in figure 5.3. The flow velocity effect is also shown in this figure. It is observed that this damping has no effect on the divergence critical velocity.

At low and room temperature, the used thermal expansion coefficients α_1=-1.6e-6, α_2=-0.5e-6, and at high temperature α_1=1.1e-6, α_2=0.8e-6. The amplitude-frequency response curves of the nonlinear free vibration of DWCNT are shown in figure 5.4. It can be seen that the amplitude- frequency curves of the inner and outer tubes are similar at lower frequencies and the difference can be discriminated at high frequencies. Figure 5.5 shows the influences of the mass of fluid and van der Waals force on the nonlinear free vibration frequencies. It can be seen that these curves tend to the case that without vdW force and the nonlinear free vibration frequencies of DWCNTs decrease with the increase of the mass of fluid. The thermal and nonlocal effects on the amplitude versus the frequency of the DWCNTs for R1=3.4 nm,

(m,n)=(1,8) and V=1e^3 ms^{-1} are shown in figure 5.6. It is demonstrated the nonlinear frequencies decrease by increasing of the nonlocal parameter and temperature.

Figure 5.7 shows nonlinear the free vibration response of double walled carbon nanotube with different axial wave numbers and n=1, L/R_o=10, R_I=3.4nm. The non-dimensional vibration frequency ω/ω_1 is employed in which ω1 denoted linear free vibration frequency of innermost tube. It is demonstrated that m has a strong on the back bone curve. For m=1, 4, 5, in fact usual in nonlinear vibration analysis of shell and beam with initial geometrical imperfect [19] the effects of the other physical and geometrical parameter of the other physical and geometrical parameter on this under critical behaviors is investigated.

In figure 5.8, the amplitudes frequency response are shown for several values of the nonlocal parameter and m=5. The dynamical behavior shows softening type non-linearity for all the nonlocal parameter range explored. It is interesting to note that the maximum amplitude of oscillation varies with the nonlocal parameter. It can be seen that the increase of the non-local parameter will increase the nonlinearity of vibration. Figure 5.9 shows the influence of the number of walls on large amplitudes-vibration frequency. It is seen that the amplitude and frequency of all tubes are similar to each other. The increase of the number of the walls results in a less nonlinear vibration response due to the influence of the vdw interaction. The influence of the circumferential wave number on the large amplitudes on vibration frequency for single and double walled carbon nanotubes with different circumferential wave number are shown in figures (5.10, 5.11). A strong effect parameter is observed. Figure 5.12 shows the influence of the fluid velocity on the large amplitudes vibration frequency response. It can be seen that the increase of the fluid velocity results in a less nonlinear vibration response.

4 Conclusion

This paper presents the dynamic instability analysis of multiwalled CNTs conveying fluid based on the nonlinear Donnell shell model. The partial differential model taking into account, the van der Waals interaction as well as the fluid-shell interaction is presented. Based on the transverse displacement at each wall, coupled nonlinear partial differential system is resulted. The dynamic instability modeling is presented in space and frequency domains. Based on the Galerkin procedure a highly nonlinear differential system is formulated in time domain. These presented formulations allow one to investigate the free vibration, the dynamic instability behavior with respect to the fluid velocity as well as the free nonlinear vibration behaviors with respect to the considered material and physical parameters. The free vibration

and flow velocity-frequency dependence are analyzed with respect to various physical and material parameters. The obtained results showed a strong dependence between the fluid velocity and the frequency of MWCNTs. The effect of the van der Waals interaction between tubes is discussed and results show that the van der Waals interaction and the small scale effects may significantly influence the stability of multiwalled CNT. It has to be noted that the nonlinear free vibration frequencies of double walled CNTs are deeply affected by temperature, fluid mass and velocity and the van der Waals interaction.

For the nonlinear free vibration, simply supported multi-walled carbon nanotubes conveying fluid are considered. The amplitude frequency dependence associated on the nonlinear free vibration MWCNT are obtained by harmonic balance method. The influences of nonlocal parameters, the vdW force and the thermal effects are discussed. Softening effect leading to under critical behaviors are obtained. The effects of the considered parameters on this under critical behavior are investigated.

References:

[1] Y. Yan, W. Q. Wang and L. X. Zhang, Noncoaxial vibration of fluid-filled multi-walled carbon nanotubes, J. Applied Mathematical Modelling 34, pp. 122–128, 2010

[2] P. Soltani, J. Sabrian, R. Bahramian, A. Farshidianfar 'Nonlinear free and forced vibration analysis of a single walled carbon nanotube using shell model'. J. of fundamental Physical Sciences, Vol. 1, No. 3, pp. 47-52, Sep. (2011)

[3] A. C. Eringen, 'On differential equations of nonlocal elasticity and solution', J. Appl. Phys. 54 pp 4703-4710, 1983.

[4] A. C. Eringen and D. G. B Edelen, On nonlocal elasticity, Int. J. Eng. Science10, pp. 233-248, 1972

[5] X. Q. He, C. M. Wang, Y. Yan, L. X. Zhang and G. H. Nie, Pressure dependence of the instability of multiwalled carbon nanotubes conveying fluids, J. of Arch Appl. Mech. 78, pp. 637–648, 2008

[6] Y. Yan, X. Q. He, L.X. Zhang and C. M. Wang, Dynamic behavior of triple-walled carbon nanotubes conveying fluid, Journal of Sound and Vibration, Journal of Sound and Vibration 319 (2009), p. 1003–1018

[7] L. Wang, Vibration analysis of nanotubes conveying fluid based on gradient elasticity theory, J. Computational Materials Science 45, pp. 584–588, 2009

[8] Y. Yan, W.Q. Wang and L.X. Zhang, Dynamical behaviors of fluid-conveyed multi-walled carbon nanotubes, J. Applied Mathematical Modeling 33, pp. 1430–1440, 2009

[9] T. P. Chang and M.F. Liu, 'Small scale effect on flow induced instability of double walled carbon nanotubes' Journal of Mechanics A/solids 30, pp 992-998, (2011).

[10] X. Y. Wang, X. Wang and G. G. Sheng, The coupling vibration of fluid-filled carbon nanotubes, J. Phys. D: Appl. Phys. 40, pp. 2563–2572, 2007

[11] K. Dong, B.Y. Liu and X. Wang, Wave propagation in fluid-filled multi-walled carbon nanotubes embedded in elastic matrix, J. Computational Materials Science 42 (2008), p. 139–148

[12] Y. G. Hu, K. M. Liew, Q .Wang, X. Q. He and B. I. Yakobson, Nonlocal shell model for elastic wave propagation in single- and double-walled carbon nanotubes, Journal of the Mechanics and Physics of Solids 56 (2008), 3475–3485

[13] Wang Lin and Ni Qiao, On vibration and instability of carbon nanotubes conveying fluid, Computational Materials Science 43 (2008), p.399–402

[14] Y. Yan, W.Q. Wang and L.X. Zhang, Nonlocal effect on axially compressed buckling of triple-walled carbon nanotubes under temperature field, Journal Applied Mathematical Modeling 34 (2010), p. 3422–3429

[15]T. Natsuki, Q. Q. Ni and M. Endo, Wave propagation in double-walled carbon nanotubes conveying fluid, J. Appl. Phys. A 90(2008), p. 441–445

[16] G. Q. Xie, X. Han and S. Y. Long, Effect of small size on dispersion characteristics of wave in carbon nanotubes, International Journal of Solids and Structures 44 (2007), p. 1242-1255

[17] A. Azrar, L. Azrar and A. A. Aljinaidi, Analytical and numerical modeling of higher order free vibration characteristics of single walled Carbon NanoTubes, submitted to Physica E, (2012).

[18] A. Azrar, L. Azrar and A. A. Aljinaidi, Length scale effect analysis on vibration behavior of single walled carbon nanoTubes with arbitrary boundary conditions, Revue de Mécanique Théorique et Appliquée, Vol. 2, pp. 475-484, 2011

[19] L. Azrar, J. Waner, S. Belouattar, *Nonlinear* vibration analysis of actively *loaded* sandwich piezoelectric beams with geometric *imperfections*, J. of Sound and Vibration , Vol. 315, 2008

[20] M. Amabili, F. Pellicano and M. P. Paidoussis 'Non-linear dynamics and stability of circular cylindrical shells conveying flowing fluid' J. Computers and Structures 80, pp 899–906, (2002)

[21] M. Amabili, F. Pellicano and M. P. Paidoussis 'Nonlinear vibrations of simply supported, circular cylindrical shells, coupled to quiescent fluid' Journal of Fluids and Structures 12 pp 883-918, (1998)

[22] M. Amabili, F. Pellicano and M. P. Paidoussis 'Non-linear dynamics and stability of circular cylindrical shells containing flowing fluid, part III: truncation effect without flow and experiments' Journal of Sound and vibration 237 pp 617-640, (2000)

Table 5.1 Linear resonant frequencies of a three WCNTs, L=10 m R_3, e_0=0.

With fluid $\rho_f = 1000$, V_0=0											
Variables				Present (10^{12}Hz)	[1]	Present	[1]	Present (10^{12}Hz)	[1]	Present	[1]
R_1	m	n	$1/R_2$	ω_1	ω_1	A1/A2	A1/A2	ω_2	ω_2	A1/A2	A1/A
3.4	1	5	10	5.1859	5.186	1.0590	1.059	1.5519	1.5518	-0.5560	-0.556
3.4	4	5	10	5.2067	5.207	1.0579	1.058	1.5545	1.5544	-0.5617	-0.562
3.4	1	5	20	5.1849	5.185	1.0590	1.059	1.5517	1.5516	-0.5557	-0.556
3.4	1	8	20	5.7720	5.772	1.0338	1.034	1.6173	1.6173	-0.6891	-0.689
6.8	1	5	20	2.3054	2.305	1.0302	1.030	1.3981	1.3980	-0.3722	-0.372

Table5.2 Linear resonant frequencies of a Six WCNTs, L=10 m R_6.

With fluid (x10^{12} Hz), V_0=0									
	R_1	m	n	ω_1	ω_2	ω_3	ω_4	ω_5	ω_6
e_0=0	3.4	1	5	4.9116	7.1004	11 .772	16.621	20.631	23.224
	3.4	4	5	4.9164	7.1109	11.779	16.625	20.633	23.225
	6.8	1	5	2.5455	5.3883	10.675	15.858	20.081	22.799
	6.8	4	5	2.5506	5.3994	10.683	15.863	20.083	22.800
e_0=0.33	3.4	1	5	4.9039	7.0942	11.7690	16.6180	20.6284	23.2217
	3.4	4	5	4.9086	7.1047	11.7760	16.6224	20.6308	23.2228
	6.8	1	5	2.5442	5.3878	10.6745	15.8580	20.0808	22.7991
	6.8	4	5	2.5493	5.3989	10.6824	15.8624	20.0828	22.7996

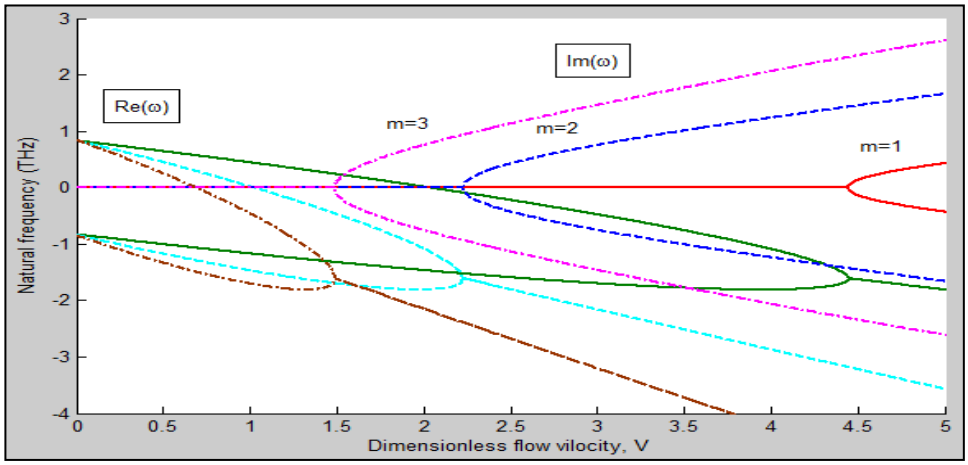

Figure 5.1 Real and imaginary frequency parts with respect to the fluid velocity V of a double WCNTs (L/R2=12, n=2) and e_0a=0 for different wave numbers m.

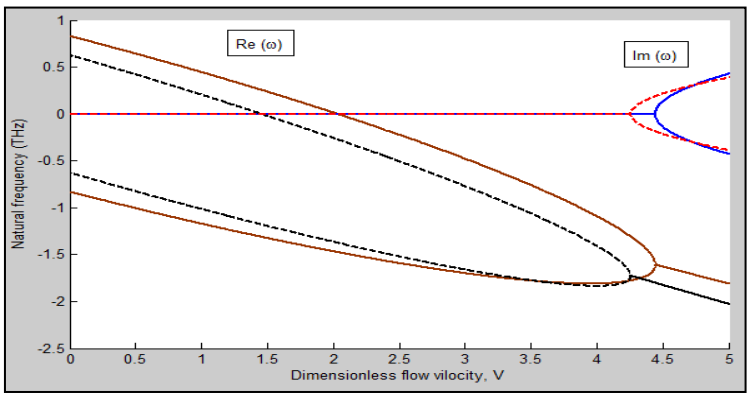

Figure 5.2 Real and imaginary frequency parts with respect to the dimensionless fluid velocity V of a DWCNTs (L/R_2=12, n=2) and e_0a=0. Dotted lines, model without vdW, solid lines, model with vdW.

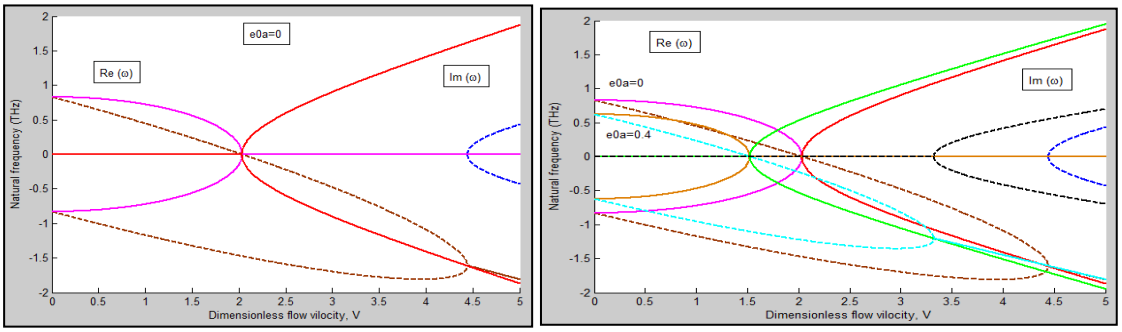

Figure 5.3 Real and imaginary frequency parts with respect to the dimensionless velocity V and e_0a=0 and e_0a=4nm. Dotted lines, model with damping, solid lines, without damping of double WCNTs (L/R_2=12, n=2, m=1).

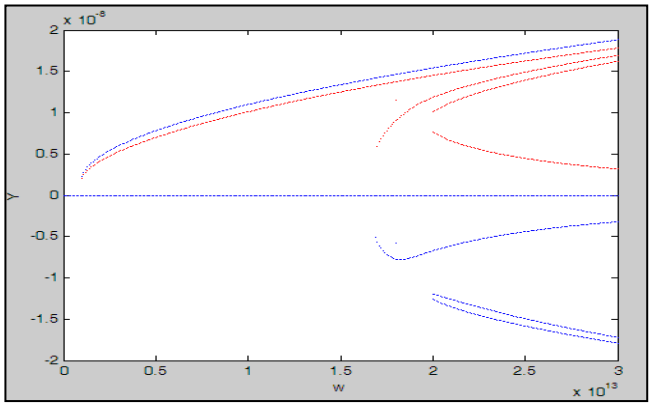

Figure 5.4 Nonlinear amplitude-frequency curves associated to free vibrations of DWCNTs for the case R_1=6.8nm, (n,m)=(1,5), L=20R_1 for ρ_f=0, V_0=0, e_0=0 and T=0k

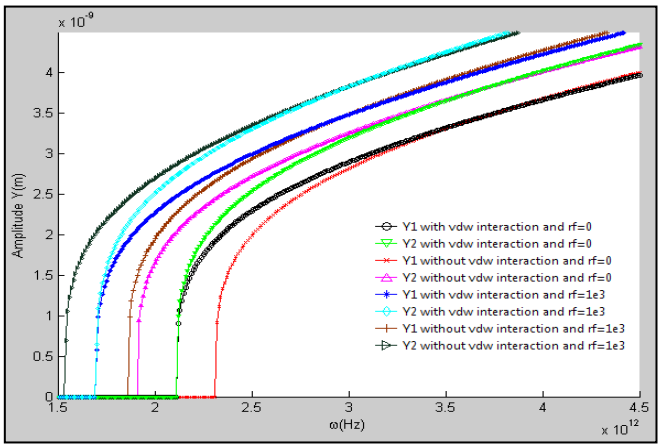

Figure 5.5 Amplitude frequency backbone curves with and without fluid and vdW interaction for R1=3.4 nm, (m,n)=(1,8) and V=1e^3 ms^{-1}

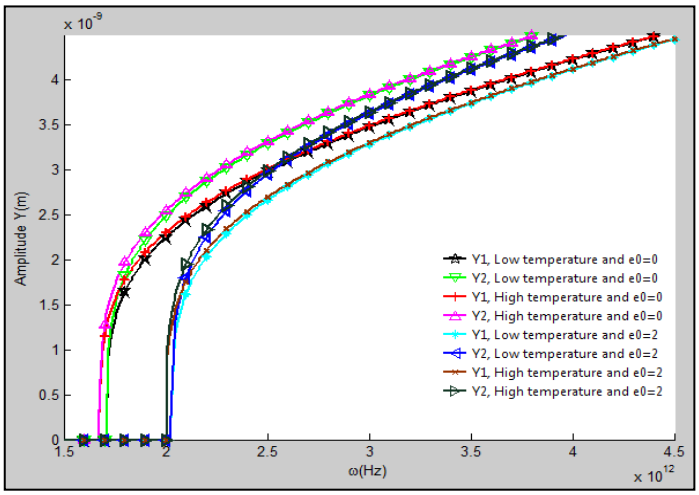

Figure 5.6 Thermal and nonlocal parameter effects on the nonlinear amplitude versus the frequency of the DWCNTs for R1=3.4 nm, (m,n)=(1,8), V=1e^3 ms^{-1} and T=40K

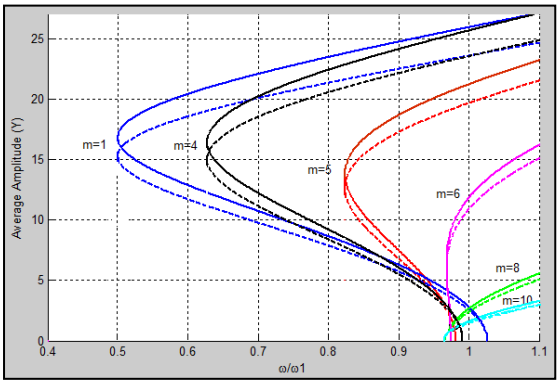

Figure 5.7 Axial wave number effects on the large amplitude frequency response associated to the free vibration of DWCNT with n=1, L/R_o=10, R_I=3.4nm.

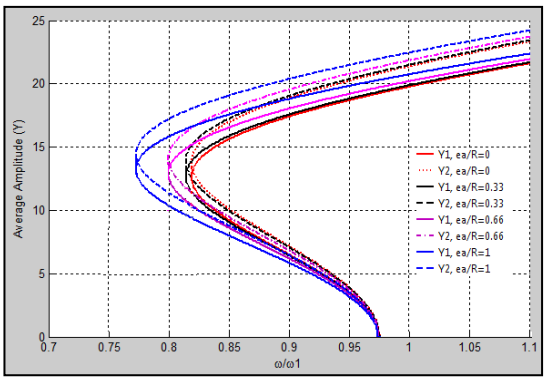

Figure 5.8 Nonlocal parameter effects on the large amplitudes frequency response associated to the free vibration of DWCNT with m=5, n=1, L/R_o=10, R_I=3.4nm.

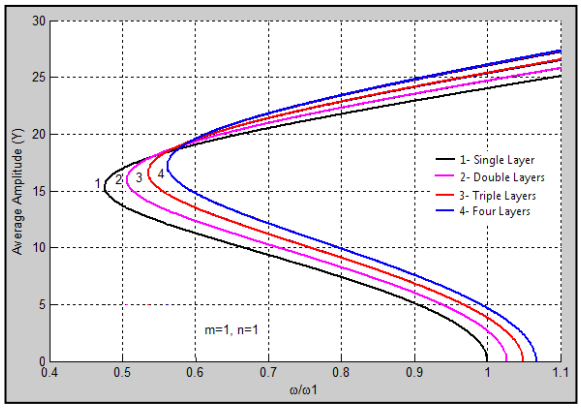

Figure 5.9 Layers number effects on the large amplitudes frequency response associated to the free vibration of MWCNT with L/R_o=10, R_I=3.4nm.

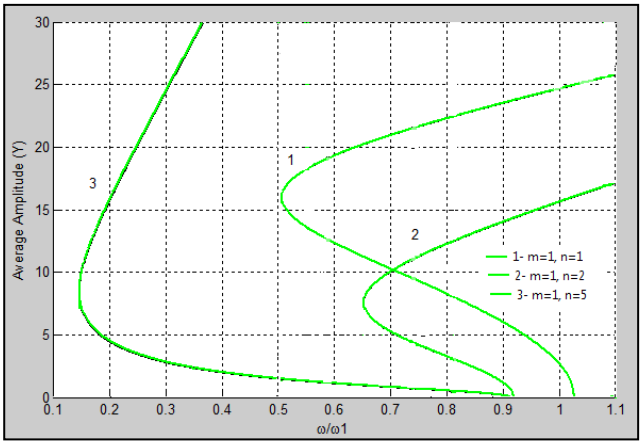

Figure 5.10 Circumferential wave number effect on large amplitude frequency response for DWCNT with L/R_o=10, R_I=3.4nm.

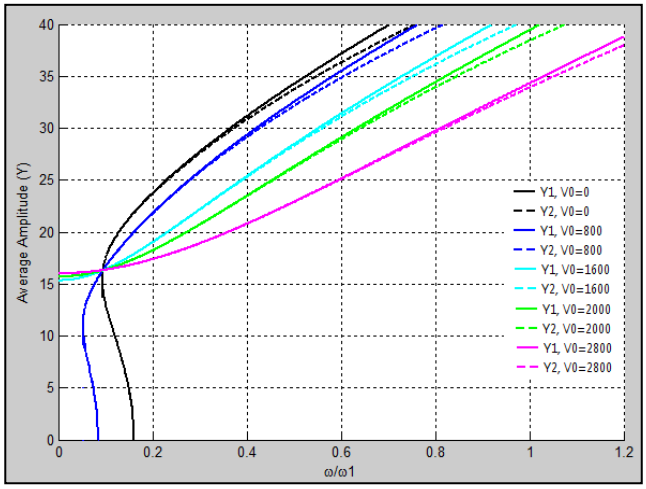

Figure 5.11 Fluid velocity effect on the large amplitude frequency response for DWCNT with L/Ro=10, RI=3.4nm, m=1; n=1; ρ_f=1e3; e_0=0.3; T=40;

Chapiter VI:

Parameters uncertainty effects on the dynamic behavior of fluid conveying carbon nanotubes under a random excitation

Abstract

The influence of parameters uncertainties on the dynamic behavior of carbon nanotubes conveying fluid and subjected to a random harmonic transverse excitation is elaborated. The parameters are assumed to be random and may follow Gaussian, exponential and uniform distribution laws. Based on the nonlocal Bernoulli beam model, several random parameters are considered. The resulted coefficients depend nonlinearly on the random coefficients and the number of considered random parameters 10, the resulting stochastic problem needs powerful stochastic methods to get accurate results. Frequency and time domains are considered and various stochastic methodological approaches are adopted for numerical analysis. For the space domain, the differential quadrature method is used. This leads to a random differential system that needs to be solved using stochastic procedures.

To shed some light on the parameters uncertainly effects on the behaviors of CNT, frequency domain as well as one mode and multimodal time domain formulations are used. Monte Carlo and an internal random coefficient method based on the general polynomial chaos are used herein for the dynamic analysis.

This work is under finalization
Title: **Parameters uncertainty effects on the dynamic behavior of fluid conveying carbon nanotubes under a random excitation**
Authors: **A. Azrar, M. Bensaid, L. Azrar and A. A. Aljinaid**

1. Introduction

In recent years, Carbon NanoTubes (CNT) have been considered good candidates for many refined nanoscaled technologies and devices due to their impressive mechanical and electrical properties. In Nanoscale design, the prediction of geometrical and physical parameters or properties and particularly the prediction of the uncertainty effects of these parameters and its propagation are presently the main challenges. During the fabrication process or experimental measurements, it is difficult to control and predict, accurately, the physical and geometrical parameters. The values of these parameters are then subjected to significant uncertainties and thus the performance of the designed nano structures is inevitably altered.

In fact, uncertainties are inherent in measuring/testing, understanding, and modeling of these downscale nanostructures. Efficient numerical models are required for the behavior analysis of these small scale structures accounting for parameters uncertainties. This deeply motivates the present study on the effects of the parameters uncertainty on the dynamic and static behaviors of Carbon NanoTubes.

In the open literature; the most available models; namely the continuum elasticity and molecular dynamics are used to simulate nano behaviors in either the frequency or time domains. However, the main limitation of the available approaches is that the proposed CNT models are deterministic. The nanostructure is described with predefined values of its mechanical, electrical and geometrical parameters. At this down scale, the impact of parameters uncertainty can be increasingly significant and needs to be taken into account.

Uncertainties in model parameters or inputs are characterized by their probability density functions (pdfs). For uncertainty analysis, the propagation of these pdfs through the model equations and the final pdfs of the model outputs have to be investigated. A number of techniques are available for uncertainty sensitivity and propagation such as Monte Carlo procedure [1], perturbation method, sensitivity analysis methods [2] and polynomial chaos [3,4] among others. Monte Carlo (MC) method has been the mainstream uncertainty quantification technique for decades. It is the most used method and is valid for a wide range of problems. However, it is very computationally expensive since it requires a large number of simulations using the full model.

An alternative approach is based on the expansion of the response in terms of a series of polynomials that are orthogonal with respect to mean value operations. Polynomial chaos was first introduced by Wiener [5] where Hermite polynomials were used to model stochastic

processes with Gaussian random variables. It is noted that a number of other expansions have been proposed in the literature for representing non-Gaussian process [6]. Recent review papers by Schueller and Pradlwarter [7] and by Stefanou [8] summarized the assessment of the past and current status of the procedure for stochastic structural analysis. The potential and applicability of various available methods are assessed.

For random variables and stochastic processes, Polynomial Chaos (PC) representations are infinite series of Hermite polynomials of standard Gaussian random variables with deterministic coefficients. These series converge in mean square to the functions they replace, provided these functions are in L_2. For numerical computation, the infinite series are truncated leading to a PC based approximation. This polynomial representation provides a framework suitable for computational simulation and then widespread in mathematical and numerical analysis of many engineering problems. Various problems have been solved based on this approximation such as solution of stochastic differential equations [9], linear structural dynamics [3,4], nonlinear random vibration [10,11]; soil–structure interaction [12], structural reliability [13], etc. The accuracy of the PC approximation has been evaluated by Field and Grigoriu [14]. Note that in these studies, only few terms random coefficients are used in the PC approximations.

Free vibration of Euler and Timoshenko nanobeams using boundary characteristic orthogonal polynomials are studied by Laxmi-Behera and Chakraverty [15]. Adhikari et al [16] studied the axial vibration of nonlocal rods using finite element method. M Abu-Hilal [17] proposed the vibration of beams with general boundary conditions due to a moving random load.

In structural mechanics, several methods are currently available to solve a large number of problems involving uncertain quantities. In the last decades, the stochastic finite element method (SFEM) was used for solving the dynamic response of structures with stochastic parameters [3,6,8,12]. For large and decomposed structures, the component mode synthesis method has been coupled with polynomial chaos expansions at first and second orders to compute the frequency transfer functions of stochastic structures by Sarsri et al [18] and their time response by Sarsri and Azrar [19]. This coupling procedure is well adapted to large structures that can be decomposed in simple ones with few random coefficients.

The polynomial chaos methods are well suited for the random dynamical systems with a very few number of random coefficients. If the number of random variables increases; the main limitation of the chaos methods is that the number of unknowns to be determined for solving the random systems increases very rapidly with the degree of the classical polynomial chaos

needed for accurate solutions. This limitation makes impossible the use of the polynomial chaos of higher degrees for systems with a large number of random variables. The CPU time and memory required may be prohibitive.

An alternative approach called Internal Random Coefficient Method; (IRCM), has been recently developed by Ben Said et al [20]. This method is based on generalized polynomial chaos and the superposition principle. It can be used to solve random differential equations with a large number of random parameters following various distribution laws and an excitation decomposed in an arbitrary number of random coefficients. The random parameters may be linear or non-linear.

There two main motivations of the present work. The first one if that there are very few research works on the dynamic behavior of nano tubes with random parameters. In nano scale, the physical and geometrical parameters are inevitably uncertain. For efficient numerical procedures predicting the behaviors of CNT; the uncertainties have to be taken into account. The second motivation is that the mathematical modeling used for CNT, depends on too many parameters that are nonlinearly dependent on each other. The order of non-linearity can be up to six and the number of the random parameters can be up to 10 or even more. This kind of problems cannot be accurately handled by the classical polynomial chaos. This kind of problems is giving a field of applications to the internal random coefficient method (IRCM).

In this chapter, the random partial differential equations modeling the dynamic behavior of CNT conveying fluid and subjected to a random excitation is presented. Based on the differential quadrature method, random algebraic systems are formulated for the free and random harmonically forced vibrations. Using the numerically obtained deterministic eigenmodes, a multimodal random formulation is resulted in time domain. The internal random coefficient method is adapted here to the obtained random differential equation. For numerical results, the Monte-Carlo and the IRCM are used. The used parameters are assumed to follow uniform; Gaussian and exponential distribution laws with variances of orders 2%; 5% and 10%. The obtained results are compared to the deterministic prediction in order to demonstrate the uncertainty effects on the elaborated numerical results.

2. Mathematical formulation

2.1 Modeling

The flexural vibration of a slender carbon nanotube conveying fluid and subjected to random transverse excitation, fluid flow and fluid pressure can be modeled by the following partial differential equation based on the nonlocal Euler-Bernoulli beam model:

$$\left(1+c\frac{\partial}{\partial t}\right)EI\frac{\partial^4 W}{\partial x^4}+m_f V^2\frac{\partial^2 W}{\partial x^2}+\left(m_f+m_t\right)\frac{\partial^2 W}{\partial t^2}+2m_f V\frac{\partial^2 W}{\partial x\partial t}-\vartheta A_f\left(V\frac{\partial^3 W}{\partial x^3}+\frac{\partial^3 W}{\partial x^2\partial t}\right)$$
$$-\left(e_0 a\right)^2\left[\left(m_f+m_t\right)\frac{\partial^4 W}{\partial x^2\partial t^2}+m_f V^2\frac{\partial^4 W}{\partial x^4}+2m_f V\frac{\partial^4 W}{\partial x^3\partial t}\right]=q(x,t)-\left(e_0 a\right)^2\frac{\partial^2 q(x,t)}{\partial x^2} \qquad (6.1)$$

in which $W(x,t)$ is the transverse displacement, V is the static mean flow velocity and $q(x,t)$ the random transverse excitation. $E,\ c,\ e_0 a$ and m_t are the Young modulus, viscoelastic coefficient of the tube, nonlocal parameter and the mass of the tube respectively. m_f is the mass of the fluid per unit axial length, A_f and ϑ are the cross sectional area and the viscosity of the internal fluid respectively. These parameters are considered to be random coefficients, following some distribution laws. As the main focus of this work is the parameter uncertainty effect on the dynamic response of CNT, the used parameters and their dependences are explicitly given. The tube section A, inertia moment I, fluid mass m_f, the tube mass m_t are given by:

$$A=\left[\left(R+\frac{h}{2}\right)^2+\left(R-\frac{h}{2}\right)^2\right],\ I=\frac{\pi}{4}\left[\left(R+\frac{h}{2}\right)^4+\left(R-\frac{h}{2}\right)^4\right],$$
$$m_f=\rho_f\pi\left(R-\frac{h}{2}\right)^2,\ m_t=\rho_s\pi A, \qquad (6.2)$$

The following material and geometrical parameters are assumed to be random parameters following arbitrary distribution laws:

$$E=E_0(1+\sigma_E\xi_1);\ R=R_0(1+\sigma_R\xi_2);\ h=h_0(1+\sigma_h\xi_3);\ L=L_0(1+\sigma_L\xi_4)$$
$$c=c_0(1+\sigma_c\xi_5);\ \vartheta=\vartheta_0(1+\sigma_\vartheta\xi_6);\ a=a_0(1+\sigma_a\xi_7);\ e_0=e_0^1(1+\sigma_{e_0}\xi_8) \qquad (6.3)$$
$$\rho_f=\rho_0^f(1+\sigma_{\rho_f}\xi_9);\quad \rho_s=\rho_0^s(1+\sigma_{\rho_s}\xi_{10});\quad V=V_0(1+\sigma_V\xi_{11});\ \delta=H$$

where ξ_j, j=1 to11 are the reduced considered random variables and σ is the ratio

$$\sigma_{X_j}=\frac{SD(X_j)}{mean(X_j)} \qquad (6.4)$$

where X_j, $X = \{E, R, h, L, c, \vartheta, a, e_0, \rho_f, \rho_s, V\}^t$. and SD is the standard deviation.

It should be noted that the considered coefficients $c, E, I, m_f V^2, m_f, m_t, \vartheta A_f V$ and $(e_0 a)^2 (m_f + m_t)$ are nonlinear random coefficients and the higher order of nonlinearity is six. This higher nonlinearity order may make strong the uncertainty effects of these parameters.
In addition to the parameters uncertainty effects a random excitation q(x,t) is considered. The partial differential equation (6.1) is thus a stochastic partial differential equation and its solution necessitates well adapted numerical methods.

2.2 Quick uncertainly quantification.

Before elaborating solution procedures of eq. (6.1), a quick uncertainly quantification procedure can be established. There are various methods for uncertainly quantification and the classical ones are reliability analysis methods based on the probability of structural failure [2]. Mostly, the forward uncertainty propagation is analyzed by evaluating the lower order moments, means and variance of the output. This procedure will be elaborated based on the mainly used methods: Monte-Carlo simulation and general polynomial chaos expansion.
Note that as the components of the parameters vector X can follow arbitrary distribution laws, the probability density function of the vector is not known. In addition, the considered coefficients are highly nonlinearly dependent and thus their probability density function is also not known. Monte-Carlo methods can be used to get an approximation of the lower order moments of the considered coefficients. This can give a quick uncertainty quantification of these coefficients.

2.3 Differential Quadrature discretization.

For numerical solution, the differential quadrature method is used the space domain. Based on this method and after space discretization, the partial differential equation (6.1) can be written in the following differential system:

$$\frac{EI}{L^4}\left(\sum_{k=1}^{n} H_{ik}^4 w_k + c\sum_{k=1}^{n} H_{ik}^4 \dot{w}_k\right) + \frac{m_f V^2}{L^2}\sum_{k=1}^{n} H_{ik}^2 w_k + \left(m_f + m_t\right)\ddot{w}_i + \frac{2m_f V}{L}\sum_{k=1}^{n} H_{ik}^1 \dot{w}_k$$

$$-\frac{\vartheta A_f}{L^2}\left(\frac{V}{L}\sum_{k=1}^{n} H_{ik}^3 w_k + \sum_{k=1}^{n} H_{ik}^2 \dot{w}_k\right) - \frac{\left(e_0 a\right)^2}{L^2}\left[\left(m_f + m_t\right)\sum_{k=1}^{n} H_{ik}^2 \ddot{w}_k + \frac{m_f V^2}{L^2}\sum_{k=1}^{n} H_{ik}^4 w_k\right.$$

$$\left. + \frac{2m_f V}{L}\sum_{k=1}^{n} H_{ik}^3 \dot{w}_k\right] = q(x,t) - \left(e_0 a\right)^2 \frac{\partial^2 q(x,t)}{\partial x^2} \qquad (6.5)$$

The detail of this development is given in the appendix A. The system (6.5) can thus be rewritten in the following matrix form:

$$[M]\{\ddot{w}\} + [C]\{\dot{w}\} + [K]\{w\} = Q(t) \qquad (6.6)$$

where

$$M = \left(m_f + m_t\right)\left(I - \frac{\left(e_0 a\right)^2}{L^2} H^2\right)$$

$$K = \left(\frac{EI}{L^4} - \frac{\left(e_0 a\right)^2}{L^2}\frac{m_f V^2}{L^2}\right)H^4 + \frac{m_f V^2}{L^2} H^2 - \frac{\vartheta A_f V}{L^3} H^3$$

$$C = \frac{2m_f V}{L} H^1 - \frac{\vartheta A_f}{L^2} H^2 - \left(e_0 a\right)^2 \frac{2m_f V}{L^3} H^3 + \frac{EI\, c}{L^4} H^4$$

$$w = \left[w_1, w_2, ..., w_n\right]^T,\ Q = \left[q_1(t), q_2(t), ..., q_n(t)\right]^T,\ H^j = \sum_{k=1}^{n} H_{ik}^j I_k$$

where H_{ik}^j are given in appendix A.

Note that the matrices [M], [C] and [K] depend nonlinearity on the considered random coefficients and are then random matrices.

For dynamic analysis, the frequency and time domains are considered and the focus is first on the frequency domain.

3. Frequency domain

3.1 Frequency-excitation system

For the frequency analysis, the solution is assumed to be $\{W\}(t) = \{W\}e^{i\Omega t}$ and the excitation $\{Q\}(t) = \{Q\}e^{i\Omega t}$. The system (6) is then reduced to:

$$-\Omega^2[M]\{W\} + i\Omega[C]\{W\} + [K]\{W\} = \{Q\} \qquad (6.7)$$

The numerical solution of this system leads to the frequency-amplitude relation for the considered excitation amplitude and physical parameters. As the system (6.7) is a random system, stochastic methods have to be elaborated for numerical solution.

3.2 Eigenproblem

For the analysis of eigenmodes and associated eigenfrequencies, the problem (6.7) is reduced to the following eigenvalue problem:

$$\begin{cases} \Gamma Y = \omega Y, \\ \Gamma = \begin{pmatrix} M_s & 0 \\ 0 & M_s \end{pmatrix}^{-1} \begin{pmatrix} 0 & K_h \\ K_h & C_S \end{pmatrix}, \; Y = \begin{Bmatrix} W_s \\ \omega W_s \end{Bmatrix}, \; K_h = [K_S] - [K_D][K_B]^{-1}[K_C] \end{cases} \tag{6.8}$$

The detail of this transformation and matrices are given in the appendix B.

As the matrices M_s, K_h and C_S are random matrices, this leads to a random eigenvalue problem. To get the mean and standard derivation of eigenfrequencies and eigenmodes, well adapted methods are necessary.

In this analysis, the Monte-Carlo method is first used. The numerical solution of equations (6.7) and (6.8) allows one to get amplitude-frequency dependence as well as the eigenvalues and eigenvectors associated to given boundary conditions and physical parameters. The frequency velocity $(\omega - V)$ dependence can be analyzed with respect to the considered random coefficients.

3.3 Simplified frequency amplitude response

For a simplified frequency-amplitude response, the one mode frequency analysis is first considered. Deterministic eigenmodes, obtained from (6.8) by considering $\sigma_{X_j} = 0,$ are used. The matrix problem (6.7) is then reduced to a simple algebraic one by considering a selected eigenmode.

Let us assumed that the excitation is decomposed into a deterministic a random harmonic parts given by: $f_1(t) = f_{10}\cos(\Omega t) + f_{11}\cos(\Omega t)$

where $f_{10}\cos(\Omega t)$ is the harmonic deterministic part and f_{11} is the random part.

The random parameter is written as $f_{11} = f_{11n}\,\xi_n$.

where f_{10} and f_{11n} are deterministic parameters and ξ_n is the associated random part.

Note that, $f_{11}\,\xi_n\cos(\Omega t)$ may be considered as a kind of load noise. This decomposition allows analyzing the departure form an ideally perfect harmonic excitation and its effect on the forced response can be analyzed.

The solution $q_1(t)$ is assumed in the form $q_1(t) = A\cos(\Omega t) + B\sin(\Omega t)$ where A and B are random function depending on the Ω, f_{10}, f_{11} as well as on the considered physical and geometrical parameters. The following random algebraic system is then resulted:

$$\begin{bmatrix} C_0 - \Omega^2 C_2 & \Omega C_1 \\ -\Omega C_1 & C_0 - \Omega^2 C_2 \end{bmatrix} \begin{bmatrix} A \\ B \end{bmatrix} = \begin{bmatrix} f_{10} + f_{11} \\ 0 \end{bmatrix} \tag{6.9}$$

where $C_2 = \langle Mw_1, w_1 \rangle$, $C_1 = \langle Cw_1, w_1 \rangle$, $C_0 = \langle Kw_1, w_1 \rangle$ and w_1 is a selected deterministic eigenmode.

For clamped-clamped boundary conditions and using the same deterministic CNT parameters given in numerical results, the following scalar products are numerically obtained

$\langle w_1, w_1 \rangle$ = 1.9938e-03; $\left\langle \frac{\partial^2 w_1}{\partial x^2}, w_1 \right\rangle$= -2.2422e-02; $\left\langle \frac{\partial^4 w_1}{\partial x^4}, w_1 \right\rangle$=1.0454e+00;

$\left\langle \frac{\partial w_1}{\partial x}, w_1 \right\rangle$ = -2.6291e-14; $\left\langle \frac{\partial^3 w_1}{\partial x^3}, w_1 \right\rangle$ =1.9368e-12;

This random algebraic system can be solved by Monte Carlo or generalized polynomial chaos for the considered parameters

4. Time domain

For time domain analysis, the differential system (6.9) can be solved by numerical method such as, New Mark or θ-Wilson methods combined to stochastic procedures. But, as the system dimension is large this will necessitates a huge amount of computation time. For this reason the modal analysis is preferred here. The deterministic eigenmodes are used as a modal basis decomposition.

4.1 Multimodal formulation

The response is $W(x,t)$ assumed in the following form:

$$W(x,t) = \sum_{i=1}^{N} w_i(x)\, q_i(t) \tag{6.10}$$

where $w_i(x)$ are deterministic eigenmodes.

Based on this decomposition, the differential system (6.6) is transformed into the following reduced matrix problem:

$$[C_2]\{\ddot{q}\}+[C_1]\{\dot{q}\}+[C_0]\{q\}=\{F(t)\} \tag{6.11}$$

where the components of the matrices $[C_2],[C_1],[C_0]$ and the vector $\{F(t)\}$ are given by:

For i=1 to N and j=1 to N.

$$C_{2ij}=\left(m_f+m_t\right)\left(\langle w_i,w_j\rangle-\left(e_0a\right)^2\left\langle\frac{\partial^2 w_i}{\partial x^2},w_j\right\rangle\right)$$

$$C_{1ij}=c\,EI\left\langle\frac{\partial^4 w_i}{\partial x^4},w_j\right\rangle+2m_fV\left\langle\frac{\partial w_i}{\partial x},w_j\right\rangle-\vartheta A\left\langle\frac{\partial^2 w_i}{\partial x^2},w_j\right\rangle-2m_fV\left(e_0a\right)^2\left\langle\frac{\partial^3 w_i}{\partial x^3},w_j\right\rangle;$$

$$C_{0ij}=\left(EI-m_fV^2\left(e_0a\right)^2\right)\left\langle\frac{\partial^4 w_i}{\partial x^4},w_j\right\rangle+m_fV^2\left\langle\frac{\partial^2 w_i}{\partial x^2},w_j\right\rangle-\vartheta AV\left\langle\frac{\partial^3 w_i}{\partial x^3},w_j\right\rangle; \tag{6.12}$$

$$F_j(t)=\langle q(x,t),w_j\rangle-\left(e_0a\right)^2\left\langle\frac{\partial^2 q(x,t)}{\partial x^2},w_j\right\rangle;$$

4.2 One-mode analysis

For the sake of clarity, the one mode is first considered. In this case, the random differential system (6.11) is reduced to the following simplified random differential equation.

$$C_{211}\ddot{q}_1(t)+C_{111}\dot{q}_1(t)+C_{011}q_1(t)=f_1(t) \tag{6.13}$$

where

$$C_{211}=\left(m_f+m_t\right)\left(\langle w_1,w_1\rangle-\left(e_0a\right)^2\left\langle\frac{\partial^2 w_1}{\partial x^2},w_1\right\rangle\right)$$

$$C_{111}=c\,EI\left\langle\frac{\partial^4 w_1}{\partial x^4},w_1\right\rangle+2m_fV\left\langle\frac{\partial w_1}{\partial x},w_1\right\rangle-\vartheta A\left\langle\frac{\partial^2 w_1}{\partial x^2},w_1\right\rangle-2m_fV\left(e_0a\right)^2\left\langle\frac{\partial^3 w_1}{\partial x^3},w_1\right\rangle;$$

$$C_{011}=\left(EI-m_fV^2\left(e_0a\right)^2\right)\left\langle\frac{\partial^4 w_1}{\partial x^4},w_1\right\rangle+m_fV^2\left\langle\frac{\partial^2 w_1}{\partial x^2},w_1\right\rangle-\vartheta AV\left\langle\frac{\partial^3 w_1}{\partial x^3},w_1\right\rangle; \tag{6.14}$$

$$f_1(t)=\langle q(x,t),w_1\rangle-\left(e_0a\right)^2\left\langle\frac{\partial^2 q(x,t)}{\partial x^2},w_1\right\rangle;$$

This simplified equation can be handled by the Monte Carlo simulation and also by the conditional expectation method. It is well known, as also tested here, that the Monte Carlo and conditional expectation methods generally need a huge amount of computational effort to obtain converged results. Another procedure to handle this problem is the classical polynomial chaos [21]. But, as the number of random parameter is large, this procedure will not provide accurate results.

Let us note that for the considered problem, we have 10 random variables with a nonlinearity of order six. It should be noted that with this order of nonlinearity and the number of random

coefficients, the polynomial chaos necessitate a very large CPU time and memory spaces for acceptable accuracy. For this reason, the newly developed method called Internal Random Coefficient Method (TRCM) is adopted here. An overview of this method is given bellow.

4.3 Internal random coefficient method

Let us consider the differential equation (6.13) with the deterministic boundary conditions where the multi- indices are dropped:

$$\begin{cases} C_2\ddot{q}_1(t) + C_1\dot{q}_1(t) + C_0 q_1(t) = f_1(t) \\ q_1(0) = q_{10} \ \ and \ \dot{q}_1(0) = \dot{q}_{10} \end{cases} \tag{6.15}$$

For more generality, the excitation $f_1(t)$ is supposed to be a random excitation and its expression is given in the following form:

$$f(t) = \sum_{j=12}^{n} (a_{0j} + a_{1j}\xi_j)\, g_j(t) \tag{6.16}$$

where a_{0j} and a_{1j} are deterministic constants and g_j is a deterministic function, $\xi_1, \xi_2, ...\xi_{11}$ are the associated to system parameters, ξ_j for $j > 12$ are used for the random excitation. The random variables ξ_j are supposed pair wise independent random variables having a distribution function with respect to the Lebesgue measure denoted by f_j with zero mean and one for standard deviation.

Based on the internal random coefficients methods, introduced by Ben-Said et al [21], the random coefficients of equation (6.15) are rewriting in the following form:

$$C_0(\omega_1) = E(C_0) + \sigma_0 X_0 \tag{6.17a}$$

$$C_1(\omega_1) = E(C_1) + \sigma_1 X_1 \tag{6.17b}$$

$$C_2(\omega_1) = E(C_2) + \sigma_2 X_2 \tag{6.17c}$$

where $E(C_i)$ is the mean and σ_i is the standard deviation of the random coefficient C_i.

Using these new expressions, the initial value problem (6.15) is reduced to the following simplified random differential equation:

$$\sum_{i=0}^{2} \left(E(C_i) + \sigma_i X_i^1 \right) \frac{d^i U(t, X^1)}{dt^i} = \sum_{j=6}^{n} (a_{0j} + a_{1j}\xi_j)\, g_j(t) \tag{6.18}$$

The random variables X_i are gathered on the random vector X^1 by:

$$X^1 = \left(X_0, X_1, X_2 \right) \tag{6.19}$$

Noted by f^1 the distribution function with respect to the Lebesgue measure associated to the random vector X^1, this distribution function is explicitly given from the distribution function associated to the random variables $(\xi_j)_{1 \le j \le 5}$. by Ben Said et all [21],

The random variables ξ_j, appearing in the right hand side of the stochastic equation (6.15), are gathered on the random vector X^2 by:

$$X^2 = (\xi_3, ..., \xi_n) \tag{6.20}$$

Using the independence of the random variables ξ_j, this random vector has the distribution function with respect to the Lebesgue measure noted by f^2 and defined by:

$$f^2(x^2) = \prod_3^n f_k(x_k^2) \tag{6.21}$$

The random vector X^1 and X^2 are gathered in the random vector X by:

$$X = (X^1, X^2) \tag{6.22}$$

Let f be the distribution function with respect to the Lebesgue measure associated to the random vector X. This distribution is given using the independence between the random vector X^1 and X^2 by:

$$f(x)dx = f^1(x^1) f^2(x^2) dx^1 dx^2 \tag{6.23}$$

$L_f^2(\mathbb{R}^{n-2})$ denotes the set of square-integrable functions with respect to the weight measure *f*:

$$L_f^2(\mathrm{R}^{n-2}) = \left\{ H : \int_{\mathrm{R}^{n-2}} H^2(x) f(x) dx < +\infty \right\} \tag{6.24}$$

with the following associated inner product:

$$\langle H, G \rangle = \int_{\mathrm{R}^{n-2}} H(x) G(x) f(x) dx < +\infty \tag{6.25}$$

Let us consider the polynomial chaos associated to the random vector X. These polynomials are be noted by:

$$\{\Psi_k, k \in N\} \tag{6.26}$$

The set of these polynomials satisfies the orthogonal conditions:

$$\langle \Psi_k, \Psi_i \rangle = \alpha_k \delta_{ki} \tag{6.27}$$

where:

$$\alpha_k = \langle \Psi_k, \Psi_k \rangle \tag{6.28}$$

The solution U(t, X) of the stochastic differential equation (6.18) is a stochastic process depending on t and X. The decomposition of this solution according to the polynomials chaos basis, is given by:

$$U(t, X) = \sum_{k \geq 0} \Psi_k(X) u_k(t) \tag{6.29}$$

Using the M^{th} first terms of the series (6.29), the process $U(t, X)$ can be approximated by:

$$U_M(t,X) \cong \sum_{k=0}^{M} \Psi_k(X) u_k(t) \tag{6.30}$$

Inserting these expressions in equation (6.18) the following random differential equation is resulted:

$$\sum_{k=0}^{M} \sum_{i=0}^{2} \left(E(C_i) + \sigma_i^1 X_i^1 \right) \Psi_k(X) \frac{d^i u_k(t)}{dt^i} = \sum_{j=6}^{n} (a_{0j} + a_{1j} \xi_j)\, g_j(t) \tag{6.31}$$

Projecting this equation with respect to Ψ_1 for l=0 to M, leads to:

$$\sum_{k=0}^{M} \sum_{i=0}^{2} \left\langle \left(E(C_i) + \sigma_i^1 X_i^1 \right) \Psi_k, \Psi_1 \right\rangle \frac{d^i u_k(t)}{dt^i} = \sum_{j=6}^{n} \left\langle (a_{0j} + a_{1j} \xi_j), \Psi_1 \right\rangle g_j(t) \tag{6.32}$$

For a compact formulation the square matrices T^i of order (M+1) and the time dependent vector D_i of dimension (M+1) are introduced for all integers k, $l \in [0, M]$ by:

$$T_i(k,l) = E(C_i)\alpha_k \delta_{kl} + \sigma_i^1 \langle X_i \Psi_k, \Psi_1 \rangle \tag{6.33}$$

$$D_1(t) = \sum_{j=6}^{n} \left(a_{0j} \delta_{0l} + a_{1j} \langle \xi_j, \Psi_1 \rangle \right) g_j(t) \tag{6.34}$$

The differential system (6.31) is rewritten in the following compact form, for $l \in [0, M]$ as:

$$\sum_{k=0}^{M} \sum_{i=0}^{2} T_i(k,l) \frac{d^i u_k(t)}{dt^i} = D_1(t) \tag{6.35}$$

This method is first used here to solve the simplified random differential equation (6.15). It will be extended next for the reduced random differential systems of kind (6.11) and in the next work to the more general random system (6.6).

5. Numerical results and discussion

For numerical results, a CNT conveying fluid with the following parameters is considered.

$E_0 = 10^{12}$ Pa; $R_0 = 0.510^{-9}$m; $h_0 = 0.3410^{-9}$m; $L_0 = 10^{-8}$m, $c_0 =$ 13.620; $\vartheta_0 = 1.1210^3$ Pa;
$a_0 = 0.4210^{-10}$m; $e_0^1 = 23.8$, $\rho_0^f = 1000\text{kg/m}^3$; $\rho_0^s = 2300\text{kg/m}^3$; $V_0 = 500 m/s$
$\sigma_E = \sigma_R = \sigma_h = \sigma_L = \sigma_c = \sigma_\vartheta = \sigma_a = \sigma_{e_0} = \sigma_{\rho_f} = \sigma_{\rho_s} = \sigma_V = \sigma$

The random variables ξ_j, $j = 1,2,...,n$ are assumed to follow various distribution laws with the ratio σ given in (6.4). It is assumed here that all the considered variables have the same ratio σ_X. Three different ratios, 2%, 5% and 10% are considered in the performed numerical analysis.

5.1. Dynamic instability analysis.

In this work, we restrict ourselves to the use of Monte-Carlo method. The random parameters are assumed to follow simultaneously uniform, normal and exponential distribution laws.

For the dynamic instability analysis, the frequency-fluid velocity relationship is analyzed when the excitation is neglected. For this analysis the random variables are assumed to be exponential, uniform and normal centered variables with $\sigma_j = 2\%, 5\%$ and 10% for j=1,5

5.2. Fluid velocity buckling problem case $\omega = 0$

The eigenvalue problem (6.8) can reduced to the fluid velocity buckling eigenvalue problem by assuming that ω=0. The following eigenproblem is resulted.

$$\left[K_{ela}\right]\{W\} = V_c^2 \left[K_{geo}\right]\{W\} \tag{6.36}$$

Where V_c^2 is the buckling fluid velocity, K_{ela} and K_{geo}, the stiffness and geometric matrices, are given by:

$$\left[K_{ela}\right] = \frac{EI}{L^4} H^4;$$

$$\left[K_{geo}\right] = -\left[\left(\frac{(e_0 a)^2}{L^2}\frac{m_f}{L^2}\right)H^4 - \frac{m_f}{L^2}H^2\right];$$

The numerical solution of the random eigenvalue problem (6.36) allows one to get the buckling fluid velocity and associated eigenmodes respectively for the considered random coefficients and boundary conditions. The Monte Carlo method is used and ξ_j are assumed to be uniform, normal and exponential simultaneously and the random coefficients are with $\sigma_j = 2\%, 5\%, 10\%$. The Monte Carlo is used here with 500 random numbers.

Table 6.1 shows the critical buckling fluid velocity associated to clamped boundary conditions for different laws. It is demonstrated from this table that for small deviation, the obtained expectations are very close to the deterministic variances. The output results for the critical loads are in the confidence interval [mean(Vi)(1-σ(Vi)), mean(Vi)(1+σ(Vi))] with an approximate probability. The effects of the input random coefficients σj are presented. The accuracy of the obtained results can be improved by increasing the number of random numbers.

5.3. Dynamic instability analysis

For the dynamic instability analysis, the random eigenvalue problem (6.8) is solved for different values of the fluid speed V by means of the Monte Carlo method. The numerical solution of this problem allows one to get the natural frequencies and the associated

eigenmodes for different values of the deterministic fluid velocity. For V=0, the obtained results correspond to the free vibration characteristics. Table 6.2 presents the numerical results obtained by Monte Carlo method with N=1000 random numbers. The first three natural frequencies are given where the random parameters follow uniform, normal and exponential laws with the input σ_x =2%, 5% and 10%. Deterministic results (σ_x =0) are presented for comparison.

The mean, variance and the corresponding ratio $\sigma(\omega_i)$ are presented for the input σ_i =2%, 5% and 10%. It has to be noted that more random numbers are needed for large input variances. For the dynamic instability, the frequency velocity curves are needed at a large range of the velocity. This leads to a very large amount of computation with the Monte-Carlo method. Figure 6.1 shows the deterministic curve and the mean value of the first frequency with respect to the velocity when the random parameters follow the uniform distribution low with σ_x =2% and 5%. Only 500 random numbers are used. It is demonstrated that the mean values agree well with the deterministic values and the confidence interval obtained by the bounds increases by increasing the input σ_i. It is also demonstrated that near the critical buckling velocity more random numbers are needed and near the flutter critical velocity a very large number of random numbers is needed for accurate results. As the amount of computation is huge, we restrict ourselves here to the presented results. It should be noted that the used number of random number is not enough for the flutter behavior. The obtained results can be improved by using parallel computation or using a supercomputer. These huge computations show clearly the limitation of the Monte-Carlo method and then the great need to develop alternative methods.

5.4. Frequency-Amplitude response

For the frequency-amplitude analysis, the one mode case is first considered. The simplified equation (6.8) is first analyzed; the Monte-Carlo and conditional procedures are used. The mean and standard deviation of the of displacement response in time for CC-CNT by IRCM, chaos, conditional and Monte-Carlo methods are presented in figures (6.5 to 6.8). It is demonstrated that a good accuracy is observed between these methods. It is observed from these figures that for higher deviation coefficient σj the magnitude of the means displacement response decreases but the associated standard deviation are increases.

The Monte-Carlo method can be used efficiently for small systems for which few CPU time is needed. This is demonstrated for the amplitude frequency analysis based on one mode. The

forced harmonic responses with respect to the first mode are presented in figures 6.2 and 6.3 when the random parameters follow uniform, exponential and normal distribution laws. The Monte-Carlo method with 500 random numbers is used. The variance effects are presented in figure 6.2 for uniform law. The deterministic frequency response is presented to show clearly the random parameters effects. This effect is clearly demonstrated and the dispersion of the results increases by increasing the input variance σ_i. Figure 6.3 shows the mean and the variance results when the input random coefficients follow normal, uniform and exponential distribution laws with σ_i =5%.

It should be noted that the same analysis can be done by considering the other modes. Response curves can be then obtained in the vicinity of the 2^{nd} and 3^{rd} and so on resonances. More generally, the multi-modal analysis can be done by considering the frequency problem (6.6).

5.5. Time response

For the time response only the one mode time response equation (6.12) is solved. For numerical analysis, the Monte-Carlo and conditional methods as well as the Internal Random Coefficient Method are used. The obtained results are presented in figures 6.4 to 6.7 for σ_j =5% and 20%. The very large variation 20% is selected in order to show the effectiveness of the IRCM even for large variation.

Let us recall that 10 random variables are used. With this number of variables and the non-linearity of order 6, presented by the coefficients, higher order of polynomial chaos is needed. This problem can not be handled accurately with the classical polynomial chaos. The results obtained by the IRCM with general polynomial chaos of order 7 are accurate as clearly presented in figures 6.4 to 6.7 and even for large variance σ_j =20%.

Figures 6.4 and 6.5 show the mean values of $q_1(t)$ with respect to time for σ_j=5% and σ_j=20%. The deterministic response is presented for comparison as well as results obtained by the Monte Carlo method with 1000 random numbers by the conditional method and by the IRCM with polynomial of order 7. The agreement between the obtained results is demonstrated. The standard deviation of $q_1(t)$ with respect to time is presented in figures 6.6 and 6.7. The agreement is observed with results obtained by the three stochastic methods.

It has to be mentioned that for numerical solutions, the Runge-Kutta method and Matlab computing codes are elaborated and programed. Monte-Carlo and conditional methods need

too much computation time in comparison to the IRCM that needs only few minutes in a simple laptop computer.

The Monte-Carlo method, conditional method and particularly the IRCM will be used to solve the multi-modal time problem (6.10) and the more general time program (6.5) in the next work.

6. Conclusion

Methodological approaches based on the differential quadrature method, Monte-Carlo and generalized polynomial chaos for random differential equation with an arbitrary number of random parameters with different types of distribution laws are developed. These parameters can be linear or nonlinear. The obtained results, based on generalized polynomial chaos and Monte-Carlo methods, are compared with deterministic ones. A good accuracy is observed between these results

Note that the Monte-Carlo method used for the eigenvalue problems and for the dynamic instability needs too much time even if only 500 and 1000 random numbers are used. For small systems, based on the one mode formulation, this method can be used with reasonably CPU time.

As the number of random parameters (10) and the order of nonlinearity is high (6), the IRCM is more adapted. This method needs some mathematical developments, but very few CPU time and memory space are required. This method will be extended to random differential systems as well as to large algebraic systems.

7. Reference

[1] S. Weinzierl, Introduction to Monte Carlo methods, NIKHEF, Theory Group, The Netherlands, Tech. Rep. NIKHEF-00-012, 2000.

[2] A. Saltelli, K. Chan, E.M. Scott, Sensitivity Analysis, Wiley, 2000.

[3] R. Ghanem and P. Spanos, Stochastic finite elements: a spectral approach. Springer-Verlag, 1991.

[4] D. Xiu, Numerical Methods for Stochastic Computations: A Spectral Method Approach. Princeton University Press, 2010.

[5] N. Wiener, The Homogeneous Chaos. American Journal of Mathematics 60, pp. 897–936, 1938

[6] H. Matthies, C. Brenner, C. Bucher, C. Soares, Uncertainties in probabilistic numerical analysis of structures and solids: stochastic finite elements. Struct Safety, 19, pp. 283–336, 1997

[7] Stefanou G. The stochastic finite element method: Past, present and future. Computer Methods in Applied Mechanics and Engineering, 198, pp.1031-1051, 2009

[8] G. I. Schueller, H. J. Pradlwarter, Uncertain linear systems in dynamics: Retrospective and recent developments by stochastic approaches. Engineering Structures, 31, pp. 2507-2517, 2009

[9] T. Banek, Chaos expansion for the solution of stochastic differential equations. Syst Control Lett, 36, pp. 351–358, 1999

[10] R. Ghanem, P. Spanos, Stochastic Galerkin expansion for nonlinear random vibration analysis. Probabilistic Engng. Mech., 8, pp. 255–264, 1993

[11] R. Li, R. Ghanem, Adaptive polynomial chaos expansions applied to statistics of extremes in non-linear random vibration. Probabilistic Engineering Mechanics, 13, pp.125-136, 1998

[12] H. Matthies, C. Brenner, C. Bucher, C. Soares, Uncertainties in probabilistic numerical analysis of structures and solids: stochastic finite elements. Struct Safety, 19, pp. 283–336, 1997

[13] J. Zhang, B. Ellingwood, Orthogonal series expansions of random fields in reliability analysis. J Engng Mech, 120, pp. 2660–2677, 1994

[14] R.V. Field Jr., M. Grigoriu, On the accuracy of the polynomial chaos approximation, Probab. Engrg. Mech. 19, 65–80, 2004

[15] L. Behera and S. Chakraverty, Free vibration of Euler and Timoshenko nanobeams using boundary characteristic orthogonal polynomials, Appl Nanosci, 2013

[16] S. Adhikari, T. Murmu and M. A. McCarthy, Dynamic finite element analysis of axially vibrating nonlocal rods, Finite Elements in Analysis and Design 63 (2013) 42–50

[17] D. Sarsri, L. Azrar, A. Jebbouri, A. El Hami, Component mode synthesis and polynomial chaos expansions for stochastic frequency functions of large linear FE models. Computers & Structures, 89, pp. 346-356, 2011

[18] M. Abu-Hilal, Vibration of beams with general boundary conditions due to a moving random load, Archive of Applied Mechanics, 72, 657,650, 2003

[19] D. Sarsri, L. Azrar, Time response of structures with uncertain parameters under stochastic inputs based on coupled polynomial chaos expansion and component mode

synthesis methods'. Submitted to Mechanics of Advanced Materials and Structures; 2014.

[20] M. Ben Said, L. Azrar and D. Sarsri, Internal random coefficient and generalized polynomial chaos for higher order differential equations with uncertain variables' Submitted to Applied Mathematical Modeling, 2014

Appendix A

Differential quadrature method

Based on the DQM, the continuous solution is approximated by functional values at discrete points. In the present paper, Chebyshev-Gauss-Lobatto quadrature points are used

$$y_i = \frac{1}{2}\left[1-\cos\left(\frac{i-1}{N-1}\pi\right)\right] \text{ for } i = 1,2,3,.....,n \qquad (A-1)$$

where $y_i = \frac{x_i}{L}$ and n is the number of grid points in the domain [0, 1].

For a function *f(y)*, DQ approximation of the mth order derivative at the ith point is given by:

$$f(y,t) = \sum_{j=1}^{n} l_j(y) f(y_j,t) \qquad (A-2a)$$

$$\frac{d^m}{dy^m}\begin{Bmatrix} f(y_1) \\ f(y_2) \\ \vdots \\ f(y_n) \end{Bmatrix} = H_{ij}^m \begin{Bmatrix} f(y_1) \\ f(y_2) \\ \vdots \\ f(y_n) \end{Bmatrix}, \; i, j = 1,2,...,n \qquad (A-2b)$$

in which $l_j(y)$ are the Lagrange interpolation polynomials and H_{ij}^m represent the weighting coefficients given by [21].

$$f(y_i) = \frac{G(y)}{(y-y_i)M_1(y_i)}, \; for\, i = 1,2,...,n \qquad (A-3a)$$

$$G(y) = \prod_{j=1}^{n}(y-y_i) \qquad (A-3b)$$

$$G_1(y_i) = \prod_{j=1,\, j\neq i}^{n}(y-y_i), \; for\; i, j = 1,2,...,n \qquad (A-3c)$$

$$H_{ij}^1 = \frac{G_1(y_i)}{(y_i-y_j)G_1(y_i)} \quad for\; i, j = 1,2,...,n;\; i \neq j \qquad (A-3d)$$

$$H_{ii}^1 = -\sum_{\substack{j=1 \\ j\neq i}}^{n} H_{ij}^1 \qquad (A-3e)$$

The higher derivative, mth, can be calculated as:

$$H_{ij}^m = m\left(H_{ij}^1 H_{ii}^{m-1} - \frac{H_{ij}^{m-1}}{x_i - x_j}\right) \qquad for\, i = 1,2,...,n,\; j \neq i \qquad (A-3f)$$

$$H_{ii}^m = -\sum_{\substack{j=1 \\ j\neq i}}^{n} H_{ij}^m \qquad (A-3g)$$

The discrete classical boundary conditions at y=0 and y=1, using the DQ method, can be written as:

$$w_1 = 0 \qquad (A-4a)$$

$$\sum_{k=1}^{n} H_{1k}^{n0} w_k = 0 \qquad (A-4b)$$

$$w_n = 0 \qquad (A-4c)$$

$$\sum_{k=1}^{n} H_{nk}^{n1} w_k = 0 \qquad (A-4d)$$

where n_0 and n_1 may be taken as either 1, 2 or 3 and $W_k = W(y_k)$. Choosing the values of n_0 and n_1 can give the following classical boundary conditions: [23]
simply supported: n_0 =2; n_1 =2
clamped-clamped: n_0 =1; n_1 =1
clamped-simply supported: n_0 =1; n_1 =2
clamped-free: n_0 =1; n_1 =3
free-free: n_0 =2; n_1 =3
Applying equations (A-3) and (A-4) to equations (1), one obtains the following ordinary differential system for i=1,2,3,…,n.

$$\frac{EI}{L^4}\left(\sum_{k=1}^{n} H_{ik}^4 w_k + c\sum_{k=1}^{n} H_{ik}^4 \dot{w}_k\right) + \frac{m_f V^2}{L^2}\sum_{k=1}^{n} H_{ik}^2 w_k + \left(m_f + m_t\right)\ddot{w}_i + \frac{2m_f V}{L}\sum_{k=1}^{n} H_{ik}^1 \dot{w}_k$$
$$-\frac{\vartheta A_f}{L^2}\left(\frac{V}{L}\sum_{k=1}^{n} H_{ik}^3 w_k + \sum_{k=1}^{n} H_{ik}^2 \dot{w}_k\right) - \frac{\left(e_0 a\right)^2}{L^2}\left[\left(m_f + m_t\right)\sum_{k=1}^{n} H_{ik}^2 \ddot{w}_k + \frac{m_f V^2}{L^2}\sum_{k=1}^{n} H_{ik}^4 w_k\right.$$
$$\left. + \frac{2m_f V}{L}\sum_{k=1}^{n} H_{ik}^3 \dot{w}_k\right] = q - \left(e_0 a\right)^2 \frac{\partial^2 q}{\partial x^2} \qquad (A-5a)$$

Appendix B

For static fluid velocity $u(t) = V_0$ $(\eta = 0)$, the differential system (A-5b) is then reduced to assuming $w(\tau) = W e^{\omega\tau}$ and $\{Q\} = 0$ the following eigenvalue problem is resulted from (4)

$$\left(\omega^2[M] + \omega[C] + [K]\right)\{W\} = 0 \qquad (B-1)$$

where $\{W\}$ denotes the unknown dynamic displacement vector defined as:

$$\{W\} = \{\, w_1 \;\; w_2 \cdots w_n \,\}^T \qquad (B-2)$$

and [K], [M] and [C] are the resulting stiffness, mass and damping matrices respectively.
The assumed boundary conditions can also be expressed in a matrix form using (A-4)

$$[K_B]\{W_B\} + [K_C]\{W_S\} = 0 \qquad (B-3)$$

where $\{W_B\} = \{\, w_1 \;\; w_2 \;\; w_{n-1} \; w_n \,\}^T$ and $\{W_S\} = \{\, w_3 \;\; w_4 \cdots w_{n-2} \,\}^T$. $[K_B]$ and $[K_C]$ are 4×4 and $4\times(n-4)$ matrices respectively, the similar approach Eq. (18) can be written as:

$$[K_D]\{W_B\} + [K_S]\{W_S\} + \left(\omega[C_S] + \omega^2[M_S]\right)\{W_S\} = 0 \qquad (B-4)$$

Coupling equations (B-3) and (B-4), one gets:

$$\left\{\left[K_S\right]-\left[K_D\right]\left[K_B\right]^{-1}\left[K_C\right]+\omega\left[C_S\right]+\omega^2\left[M_S\right]\right\}\left\{W_S\right\}=0 \qquad (B-5)$$

where $\left[K_S\right]$, $\left[M_S\right]$ and $\left[C_S\right]$ are $(n-4)\times(n-4)$ matrices respectively.

This relation is rewritten in the following eigenvalue problem form:

$$\begin{cases}\Gamma Y=\omega Y,\\ \Gamma=\begin{pmatrix}M_s & 0\\ 0 & M_s\end{pmatrix}^{-1}\begin{pmatrix}0 & K_h\\ K_h & C_S\end{pmatrix},\ Y=\begin{Bmatrix}W_s\\ \omega W_s\end{Bmatrix},\\ K_h=\left[K_S\right]-\left[K_D\right]\left[K_B\right]^{-1}\left[K_C\right]\end{cases} \qquad (B-6)$$

Table 6.1 Critical flow velocity buckling associated CC-CNT with uniform, normal, exponential laws and N=500

Uniform, N=500 random numbers									
V	V1			V2			V3		
σ_i=0	2.8245e+03			3.5487e+03			4.1542e+03		
	Mean(V1)	SD(V1)	σ(V1)	Mean(V2)	SD(V2)	σ(V2)	Meam(V3)	SD(V3)	σ(V3)
σ_i=2%	2.8242e3	7.0452e1	2.4946%	3.5486e3	8.8807e1	2.5026%	4.1550e3	1.0948e2	2.6349%
σ_i=5%	2.8364e3	1.7277e2	6.0912%	3.5660e3	2.1988e2	6.1660%	4.1798e3	2.7377e2	6.5498%
σ_i=10%	2.7957e3	3.3060e2	11.825%	3.5186e3	4.2321e2	12.028%	4.1355e3	5.2940e2	12.801%
Normal, N=500 random numbers									
V	V1			V2			V3		
σ_i=0	2.8245e+03			3.5487e+03			4.1542e+03		
	Mean(V1)	SD(V1)	σ(V1)	Mean(V2)	SD(V2)	σ(V2)	Meam(V3)	SD(V3)	σ(V3)
σ_i=2%	2.8242e3	6.9330e1	2.4549%	3.5469e3	8.7291e1	2.4611%	4.1510e3	1.0776e2	2.5960%
σ_i=5%	2.8245e3	1.7010e2	6.0223%	3.5509e3	2.1465e2	6.0449%	4.1618e3	2.6550e2	6.3795%
σ_i=10%	2.8128e3	3.4207e2	12.161%	3.5242e3	4.2864e2	12.163%	4.1228e3	5.2511e2	12.737%
Exponential, N=500 random numbers									
V	V1			V2			V3		
σ_i=0	2.8245e+03			3.5487e+03			4.1542e+03		
	Mean(V1)	SD(V1)	σ(V1)	Mean(V2)	SD(V2)	σ(V2)	Meam(V3)	SD(V3)	σ(V3)
σ_i=2%	2.8267e3	6.3117e1	2.2329%	3.5507e3	8.1983e1	2.3089%	4.1562e3	1.0420e2	2.5071%
σ_i=5%	2.8171e3	1.5970e2	5.6690%	3.5371e3	2.0655e2	5.8395%	4.1403e3	2.5974e2	6.2735%
σ_i=10%	2.8395e3	3.2571e2	11.471%	3.5684e3	4.2040e2	11.781%	4.1858e3	5.1897e2	12.398%

Table 6 2 Predictions of the first dimensionless frequencies associated CC-CNT with random coefficients following uniform, normal, exponential laws used on the Monte-Carlo method with 1000 random numbers.

Normal, N= 1000 random numbers									
ω	ω1			ω2			ω3		
σ_i=0	8.6006e+10			2.0772e+11			3.4924e+11		
	Mean(ω1)	SD(ω1)	σ(ω1)	Mean(ω2)	SD(ω2)	σ(ω2)	Mean(ω3)	SD(ω3)	σ(ω3)
σ_i=2%	8.5934e10	3.5645e9	4.1479%	2.0754e11	8.1235e9	3.9142%	3.4895e11	1.3280e10	3.8056%
σ_i=5%	8.6714e10	8.8370e09	10.191%	2.0924e11	2.0000e10	9.5582%	3.5181e11	3.2647e10	9.2795%
σ_i=10%	8.7840e10	1.9131e10	21.779%	2.1095e11	4.2833e10	20.305%	3.5422e11	6.9542e10	19.633%
Uniform, N= 1000 random numbers									
ω	ω1			ω2			ω3		
σ_i=0	8.6006e+10			2.0772e+11			3.4924e+11		
	Mean(ω1)	SD(ω1)	σ(ω1)	Mean(ω2)	SD(ω2)	σ(ω2)	Mean(ω3)	SD(ω3)	σ(ω3)
σ_i=2%	8.5977e10	3.6557e9	4.2519%	2.0764e11	8.1544e9	3.9272%	3.4912e11	1.3069e10	3.7433%
σ_i=5%	8.6295e10	9.0249e9	10.458%	2.0819e11	2.0148e10	9.6776%	3.5000e11	3.2410e10	9.2600%
σ_i=10%	8.8335e10	1.9225e10	21.764%	2.1214e11	4.2911e10	20.228%	3.5615e11	6.9028e10	19.382%
Exponential, N= 1000 random numbers									
ω	ω1			ω2			ω3		
σ_i=0	8.6006e+10			2.0772e+11			3.4924e+11		
	Mean(ω1)	SD(ω1)	σ(ω1)	Mean(ω2)	SD(ω2)	σ(ω2)	Mean(ω3)	SD(ω3)	σ(ω3)
σ_i=2%	8.6223e10	3.4307e9	3.9789%	2.0820e11	7.7796e9	3.7365%	3.5003e11	1.2651e10	3.6144%
σ_i=5%	8.6298e10	8.7298e9	10.116%	2.0830e11	1.9965e10	9.5847%	3.5028e11	3.2563e10	9.2963%
σ_i=10%	8.6953e10	1.6332e10	18.782%	2.0940e11	3.7659e10	17.984%	3.5203e11	6.1810e10	17.558%

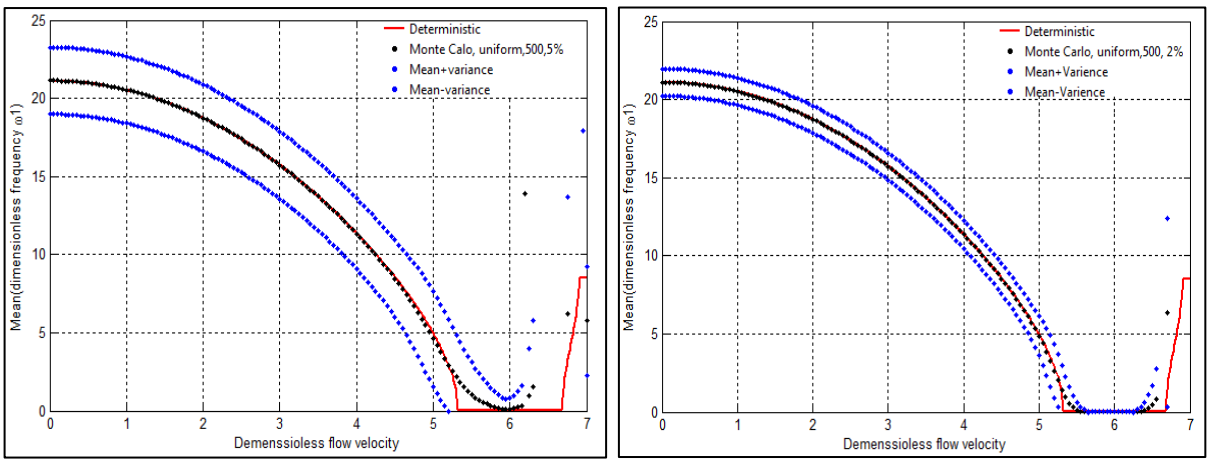

Figure 6.1 Mean ± the standard deviation of first dimensionless frequency of a CC-CNT with dimensionless deterministic flow velocity: the random parameters follow the uniform probability density with σx=2% and 5%

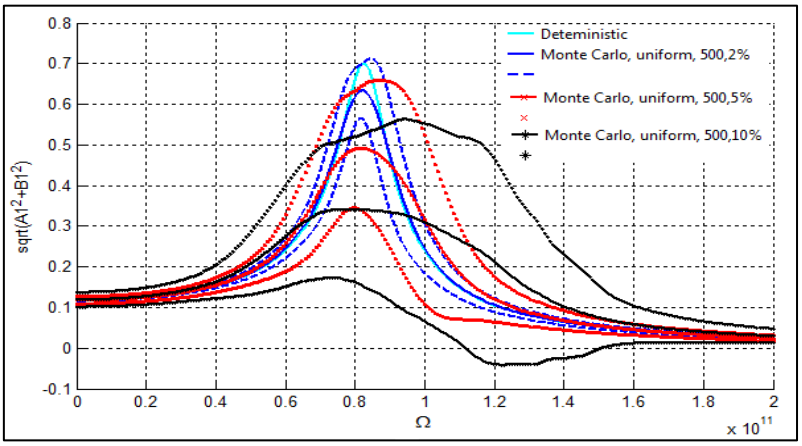

Figure 6.2 Mean ± the standard deviation of the displacement response norm with respect the frequency associated the first mode.

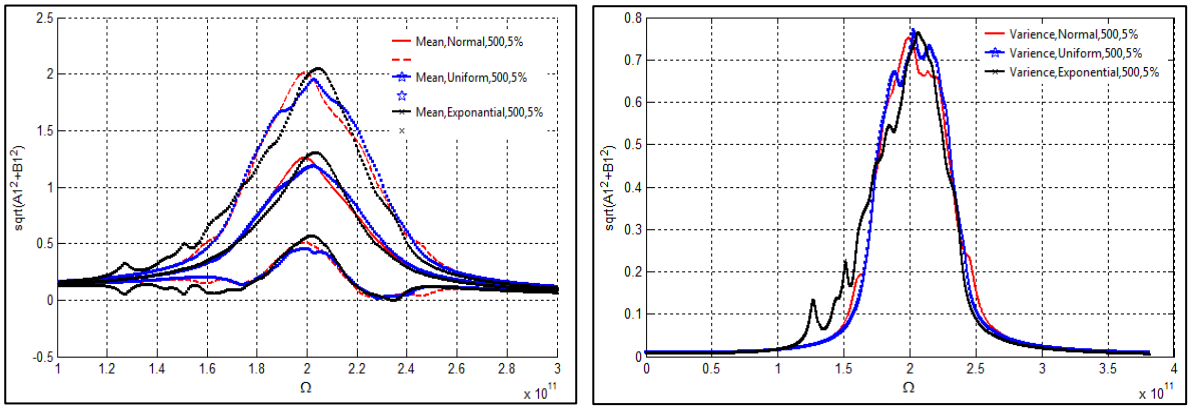

Figure 6.3 Mean ± the standard deviation and the expected value of of the displacement response norm with respect the frequency associated the first mode.

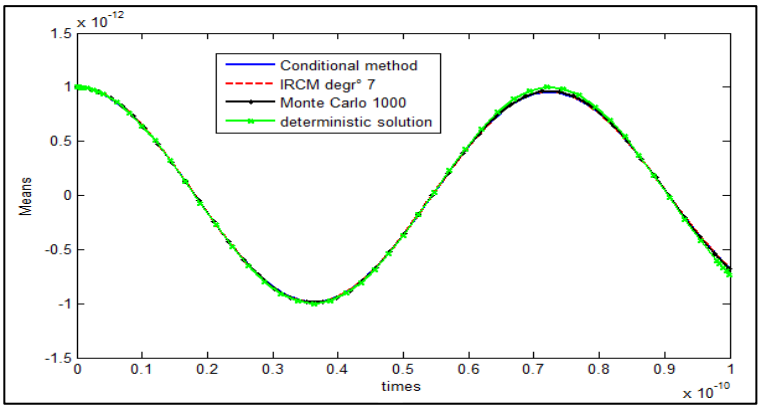

Figure 6.4 Means displacement response of $q_1(t)$ for CC-CNT, based on one mode σj=5%, uniform law.

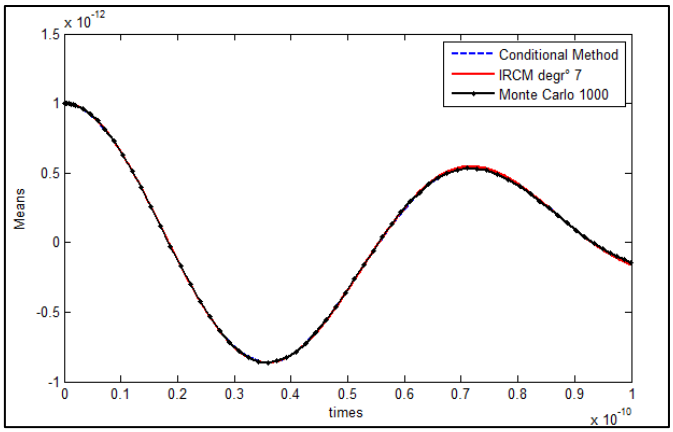

Figure 6.5 Means displacement response $q_1(t)$ for CC-CNT, based on one mode σj=20%, uniform low

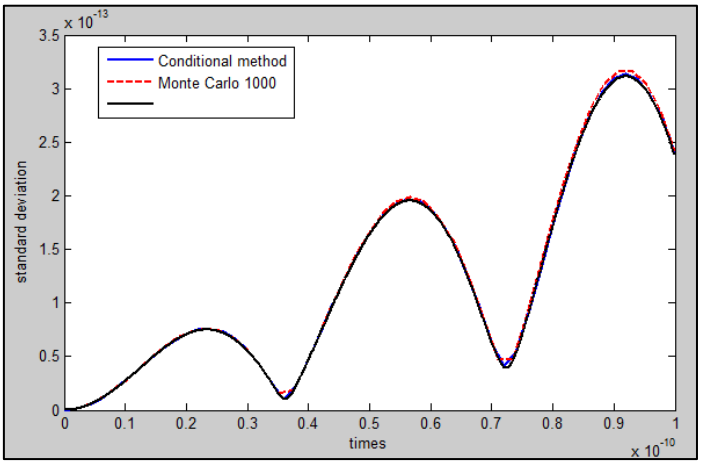

Figure 6.6 Standard deviation of displacement response of $q_1(t)$ for CC-CNT, based on one mode σj=5%, uniform law.

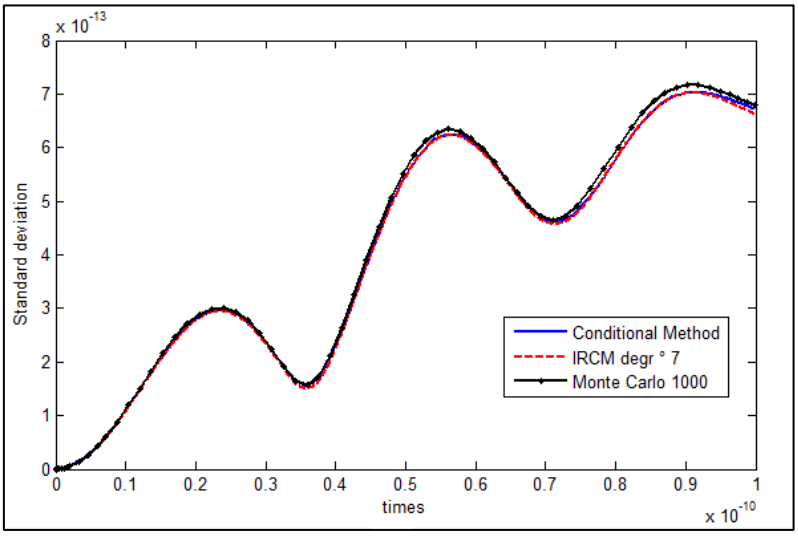

Figure 6.7 Standard deviation of displacement response of $q_1(t)$ for CC-CNT, based on one mode σj=20%, uniform law

Chapter VII

GENERAL CONCLUSION AND PERSPECTIVES

1. General conclusion

Studying the dynamic instability behaviors of carbon nanotubes (CNT) is the focus of this thesis. These structures have attracted attention because of their exceptional physical, chemical, mechanical, optical and electrical characteristics. The mastery of the static and dynamic instability behaviors of this type of structure is of great interest for miniaturized and advanced NEMS technology.

Several methods and models which were used in the literature for the study and analysis of nano-structures are introduced in the first chapter of this thesis. Mathematical models and numerical simulation for vibration problems, dynamic and parametric instabilities of single carbon nanotubes and carbon nanotube conveying fluid are developed in this thesis. Single walled carbon nanotube (SWCNT) and multi-walled carbon nanotubes (MWVNTs) are considered. Analytical and numerical simulations based on the differential quadrature method are used in this thesis to study the dynamic behaviors of carbon nanotubes. The effects of the nonlocal parameter, the fluid pulsation, viscosity, the viscoelastic coefficient and the thermal on the dynamic behaviors of the CNT-fluid system are analyzed. Various types of instabilities such as divergence, flutter and parametric instabilities as well as their interactions are analyzed. The sensitivity of the physical and geometrical parameters of carbon nanotubes, according to random parameters following different probability laws is investigated. The frequency and time analyses are elaborated by solving random algebraic and differential equations using various stochastic methods.

In the first chapter, representing a general introduction, the remarkable properties of carbon nanotubes and their applications in various fields are discussed. A broad literature review has made to cover a wide range of studies carried out in this area. Emphasis has been placed on the nonlocal elasticity theory and beams and shells models used as well as on the static and dynamic phenomena studied in this thesis.

In the second chapter, the small length scale parameter and the general boundary conditions effects on the vibration frequencies are studied. It was demonstrated that the clamped-free

CNT will flutter at critical values of (e_0a/L). This instability limit can be used as a limit of predicted values of the small length scale. Presented below is a list of main conclusions of this chapter:

- Analytical modeling and numerical simulation are elaborated for the dynamic instability analysis of CNT.
- The small length scale parameter and the generalized boundary conditions effects on the resonant frequencies are analyzed.
- The C-F CNT can flutter at critical values of (e_0a/L). This instability limit can be used as a limit of predicted values of the small length scale.

In chapter three, the higher vibration characteristics of single walled CNT based on the nonlocal elasticity, Timoshenko and Euler-Bernoulli beam theories are analytically and numerically investigated. Below is a list of conclusions that are made in this chapter:

- The differential quadrature method has been adapted for the vibration analysis of CNT.
- The small as well as the very higher eigenmodes and the associated eigenfrequencies are developed for various boundary conditions.
- New mathematical models for higher and very higher eigenmodes and frequencies are elaborated for CNT with various boundary conditions.
- The small scale length has a stabilizing effect on some few first modes.
- The developed eigenmodes at higher orders are numerically stable and can then be used as a basis for modal analysis at any desired frequency range.

In chapter four, dynamic and parametric instabilities of CNT conveying pulsating fluid are analyzed based on the nonlocal elasticity, differential quadrature method, fluid interaction and Euler-Bernoulli beam theory. The multimodal approach has been formulated based on the numerically computed eigenmodes, for dynamic and parametric instabilities. The influences of the internal fluid velocity, the nonlocal parameter, the viscosity, the viscoelastic coefficient as well as the thermal effects on the dynamic behaviors and flow-induced structural instability of CNTs are studied. Various types of instabilities such as divergence, flutter and parametric instability and their interactions are investigated. Below is a list of conclusions that are made in this chapter:

- Mathematical modeling and methodological approaches are developed for the dynamic and parametric instability analyses of CNT conveying fluid.

- The differential quadrature method has been adapted to dynamic instability of the CNT conveying fluid.
- Complex modes are computed and analyzed with respect to the fluid velocity.
- The principal parametric instability regions are numerically determined and discussed based on one and two real modes approaches as well as on complex modes.
- The influences of physical, material parameters on the flow-induced structural instability of CNTs are studied.
- Various types of instabilities such as divergence, flutter and parametric instability are investigated with respect to fluid velocity.

In chapter five, the linear and nonlinear free vibration and dynamic instability analysis of multi-walled CNTs conveying fluid based on the nonlocal elasticity and Donnell shell model are investigated. The van der Waals interactions between layers of carbon nanotube as well as the fluid-shell interaction are modeled. The free vibration and flow velocity-frequency dependence are analyzed with respect to various physical and material parameters. The obtained results showed a strong dependence between the fluid velocity and the frequency of MWCNTs. The effect of the van der Waals interaction between tubes is discussed and results show that the van der Waals interaction and the small length scale effects may significantly influence the stability of multiwalled CNT. For the nonlinear free vibration, the amplitude-frequency dependence associated to the nonlinear free vibration of MWCNT is obtained by harmonic balance method. The influences of nonlocal parameters, the vdW force and the thermal effects are discussed. The following conclusions from this chapter can be made.

- Mathematical modeling and methodological approach are developed for nonlinear vibration and the dynamic instability analysis of MWCNT conveying fluid based on a shell model.
- The influence of nonlocal parameter, the temperature, the number of tubes, the fluid velocity and the circumferential wave numbers on the nonlinear vibration are examined.
- It is demonstrated that the increase of the axial wave numbers will decrease the nonlinearity vibration effect.
- The increase of the nonlocal parameter will increase the nonlinearity vibration effect.

- The increase of the fluid velocity results in a less nonlinear vibration response effect
- The increase of the number of the walls results in a less nonlinear vibration response effect due to the influence of the vdW interaction
- The amplitude and frequency of all tubes are similar to each other.

Chapter six aims to develop models and simulations for the sensitivity analysis of CNT, physical and geometrical parameters. Given the size effect, the parameters associated to CNT models are inevitably non deterministic. These parameters are considered random and can be approximated by different probability laws. The static and dynamic behaviors of CNTs are then modeled by random equations or stochastic processes. Below is a list of conclusions that are made in this chapter:

- Models are elaborated for parameters uncertainty effects on the dynamic behavior of CNT.
- Various distribution laws are considered.
- Monte-Carlo, conditional expectation methods as well as the Internal Random Coefficients Method are adapted and numerically used.
- The effects of random parameters on vibration, buckling and dynamic instability are analyzed.
- The time responses are also developed for a wide number of random parameters.
- The models and simulations, developed in this chapter, are an outline, scientifically promising, for random analysis of the dynamic behavior of nanotubes.

2. Perspectives

- Elaboration of the differential quadrature method for plates and shells.
- Elaboration of dynamic stability analysis of nanoplates based on the nonlocal elasticity.
- Elaboration of dynamic stability analysis of multiwalled spherical carbon nanostructures.
- Dynamic instability of carbon nanotubes conveying nanofluid.
- Numerical simulation based on the Molecular Dynamics for:
    - Dynamic analysis of CNT
    - Dynamic analysis of CNT conveying fluid.
- Parameters uncertainty effects on static and dynamic behaviors of:
    - Carbon nano plate
    - Carbon nano spheres
    - Multiwalled CNT
- Development of stochastic methodological approaches for structural problems such as vibration, buckling and post buckling of the tubes and shells.